UNIVERSITÀ DEGLI STUDI DI TRIESTE

UNIVERSITÀ DEGLI STUDI DI TRIESTE

XXXVIII CICLO DEL DOTTORATO DI RICERCA IN

INGEGNERIA INDUSTRIALE E DELL' INFORMAZIONE

Funded by the European Union - NextGenerationEU

NOVEL METHODOLOGY BASED ON OPERATIVE SIMULATION AND 3D MODELING FOR THE CONCEPT DESIGN OF LUXURY PASSENGER SHIP

Settore scientifico-disciplinare: ING/IND - 02

Ph.D. Student
SAMUELE UTZERI

Ph.D. Program Coordinator
PROF. FULVIO BABICH

Thesis Supervisor
PROF. ALBERTO MARINÒ

Thesis Co-Supervisor
PROF. LUCA BRAIDOTTI, PhD

ANNO ACCADEMICO 2024/2025

Finanziato dall'Unione europea NextGenerationEU | Ministero dell'Università e della Ricerca | Italiadomani | UNIVERSITÀ DEGLI STUDI DI TRIESTE

Abstract

The ship design of a luxury cruise ship has long represented a complex engineering challenge. Traditionally, it relies on iterative and often time-consuming techniques, such as the design spiral or basic multi-attribute decision-making methods. However, with the emergence of increasingly effective technologies, such as three-dimensional parametric modelling and, in the future, artificial intelligence, traditional design frameworks can be reconsidered by integrating parametric 3D models already in the early design stages. Moreover, the enforcement of increasingly stringent regulations on pollutant emissions makes it sensible to adopt operational models to support the selection of the best possible design.

This work therefore proposes a multi-stage approach to concept design based on the integration of parametric modelling with a mathematical model for luxury cruise ships, together with the use of probabilistic software to estimate fuel consumption and pollutant emissions.

The first stage consists of generating design solutions through Monte Carlo sampling, starting from a parametric model of a luxury cruise ship. Each individual design is analysed by a mathematical model that discards configurations not satisfying technical, topology, propulsion, stability, and shipowner constraints. By defining design attributes and their associated objective or subjective weights, multi-attribute decision-making techniques can be applied to obtain, after Pareto filtering, a ranking of the non-dominated solutions.

The second stage then follows, in which, after defining one or more typical itineraries of a luxury cruise ship, a probabilistic operational simulation software is used to determine a realistic average of fuel consumption and pollutant emissions only for non-dominated designs from the first step. Hence, the first stage acts as a pre-screening process to reduce the computational load associated with the simulations. After defining additional operational attributes and their corresponding weights, a second and final ranking can be defined. The main objectives are to assess how operational conditions influence the decision-making process, while also exploiting parametric modelling to accurately define passenger areas, spaces, and volumes from a three-dimensional model from the very beginning of the design process.

Contents

List of Figures

Nomenclature

RSM Response Surface Methodology

DBD Decision Based Design

CLIA Cruise Line International Association

SWF Social Welfare Function

LSM Least Square Estimation Method

LES Least Square Estimators

DoE Design of Experiments

CCD Central Composite Designs

SPV Scaled Prediction Variance

CCC Central Composite Circumscribed

CCI Central Composite Inscribed

CCF Central Face Centered

MC Monte Carlo sampling

NURBS Non Uniform B-Spline

MAUT Multi-Attribute Utility Function

MDM Mathematical Design Model

MCDM Multi-Criterial Decision-Making

MADM Multi-Attribute Decision-Making

MODM Multi-Objective Decision-Making

AHP Analytic Hierarchy Process

TOPSIS Technique for Order of Preference by Similarity to Ideal Solution

POD Propulsion Orientable Device

DG Diesel Generator

MFZ Main Fire Zone

LSA Life-Saving Appliances

SOLAS (Safety of Life at Sea)

MES Marine Evacuation Systems

ILLC International Load Line Convention

PEM Propulsion Electric Motor

SFOC Specific Fuel Oil Consumption

SRtP Safe Return to Port

FW Fresh Water

GBW Gray Black Water

BW Ballast Water

MGO Marine Gasoil Oil

PMS Power Menagment System

HVAC High Ventilation and Conditioning

CII Carbon Intensity Indicator

GHG_{int} Greenhouse intensity factor

GT Gross Tonnage

BD Bulkhead deck

DWT Deadweight

L_{OA} Length overall

B Ship beam

L_{BP} Length bewtween perpendiculars

L_{WL} Waterline length

T_{des} Design draught

V_{des} Design speed

V_{max} Maximum speed

C_B Block coefficient

C_X Midship coefficient

C_{WP} Waterplane area coefficient

C_{VP} Vertical prismatic coeffcient

LCB Longitudinal position of centre of Buoyancy

LCF Longitudinal position of centre of floating

A_{BT} Transverse bulb area

h_B Bulb center height above keel

A_{WP} Waterplane area

C_{WP} Waterplane area coefficient

A_T Transom immersed area at zero speed

S Wetted hull surface

i_E Entrance angle coefficient

LE Bow waterline entrance length

LR Stern waterline entrance length

kyy Longitudinal inertia radius

A_{l_a} Lateral projected area exposed to air

sl Lateral-plane centroid position

A_{f_a} Frontal projected area exposed to air

sl Lateral-plane centroid height

A_{l_w} Lateral projected area underwater

A_{f_w} Frontal projected area underwater

P/D Pitch diameter ratio

A_E/A_0 Expanded area ratio

S_{pod} Pod wetted surface

D Propeller diameter

Z Number of blades

W_{LS} Lightship Weight

DW Payload Deadweight

D_A Correct moulded depth to the highest continuos deck

KG Vertical centre of gravity

KG_{limit} Limit vertical centre of gravity

P_{tot} Installed Power

PAX Passegenrs on board

$CREW$ Crew member

$A_{Pax_{tot}}$ Total passenger area

$A_{Crew_{tot}}$ Total passenger area

$TrunkTec_{tot}$ Total Trunk and techinical area

$A_{Gal_{tot}}$ Total galleys area on board

$A_{Pub_{tot}}$ Total public area on board

$A_{Ext_{tot}}$ Total external area on board

n_{Evap} Number of evaporators

n_{Osmos} Number of reverse osmosis units

Chapter 1

Introduction

Despite the initial outbreak of the COVID-19 pandemic in China, its impact on the travel and tourism industry was significantly underestimated [4]. In recent years, however, cruise travel has experienced a notable resurgence, driving a gradual recovery of the cruise sector [5]. According to the Cruise Line International Association (CLIA) [6], global passenger numbers reached 31.7 million in 2023, compared to 29.7 million in 2019, representing a growth rate of 6.8%. This upward trend is expected to continue, with projections of 35.7 million passengers in 2024 and nearly 40 million by 2027.

In 2023, CLIA reported that the largest share of cruise passengers was American, totalling 16.9 million travellers. The United States recorded a 19% increase compared to 2019, consolidating its position as the leading contributor to the global cruise market. Germany ranked second with 2.5 million passengers, showing a 3% decline relative to 2019 [6]. The United Kingdom followed in third place with 2.2 million passengers, marking a 15% increase. Italy and Brazil also demonstrated significant growth, with increases of up to 30%. In contrast, China experienced a sharp decline: from 1.9 million passengers in 2019 to fewer than $157\,000$ in 2023, highlighting persistent challenges in that region.

Regarding destinations, the Caribbean, the Bahamas, and Bermuda remained the most popular cruise regions [7], attracting approximately 12.6 million passengers in 2023, a 7.3% increase compared to 2019. The Mediterranean exhibited strong growth, welcoming 5.5 million passengers, an increase of 23% [8]. Other European regions also benefited, with 3 million passengers, representing a 6.6% rise over pre-pandemic levels. Significant increases were observed in Alaska, South America, and the west coast of North America. Conversely, Asia recorded a 35.6% decline, falling to 2.6 million passengers.

Although cruises account for only 2% of global tourism, the sector occupies a strategic position within the international economic landscape, generating direct, indirect, and induced benefits [9]. In 2022, despite passenger volumes reaching only 70% of pre-pandemic levels, revenues recovered to 90% of 2019 figures, amounting to 138 billion, sustaining 1.2 million jobs world-

wide and generating 43 billion in wages [6].

The expansion of the cruise industry, like any economic activity, entails externalities that raise social, economic, and environmental challenges for ports and surrounding areas [10]. Among the proposed solutions, the adoption of shore-side electricity (cold ironing), i.e. the process of supplying power from shore to meet ships' energy needs while berthed, has gained relevance [11]. This technology eliminates emissions from auxiliary engines during port stays, contributing to global emission reductions when the shore grid relies on renewable energy sources [12]. The number of cruise ships equipped with shore-side power capability is expected to more than double by 2028 [13]. During this period, all new ships ordered by CLIA member companies, except expedition vessels, will include this feature. However, the main limitation remains the low availability of port infrastructure: currently less than 2% of cruise ports are equipped, with an increase to 3% projected by 2025.

noindent Cruise lines are typically classified by market segment into four categories: Contemporary, Premium, Luxury, and Niche [14]. Contemporary cruises target families and couples, offering activities at accessible prices (up to $249 per day). The Premium segment caters to travellers seeking higher-quality experiences at moderate prices ($250–$299 per day). Luxury cruises serve affluent customers, with costs exceeding $500 per day [15]. Finally, the Niche segment, an extension of Luxury, includes small and medium-sized expedition and exploration vessels.

Luxury cruises aim to attract sustainability-conscious passengers and younger demographics, offering all-inclusive experiences in an informal yet refined setting. Innovations include an increased number of balcony cabins, single-occupancy options, combinable balconies for families, gourmet dining, entertainment, and multiple relaxation opportunities. The target clientele consists of affluent travellers seeking exclusive experiences worldwide. On board, maximum comfort is ensured through first-class restaurants and high-level entertainment. Transport capacity ranges from 200 to 900 passengers, with daily costs typically between $500 and $1,000 per person. Gross Tonnage (GT) varies from 10,000 to 80,000 tons [16].

Considering the design process of Luxury cruise ships, meeting shipowners' requirements is therefore essential to maintain competitiveness in the market. In this context, the early design stages are crucial. In particular, the objective of concept design is to translate these requirements into graphical and numerical representations of the design alternative that best satisfies them. The quality of a technical product depends on multiple activities, among which the development of the design process is paramount. The term design process refers to the set of actions and procedures structured to guide design activities through a step-by-step decision-making framework [17].

The overall design process can be regarded as a decision-making process involving analysis, synthesis, evaluation, feedback, modification, and control. A rational approach starts from the

identification of customer requirements and extends through conceptual design, basic design, and production, up to the end-of-life phase of the product [18].

In today's competitive market, there is a continuous need to develop and produce technical systems that satisfy customer requirements while ensuring reliability and an adequate cost–benefit ratio. The early design stages are of paramount importance for the success of a product. A rational design approach is therefore required to increase both the efficiency and the effectiveness of the decision-making process. Efficiency is defined as the speed at which reliable information is generated, whereas effectiveness measures the quality of design decisions, i.e. their accuracy and applicability. The primary objective of design is to satisfy customer requirements at the minimum cost. The life-cycle cost of a product includes design, construction, and operating costs [17].

The design process of a ship is the articulated and lengthy production pathway that runs from the initial concept to the delivery of the ship. It is typically divided into basic design and product realisation.

Basic design is subdivided into several phases:

Concept design. This is the phase in which the foundations for the entire life cycle of the ship, from preliminary design to construction and production, are laid. It is the phase that offers the greatest potential for improvement at relatively low cost and presents the most demanding challenges for the design team. Engineering knowledge, practical experience, production methods, and economic aspects are integrated in order to make the most important and far-reaching decisions. In this phase, the operational requirements are defined, the design criteria are selected, and a baseline configuration is developed to meet the customer's needs under regulatory and engineering constraints. Decisions taken at this stage are strategic and influence the entire product life cycle in terms of performance and cost.

Preliminary design. This phase uses the outputs of the conceptual design to assess performance through direct calculations and to evaluate performance and/or optimise individual systems using analytical and numerical tools. Operational, spatial, and layout requirements, redundancy, weight, life-cycle cost, maintenance, reliability, and crew requirements are all considered. At the end of this phase, the preliminary ship specifications are issued, which definitively establish the main requirements and constraints for the final product.

Contract design. The preliminary design is further optimised in its subsystems using numerical codes and physical experiments. Each system, such as the hull, machinery, and electrical systems, is analysed in detail. The principal dimensions and main characteristics of the ship are no longer modified during this phase. The outcome is a complete final

specification, including calculations and drawings submitted to the selected Classification Society for approval. The final outputs of this phase are the general arrangements and the final specification attached to the contract between shipowner and shipyard.

Functional design. After contract signing, in this phase the final design is refined in terms of functionality through the optimisation of overall system performance and costs. It concludes with the definition of one-line diagrams of all the systems and their components, and procurement documentation for long-lead items.

Transition & Work Instructions. Once the functional design phase is completed, the detailed engineering of the ship begins, aiming to define how the systems and their components are actually positioned and installed onboard. The main outputs are the detail drawings and work instructions for the shipyard. This design phase, although characterised by simpler tasks, is the most time-consuming and usually proceeds partially in parallel with ship construction.

Figure 1.1 summarises the phases described above.

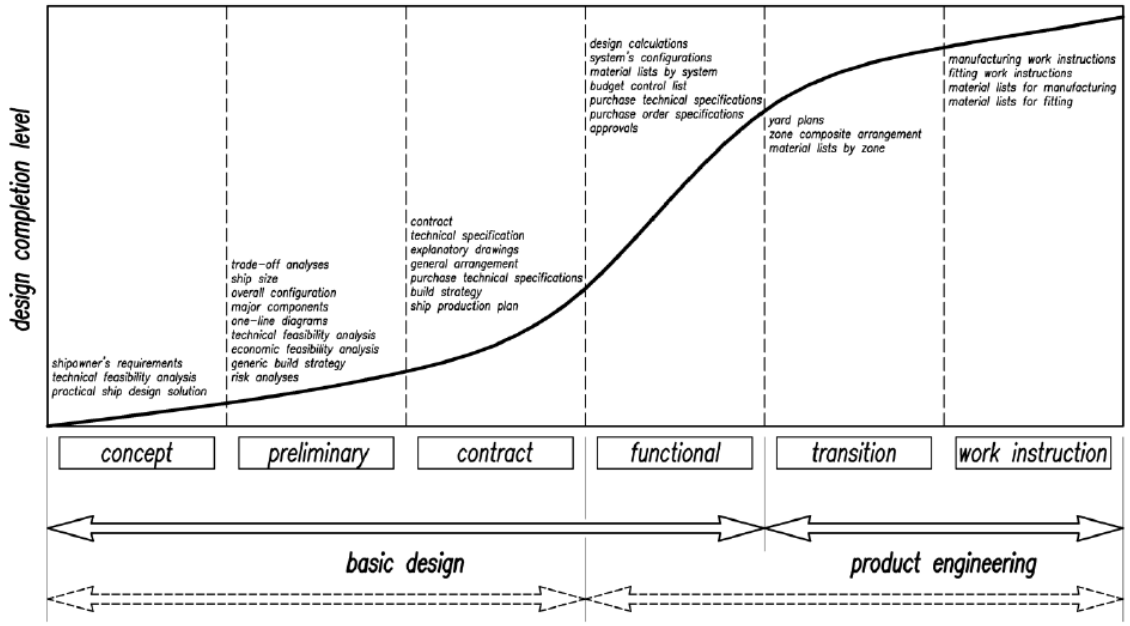

Figure 1.1: Ship deign flow [1]

The traditional ship design approach is represented by the design spiral, which focuses on a series of iterative activities aimed at converging, as efficiently and rapidly as possible, to a single feasible solution for a given project. This approach often leads to decisions based on incomplete information or compromises, requiring extensive rework through iterations in order to reach an

acceptable outcome. Naval architects move through the design process in a serial manner, gradually increasing the level of detail at each loop of the spiral until a feasible solution satisfying all constraints is reached. However, at the end of one cycle, the design is rarely balanced or even feasible, and a second cycle is therefore initiated, carrying out all the activities starting from assumptions proved unrealistic. The number of iterations required to converge to a feasible solution is not known a priori. This approach can be classified as point-based design, since it identifies a single point in the design space. One of the main limitations of this method is that there is no way to verify whether better solutions exist than the one obtained. Consequently, alternative design methods based on the comparison and selection among multiple feasible designs are required. One such method is Decision Based Design (DBD). DBD is a rational design methodology that provides multiple high-quality design solutions in a reduced time. It is based on the axiom that the primary role of engineers is to make decisions. It incorporates the principles of concurrent engineering throughout the product life cycle and is particularly effective in the early design stages, as it relies on multi-criteria decision-making techniques. Because the conceptual and preliminary phases have a dominant influence on final costs and performance, DBD offers the greatest potential to maximise product value.

The DBD approach [19] was developed to model design as a decision-making process aimed at maximising product value. In order to select the best designs, a ship-specific Mathematical Design Model (MDM) must be developed. Given the complexity of a ship, a single monolithic code is not feasible, and the problem must be decomposed into several subsystems. The design team therefore develops a set of metamodels describing, for instance, propulsion, manoeuvrability, resistance, seakeeping, construction costs, operating costs, etc. The inputs to the metamodels consist of the primary ship characteristics, which are defined during the early design stages through interactions between the design team and the client. The outputs of the mathematical model comprise a set of attributes spanning regulatory, technical, and economic domains, which collectively determine the vessel's technical quality and overall value. For a given ship type, the metamodels are usually mathematical–statistical models derived from databases of existing ships using multivariate regression techniques, so that the attributes depend only on the primary design variables. A comprehensive and reliable ship database is therefore a prerequisite for the effective development of such models. By feeding the mathematical design model with random variables generated through Monte Carlo methods, a large number of conceptual designs with known attributes can be generated. Given this set of alternative designs, the design team faces the problem of selecting the best one. Such decisions should not be based on intuition, experience, or arbitrary judgement, but rather on rational multi-criteria procedures, such as those provided by Multi-Criterial Decision-Making (MCDM) and, in particular, Multi-Attribute Decision-Making (MADM).

In the ship concept design, the ship's main characteristics and principal dimensions are typically

established. The calculations performed should be sufficiently accurate in order to avoid major modifications in subsequent phases. At this point in the process, the following are defined: the mission profile of the ship, the performance targets, and a preliminary estimate of production and operational costs [18].
A ship is an extremely complex industrial product, featuring a non-analytical hull form and multiple interacting systems. The properties used to describe the ship are often interdependent, even when simplified mathematical models are adopted. For instance, if the ship length were increased, this would imply a larger hull volume, requiring a more powerful air-conditioning system, which would increase the ship's weight and consequently reduce its speed [20].
The goal of the concept design phase is to evaluate the fundamental aspects of the system under study and select the solution that best satisfies the shipowner's requirements.
The development of increasingly efficient and effective computational techniques has allowed for the establishment and widespread adoption of design methods, such as DBD, as alternatives to the traditional design spiral, based on multi-criteria decision-making approaches [21]. The "chosen" solution is the one that performs best, according to predefined criteria, among all feasible alternatives within the design space. Thus, the challenge is not merely to find a solution, but to find the best possible one. Several methodologies can be employed to achieve this. Indeed, an entire scientific discipline exists dedicated to the study of design processes [22].
The application of multi-attribute decision-making techniques requires the definition of a design space within which the best possible solution can be identified. Given the difficulty of retrieving reliable data from the literature concerning ship spaces, layouts, and weight distributions, it is advisable to implement parametric modelling already in the early stages of design. It is possible to provide, from the very first conceptual phases, a three-dimensional model of the ship that can serve as the basis for the subsequent technical development.

1.1 Literature Review

A review of the literature shows that contributions focusing on cruise ships are particularly relevant. These studies confirm that industry know-how is progressively shifting from hull form design towards interior design and passenger experience [23]. A specific example is provided by the study of Zhang, which uses the cruise ship *Tianhai New Century* to develop a virtual reality simulation [24]. This demonstrates that the success of a luxury cruise ship is not only engineering-driven, but also perceptual and architectural, thus requiring complex three-dimensional models from the earliest design stages. The use of virtual reality for the review of interior design on a ship under construction is particularly critical for the luxury segment, where an error in the layout of a suite or a public area can significantly compromise the product's value [25]. All these studies suggest that it is mandatory to increase focus on the payload

(cabins, internal and external public spaces) since the very beginning of the luxury cruise ship design process, possibly supported by 3D models.
Energy efficiency and Safe Return to Port studies for cruise ships confirm that parametric models are already used to assess safety-related and performance aspects for large ships [26, 27]. The literature also presents well-established approaches for hull optimisation. There are parametric models coupled with genetic algorithms applied to SWATH hulls and catamarans [28, 29], and high-speed naval ships [30]. With regard to General Arrangement plans, the parametric approach proposes a flexible layout-generation approach that overcomes the limitations of 2D CAD [31]. However, a direct link between the generated geometry and the ship's physics, particularly in terms of stability and weight distribution, is usually missing. Currently, no studies have been carried out aiming to couple parametric modelling with a mathematical design model capable of comprehensively analysing the studied design alternative and assessing both its technical and economic feasibility, using databases of real ships from which unknown quantities at the early design stage can be estimated through regression techniques.
A second aspect that is neglected by the current literature on ship design concerns the estimation of operational efficiency, which is typically studied only after the ship has been delivered. The literature is rich in examples of ex-post operational optimisation, such as applying mixed-integer linear programming to optimise cruise ship itineraries by maximising attractiveness and minimising costs [32], or using algorithms to manage ship speed and waste disposal under Emission Control Area (ECA) regulations [33, 34]. However, to date, no early-stage design studies exist that identify the best possible ship design based on realistic operational attributes.

1.2 Objectives of the thesis

The present work aims to develop a novel multi-stage methodology for ship concept design based on MADM, incorporating advanced probabilistic operational simulations. Specifically, a ship 3D parametric model coupled with a MDM for luxury cruise ships is formulated, enabling the parametric modelling of the hull and internal spaces for the accurate definition of ship geometry. Once the principal design variables have been identified, a set of design alternatives is generated through Monte Carlo sampling, exploiting the 3D parametric ship model, and evaluated using a MDM to characterise each alternative in terms of topology, propulsion, power generation, and stability, discarding those that fail to meet technical or owner-imposed constraints. An appropriate set of attributes is then defined to enable a first-stage selection, which screens the most promising alternatives. This stage employs Pareto filtering combined with ranking based on the Technique for Order of Preference by Similarity to Ideal Solution (TOPSIS) method. The second major objective of the thesis is addressed in the subsequent stage, where the shortlisted designs undergo further analysis to incorporate an enriched set of attributes for final screen-

ing and TOPSIS ranking, ultimately leading to the selection of the optimal ship configuration. These additional attributes are derived from average fuel consumption and emissions estimated through operational simulations of itineraries representative of the vessel's service life, accounting for the actual influence of environmental conditions encountered during operation.
The main contribution of this work lies in addressing the inherent limitations of traditional MADM-based concept design frameworks, and it is twofold. First, the integration of a three-dimensional parametric ship model with the MDM eliminates the need to estimate geometric characteristics through regressions or empirical estimates. This approach enhances flexibility in exploring alternative platforms and payload configurations, while improving the accuracy, completeness, and reliability of geometric and topological quantities employed by the MDM, thereby increasing the reliability of its outputs as well. Second, this study introduces operational simulation into the concept design stage for the first time, albeit restricted to a shortlist of design alternatives to control the computational burden associated with probabilistic simulations. This task is often neglected even in subsequent design phases, yet it is of critical importance as it enables the inclusion of attributes within the MADM framework that reflect real-life operational efficiency, rather than relying solely on standard or unrealistic design assumptions.

1.3 Thesis organisation

The thesis is organized as follows: Chapter 2 presents the theoretical foundations of the MADM framework. Chapter 3 describes the proposed methodology, focusing on the integration of the three-dimensional parametric ship model with the MDM and the incorporation of probabilistic operational simulations. Chapter 4 presents the application of the methodology and the results obtained from a case study involving a luxury passenger ship characterised by multiple payload configurations, including cabins, public spaces, and external areas. Chapter 5 discusses the impact of introducing the second stage on the selection of the optimal ship design, while Chapter 6 provides the concluding remarks.

Chapter 2

Theoretical basis

The design of a ship develops through multiple stages, during which the level of knowledge increases while the degrees of freedom for design choices progressively shrink. Implementing changes in the later phases of design can be highly costly and may cause significant scheduling delays [35]. For this reason, the concept and preliminary design phases, the early stages of the design process, exert a decisive influence on the final outcome. This chapter presents the theoretical foundations of Design Science based on MCDM, with a specific focus on MADM methodologies. It introduces intra- and inter-attribute preference modeling and ranking techniques, including attribute normalization based on fuzzy set theory, the AHP method for deriving subjective weights, and the TOPSIS method for alternative selection. Finally, RSM is discussed as a tool for developing regression models that support concept design, using historical or newly generated datasets.

2.1 Design Science

Design Science is a discipline that studies the creation of artifacts and their introduction into physical, psychological, economic, social, and technological environments, with the aim of developing processes capable of solving problems and producing practical impact in specific scenarios [36]. The need to optimize design processes arises primarily from market demands for increasingly high quality standards, without compromising delivery times.
Two major branches of Design Science may be identified:

- Theory of tecnical systems
- Theory of design process

The theory of technical systems aims to describe the design object from a technical perspective, decomposing it into its most significant components for the design process [19]. A technical system may be represented through a behavioural model, typically used in early design

phases, where properties are simulated or approximated through mathematical models; a structural model, used in later phases, where detailed 3D representations and construction-relevant information are produced.
The following elements are essential for defining a behavioural technical system and its characteristics:

- **Variables**: Discrete or continuous properties that uniquely distinguish one design alternative from another.
- **Design Space**: The multidimensional domain defined by the ranges of the design variables; each point within this space corresponds to a specific combination of variable values and represents a distinct design alternative.
- **Parameters**: Properties of the design assumed to remain constant across all design alternatives.
- **Soft Constraints**: Quantifiable properties that characterize components of a technical system and serve as indicators for evaluating its overall performance or suitability.
- **Hard Constraints**: Prescribed limits imposed on specific properties, defining the feasible region of the design space.

The theory of design process focuses on analysing and generalizing the design process itself. A design process theory allows the distinction between design science and design practice, providing a framework for understanding and explaining key phenomena [37]. It enables designers to validate or challenge existing knowledge and to construct new knowledge in a systematic manner[38]. The goal is to generalize the phases of the design process so that they become applicable across a wide range of contexts and problems [39].
There are two main approaches to the design process:

1. **Evolutionary approach** (**traditional spiral method**), which consists of a recursive method that guarantees the feasibility of a solution for creating a product through successive iterations.
2. **Multi-criteria decision-making approach**, which allows for selecting the best solution in a vast set of technically feasible alternatives [40].

The first proposed approach, however, presents notable critical issues. One of the main problems concerns the complexity in managing the process. The model involves continuous iterations that must be carefully monitored to avoid wasting time and resources. Each iteration of the process involves additional costs in terms of time, budget, and personnel involved, and

if not managed correctly, this characteristic can drive up project costs, making the method inconvenient for small or medium-scale projects. Furthermore, the spiral method can lead to a proliferation of modifications. The continuous refinement of the project and the possibility of introducing new functionalities in each iteration can give rise to an uncontrolled growth in system complexity, making it more difficult to manage and implement. Finally, another significant problem is the difficulty in defining a clear endpoint. Since the method involves progressive system improvement through successive cycles, it can be complicated to establish when the project is mature enough to be completed and released. This can lead to excessive work extension, with the risk of not meeting deadlines. Moreover, the endpoint strongly depends on the starting product considered, which suggests that it is not always possible to arrive at the best possible solution, especially for innovative projects [41]. The MCDM approach presents several advantages over the evolutionary approach. MCDM allows for addressing design complexity by simultaneously considering multiple criteria, supporting the management of complex decision problems with multiple and often conflicting objectives. This method favors a more transparent and rational decision-making process, thanks to an organized structure that allows for analyzing and comparing different alternatives [41].
Furthermore, it helps to identify balanced solutions among the various criteria, optimizing the use of available resources. Despite its numerous advantages, MCDM presents some critical issues. Among these are the subjectivity in the selection of criteria, in the assignment of weights, and in the choice of evaluation methods, which can influence the objectivity of the decision-making process. Moreover, computational complexity can represent a critical issue when the number of criteria and alternatives increases, making the process extremely computationally expensive [41]. In the context of design, MCDM proves particularly effective for managing problems where it is necessary to balance technical, economic, social, and environmental aspects [42]
This makes it an efficient method, especially in the initial phases of the design process. However, to ensure its effectiveness, careful application is fundamental, in order to mitigate the critical issues related to subjectivity and computational complexity.

2.1.1 Multi-Attribute Decision Making

During the concept design phase, it is crucial to clearly identify and define the design attributes that will serve as the basis for evaluating alternative solutions [43]. These attributes represent measurable characteristics that influence the decision-making process. Establishing the evaluation criteria at the outset provides a robust foundation for comparing alternatives and ensures that all relevant variables are considered from the beginning [44].
It is important to specify that criteria in MADM can be divided into two main categories:

1. Design constraints (hard constraints);

2. Design attributes (soft constraints).

Hard constraints are requirements that must be absolutely met to ensure the design alternative feasibility, such as physical laws or specific technical regulations, while soft constraints are more flexible requirements that can be subject to compromise to select the best possible alternative. The latter reflect the preferences of the design team or the owner's desires and can be adapted based on the circumstances. The distinction between hard and soft constraints is crucial for managing uncertainties and inaccuracies in the early design phases, allowing for the exploration of more creative solutions and optimizing compromises between different attributes. This flexibility is essential for developing an optimal and efficient design in the context of conceptual design for innovative solutions [44].
Hard constraints are essential for defining the boundary of the design space ($\mathbf{X}$-space), in which design alternatives are identified through the variables' values. Hard constraints, therefore, ensure that the evaluated alternatives are all feasible and conform to essential requirements. Every alternative in the design space is evaluated through the MDM, which is capable of mapping them to the attribute space ($\mathbf{Y}$-space). This process allows for translating the characteristics of the alternatives into quantifiable performances, through which it is possible to define the best solutions based on the established criteria. This is called the evaluation phase [45]. The design process, on the other hand, represents the inverse mapping from the attribute space to the design space, through which the values of the design variables leading to the best possible alternative are determined.
Figure 2.1 illustrates the spaces just mentioned and the mapping process through the function $y = f(x)$, which summarizes the task of the mathematical model, and the function $x = f^{-1}(y)$. The conceptual design process was built with a prescriptive model, based on a schematic organization and capable of utilizing prior knowledge through algorithms. The Multi-Attribute Concept Design phase was subdivided into three interconnected phases [46]:

1. Design Analysis: the evaluation of multiple design alternatives, meeting constraints. These solutions were obtained through a Monte Carlo generation, to adequately cover the design space.

2. Design Synthesis: a filter is applied to identify the feasible designs and select, from these, the non-dominated ones that populate the Pareto frontier.

3. Design Selection: which is based on multiattribute metrics, aiming for the selection of the optimal solution.

Ultimately, the strategy involves combining the MADM approach with filtering and selection/ranking techniques [47].

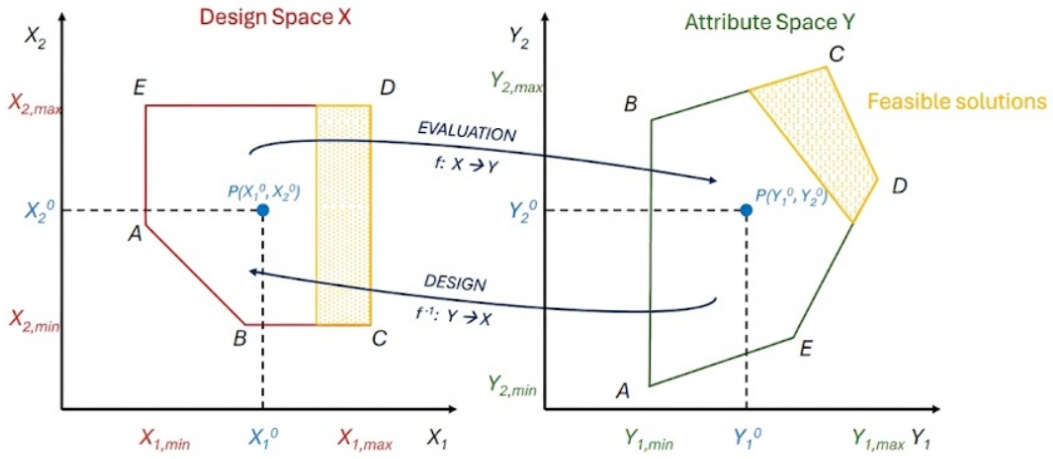

Figure 2.1: Mapping of X and Y spaces

2.2 Preference and selection

Within the MADM framework, the concepts of attribute preference and selection based on weighted attribute values are of paramount importance [21]. Preferences can be categorized into two main types: intra-attribute and inter-attribute preferences. The former relates to the attribute values themselves and, when applicable, their normalization process, implemented in this work using fuzzy set theory. The latter concerns the subjective priorities of the design team, which are used to define attribute weights. Once normalized and weighted attribute values are established, they serve as the basis for Pareto filtering and ranking feasible design alternatives. The following sections present the approaches adopted in this study to address preference modeling and selection.

2.2.1 Intra-attribute Preferences and fuzzification

Intra-attribute preferences refer to the objective importance assigned to the values of a single attribute in relation to the target thresholds defined by the design team [46]. Here, the approach used to define intra-attribute preferences is the fuzzy set theory [44], which consists, by definition, in associating a value between 0 and 1 with each element of a set of attributes using a function called the membership function. This value expresses the degree of membership of the element to the attribute set. The choice of the membership function intrinsically affects the selection process, as the values associated with each single element of the attribute set change

depending on the shape intended for the function. For this reason, it is very important to accurately decide the membership functions with which the single attribute is to be fuzzified. It is also fundamental to carefully choose the thresholds for each attribute set, i.e., the limit values to which 0 and 1 correspond.
The triangular membership functions are used for this purpose [48]. It defines y_{jk} as the elements of an attribute set containing m attributes and k design alternatives. Then, U_{jk} can be defined as as the fuzzified attribute set. In the present study, the following membership functions are employed to normalise attributes:

1. For attributes to be maximized:

$$U_{jk} = \frac{y_{jk} - x_{j_*}}{y_j^* - y_{j_*}}$$

2. For attributes to be minimized:

$$U_{jk} = 1 - \frac{y_{jk} - y_{j_*}}{y_j^* - y_{j_*}}$$

3. For attributes that are desired to converge towards the value $\overline{y}$:

   - if $y_{jk} < \overline{y}$ then the function is used:

$$U_{jk} = \frac{y_{jk} - y_{j_*}}{\overline{y} - y_{j_*}}$$

   - otherwise:

$$U_{jk} = 1 - \frac{y_{jk} - \overline{y}}{y_j^* - \overline{y}}$$

4. For attributes that are desired to diverge from the value $\overline{y}$:

   - if $y_{jk} < \overline{y}$ then the function is used:

$$U_{jk} = 1 - \frac{y_{jk} - y_{j_*}}{\overline{y} - y_{j_*}}$$

   - otherwise:

$$U_{jk} = \frac{y_{jk} - \overline{y}}{y_j^* - \overline{y}}$$

where for cases 1 and 2, $y_{j_*} = \min_k(y_{jk})$, $y_j^* = \max_k(y_{jk})$, $U_{jk}(y_{j_*}) = 0$ and $U_{jk}(y_j^*) = 1$, while for cases 3 and 4 the values of y_{j_*}, y_j^* and $\overline{y}$ are arbitrarily decided based on practice and experience.

2.2.2 Inter-attribute Preferences

Inter-attribute preferences refer to the assignment of weights to the attributes, a fundamental step for the selection of the optimal alternative. The attribution of weights allows for reflecting the relative importance of each attribute and establishing a hierarchy among them. The determination of these weights is usually carried out by the design team, who define them based on their own preferences and the owner's requests.

The AHP [48] is a well-established method for converting subjective evaluations of the relative importance of attributes into quantitative weights. In this approach, experts express their preferences by performing pairwise comparisons of the criteria (in this study, only criteria are considered) using a predefined linguistic scale. These judgments are then translated into a pairwise comparison matrix, from which the priority weights are obtained as the normalized principal eigenvector.

A critical step in the procedure is the verification of the matrix consistency, which ensures the reliability of the judgments [49]. In the present work, pairwise comparisons were carried out by the author and supervisors, with consistency checks applied to each matrix. Individual judgments were subsequently aggregated using the geometric mean method [50]

2.2.3 Pareto Dominance Principle

The Pareto dominance principle allows for an additional screening among the feasible alternatives, identifying all those that are non-dominated. According to the definition given by the principle, a solution 2 is dominated by a solution 1 if, moving from 2 to 1, at least one attribute is improved while leaving the others unchanged. Substantially, solution 1 is non-dominated if it respects the following two conditions: no other solution must exist that has the same or better performance in all attributes, and the performance improvement of one attribute leads to the deterioration of another.

Mathematically, the principle can be described as follows: We define the two solutions $\mathbf{U}_1$ and $\mathbf{U}_2$:

$$\mathbf{U}_1 = \{U_{11}, ..., U_{m1}\}, \quad \mathbf{U}_2 = \{U_{12}, ..., U_{m2}\}$$

$\mathbf{U}_1$ dominates $\mathbf{U}_2$ if:

$$\forall j \in \{1, ..., m\}, \quad U_{j1} \geq U_{j2}$$

$$\exists j \in \{1, ..., m\} \quad | \quad U_{j1} > U_{j2}$$

Or with direct comparison:

$$\mathbf{U}_1 \geq \mathbf{U}_2 \quad \text{and} \quad \mathbf{U}_1 \neq \mathbf{U}_2$$

It is important to note that the dominance principle can be applied exclusively to attributes classified as either benefits or costs. Consequently, attributes that are intended to converge toward or diverge from a specific target value must undergo a fuzzification process prior to applying the dominance rule. The fuzzification procedure, described in Section 2.2.1, transforms all attributes into benefit-oriented membership functions, thereby ensuring that every attribute type can be consistently utilized within the decision-making framework.

2.2.4 TOPSIS

The TOPSIS method is a well-established multi-criteria decision analysis technique employed to rank non-dominated alternatives based on their attribute values and corresponding weights. In this approach, the ranking is determined by evaluating the relative proximity of each alternative to the ideal solution and its remoteness from the anti-ideal solution. The ideal solution is defined as the hypothetical alternative composed of the maximum value for each attribute, whereas the anti-ideal solution consists of the minimum values.
Since attribute normalization has already been performed through the fuzzification process described in Section 2.2.1, no additional normalization is required in this step. Let U_{jk} denote the normalized value of attribute j for alternative k, and w_j the weight associated with attribute j. The euclidean distances to the ideal (d_k^+) and anti-ideal (d_k^-) solutions are computed as:

$$d_k^+ = \sqrt{\sum_{j=1}^{m} w_j \big(U_{jk} - U_j^+\big)^2}, \qquad d_k^- = \sqrt{\sum_{j=1}^{m} w_j \big(U_{jk} - U_j^-\big)^2}$$

where U_j^+ and U_j^- represent the ideal and anti-ideal values for attribute j, respectively. The relative closeness coefficient for alternative k is then given by:

$$C_k = \frac{d_k^-}{d_k^+ + d_k^-}, \qquad C_k \in [0, 1]$$

Higher values of C_k indicate alternatives that are closer to the ideal solution and farther from the anti-ideal, thus ranking them as more desirable. [51].

2.3 Response Surface Methodology

Response Surface Methodology (RSM) is a collection of mathematical and statistical techniques designed to support the development, improvement, and optimization of complex processes. Within the context of ship concept design, RSM is particularly valuable for predicting the outcomes of intricate design processes without resorting to costly and time-consuming analyses. This is achieved by leveraging past knowledge or newly generated databases constructed

with a minimal number of records. Such an approach is especially relevant when investigating innovative ship concepts that significantly deviate from conventional designs. RSM is typically applied in scenarios where multiple input variables influence the quality or magnitude of a response. These input variables are referred to as *independent variables*, while the resulting performance measures are termed *dependent variables*. The primary objective of RSM is to employ statistical and empirical modeling techniques to establish an approximate functional relationship between the independent and dependent variables.
In the following subsections, the general nomenclature will be introduced, followed by the theoretical background for estimating regression coefficients. Furthermore, the strategy based on Design of Experiments (DoE) will be presented, illustrating how it can be employed to construct an effective database for regression purposes when historical data are unavailable.

2.3.1 Linear Regressions

The basis of this method is the search for a function f that links n independent variables to a response y:

$$y = f(x_1, x_2, ..., x_n) + \epsilon \tag{2.1}$$

where ϵ includes all measurement errors, errors due to interference among variables, and a statistical error; $\mathbf{x} = (x_1, x_2, ..., x_n)$ are the independent variables and f the unknown function.
The set of all admissible combinations of $\mathbf{x}$ within their prescribed ranges is known as the Experimental Region, denoted by $S(\mathbf{x})$. This region forms a subset of the n-dimensional predictor space, and its geometry is determined by the intervals specified for each independent variable.
If this function is approximated by a polynomial of degree d, it becomes:

$$y = p(\mathbf{x}, \beta) + \epsilon \tag{2.2}$$

where β is the vector of the polynomial coefficients and ϵ an approximation error of f. In general, the response y may be related to the k independent variables by a first-degree multiple linear regression:

$$y = \beta_0 + \sum_{i=1}^{k} \beta_i x_i + \epsilon \tag{2.3}$$

2.3.2 Least Squares Method

The LSM is employed to estimate the coefficients of a multiple linear regression model. TO apply this method, it is assumed that the error term, denoted by ϵ, has an expected value of zero and a variance equal to σ^2. Furthermore, for the LSM to be solvable, the condition $l > m$ must

hold. Under these assumptions, Equation 2.3 can be expressed in matrix form as follows:

$$\mathbf{y} = \mathbf{X}\boldsymbol{\beta} + \boldsymbol{\epsilon} \tag{2.4}$$

Where, $\mathbf{y}$ denotes the $l \times 1$ vector of observations, $\mathbf{X}$ is an $l \times n+1$ design matrix that includes the considered independent variables and a column of ones to represent the intercept, $\boldsymbol{\beta}$ is the $n+1 \times 1$ vector of regression coefficients, and $\boldsymbol{\epsilon}$ is the $l \times 1$ vector of random errors:

$$\mathbf{y} = \begin{bmatrix} y_1 \\ y_2 \\ \vdots \\ y_l \end{bmatrix}, \mathbf{X} = \begin{bmatrix} 1 & x_{11} & x_{12} & \dots & x_{1n} \\ 1 & x_{21} & x_{22} & \dots & x_{2n} \\ \vdots & \vdots & \vdots & \vdots & \vdots \\ 1 & x_{l1} & x_{l2} & \dots & x_{ln} \end{bmatrix}, \boldsymbol{\beta} = \begin{bmatrix} \beta_0 \\ \beta_1 \\ \vdots \\ \beta_k \end{bmatrix}, \boldsymbol{\epsilon} = \begin{bmatrix} \epsilon_1 \\ \epsilon_2 \\ \vdots \\ \epsilon_l \end{bmatrix}$$

The LSM determines the coefficients $\boldsymbol{\beta}$ such that the sum of squared errors is minimized. Formally stated, the problem is expressed as:

$$L = \sum_{i=1}^{n} \epsilon_i^2 = \boldsymbol{\epsilon}'\boldsymbol{\epsilon} = (\mathbf{y} - \mathbf{X}\boldsymbol{\beta})'(\mathbf{y} - \mathbf{X}\boldsymbol{\beta}) = \mathbf{y}'\mathbf{y} - 2\boldsymbol{\beta}'\mathbf{X}'\mathbf{y} + \boldsymbol{\beta}'\mathbf{X}'\mathbf{X}\boldsymbol{\beta}$$

The coefficients $\boldsymbol{\beta}$ can be determined as [52]:

$$\boldsymbol{b} = (\mathbf{X}'\mathbf{X})^{-1}\mathbf{X}'\mathbf{y} \tag{2.5}$$

Hence the predicted values $\hat{\boldsymbol{y}}$ obtained applying the regression equation are computed as:

$$\hat{\boldsymbol{y}} = \mathbf{X}\boldsymbol{b} \tag{2.6}$$

2.3.3 Statistical Indices

It is essential to ensure that the model provides an adequate approximation of the real phenomenon and to verify that none of the assumptions underlying the LSM are violated, while also confirming that the model achieves a satisfactory level of accuracy [53]. To this end, several indices can be used to check the goodness of fit and perform proper selection of the indipendent variables of the model.

The difference between the observed value y_k and its predicted counterpart $\hat{y}_k$ is referred to as the residual. Collectively, these residuals form an $l \times 1$ vector, denoted as

$$\boldsymbol{e} = \boldsymbol{y} - \hat{\boldsymbol{y}} \tag{2.7}$$

The sum of squares of the residuals [52]:

$$SS_E = \sum_{k=1}^{l} (y_k - \hat{y_k})^2 = \sum_{k=1}^{l} e_k^2 = \boldsymbol{e}'\boldsymbol{e} \tag{2.8}$$

Recalling equation 2.7 and substituting into it one obtains:

$$SS_E = (\mathbf{y} - \mathbf{X}\boldsymbol{b})'(\mathbf{y} - \mathbf{X}\boldsymbol{b}) = \mathbf{y}'\mathbf{y} - 2\boldsymbol{b}'\mathbf{X}'\mathbf{y} + \boldsymbol{b}'\mathbf{X}'\mathbf{X}\boldsymbol{b} \xrightarrow{\mathbf{X}'\mathbf{X}\boldsymbol{b}=\mathbf{X}'\mathbf{y}} SS_E = \mathbf{y}'\mathbf{y} - \boldsymbol{b}'\mathbf{X}'\mathbf{y}$$

Considering l observations, n coefficients of the multiple regression and that the variance is linked to the expected value of SS_E one can consider:

$$\hat{\sigma}^2 = \frac{SS_E}{l - n} \tag{2.9}$$

In the subsequent phase after regressions it is useful to consider the mean square error (MS_E):

$$MS_E = \frac{1}{(l - 1 - n)} SS_E = \frac{1}{(l - 1 - n)} \sum_{k=1}^{l} (y_k - \hat{y_k})^2 \tag{2.10}$$

From SS_E other statistical indices can be computed useful to identify the measure of the relationship between the variability of the data and the correctness of the statistical model used: the coefficient of determination R^2 and the adjusted one R^2_{adj}, the first used for simple linear regressions and the second, in the case of multiple linear regressions, makes the value independent of the number of independent variables. In general adding an independent variable increases the value of R^2 even if the variable is not significant.

$$R^2 = 1 - \frac{SS_E}{SS_{tot}} \tag{2.11}$$

where with SS_{tot} one defines the sum of squares of deviations from the mean value:

$$SS_{tot} = \sum_{k=1}^{l} (y_k - \overline{y})^2$$

$$R^2_{adj} = 1 - \frac{\frac{SS_E}{l-n}}{\frac{SS_{tot}}{l-1}} = 1 - \frac{l-1}{l-n}(1 - R^2) \tag{2.12}$$

2.3.4 Coefficient's p-value

In the context of regression analysis, the *p-value* associated with each estimated coefficient quantifies the probability of observing a test statistic at least as extreme as the one computed,

assuming that the null hypothesis (typically that the corresponding coefficient is equal to zero) is true. A small p-value indicates that the observed effect is unlikely to be due to random sampling variation alone, suggesting that the variable has a statistically significant impact on the response.
To assess significance, a threshold value α (commonly set at 0.05) is used to define the level of statistical significance. If $p < \alpha$, the null hypothesis is rejected, and the variable is considered statistically significant. Common significance levels include:

- $p < 0.05$: statistically significant;
- $p < 0.01$: highly significant;
- $p < 0.001$: very highly significant.

2.3.5 Stepwise Regression Method

Since evaluating all possible regression models can be computationally expensive, several procedures have been developed to identify a limited set of candidate models by sequentially adding or removing independent variables. According to Carley [53] they can be classified into three main categories: forward selection, backward elimination and stepwise regression, the latter being a hybrid technique that combines the first two.

2.3.5.1 Forward Selection

The procedure starts by assuming that the model is defined by a function in which only the intercept appears. The key point of the process is to insert the independent variables one at a time. The first variable x_i is the one that most influences the response y. The independent variable is included if its p-value does not exceed an initial significance level P_{in}. Thereafter a second independent variable is inserted which will enter only if it influences the response and increases the chosen statistical parameter. The process proceeds with all independent variables and only those significant for the response and having a value less than P_{in} will be inserted. Combined variables are also considered and the process ends when all possible combinations among the available independent variables are exhausted.

2.3.5.2 Backward Elimination

Backward elimination seeks to find a good model by working in the opposite direction, starting with a model that includes all candidate independent variables to define the response. The p-value is calculated for each variable and the variable having the highest p-value is removed if it

is greater than a chosen P_{out}. The the coefficients and the related p-values are recalculated and the procedure continues until the regression is improved or all candidate variables have been removed.

2.3.5.3 Stepwise Regression

The two procedures described produce a certain number of possible combinations. Stepwise regression modifies forward selection by re-evaluating the significant characteristics at each step. An independent variable is entered if it is significant, i.e. has a p-value below the threshold P_{in}, but it may be removed at later stages if its level of significance is superseded by other variables. Consequently the variable becomes redundant in the regression having a p-value > P_{out} and is discarded. The procedure continues until all possible combinations are exhausted. It requires both threshold values P_{in} and P_{out} where generally $P_{in} > P_{out}$.

2.4 Design of Experiments

RSM depends directly on the distribution of input data [54]. When sufficient historical data are not available, an engineered dataset can be generated, often by simulations.To this purpose, Design of Experiments (DoE) might be used in order to keep the number of simulations/designs required to fit the model as low as possible preserving the quality of the regression [55].
In ship design, Design of Experiments is a methodological framework that allows engineers to manage the complexity arising from the simultaneous influence of many design variables, such as hull geometry ratio. Unlike traditional spiral derign approach, DoE structures the set of simulations or experiments so that both individual effects and interactions between parameters can be identified. This is particularly important in ship design applications, where interactions often dominate overall performance. DoE makes it possible to explore large design spaces with a relatively small number of high-fidelity simulations, reducing computational effort while enabling the construction of response surfaces for sensitivity analysis and multi-attribute decision making techniques.
At the same time, the reliability of DoE strongly depends on the correct definition of the design space and on the quality of the underlying physical and numerical models. Poorly chosen parameter ranges or inaccurate models can lead to misleading conclusions. Moreover, because DoE delivers statistical relationships rather than physical laws, it cannot replace engineering judgment: mathematically optimal solutions must always be checked against structural, regulatory, operational and manufacturability constraints. In this sense, DoE is a powerful decision-support tool, but not an automatic design solution. There are various types of CCDs; Figure 2.2 shows an example.

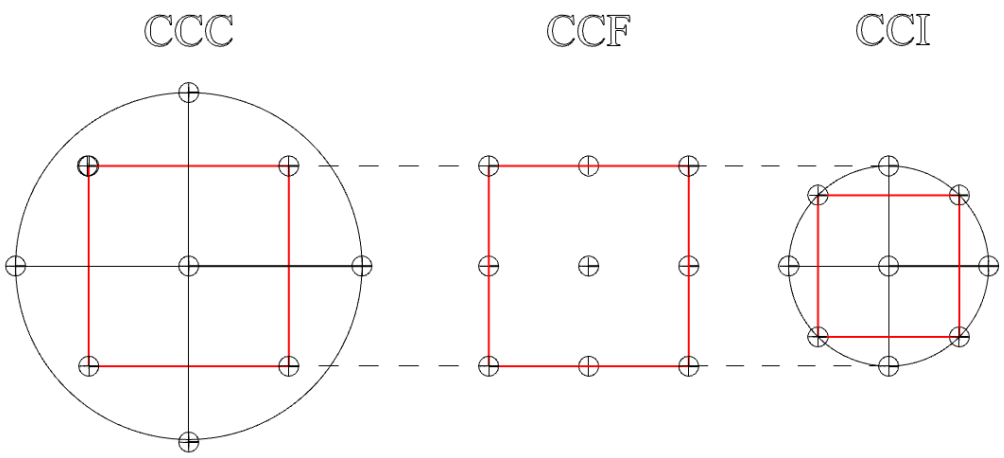

Figure 2.2: Examples of CCD designs

The reasons for choosing these models are linked both to the importance of rotatability of the design and to the constraints imposed on the ranges in which the variables may lie. They allow the experimenter to build an effective second-order model that explores the experimental region symmetrically, preventing zones where the lack of information negatively affects the model.

2.4.1 CCC

CCC is the most common method; it identifies a design space formed by a cube circumscribed by a sphere. The optimal points are those located at the vertices of the cube and at the cardinal points of the sphere. The design matrix for the present case is reported below.

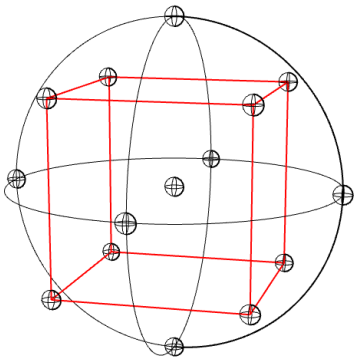

$$\boldsymbol{D} = \begin{bmatrix} 1 & 1 & 1 \\ 1 & 1 & -1 \\ 1 & -1 & 1 \\ 1 & -1 & -1 \\ -1 & 1 & 1 \\ -1 & 1 & -1 \\ -1 & -1 & 1 \\ -1 & -1 & -1 \\ 1.732 & 0 & 0 \\ -1.732 & 0 & 0 \\ 0 & 1.732 & 0 \\ 0 & -1.732 & 0 \\ 0 & 0 & 1.732 \\ 0 & 0 & -1.732 \end{bmatrix}$$

2.4.2 CCF

CCF method in which the axial points are placed one unit away from the centre. The design space is a cube with characteristic points at the vertices and at the midpoints of the faces. Non-rotatable design.

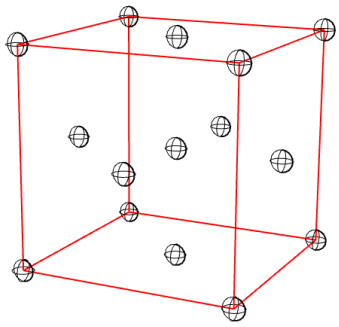

$$\boldsymbol{D} = \begin{bmatrix} 1 & 1 & 1 \\ 1 & 1 & -1 \\ 1 & -1 & 1 \\ 1 & -1 & -1 \\ -1 & 1 & 1 \\ -1 & 1 & -1 \\ -1 & -1 & 1 \\ -1 & -1 & -1 \\ 1 & 0 & 0 \\ -1 & 0 & 0 \\ 0 & 1 & 0 \\ 0 & -1 & 0 \\ 0 & 0 & 1 \\ 0 & 0 & -1 \end{bmatrix}$$

2.4.3 CCI

CCI method in which the design space is a sphere in which a cube is inscribed. It is the smallest design space among those presented.

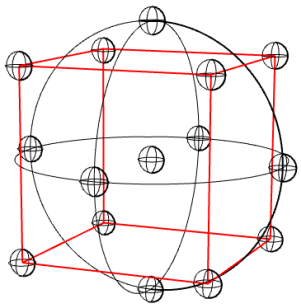

$$\boldsymbol{D} = \begin{bmatrix} \frac{\sqrt{2}}{2} & \frac{\sqrt{2}}{2} & \frac{\sqrt{2}}{2} \\ \frac{\sqrt{2}}{2} & \frac{\sqrt{2}}{2} & -\frac{\sqrt{2}}{2} \\ \frac{\sqrt{2}}{2} & -\frac{\sqrt{2}}{2} & \frac{\sqrt{2}}{2} \\ \frac{\sqrt{2}}{2} & -\frac{\sqrt{2}}{2} & -\frac{\sqrt{2}}{2} \\ -\frac{\sqrt{2}}{2} & \frac{\sqrt{2}}{2} & \frac{\sqrt{2}}{2} \\ -\frac{\sqrt{2}}{2} & \frac{\sqrt{2}}{2} & -\frac{\sqrt{2}}{2} \\ -\frac{\sqrt{2}}{2} & -\frac{\sqrt{2}}{2} & \frac{\sqrt{2}}{2} \\ -\frac{\sqrt{2}}{2} & -\frac{\sqrt{2}}{2} & -\frac{\sqrt{2}}{2} \\ 1 & 0 & 0 \\ -1 & 0 & 0 \\ 0 & 1 & 0 \\ 0 & -1 & 0 \\ 0 & 0 & 1 \\ 0 & 0 & -1 \end{bmatrix}$$

Chapter 3

Methodology

The ship design process is a complex and inherently multidisciplinary activity, requiring careful evaluation of multiple technical, operational, and economic aspects.
This chapter presents a systematic approach to the concept design of a luxury cruise ship. The methodology involves the generation, modelling, and selection of the best feasible solution from a set of design alternatives, ensuring strict adherence to rigorous geometric, propulsive, electrical, operational, and stability constraints.
The approach adopted in this work represents an innovation compared to the traditional spiral iterative design used in naval engineering and MADM. The goal is to obtain the maximum amount of information as early as possible in the initial phases of the design process.
To this end, a MDM of the ship under study was developed, conceived to support a multi-attribute decision-making criterion in the selection of design alternatives. A MDM can be defined as a mathematical abstraction of reality, which uses equations and analytical structures to replicate and describe the real-world behaviour of a subject of study. In other words, a mathematical model provides a simplified representation of a complex system, allowing its behaviour to be analysed and predicted without resorting to direct simulations or experiments.
Mathematical models are typically "trained" using databases that incorporate past knowledge and experience. This approach allows for the development of reliable predictive models and significantly reduces the need for complex and costly computational simulations, both in terms of time and economics.
However, this methodology is not always feasible. In cases of completely innovative projects, past experience is insufficient to achieve reliable predictions. In such circumstances, it becomes essential to adopt an alternative approach for the construction of the mathematical model. In the context of designing a new-concept luxury cruise ship, and given the absence of a reference hull and the scarcity of information available in the literature, the choice was made to adopt parametric 3D modelling.
The crucial innovative element is represented by the introduction, as early as the initial design

phases, of a complete 3D model of the entire luxury cruise ship, which integrates essential data related to public spaces, passenger estimates, and available volumes on board related to model variables such as the number of passengers, type of propulsion, and whether there are external areas on passenger and public decks.

The flowchart of the methodology adopted is presented in Figure 3.1 and is a topic detailed in the following chapter. Once the base ship concept is established, the geometric design variables are identified. Utilising a database of existing luxury cruise ships, the variability ranges are defined, enabling the subsequent generation of n projects using Monte Carlo sampling. The outputs provided by the parametric model include all the principal geometric quantities of the ship. The approach focused on the parametric definition of not only the hull forms but also the entire superstructure, allowing for a detailed, deck-by-deck control of the geometries and the onboard arrangement of passenger cabins, public, and technical spaces. The parameterisation provides specific results on the areas and geometric centroids of internal and external spaces dedicated to passengers, crew, and technical areas above the bulkhead deck. For the zones below this deck, the volumes of the room compartments are made available.

noindent These detailed geometric outputs from the parametric ship model serve as input for the core mathematical design model developed for luxury cruise ships, which implements regression formulae created from a database of existing ships. The use of this database enables the creation of ad hoc metamodels for preliminary estimates of weight breakdown, electrical balance, and stability. This information is crucial for defining the design constraints necessary to immediately discard ships that do not meet rule requirements or shipowner specifications.

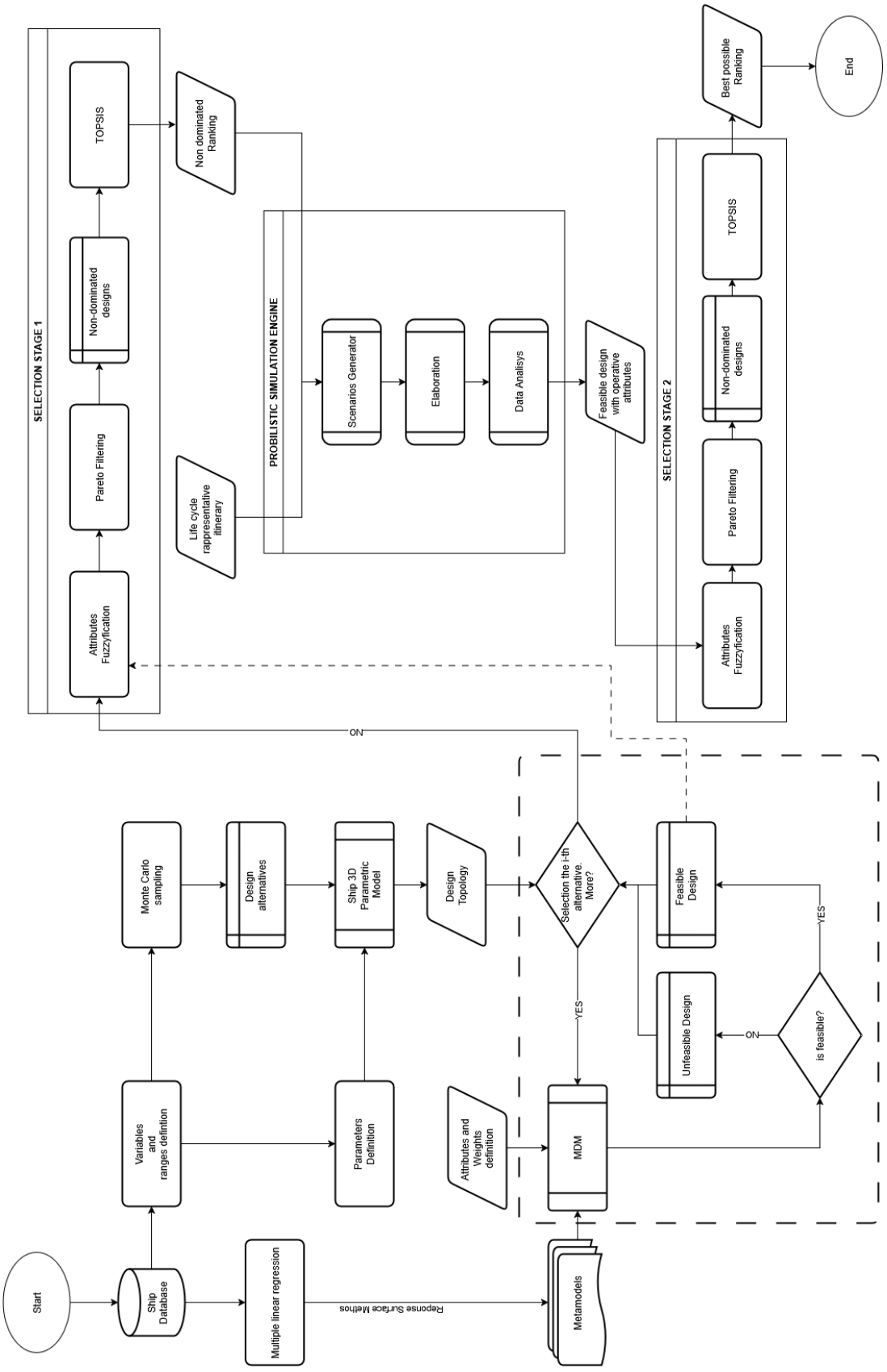

Figure 3.1: Methodology flowchart

Subsequently, the Alternatives Matrix is identified, composed of n rows identifying the design alternatives and m coloumns identifying the design variables and parameters. The attributes are derived from this matrix by applying a fuzzification process, allowing operation within the [0,1] interval. A further filter is then applied, eliminating all alternatives dominated according to the definition of Pareto. The resulting product is the Decision Matrix, defined in the Y-space (the attribute space), which contains all the non-dominated ships populating the Pareto front. Among these alternatives, the best possible solution is selected through a classification method. The ranking method used is TOPSIS , which classifies the design alternatives in the Decision Matrix by assessing their distance from the ideal solution (the highest value for every attribute) and/or the anti-ideal solution (the lowest value for every attribute). This enables the creation of a preliminary ranking (1^{st} selection stage) of all solutions on the Pareto front, facilitating the decision on the provisional best design.
Usually the final phase would involve returning immediately to the X-space, the space where alternatives are defined by the design variables. This step, known as the design phase, allows tracing back from the attribute space to the variable space, identifying the variable values corresponding to the solutions with the best performance. In the proposed methodology, instead a single project is not immediately selected; instead, a subset of k best non-dominated alternatives is chosen to undergo a operative simulation study and the 2^{nd} selection stage. After identifying typical luxury cruise ship itineraries, a probabilistic software is used to calculate average values of environmental emissions and fuel consumption in a realistic operative environment. By defining these new attributes for selecting the best design alternatives, after updated weights definition, attributes fuzzification and Pareto filtering, the TOPSIS method is reapplied to the k alternatives to select the final best possible ship. The simulation code is structured into three main steps. Scenario Generation: selected itineraries are combined with environmental data on wind, waves, currents, and sea/air physical properties to construct a set of deterministic scenarios; Elaboration: each deterministic scenario is simulated to evaluate key outputs such as fuel consumption and emissions; Data Analysis: outputs from all scenarios are aggregated to build empirical probability distributions, which are then used to extract average values.

3.1 3D Parametric Design

The methodology followed for the creation of a parametric luxury cruise ship model is illustrated below. The starting point was a reference taken from a real-world existing cruise ship. A preliminary analysis of the general arrangement plans allowed for the study of a possible configuration of the onboard spaces, with a particular focus on the ship's longitudinal profile section. The corresponding lines plan were subsequently used to study the ships' cross-sections. The modelling process was logically divided into two main parts: the creation of the ship's un-

derwater hull and, subsequently, the focus on the superstructure decks. The bulkhead deck was utilised as the key geometric reference point, making it possible to identify clearly in the design outputs both the volumes below it and the areas designated for accommodation or public spaces above it.

3.1.1 Parametric Hull Form

This subsection addresses the parametric modelling of the hull. NURBS curves were utilised for its creation. The hull study required the careful definition of the control points' positions in the following key geometric elements:

- The transom section;
- The stern profile;
- The midship section;
- The bulb cross-section;
- The longitudinal profile of the stem.

The transom section has been modelled using ten main control points, allowing the reconstruction of the most common geometries, such as the classical U-shaped form, the V-shaped form, or the U-shaped configuration featuring semi-tunnels. The high number of points has been introduced specifically to provide the flexibility required to explore different geometric configurations.

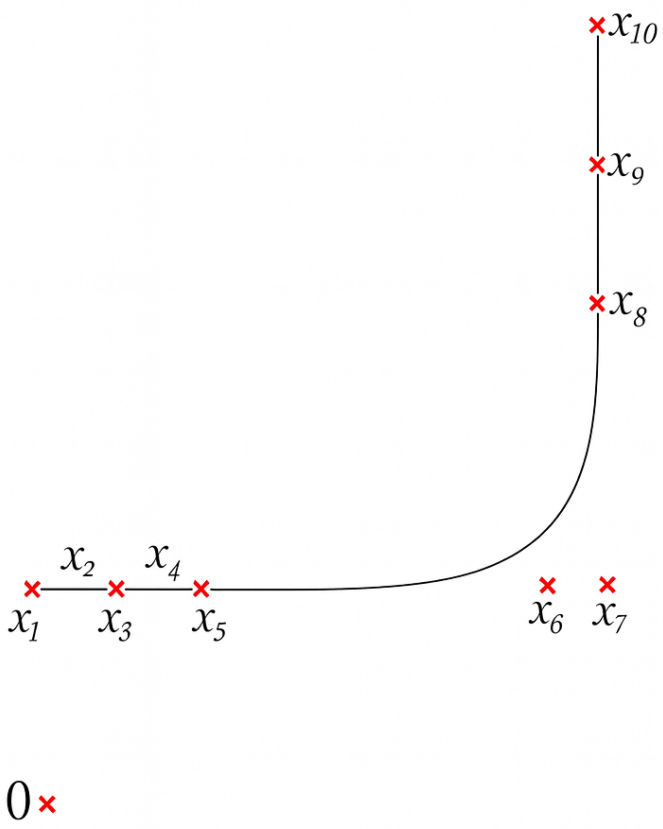

Figure 3.2: Transom modellation

Figure 3.2 shows an example of the transverse semi-section, illustrating the arrangement of the control points and the Non Uniform B-spline curve interpolating them. The key points are:

- The point x_1, located on the centerline, which receives as input the variable associated with the transom height.
- The point x_{10}, positioned on the ship's side at the maximum Z coordinate.
- The point x_6,x_8 used to control the radius of the transom knuckle.

The alignment of the points x_8, x_9, and x_{10} ensures the planarity of the ship's side. Conversely, the displacement of the points x_2, x_3, x_4, x_5, and x_6 allows the creation of either a flat transom bottom, when they are aligned, or a curved bottom when a semi-tunnel configuration is required.
Similarly to the transom, the midship section was also modelled. This section was used as a key reference for the creation of a potential parallel body.
The logic employed for generating the parallel body involves translating the midship section

both aft and forward, using a different translation length which is introduced as a design variable. For a ship without a parallel body, the two translated midship sections are designed to collapse (or coincide) onto the original midship section.

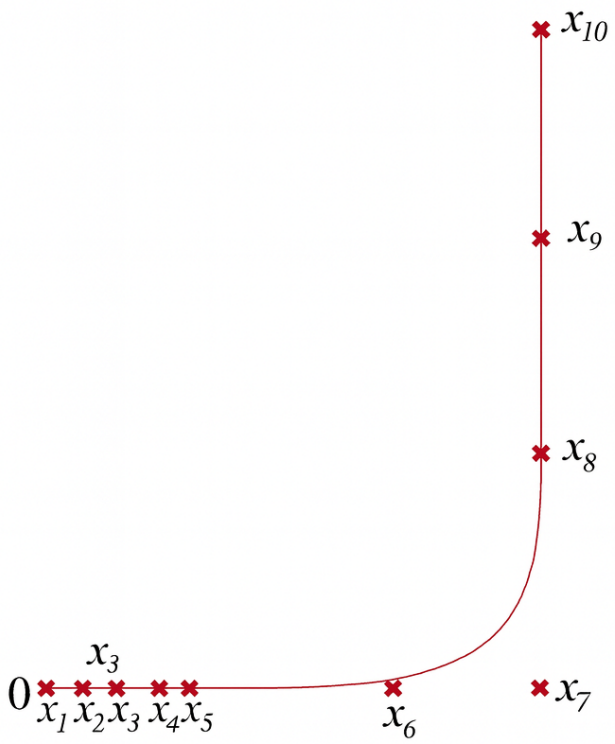

Figure 3.3: Midship section

The cross section at the forward perpendicular is consistent with the presence or absence of the bulbous bow. The displacement of the relevant control points allows for the creation of typical bulb profiles found in the literature. Specifically, this section provides crucial indications regarding the size and thickness of the bulb itself.
Since the modelling is entirely parametric, the arrangement of the points also allows for the modelling of bows (raked), or straight bows, ensuring maximum design versatility.

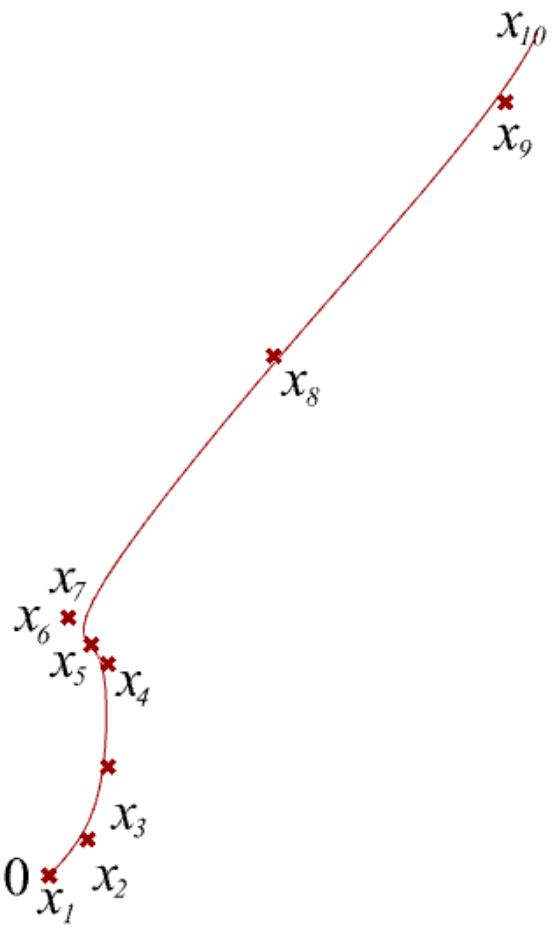

Figure 3.4: Forward perpendicular section

The longitudinal profile of the stem in Figure 3.5 was modelled to offer considerable geometric flexibility. The arrangement of the control points allows for the easy modelling of various configurations, including a bulbous bow, a classic non-bulbous bow, or, alternatively, a straight bow, which is achieved when the points are aligned.

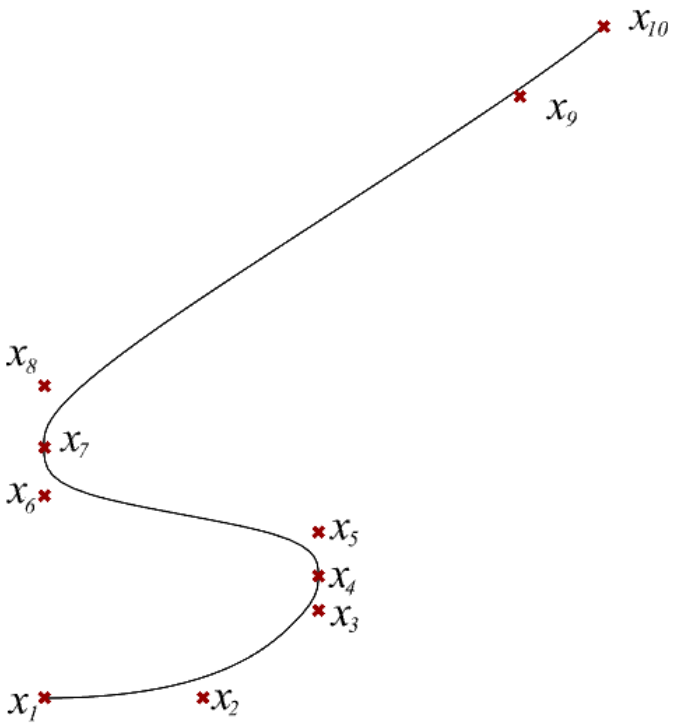

Figure 3.5: Bow profile modellation

The final reference line used for hull generation is the stern profile. A smaller number of control points were utilised for its modelling in order to effectively simulate the two typical configurations found in luxury cruise ships.The hull of a luxury cruise ship is typically twin-screw (meaning it is designed to accommodate two propellers), which necessitated the parameterisation and creation of the skeg.

The stern curve changes based on the presence or absence of the Propulsion Orientable Device (POD). As highlighted in Figure 3.6 and Figure 3.7, the substantial difference lies in achieving a flat bottom at the transom, between points x_1 and x_2 to allow for the accommodation of machinery designated for the POD's ventilation and operation. The modelling was designed to ensure a double curvature.

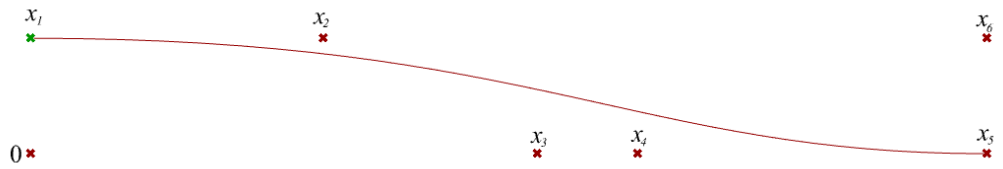

Figure 3.6: Stern profile for traditional propulsion configuration

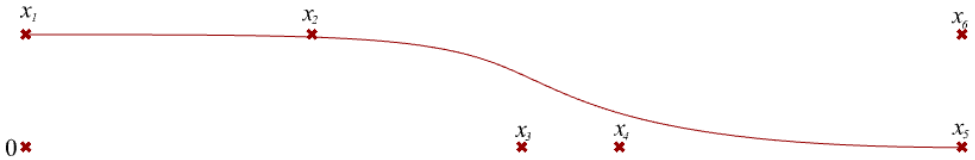

Figure 3.7: Stern profile for POD configuration

The variable used to modify the stern profile is the position of point x_5 which is placed tangent to the keel line. The longitudinal position of this point was chosen as the variable to simulate ships with either traditional propulsion or POD propulsion, making the stern respectively fuller or slender.

Using the previously proposed curves as references, it was possible to generate a complete parametric hull as a function of the Length overall (L_{OA}), the $B/2$ and the longitudinal position of the midship section, thus allowing for the simulation of the presence or absence of a parallel body. An example of this can be seen in Figure 3.8.

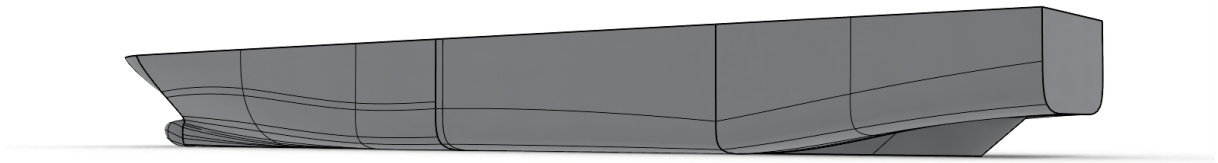

Figure 3.8: Hull form

The distinctive feature of this modelling approach is strictly related to the use of NURBS curves, which can be joined to create a single, continuous surface.The final hull is modelled as a continuous surface, where adjustments to the section control points enable the precise introduction or suppression of double curvature. Should localised irregularities occur, corrective measures are applied selectively to the specific points involved, ensuring the overall geometry remains intact.

3.1.2 Parametric modelling of Luxury Cruise Ship

The internal space of the cruise ship was divided into two main methodologies: area modelling was applied to the decks located above the bulkhead deck, while volume modelling was used for the decks below the bulkhead deck.
This modelling was based on a reference luxury cruise ship featuring a techincal space in the centerline, herinafter refferred as central spine. Given the hull geometry, the vertical position of the double bottom was first determined. According to the (Safety of Life at Sea) (SOLAS) regulations, this is placed at a maximum height of B/20 (where Ship beam (B)). Above the double bottom, the deck is allocated to engine rooms, auxiliary spaces, service tanks, and the propulsion rooms (either two Propulsion Electric Motor (PEM) rooms or two POD rooms).
The third deck above the Base Line is typically designated as the bulkhead deck, whereas the second deck (the first deck below the bulkhead deck) is usually partial due to the presence of main machinery rooms and tanks. This deck accommodates crew quarters and small machinery. The bulkhead deck is primarily allocated for crew accommodations, crew common areas, provision storage, and embarkation zones. It also features a service corridor running along the

central spine of the ship, connecting the stern and bow and passing through the engine casing, as illustrated in Figure 3.9.

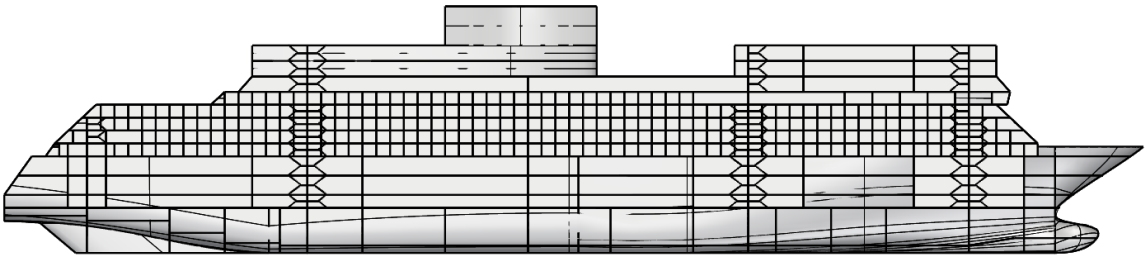

Figure 3.9: Luxury Ship longitudinal profile

For both crew and passenger decks, a fixed deck height of 2800 mm was assumed, as indicated from regulations. The deck immediately above the bulkhead deck is designated for public areas. This typically includes the atrium for passenger reception, restaurants, and theaters. The deck height assumed for the public areas was made parametric, ranging between 3500 mm and 4200 mm, consistent with regulatory standards and the functional designation of the areas on that deck. Moving vertically, the embarkation deck is positioned, where lifeboats are stowed and, consequently, large open public spaces are designated as safe areas for receiving passengers during an emergency. These areas must meet all necessary requirements for the ship to comply with the Safe Return to Port (SRtP) regulations. Above this second public deck begins the arrangement of decks dedicated exclusively to passengers, followed by the wheelhouse deck, the external deck, and the deckhouses.

The input variables for the parametric modelling of a luxury cruise ship include the number of passengers, number of crew, cabin dimensions, and the previously modelled hull. The design choice regarding the cabins involved separating the cabin area itself from the balcony, to allow for greater freedom in dimension variation. For the modelling process, the vertical position of the bulkhead deck and the longitudinal position of the engine casing were fixed as parameters.

The modelling began by defining a frame spacing interval. It was assumed that the width of the cabins covers four ordinary frames; once the overall length was defined, an initial longitudinal reference was determined for the positioning of bulkheads, Main Fire Zone (MFZ), and other ship structures. The first MFZ was positioned based on the location of the funnel, separating the two engine rooms (forward and aft). By adhering to regulatory constraints regarding the maximum distance between MVZs (maximun 48 m), the remaining zones were positioned.

Given the forward forms, the collision bulkhead was also defined at the bow according to the International Load Line Convention (ILLC). The positioning of the MFZ was carried out by placing the bulkheads at the nearest web frame, ensuring the length was less than 48 meters.

As mentioned, the first public deck was arranged at a height of 2800 mm above the bulkhead deck. The deck height of this second public deck was determined by considering the size of the lifeboats to allow lifeboat embarkation from the next deck.
The number of lifeboats was determined as a function of the total persons on board, in accordance with Life-Saving Appliances (LSA) requirements. SOLAS regulations require that, in the event of an emergency, sufficient life-saving appliances (lifeboats, rescue boats, and other MES) shall be provided to accommodate all persons onboard for each side.
Applying SOLAS and using the geometric and capacity references of the main lifeboats, the calculation for the number of life-saving appliances was performed. Considering a maximum capacity of 150 people for lifeboats and 35 for rescue boats, the methodology specified covering 75% of the total LSA with lifeboats and the remaining 25% with MES for each side.
The lifeboat arrangement was parametrically defined, offering either a single continuous row along each side or two separate clusters. The latter configuration was introduced to fit a midship public area adjacent to the ship's side, intended for functions such as a sea-view restaurant.
The arrangement of life-saving appliances on the embarkation deck was aligned with MFZ bulkhead locations to maximize evacuation efficiency during emergency conditions.
The width of the deck recess, dictated by the positioning of survival craft, constitutes a key determinant for the transverse placement of the lateral pillar lines ending on the lateral girders. The central pillar line and girders are located at the breadth of the central spine.
The deck modelling was conceived to include a possible external area for example dedicated to the passenger pool zone. The choice of the deck recess relative to the stern was made parametric, ensuring that the supporting structures always begin at the position of the first available ordinary frame.
After finalising the embarkation deck, the parameterisation of the first passenger deck was addressed. For this deck too, the option to include an external area was provided, both aft, for passengers and forward for crew or mooring spaces. The structure was parameterised to determine whether it should extend fully to the side shell or include an external corridor along the perimeter. Based on the total passenger capacity and the specific dimensions of the balcony cabins (assuming an average occupancy of two persons per unit), the maximum cabin density for the initial deck was determined. By comparing the total cabin requirement against this initial layout, the minimum number of additional decks was dynamically calculated. To maintain a standard cruise ship profile, deck lengths were progressively reduced on upper levels. This calculation aims for the minimum necessary deck count, as the methodology integrates the bridge deck to accommodate any remaining cabins. Furthermore, the bridge deck configuration is flexible, allowing for either a set-back lateral walkway or a full-length extension to the stern. The logic used to model this deck was to allocate it to officer cabins and any residual passenger cabins. If sufficient area was available, the option was included to place larger suites (considering

double the standard cabin width) instead of the base input cabins.
Finally, the external deck was modelled, and the upper superstructures were realised, using the length of a potential pool on the highest deck, typical of these ships, as an input. The deckhouses are designed to occupy a portion of the ship's total width rather than extending fully to the sides, ensuring a functional and typical cruise ship layout.
For the decks located below the bulkhead deck, the modelling began by positioning a deck allocated for crew accommodation, and by defining the double bottom, which is essential for placing the void or water tanks. Consequently, the necessary space for the engine room and all auxiliary rooms was derived.
Once the pillar lines position is assessed according to central spine and lifeboats, it was possible to proceed with a preliminary general subdivision. Knowing the position of the MFZ, and understanding that the engine room requires two pillars lines due to the dimensions of the diesel generators, the preliminary positioning of the watertight bulkheads was carried out.
Based on MFZ position, the number of compartments was set at 15. The underwater hull was divided into compartments following the hull forms; specifically, the two engine rooms were positioned astride the casing bulkhead.
With the subdivision established, the actual double bottom modelling was finalized, consistently following the shapes of the skeg and the rooms.
Figure 3.10 reports an example of the parametric 3D modelling of the rooms and the internal spaces described.

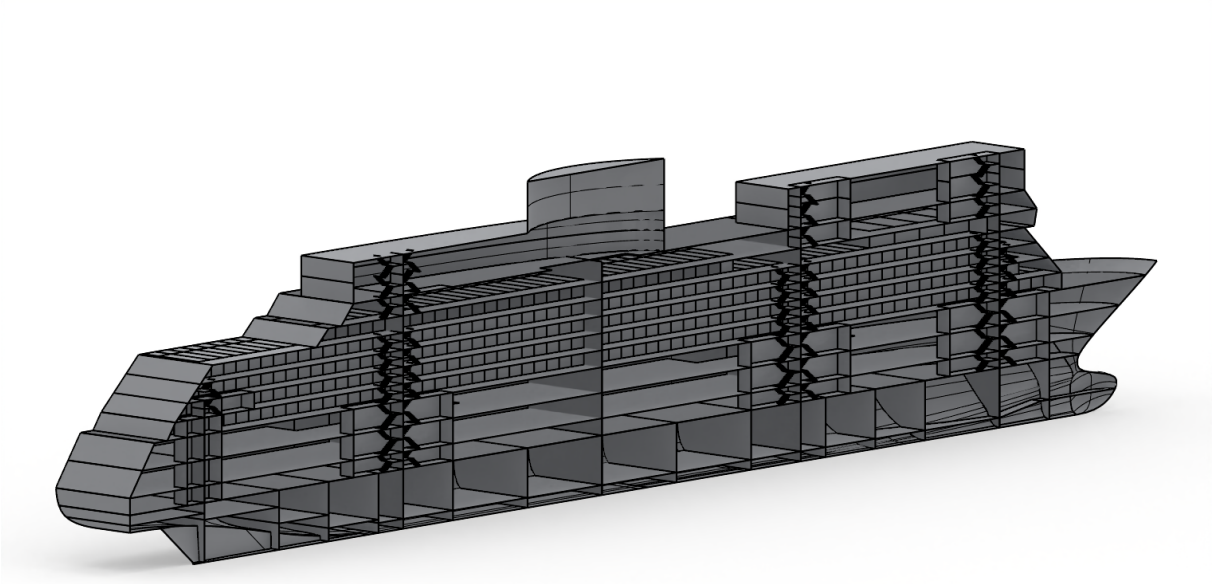

Figure 3.10: 3D Parametric Luxury cruise ship

3.1.3 3D Parametric output

Once the design draught is established, the main geometric and hydrostatic parameters of the hull can be derived. These data are essential in the preliminary design phases for conducting stability studies, weight exponent evaluations, and volume space analysis.
Consequently, specific outputs have been selected and extracted from the parametric model, which are indispensable for supporting both the MDM and the subsequent applications of the probabilistic simulation.
The most of relevant of these are summarised below:

- Main Geometric and Hydrostatic Parameters: these variables define the hull form and its stability and buoyancy properties:
- Dimensions: GT,L_{OA}, Length bewtween perpendiculars (L_{BP}), Waterline length (L_{WL}), B.
- Coefficients & Stability: Displacement, hull coefficients (Block coefficient (C_B), Midship coefficient (C_X), Waterplane area coefficient (C_{WP}), Vertical prismatic coeffcient (C_{VP})), Longitudinal position of centre of Buoyancy (LCB), Longitudinal position of centre of floating (LCF).
- Specific Areas: Wetted Hull Surface, Transom Area, Windage areas, Bulb area.
- Volumes and room Variables related to the internal subdivision of the hull below the bulkhead deck:
  - Rooms: Room volumes, Volume centroids number and position of room, room type (Ballast room, Thruster room, Tank room, Engine room, PEM room, auxilieries room, techical room).
  - Position and number of MFZ
- Superstructure and Passenger and Crew Areas Geometric data related to the upper decks and space distribution:
  - Deck Dimensions: Deck heights and breadths, Central spine and funnel dimensions.
  - Areas and Centroids:
    * Passenger Cabins.
    * Internal Public Spaces.
    * External Public Spaces.
    * Crew Areas.

* Wheelhouse area
* Deckhouse space
* Casings and Trunks and techical areas.

3.2 Luxury ship Matematical Model

Once the ship topology is defined, a MDM for luxury cruise ships is defined. It is crucial to emphasise that the methodology developed here is exclusively applicable to small luxury cruise ships with a diesel-electric propulsion system, where a central generation plant powers both hotel loads and propulsion (whether traditional or POD, as long as it is electric). The model's validity is also limited to cruise ships featuring a techical space at central line; other configurations would require modifications to the initial parametric ship model.
The mathematical model, as shown in the flowchart in Figures 3.11 and 3.12, has been defined according multiple sources: on one hand, by the 3D parametric model of the luxury cruise ship, and on the other, by an existing ship database crucial for identifying specific regression formulae.
The operating logic of the mathematical model involves identifying the design variables, which are dependent on the previously performed hull parameterisation. Determining these design variables and their respective variability range is essential for generating n projects within the design space, utilising techniques such as the Monte Carlo sampling.
The mathematical model was developed in MATLAB. It includes the analysis of several fundamental phases of ship design. In the specific case of cruise ships, the topology of the internal spaces is critical for a future economic estimation of the ship.
The model performs a preliminary estimation of propulsive resistance using the Holtrop-Mennen method follow by propeller selection. Based on the determination of a design speed (whether defined by the owner or not), a choice between PEM or POD can be made, according to the chosen configuration.
Subsequently, a preliminary electrical balance estimation is conducted, which allows for the sizing of the onboard power plant and the subsequent selection of diesel generators from an available engine database. It is also possible to provide a rough estimate of the most important machinery to be installed on board, such as chillers for ventilation or machinery for onboard fresh water generation.
From the volumes below the bulkhead deck and from regressions based on existing tank volumes, it is possible to calculate the necessary number of tanks and their respective volumes for fuel, ballast tanks, and fresh water tanks.
Subsequently, a weight estimation and related load exponent calculation are performed, based on regression formulae for the various ship weights. These weights are distributed based on

the areas identified by the parametric modelling and are used to perform a preliminary stability analysis of the ship.
Given the iterative process, the identification of design constraints is foreseen at each analysis phase, leading to the classification of the project as feasible or unfeasible. If a project is feasible, it continues through the analysis to define a design space of feasible solutions. These solutions can then be selected using multi-attribute decision-making techniques, after defining their performance attributes and respective weights. Each individual phase will be analysed in detail below.

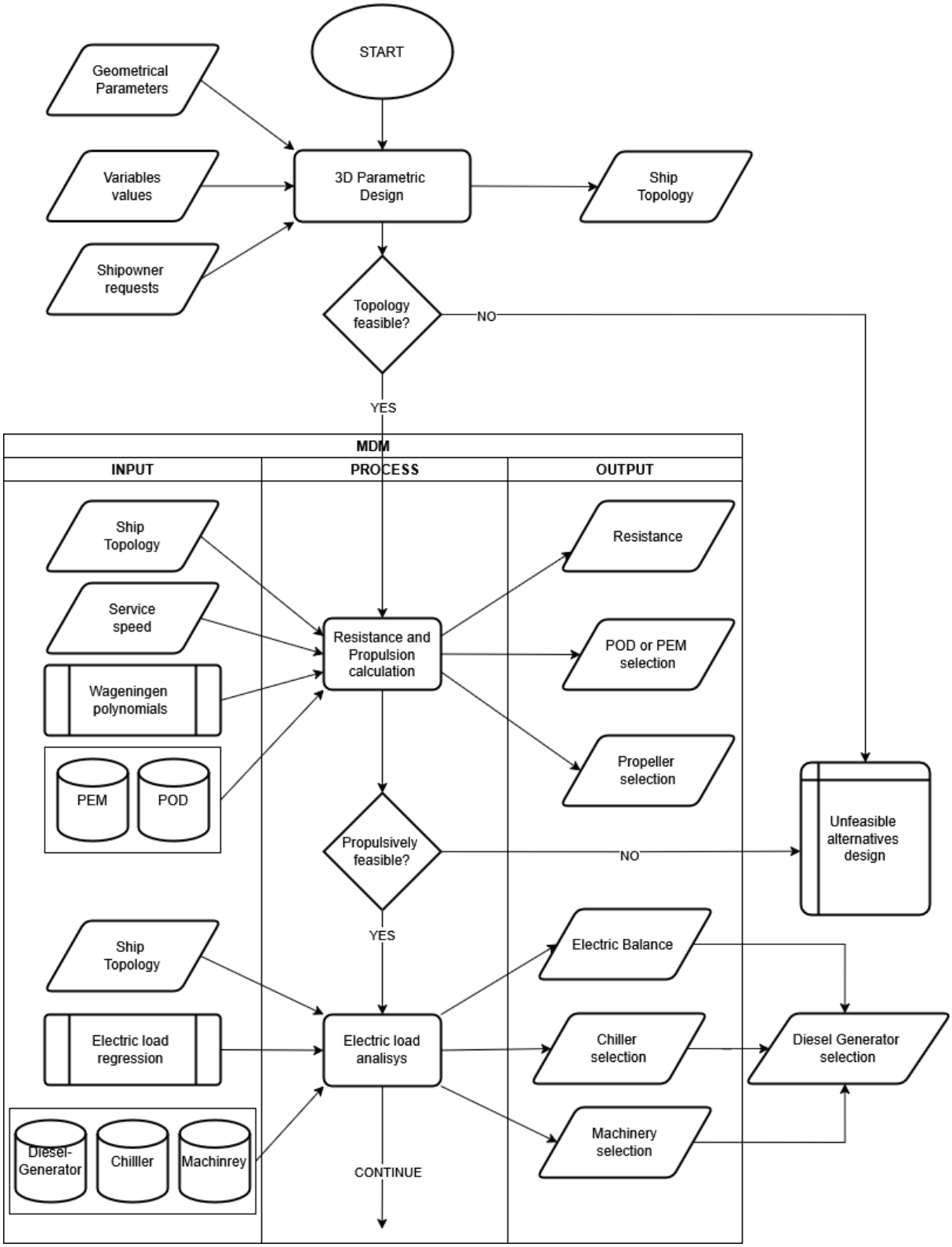

Figure 3.11: Matematical Model flowchart part 1

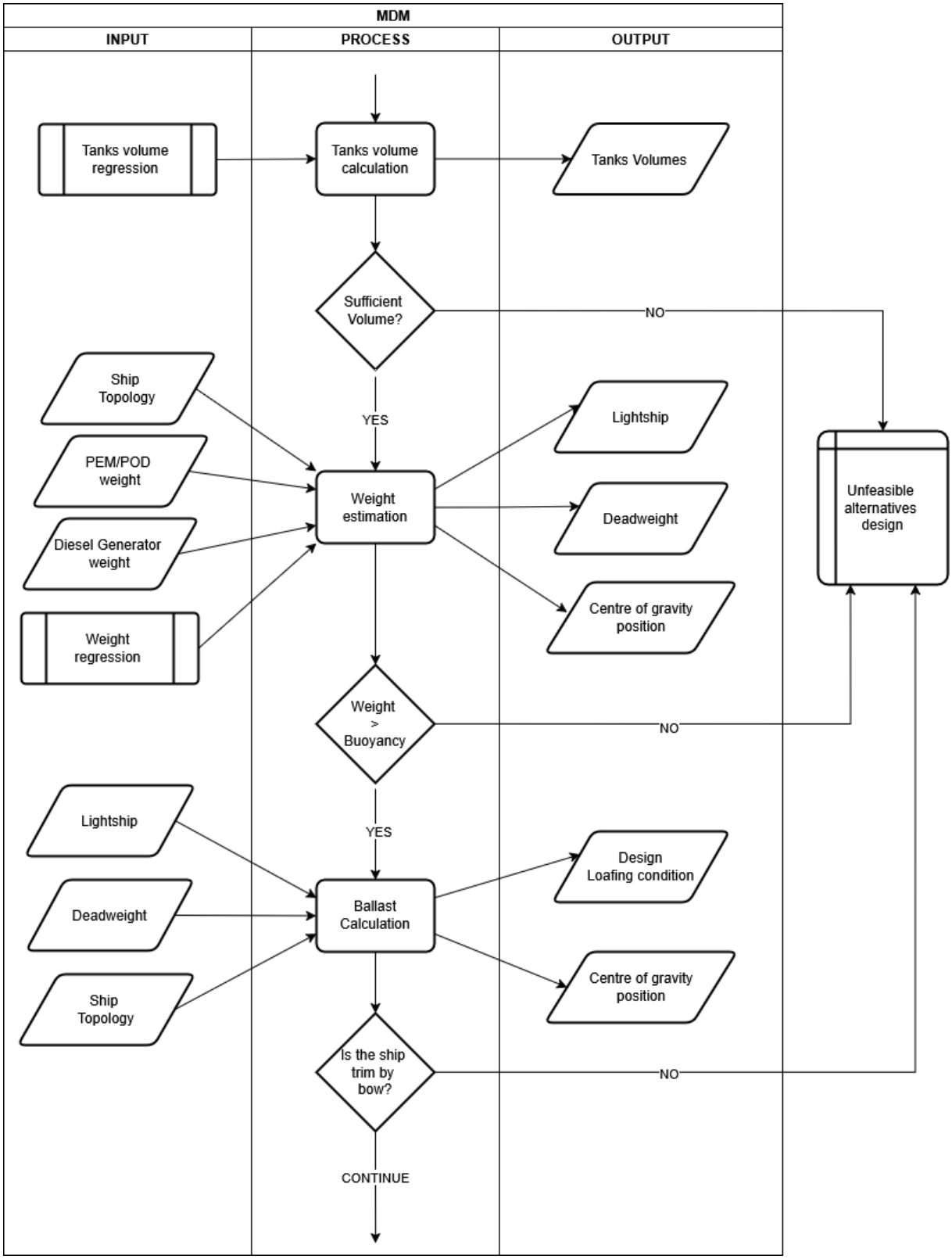

Figure 3.12: Matematical Model flowchart part 2

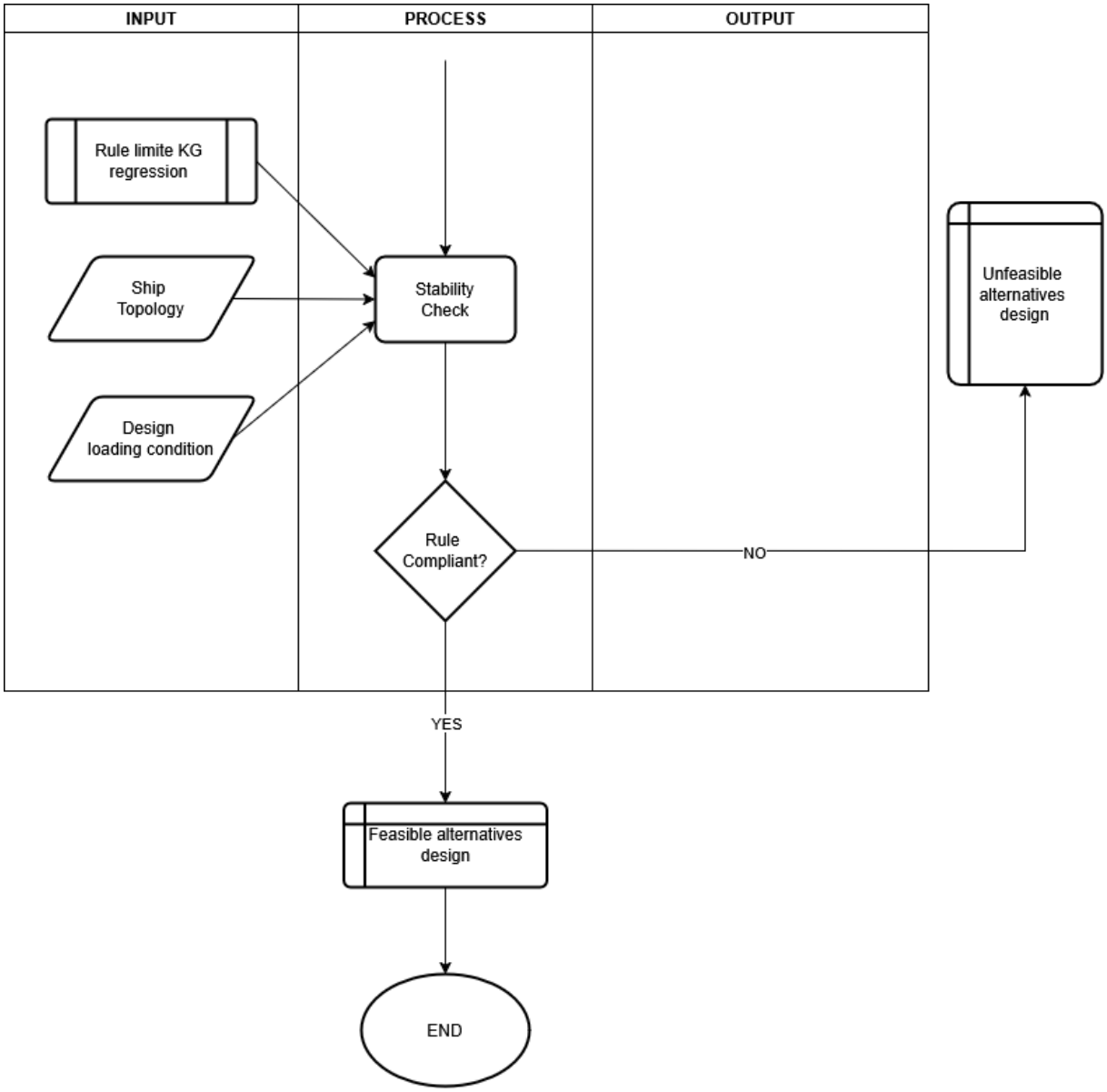

Figure 3.13: Matematical Model flowchart part 3

3.2.1 Ship topology

The first step of the methodological process consists of defining the ship's topology. The necessary inputs for this phase include:

- The number n of projects to be generated.
- The identification of the design variables in relation to how the parametric modelling was developed.
- The identification of the owner's requirements (such as the target GT of the ship or the number of passengers).

With the main outputs listed in Chapter 3.1.3 available, the 3D cruise ship projects can be generated.
A first screening in this phase is carried out by acting on the dimension of the corridor between the central spine and the end of the cabin. The dimensioning of the central spine was modelled in accordance with the SOLAS regulation (Regulation 13, Part D, Chapter II-2, Paragraph 3.2.4.5)[2]. The width of the central spine is strictly linked to the minimum width of the staircases for the escape routes of a passenger ship.
Knowing the B, the cabin length, and the dimension of the central spine, it was possible to parametrically determine the width of the corridor, measured between the central spine's longitudinal bulkhead and the cabin's extremity.
The Code establishes a minimum stairway width of 900 mm, which must be increased by 10 mm for each person exceeding the initial 90 persons. This forms the foundational requirement for designing escape stairways.
The calculation considers evacuation from enclosed spaces within each MFZ. All persons using the stairway must be included, even if they originate from a different MFZ. Two evacuation scenarios must be analysed Night case or Day case. The larger value resulting from the two scenarios determines the minimum stairway width for each deck level. The occupant load per deck includes accommodation spaces, service spaces, control stations, and machinery spaces. Public space capacity is defined either by the number of available seats or by allocating 2 m^2 per person.
To ensure timely evacuation flow towards muster stations from adjacent decks above and below, the following formulae apply:

- Two decks combined:

$$W = (N_1 + N_2) \times 10\,\text{mm} \tag{3.1}$$

- Three decks combined:

$$W = (N_1 + N_2 + 0.5N_3) \times 10\,\text{mm} \tag{3.2}$$

- Four decks combined:

$$W = (N_1 + N_2 + 0.5N_3 + 0.25N_4) \times 10\,\text{mm} \tag{3.3}$$

- Five or more decks: apply the four–deck formula to the deck under examination and the consecutive deck.

Where:

$$W = \text{required width of the stair treads measured between handrails.} \tag{3.4}$$

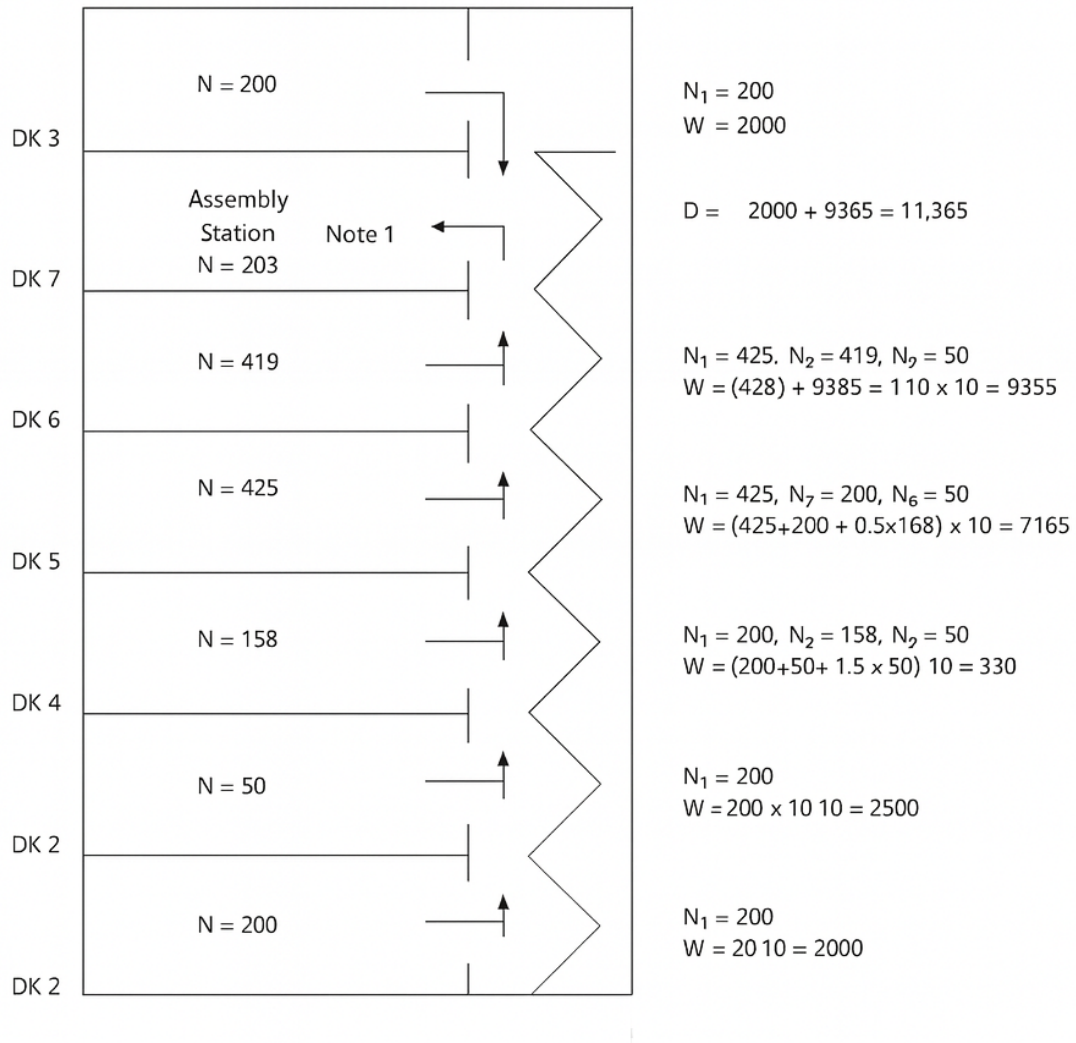

Figure 3.14: Example of a minimum stairway width calculation [2].

The calculated value of W may be reduced if a landing area S is present at the deck level. The reduction is obtained by subtracting P from Z:

$$P = S \times 3\,\text{persons/m}^2, \tag{3.5}$$

with the maximum allowable value:

$$P_{\max} = 0.25Z. \tag{3.6}$$

- Z = total number of persons to be evacuated from the deck under consideration
- P = number of persons temporarily accommodated on the stair landing (up to $0.25Z$)

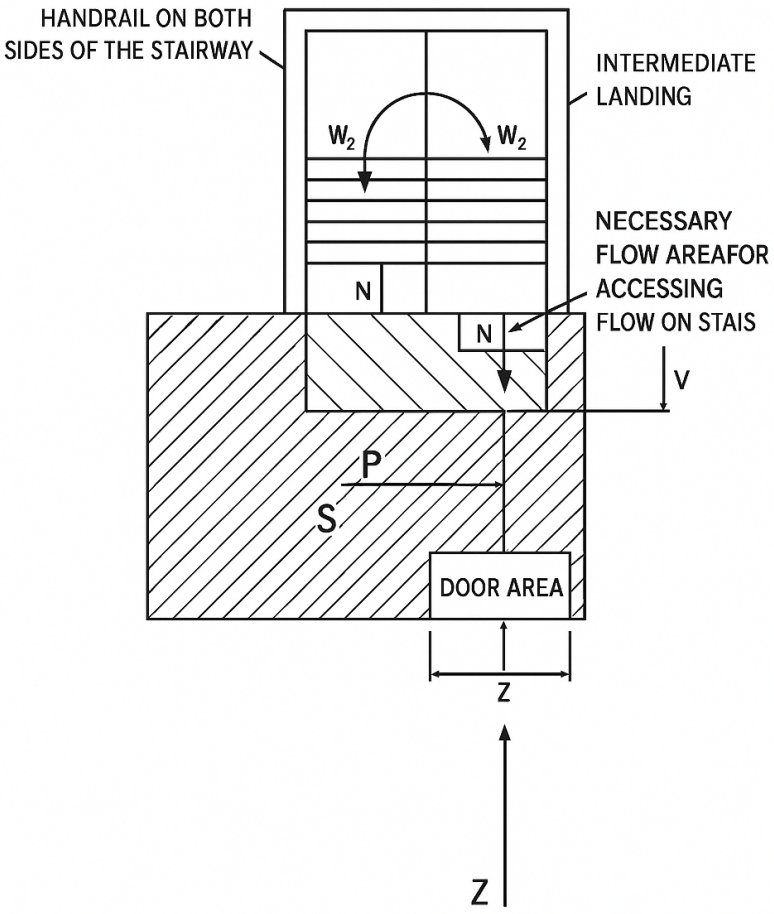

Figure 3.15: Reference diagram for calculating the minimum stairway width [2].

- S = useful landing surface area (excluding door swing and access paths)
- N =the total number of persons expected to use the stairway from each consecutive deck under consideration. N_1 refers to the deck with the highest number of persons using that stairway; N_2 refers to the deck with the next highest number of persons entering directly into the stair flow, such that when determining the stairway width for each deck level, the condition $N_1 > N_2 > N_3 > N_4$ is satisfied, as shown in Figure 3.15. These decks are considered as located upstream, further away from the embarkation deck, relative to the deck being assessed.

Thanks to parametric modelling, the three-dimensional model was subdivided into MFZ. By locating the cabins within each MFZ, it was possible to calculate the number of people on board allocated per deck to that specific zone, thus enabling the appropriate sizing of the central spine's width to accommodate the staircases for passenger escape routes.
The sole design constraint, once the cabin length and ship breadth were defined, was to verify that the corridor adhered to the same safety regulations. By regulation, the minimum clear space for the corridor, excluding fittings such as fire extinguishers and handrails, must be 900 mm. To ensure greater compliance with this constraint, the design threshold was raised to 1100 mm. Projects falling below this value are immediately excluded and categorised as non-feasible.

3.2.2 Ship Resistance and Propulsion

Following the verification of the geometric constraints pertaining to the examined design alternative, resistance and propulsion calculations are performed. In this phase, the goal is to analyse the hydrodynamic efficiency aspects of the hull associated with the i-th design solution.
The statistical method proposed by Holtrop [56] is used to estimate the propulsive power required by a ship during the initial design stages. This approach was developed through a regression analysis based on experiments conducted on random models and full-scale data collected at the Netherlands Ship Model Basin.
The Holtrop-Mennen method also provides regressions useful for calculating propulsive coefficients, although these are specifically calibrated for ships with conventional shaft lines. However, since our project also considers a POD propulsion system, it is necessary to differentiate the calculation method based on the selected propulsion type. A specific check is implemented within the code: if the ship is equipped with conventional shaft lines, the regressions from Holtrop-Mennen are utilised; conversely, if the ship employs POD propulsion, the propulsive coefficients are calculated using the regressions provided by Flikkema [57]. For twin-screw ships with traditional shaft lines, the following equations apply for thrust deduction factor t, wake fraction w and relative rotative efficiency η_R:

$$w = 0.3095C_B + 10C_V C_B - 0.23\frac{D}{\sqrt{BT}} \tag{3.7}$$

$$t = 0.325C_B - 0.1885\frac{D}{\sqrt{BT}} \tag{3.8}$$

$$\eta_R = 0.9737 + 0.111(C_P - 0.0225\,lcb) - 0.06325\frac{P}{D} \tag{3.9}$$

The formulations presented by the Flikkema method for POD-driven ships are given below:

$$t = 0.21593 + 0.099768C_B - 0.56056\frac{D}{\sqrt{BT}} \tag{3.10}$$

$$w = -0.21035 + 0.18053C_B + 56.724C_BC_V + 0.18566\frac{D}{\sqrt{BT}} + 0.090198\frac{C_{tip}}{D} \tag{3.11}$$

$$\eta_r = 1.493 - 0.18425C_P - 0.4278\,lcb - 0.33804\frac{P}{D} \tag{3.12}$$

where $\frac{C_{tip}}{D}$ is the relative clearance.

The calculation of the relative rotative efficiency, both according to the Holtrop–Mennen method and the Flikkema method, is influenced by the geometric parameters of the propeller, particularly the pitch-to-diameter ratio P/D. However, in the implemented model, propeller selection is performed after the resistance computation, and therefore the propulsive coefficient η_r is determined only after the propeller with the highest efficiency has been identified.

Propeller selection occurs immediately after the calculation of the ship's total resistance. The implemented code uses the total resistance determined by the Holtrop-Mennen method, the design speed and maximum speed (defined by the shipowner's specifications), in addition to the propulsive coefficients t and w derived from the previous phase, as inputs. It is assumed that the propeller is chosen from the models of the systematic series developed by the Netherlands Ship Model Basin in Wageningen.

While choosing from the Wageningen series is a conservative option, as it does not include specific optimization for the hull under consideration, further refinement of the propeller choice will be possible in later design phases to maximise performance relative to the hull characteristics.

Among the various possible strategies, the propeller design was performed by keeping the speed and diameter constant. In this phase, therefore, the propeller diameter and the number of blades were defined. The diameter was selected to be the largest possible size to ensure greater propulsive efficiency, while complying with size constraints and ensuring the propeller does not protrude below the keel line. Here 6 blades propellers have been used as a compromise solution between the conflicting needs to improve propeller open water efficiency and reduce irradiated noise to increase comfort.

The propeller design begins with the introduction of a sea margin, a safety factor that increases the total resistance. The increase in resistance via the sea margin used here is highly conservative, and it would be more appropriate in subsequent design phases to derive the increase using more accurate methods. This margin accounts for adverse weather conditions, hull fouling, variations in ship loading condition, and machinery performance degradation over time. From the increased total resistance R_T, the total required thrust T is derived using the thrust deduction factor t and n_S number of propellers, as expressed by the following relationship:

$$T = \frac{R_T}{(1-t)\cdot n_S} \tag{3.13}$$

Meanwhile, the advance speed (V_A) can be determined using the wake fraction coefficient w according to the following formula:

$$V_A = (1 - w) \cdot V \tag{3.14}$$

Subsequently, a suitable value for the expanded area ratio (A_E/A_O) is selected for the hull under examination. It should be noted that the choice of the A_E/A_O ratio influences both the efficiency of the isolated propeller and cavitation. The efficiency of the isolated propeller, for the same diameter and thrust, decreases as the expanded area ratio increases. This is easily explained by considering that a propeller with a larger expanded area has a greater wetted surface. Therefore, the highest efficiencies belong to propellers with a low A_E/A_O ratio. On the other hand, propellers with a low expanded area may encounter problems due to the onset of cavitation, which can be avoided by adopting a higher value for the A_E/A_O ratio. In the early design stages, the A_E/A_O ratio can be selected using Keller's formula:

$$\frac{A_E}{A_O} = \frac{(1.3 + 0.3Z)T}{(p_A + \gamma h - p_v)D^2 + k} \tag{3.15}$$

where:

- T = Thrust of each propeller, expressed in N
- Z = Number of propeller blades
- p_A = Atmospheric pressure, expressed in N/m^2
- γh = Hydrostatic head at the center of the propeller disc, expressed in N/m^2
- p_v = Vapor pressure of seawater, expressed in N/m^2
- k = A constant that varies from 0 (for naval ships with a transom stern) up to 0.20 (for single-screw ships with high installed power)
- D = Propeller diameter.

The method continues by defining a Papmel coefficient, Y, which allows us to utilise the isolated propeller diagrams of the systematic series, even though the propeller's rotational speed (n_p) is still unknown.
The variable Y is defined as the ratio of the thrust coefficient (K_T) to the square of the advance coefficient (J^2):

$$Y = \frac{K_T}{J^2} = \frac{\frac{T}{\rho n^2 D^4}}{\frac{V_A^2}{n^2 D^2}} = \frac{T}{\rho D^2 V_A^2} \tag{3.16}$$

Than can be possible to calculate the value of $\bar{Y}$, with $\bar{T}$ corresponding to the required design thrust. Through a loop over the pitch-to-diameter ratios (P/D), the Y curves are derived as a function of the advance coefficient (J) for each P/D value provided by the systematic series. The intersections of the Y curves with the value $\bar{Y}$ represent the operating points of propellers that all deliver the required thrust $\bar{T}$. It is then necessary to plot an auxiliary diagram that shows the values of the open water efficiency (η_0), the torque coefficient (K_Q), and the rotational speed (n_p) as a function of the pitch-to-diameter ratio (P/D). The rotational speed n_p can be derived from the advance coefficient J using the following relationship:

$$n_p = \frac{V_A}{JD} \tag{3.17}$$

At this stage, it is possible to determine the P/D ratio that corresponds to the maximum efficiency and subsequently derive the design values of K_T and K_Q from the isolated propeller diagrams.

At this stage of the design process, it is possible to calculate the required electric power. This power will be delivered either by the PEM in the case of a conventional shaft line configuration, or by the electric motor integrated into the POD, based on the type of stern configuration previously selected.

Thus, the brake power provided by the PEM is:

$$P_B = \frac{2\pi n_p Q}{\eta_r \eta_s} \tag{3.18}$$

where η_r and η_s are the relative rotative and shaft efficiency, respectively. Or the brake power provided by the POD is:

$$P_B = \frac{2\pi n_p Q}{\eta_{POD}} \tag{3.19}$$

where η_{POD} is the POD efficiency.

At this stage of the process, with the required electric propulsive power at the stern now known, the most suitable PEM or POD can be selected from an available model database. This selection is based on an evaluation criterion that compares the required propulsive power with the rated powers delivered by the catalog models.

It is possible to determine the electric power that must be supplied by the power plant to meet the required propulsive power

This determination is performed by working backward through the distribution chain, taking into account the inherent efficiency losses of each electrical component. It is therefore essential to include in the calculation the efficiency of the converters and transformers η_{tc}.

$$P_{prop} = \frac{n_S P_B}{\eta_{tc}} \tag{3.20}$$

where n_S is the number of propellers.

3.2.3 Electric balance and Diesel-Generator choice

Considering the power plant configuration of a typical luxury cruise ship as shown in Figure 3.16, it must be estimate the power not propulsive called P_{other} Consequently, an approximate

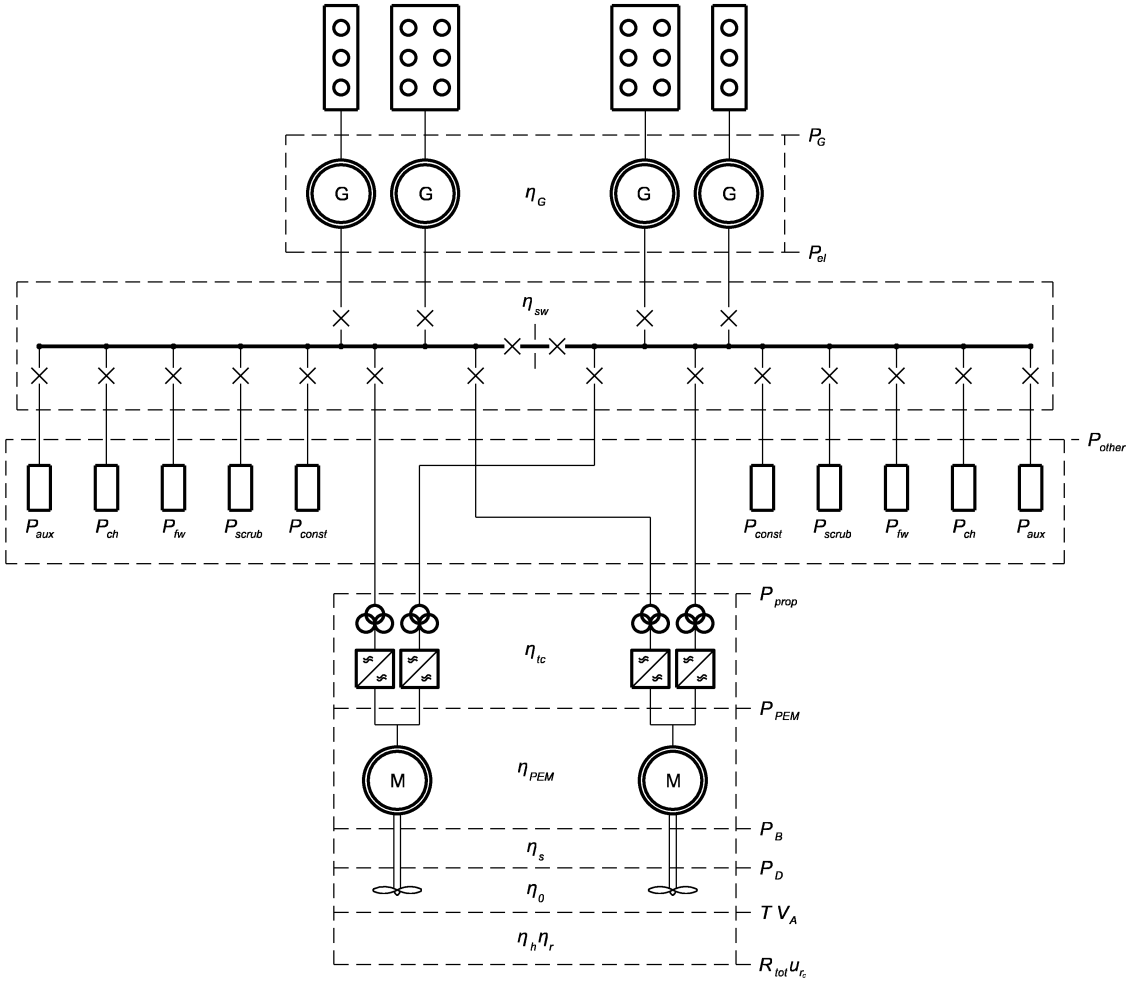

Figure 3.16: Ship's power electric system [3]

electrical load analysis was drafted. The items in this electrical load analysis were categorised into the following list: 'Hull service', 'Safety Service', 'Propulsion service', 'Engine Service', 'HVAC service', 'Galley service', 'Accommodation service', and 'Lighs service'.
For each item in the electrical load analysis, the summer and winter conditions were analysed during the various operational phases: service, maximum speed, maneuvering, and in port.
An existing ship database was utilised to regress the residual load under both the navigation at sea conditions and port stay . The theory employed is the multiple regression introduced in the

previous chapter. The aim was to derive regression formulae linked to the onboard area allocations.
The residual electrical load in the navigation condition was found to be dependent on the area designated for cabins (thus accounting for the number of passengers and air conditioning areas, one of the predominant electrical loads after propulsion), and the area designated for provisioning to account for any cold storage rooms and laundry areas.

$$P^{nav}_{other_{max}} = 0.512 \cdot A_{tot_{cab}} + 4.427 \cdot A_{tot_{prov}} + 5.421 \cdot A_{tot_{lan}} \tag{3.21}$$

Conversely, the residual load during port operations is dependent on the areas designated for the cabins and the areas designated for the laundries.

$$P^{port}_{other_{max}} = -0.085 \cdot A_{tot_{cab}} + 5.625 \cdot A_{tot_{lan}} + 5315.780 \tag{3.22}$$

Regression formulae were developed for each item in the electrical load analysis and for the different operational profiles. In cases where a regression formula could not be determined, it was decided to perform a weighted average of the coefficients of the available data to obtain a preliminary power estimate.

- Hull and deck service:
  - Service speed
    - Summer

$$P^{S}_{HD_{serv}} = P^{nav}_{other_{max}} \cdot (0.145C_B - 0.0004L_{OA}) \tag{3.23}$$

    - Winter

$$P^{W}_{HD_{serv}} = P^{nav}_{other_{max}} \cdot (0.145C_B - 0.0004L_{OA}) \tag{3.24}$$

  - Maximum speed
    - Summer

$$P^{S}_{HD_{max}} = P^{nav}_{other_{max}} \cdot (0.145C_B - 0.0004L_{OA}) \tag{3.25}$$

    - Winter

$$P^{W}_{HD_{max}} = P^{nav}_{other_{max}} \cdot (0.145C_B - 0.0004L_{OA}) \tag{3.26}$$

  - Maneuvering
    - Summer

$$P^{S}_{HD_{man}} = 0.147 \cdot P^{nav}_{other_{max}} \tag{3.27}$$

    - Winter

$$P^{W}_{HD_{man}} = 0.147 \cdot P^{nav}_{other_{max}} \tag{3.28}$$

- Port
  - Summer

$$P^{S}_{HD_{man}} = 0.003 \cdot P^{port}_{other_{max}} \tag{3.29}$$

  - Winter

$$P^{W}_{HD_{man}} = 0.003 \cdot P^{port}_{other_{max}} \tag{3.30}$$

- Safety Service:
  - Service speed
    - Summer

$$P^{S}_{Saf_{serv}} = 0.026 \cdot P^{nav}_{other_{max}} \tag{3.31}$$

    - Winter

$$P^{W}_{Saf_{serv}} = 0.026 \cdot P^{nav}_{other_{max}} \tag{3.32}$$

  - Maximum speed
    - Summer

$$P^{S}_{Saf_{max}} = 0.026 \cdot P^{nav}_{other_{max}} \tag{3.33}$$

    - Winter

$$P^{W}_{Saf_{max}} = 0.026 \cdot P^{nav}_{other_{max}} \tag{3.34}$$

  - Maneuvering
    - Summer

$$P^{S}_{Saf_{man}} = 0.028 \cdot P^{nav}_{other_{max}} \tag{3.35}$$

    - Winter

$$P^{W}_{Saf_{man}} = 0.028 \cdot P^{nav}_{other_{max}} \tag{3.36}$$

  - Port
    - Summer

$$P^{S}_{Saf_{port}} = 0.047 \cdot P^{port}_{other_{max}} \tag{3.37}$$

    - Winter

$$P^{W}_{Saf_{port}} = 0.047 \cdot P^{port}_{other_{max}} \tag{3.38}$$

- Engine Service:
  - Service speed
    - Summer

$$P^{S}_{Eng_{serv}} = 0.150 \cdot P^{nav}_{other_{max}} \tag{3.39}$$

    - Winter

$$P^{S}_{Eng_{serv}} = 0.146 \cdot P^{nav}_{other_{max}} \tag{3.40}$$

  - Maximum speed
    - Summer

$$P^{S}_{Eng_{max}} = 0.150 \cdot P^{nav}_{other_{max}} \tag{3.41}$$

    - Winter

$$P^{S}_{Eng_{max}} = 0.146 \cdot P^{nav}_{other_{max}} \tag{3.42}$$

  - Maneuvering
    - Summer

$$P^{S}_{Eng_{man}} = 0.147 \cdot P^{nav}_{other_{max}} \tag{3.43}$$

    - Winter

$$P^{W}_{Eng_{man}} = 0.145 \cdot P^{nav}_{other_{max}} \tag{3.44}$$

  - Port
    - Summer

$$P^{S}_{Eng_{port}} = 0.235 \cdot P^{port}_{other_{max}} \tag{3.45}$$

    - Winter

$$P^{W}_{Eng_{port}} = 0.238 \cdot P^{port}_{other_{max}} \tag{3.46}$$

- Air conditioning service:
  - Service speed
    - Summer

$$P^{S}_{HVAC_{serv}} = P^{nav}_{other_{max}} \cdot (3.153\frac{A_{tot_{cab}}}{A_{tot}} - 0.552) \tag{3.47}$$

    - Winter

$$P^{W}_{HVAC_{serv}} = P^{nav}_{other_{max}} \cdot (2.728\frac{A_{tot_{cab}}}{A_{tot}} - 0.478) \tag{3.48}$$

  - Maximum speed
    - Summer

$$P^{S}_{HVAC_{max}} = P^{nav}_{other_{max}} \cdot (3.153\frac{A_{tot_{cab}}}{A_{tot}} - 0.552) \tag{3.49}$$

    - Winter

$$P^{W}_{HVAC_{max}} = P^{nav}_{other_{max}} \cdot (2.728\frac{A_{tot_{cab}}}{A_{tot}} - 0.478) \tag{3.50}$$

  - Maneuvering

* Summer

$$P^{S}_{HVAC_{man}} = P^{nav}_{other_{max}} \cdot (2.714 \frac{A_{tot_{cab}}}{A_{tot}} - 0.450) \tag{3.51}$$

* Winter

$$P^{S}_{HVAC_{man}} = P^{nav}_{other_{max}} \cdot (2.353 \frac{A_{tot_{cab}}}{A_{tot}} - 0.390) \tag{3.52}$$

– Port

* Summer

$$P^{S}_{HVAC_{port}} = P^{port}_{other_{max}} \cdot (7.209 \frac{A_{tot_{cab}}}{A_{tot}} - 1.361) \tag{3.53}$$

* Winter

$$P^{S}_{HVAC_{port}} = P^{port}_{other_{max}} \cdot (7.204 \frac{A_{tot_{cab}}}{A_{tot}} - 1.379) \tag{3.54}$$

• Galley service:

– Service speed

* Summer

$$P^{S}_{Gal_{serv}} = P^{nav}_{other_{max}} \cdot (4.64 \cdot 10^{(-6)} \cdot A_{tot_{Gal}} + 0.040) \tag{3.55}$$

* Winter

$$P^{W}_{Gal_{serv}} = P^{nav}_{other_{max}} \cdot (4.84 \cdot 10^{(-6)} \cdot A_{tot_{Gal}} + 0.042) \tag{3.56}$$

– Maximum speed

* Summer

$$P^{S}_{Gal_{max}} = P^{nav}_{other_{max}} \cdot (4.64 \cdot 10^{(-6)} \cdot A_{tot_{Gal}} + 0.040) \tag{3.57}$$

* Winter

$$P^{W}_{Gal_{max}} = P^{nav}_{other_{max}} \cdot (4.84 \cdot 10^{(-6)} \cdot A_{tot_{Gal}} + 0.042) \tag{3.58}$$

– Maneuvering

* Summer

$$P^{S}_{Gal_{man}} = 0.044 \cdot P^{nav}_{other_{max}} \tag{3.59}$$

* Winter

$$P^{W}_{Gal_{man}} = 0.038 \cdot P^{nav}_{other_{max}} \tag{3.60}$$

– Port

* Summer

$$P^{S}_{Gal_{port}} = P^{port}_{other_{max}} \cdot (-4.92 \cdot 10^{(-5)} \cdot A_{tot_{Gal}} + 0.134) \tag{3.61}$$

* Winter

$$P^{W}_{Gal_{port}} = P^{port}_{other_{max}} \cdot (-5.14 \cdot 10^{(-5)} \cdot A_{tot_{Gal}} + 0.141) \tag{3.62}$$

- Accommodation service:
  - Service speed
    * Summer

$$P^{S}_{Ac_{serv}} = P^{nav}_{other_{max}} \cdot (-1.56 \cdot 10^{(-6)} \cdot GT + 0.126) \tag{3.63}$$

    * Winter

$$P^{W}_{Ac_{serv}} = P^{nav}_{other_{max}} \cdot (-1.63 \cdot 10^{(-6)} \cdot GT + 0.131) \tag{3.64}$$

  - Maximum speed
    * Summer

$$P^{S}_{Ac_{max}} = P^{nav}_{other_{max}} \cdot (-1.56 \cdot 10^{(-6)} \cdot GT + 0.126) \tag{3.65}$$

    * Winter

$$P^{W}_{Ac_{max}} = P^{nav}_{other_{max}} \cdot (-1.63 \cdot 10^{(-6)} \cdot GT + 0.131) \tag{3.66}$$

  - Maneuvering
    * Summer

$$P^{S}_{Ac_{man}} = P^{nav}_{other_{max}} \cdot (-1.76 \cdot 10^{(-6)} \cdot GT + 0.137) \tag{3.67}$$

    * Winter

$$P^{W}_{Ac_{man}} = P^{nav}_{other_{max}} \cdot (-1.84 \cdot 10^{(-6)} \cdot GT + 0.143) \tag{3.68}$$

  - Port
    * Summer

$$P^{S}_{Ac_{port}} = P^{port}_{other_{max}} \cdot (-2.47 \cdot 10^{(-6)} \cdot GT + 0.215) \tag{3.69}$$

    * Winter

$$P^{W}_{Ac_{port}} = P^{port}_{other_{max}} \cdot (-2.58 \cdot 10^{(-6)} \cdot GT + 0.225) \tag{3.70}$$

- Lighting service:
  - Service speed
    * Summer

$$P^{S}_{Light_{serv}} = P^{nav}_{other_{max}} \cdot (7.87 \cdot 10^{(-6)} \cdot A_{tot_{cab}} - 0.035) \tag{3.71}$$

    * Winter

$$P^{W}_{Light_{serv}} = P^{nav}_{other_{max}} \cdot (9.16 \cdot 10^{(-6)} \cdot A_{tot_{cab}} - 0.041) \tag{3.72}$$

- Maximum speed
  - Summer

$$P^{S}_{Light_{max}} = P^{nav}_{other_{max}} \cdot (7.87 \cdot 10^{(-6)} \cdot A_{tot_{cab}} - 0.035) \tag{3.73}$$

  - Winter

$$P^{W}_{Light_{max}} = P^{nav}_{other_{max}} \cdot (9.16 \cdot 10^{(-6)} \cdot A_{tot_{cab}} - 0.041) \tag{3.74}$$

- Maneuvering
  - Summer

$$P^{S}_{Light_{man}} = P^{nav}_{other_{max}} \cdot (2.38 \cdot 10^{(-5)} \cdot A_{tot_{cab}} - 0.175) \tag{3.75}$$

  - Winter

$$P^{W}_{Light_{man}} = P^{nav}_{other_{max}} \cdot (2.78 \cdot 10^{(-5)} \cdot A_{tot_{cab}} - 0.204) \tag{3.76}$$

- Port
  - Summer

$$P^{S}_{Light_{serv}} = P^{port}_{other_{max}} \cdot (7.87 \cdot 10^{(-6)} \cdot A_{tot_{cab}} - 0.035) \tag{3.77}$$

  - Winter

$$P^{W}_{Light_{serv}} = P^{port}_{other_{max}} \cdot (9.16 \cdot 10^{(-6)} \cdot A_{tot_{cab}} - 0.041) \tag{3.78}$$

A preliminary estimation of the power allocated to the chillers was performed. Based on the available electrical load analysis data from cruise ships, it was found that the electrical consumption of the chillers across the various operational profiles is as follows:

- For the summer service and full speed condition, the consumption is 67.557% of the total Air Conditioning Service load, and 54.905% for the winter condition.
- In the summer maneuvering condition, it is 66.616%, and 54.024% in the winter condition.
- During port operations, where ventilation and air conditioning remain active, the consumption is 56.654% in the summer and 35.219% in the winter.

Knowing these assumptions, it was possible to derive an electrical load analysis for the power consumed by the chillers. It is difficult during these preliminary phases to have an accurate idea of the chiller consumption and their required number. The calculation was carried out to try and reconstruct, as closely as possible to reality, the potential consumption during the execution of

an itinerary.
According to the publication by [3], the electrical consumption as a function of the external temperature is a bilinear function, as shown in Figure 3.17 .

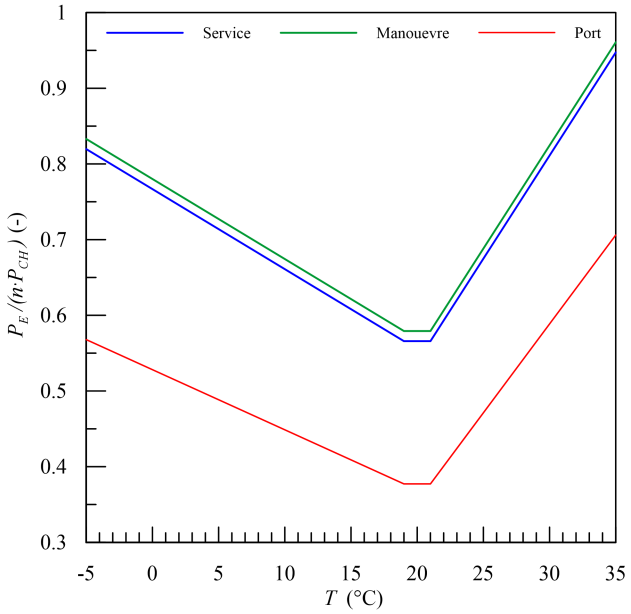

Figure 3.17: Chillers electric powert demand as a function of air temperature [3]

Knowing the calculation extremes for an electrical load analysis of cruise ships, specifically T -5°C for the winter condition and 24°C for the summer condition, it will be possible to reconstruct the chiller load function for each individual project.
In a manner analogous to what was done for the chillers, the electrical consumption of the reverse osmosis machines and evaporators for fresh water production on board was estimated. The electrical load analysis for this machinery will be useful during the operational simulation, as these machines will not always be active but will only be turned on or off during navigation segments when the ship has moved away from the coast.
Typically, one or two reverse osmosis machines and one evaporator are installed on board. Based on the available databases, it was possible to estimate how much power from the Engine Service can be attributed to this machinery without knowing their precise number in these initial design phases. In the future, with more data, it will be possible to perform a specific sizing even for these machines, given their fundamental function in producing fresh water.
Under service and maximum speed conditions, the electrical consumption of the machinery designated for fresh water production is 13.77% in summer conditions, and 13.82% in winter conditions. During maneuvering or port calls, these machines will be switched off.
Among the various generated configurations that are capable of guaranteeing the maximum required power under the operational conditions indicated in the electrical load analysis, the con-

figuration that presents the smallest deviation between the maximum deliverable power and the required power is selected. This process involves comparing different configurations, evaluating not only the power generated but also factors such as efficiency and geometric compatibility with the ship's spaces.
To ensure the feasibility of the chosen configuration, a check is performed on the dimensions of the generators against the available space in the ship's engine rooms. If the selected configuration does not satisfy the geometric constraints, the function eliminates that option and repeats the selection process until a compatible solution is found. Should no feasible configuration remain, then the design alternative would be declared unfeasible.
Finally, once the best possible configuration is identified, the code updates the electrical load analysis table with the newly calculated values and returns all the information regarding the final chosen configuration, including the number and models of the selected gensets.
Based on the information obtained, the model is now able to identify, for each analysed operational condition, the most efficient generator set arrangement from a fuel consumption perspective. For every operational condition, the function determines which combination of generators guarantees the necessary power with the lowest possible consumption, taking into account the technical characteristics of each generation group and the operational load to which it is subjected. Ultimately, the system selects, for each operational condition, which and how many generators present in the engine room should be kept in operation to minimise consumption.
The first step of the function conducting this selection consists of defining the main characteristics of the available generator set types. For each of them, the values of the maximum deliverable power are calculated, set to a maximum load limit value equal to 85% of the available generation capacity, and the minimum power, the latter fixed at 20% of the generator's nominal power. The maximum limit is imposed in such a way that it corresponds to the engine's maximum efficiency, while the lower limit is imposed because, below that load percentage, the engine is unable to guarantee proper operation.
At this point, the function proceeds to generate all possible configurations among the generation groups chosen in the previous phase. The process occurs by iterating through the maximum number of available groups and systematically combining the generators to form different configurations. Each generated configuration is then stored in an array of objects, representing the various possible combinations of Diesel Generator (DG) and their output capabilities. After generating the set of possible configurations, the function handles the selection of the most suitable configuration for each specific operational condition of the ship. For each available configuration, it is verified whether the required power falls within the range between the minimum and maximum power of the configuration itself. If the configuration is capable of meeting the energy requirement, the difference between the maximum power deliverable by the configuration and the required power is calculated. The objective is to select the configuration that

minimises this difference, thus ensuring optimal use of the generation capacity. In the event that no configuration is able to cover the power demand, a warning is generated, indicating the impossibility of finding a feasible solution for that specific operational condition.
Once the most suitable configuration for each operational condition is identified, the function calculates the load level, assuming a uniform load distribution among the operating generators.
Another fundamental aspect considered by the code concerns the Specific Fuel Oil Consumption (SFOC) of the generators. For each running generator, the SFOC value is determined by interpolating the available data as a function of the current operational load, given that the Diesel Generator database only indicates SFOC values under certain load conditions.
The generator percentage load, the maximum power available in the selected configuration, the power required by the ship, and the total hourly fuel consumption in tons are recorded. The final result consists of a table containing all this information for each operational condition, providing a clear overview of the selections automatically made by the code and the expected performance of the generation system.
Finally, for each operational condition, the function records several key parameters related to the chosen configuration.

3.2.4 Tanks volume estimation

The process then moved on to the preliminary estimation of volumes dedicated to the various service tanks, including those for fuel, Fresh Water (FW), Gray Black Water (GBW), and Ballast Water (BW).
To provide an accurate estimate, the existing ship database was utilised to derive specific regression formulae for estimating each tank volume. These formulae correlate the required tank volume to the ship's main dimensional and capacity parameters.
The results obtained from these regression analyses, specific to each tank type, are reported below.

$$\nabla_{fuel} = 0.066 \cdot P_{tot} + 0.094 \cdot P_{prop} - 1473.3 \tag{3.79}$$

$$\nabla_{FW} = 0.047 \cdot P_{tot} + 0.133 \cdot PAX + 121.66 \tag{3.80}$$

$$\nabla_{GBW} = 0.085 \cdot GT - 2878.9 \tag{3.81}$$

$$\nabla_{BW} = 0.055 \cdot \nabla \tag{3.82}$$

Following the preliminary estimation via regression, a cross-check was performed using the compartment volumes located below the bulkhead deck, which were obtained directly from the parametric solid modelling.
Each compartment was assigned a preliminary identification coefficient, based on the typical geometries of a cruise ship, to define its dedicated purpose. These destination categories in-

cluded: Ballast, PEM Room, Engine Room, Thruster Room, Void, or Auxiliaries Room.
This mapping made it possible to compare the estimated tank volumes with the actual volumes available in the rooms generated by the parameterisation. It is important to note that, when comparing the dedicated fuel volume, the spaces located beneath the double bottom were excluded. This exclusion was based on the assumption that the ship is exclusively propelled by Marine Gasoil Oil (MGO), a configuration that, for regulatory or safety reasons, does not foresee the placement of the corresponding tanks below the double bottom.

3.2.5 Weigth estimation

The process begins with the preliminary estimation of the Lightship Weight (W_{LS}), which is the weight of the ship when empty, and is essential for subsequent stability and trim verification. The weights have been broken down and categorised into the following functional classes for calculation and management purposes:

- Hull Steel Weight: Represents the weight of the steel hull structure.
- Coatings and Surface Treatments: Includes the weights related to coatings, thermal and acoustic insulation, and painting.
- Marine and Auxiliary Systems: Covers all hull auxiliary systems not directly related to propulsion, such as pumps, piping, bilge, and fire-fighting systems.
- Engine and Machinery Auxiliaries: Groups the weights of the auxiliaries strictly related to the propulsion plant, including lubrication, cooling systems, and heat exchangers.
- High Ventilation and Conditioning (HVAC): Includes the weight of the high-capacity heating, ventilation, and air conditioning systems.
- Electrical Systems: Covers the total weight of electrical distribution, including cables, switchboards, and equipment.
- Galley and Catering Equipment: Includes the weight of fixed equipment for galleys, pantries, and food service areas.
- Cabins and Accommodation: Includes the weight of the structures and fixed furnishings of the crew and passenger cabins.
- Public Area Furnishings: Includes the furniture and finishes of the ship's public areas (restaurants, lounges, etc.).
- Propulsion System: Includes the weight of electric motors (PEM/POD), shaft lines (if present), the propeller, and all direct transmission components.

Using the available database, it was possible to estimate the ship's Deadweight (DWT).

$$DWT = 0.096 \cdot P_{tot} + 1497.2; \tag{3.83}$$

By summing the DWT with the previously calculated W_{LS}, the total weight of the ship is obtained.
This total weight estimate is immediately compared against the Displacement (Δ), which is a geometric output of the parametric modelling. DWT include the fuel, the GBW and FW weight. For the stability, the centre of this weight will be a centre of floating area position. In this fase the specidic position of the tanks is unkonwn.
Consequently, projects are discarded if Δ is found to be less than the estimated total weight. The screening criterion accounts for a specified tolerance (within certain limits), ensuring that only projects where the submerged volume is geometrically sufficient to support the estimated weight are deemed feasible.
This constraint ensures that the design adheres to the fundamental principle of naval architecture: the condition of flotation.

3.2.5.1 Hull Steel Weight

The hull steel weight estimation for a cruise ship was performed by adopting the methodology formulated in [58]. Regarding the author's methodology, it is typically grounded in a statistical-parametric approach. This approach establishes a correlation between the structural weight, which acts as the dependent variable, and the main principal particulars and design parameters of the ship, such as the L_{WL}, B, Δ and Correct moulded depth to the highest continuos deck (D_A). The relationship is often represented by a multivariate regression formula, where the numerical coefficients reflect the relative influence of each parameter on the ships within a specific database. The validity of such an estimation is intrinsically linked to the quality and size of the database of existing ships used for the initial calibration.
Subsequently, the original dataset, which initially comprised only four ships, underwent a substantial augmentation through the integration of an additional nine ships, thereby yielding a final sample size of thirteen units. Following this database expansion, the process involved the recalibration of the parametric coefficients within the pre-existing derivation formulae, utilising the newly updated and extended ship database while adhering to the identical statistical methodology. This recalibration procedure is fundamental for enhancing the predictive accuracy of the conceptual design model.
The following regression equation is used for the hull steel weight calculation:

$$W_{st} = 0.090 \cdot L_{WL}^{1.317} \cdot B^{1.725} \cdot D_A^{-0.290} \tag{3.84}$$

3.2.5.2 Other Weights

Regarding the preliminary estimation of the weights for the other listed items, regression formulae derived from the available database data were utilised:

- Coatings and Surface Treatments

$$W_{ct} = 0.018 \cdot GT + 26.843 \tag{3.85}$$

- Marine and Auxiliary Systems

$$W_{ms} = 0.472 \cdot GT - 4.519 \cdot 10^{-6} \cdot GT^2 - 10459.6 \tag{3.86}$$

- Engine and Machinery Auxiliaries

$$W_{EngAux} = 0.032 \cdot P_{tot} + 0.008 \cdot GT + 168.4 \tag{3.87}$$

- HVAC

$$W_{HVAC} = 19.988 \cdot TrunkTec_{tot} - 9.579 \cdot 10^{-4} \cdot TrunkTec_{tot}^2 - 1.026 \cdot 10^5 \tag{3.88}$$

- Electrical Systems

$$W_{El} = 0.009 \cdot GT + 412.1 \tag{3.89}$$

- Galley and Catering Equipment

$$W_{Gal} = 2.884 \cdot \frac{A_{Gal_{tot}}}{PAX} + 86.414 \tag{3.90}$$

- Cabins and Accommodation

$$W_{Cab} = 0.192 \cdot A_{Pub_{tot}} - 266.8 \tag{3.91}$$

- Public Area Furnishings

$$W_{Pub} = -9304.2 \cdot \frac{PAX}{A_{Pub_{tot}}} + 1995.1 \tag{3.92}$$

- Propulsion System: for the assessment of the propulsion system weights, the chosen approach involved an initial analytical decomposition. Essentially, the weights of the primary component, specifically the PEM/POD units and the DG, were first isolated and

quantified. This was done to enable a subsequent estimation of the residual weight using regression techniques. The weights for these key elements (PEM/POD and DG) were directly retrieved and integrated from the dedicated machinery database, thereby allowing for a more accurate calculation of the total propulsion system mass.

$$W_{prop_{res}} = 0.088 \cdot P_{Prop} - 1146.2 \tag{3.93}$$

Prior to the stability verification, the ballast condition was analysed. Ballast tanks were filled to achieve a zero-trim condition by loading only the amount corresponding to the difference between the ship's weight and the displacement at the design draught. This procedure allowed for the exclusion of designs where the ship exhibited a trim by the bow, whereas configurations with an even keel or a slight trim by the stern were accepted.

3.2.6 Stability calcualtion

The preliminary stability calculation for the ship proceeds. Given the total weights of the ship, broken down by main categories, these were distributed across the available areas and volumes. Longitudinal, transverse, and vertical centres for each individual area and compartment were also determined from the parametric modelling. The following logic, based on previous experience, was used to identify the weight percentages allocated to the main macro-areas:

- Passenger Cabins
- Internal Public Spaces
- External Public Spaces
- Crew areas
- Trunk and technical spaces

The residual weights were then spread across the volumes of the compartments located below the bulkhead deck. By using static area moments and applying Varignon's Theorem, it was possible to calculate the Vertical centre of gravity (KG) for the design.
The stability constraint was imposed on the Limit vertical centre of gravity (KG_{limit}) mandated by the Intact Stability Code 2008 and the SOLAS convention (with damaged stability referring to Chapter II-1, Part B-1).
However, beforehand, bilinear regression formulae were developed for three critical criteria specific to this type of ship:

- Criterion 2.3: Severe wind and rolling

- Criterion 2.2.1: Area 30° to 40°
- Criterion 3.1.2: Turn angle of equilibrium

A ship from the database was used, its hull rebuilt, and a DoE was performed on it, specifically a CCC. The initial variable space was defined by four non-dimensionalised attributes: the geometric ratios ($B/T, L_{WL}/B, C_P, C_X$). Finding these insufficient for an exhaustive analysis, the DoE was extended by introducing a fifth attribute: the non-dimensionalised freeboard deck height, D/T. This allowed the calculation of the height D for the individual models based on the design draught T. Regarding the constraints, it was verified that height D was greater than the minimum regulatory freeboard height. Some D heights did not satisfy this requirement, but the deviation was intentionally maintained to explore the margins of design feasibility; in metamodels, in fact, optimal solutions are often found at the limits of the specifications. The final 5-attribute DoE produced 44 hulls in total, with variants characterised by three different D heights. The most restrictive criterion for determining the maximum allowable KG_{limit} was the Weather Criterion. To obtain reliable results, it was deemed unacceptable to heuristically estimate the values for the exposed lateral wind area (A_w) and the wind heeling lever (H). Therefore, the DoE was further implemented with two new non-dimensionalised variables: the normalised exposed lateral wind area and the normalised wind heeling lever. This led to a final model with 7 non-dimensionalised attributes and 143 distinct ship configurations. Once the KG_{limit} values were calculated for all 143 configurations, it was possible to obtain regression formulae using the variables selected for the DoE generation. The following regressions identify the KG_{limit} for the three different criteria considered.

$$\begin{aligned}\left(\frac{KG_{lim2.3}}{T}\right)' = &+ 0.443 + 0.479\left(\frac{B}{T}\right) + 0.034\,(C_P) + 0.020\,(C_x) + \\ &+ 0.325\left(\frac{D}{T}\right) - 0.103\left(\frac{H}{T}\right) - 0.130\left(\frac{A}{L_{WL}T}\right) + \\ &+ 0.080\left(\frac{B}{T}C_P\right) + 0.146\left(\frac{B}{T}\frac{D}{T}\right) - 0.080\left(\frac{B}{T}\frac{H}{T}\right) + \\ &- 0.096\left(\frac{B}{T}\frac{A}{L_{WL}T}\right) - 0.058\left(C_P\frac{D}{T}\right) + 0.048\left(C_x^2\right) + \\ &+ 0.116\left(\frac{D}{T}\frac{H}{T}\right) + 0.147\left(\frac{D}{T}\frac{A}{L_{WL}T}\right) - 0.698\left(\frac{D}{T}\right)^2\end{aligned} \tag{3.94}$$

$$\begin{aligned}\left(\frac{KG_{lim2.2.1}}{T}\right)' = &+ 0.387 + 0.501\left(\frac{B}{T}\right) + 0.014\,(C_x) + 0.438\left(\frac{D}{T}\right) + \\ &+ 0.080\left(\frac{B}{T}C_P\right) + 0.229\left(\frac{B}{T}\frac{D}{T}\right) + 0.022\,(C_PC_x) + \\ &- 0.716\left(\frac{D}{T}\right)^2\end{aligned} \tag{3.95}$$

$$\left(\frac{KG_{lim3.1.2}}{T}\right)' = -0.303 + 0.689\left(\frac{B}{T}\right) + 0.016\left(\frac{L}{B}\right) - 0.046\,(C_P) + \\ + 0.298\left(\frac{B}{T}\right)^2 - 0.058\left(C_P^2\right) - 0.088\left(C_x^2\right) + \\ - 0.055\left(\frac{D}{T}\right)^2 - 0.055\left(\frac{H}{T}\right)^2 - 0.055\left(\frac{A}{L_{WL}T}\right)^2 \tag{3.96}$$

The resulting value is a normalised value within the range of the database used.

Table 3.1: Maximum and minimum normalised KG_{limit} values

	y_c	y_{min}	y_{max}
KG 2.3	2.054	1.367	2.259
KG 2.2.1	2.037	1.778	2.661
KG 3.1.2	1.943	1.547	2.328

The de-normalised value will have to be found using the following formula:

$$y = y' \cdot r + c \tag{3.97}$$

where c, r, y_{max} and y_{min} are, respectively, the centre value, the radius, the maximum value, and the minimum value of the data set resume in Table 3.1.

$$c = \frac{y_{max} + y_{min}}{2} \\ r = \frac{y_{max} - y_{min}}{2} \tag{3.98}$$

To find the KG_{limit} for the criterion, it will be necessary to multiply by the ship's draught.
If the determined KG is not less than the KG_{limit} values of the three criteria considered, the design will be rejected.
Once the stability constraints have been verified, the design attributes are defined. These attributes can be selected based on technical expertise or specific shipowner requirements, ensuring they are mutually independent and accurately represent both technical aspects and future economic prospects. After defining the decision weights using objective or subjective methods, the fuzzification phase is carried out to identify which attributes are to be minimised, maximised, or converged toward a known target value. The feasible designs generated by the mathematical model are then subjected to a Pareto filter to isolate non-dominated solutions. Finally, a TOPSIS algorithm is applied to rank the non-dominated projects located on the Pareto frontier. An operational simulation, extensively discussed in the article [3], of which the author of this manuscript is one of the co-authors, will be applied to some of the non-dominated designs on the Pareto frontier.

3.3 Probabilistic simulation model

On a ship underway, the amount of consumables affects the overall displacement and therefore the ship's floating position. An even trim is assumed, while the real loading condition is taken into account to evaluate the effective draught. For cruise ships, the loading condition depends strongly on the bunkering and resupply practices adopted, as well as on statistical data collected from past voyages. For this reason, the assumptions presented here were developed in close collaboration with a leading cruise operator, so as to mirror real bunkering and resupply procedures and to make use of historical datasets for modelling passenger and crew occupancy together with consumables usage.

It should be noted that cruise ships operate using MGO, which is stored in dedicated fuel tanks on board. The use of this fuel is generally dictated by international and local regulatory requirements rather than by operational preference. In standard cruise ship operations, MGO bunkering may take place at any port when needed. Accordingly, this study assumes that MGO refuelling is automatically carried out at the departure from each port whenever the filling level of the relevant tanks drops below 30%. In such cases, the tanks are replenished up to a filling level of 90%. Consistent with this operational practice, the initial filling levels of the MGO tanks at the first port of the itinerary are randomly assigned within the range of 30% to 90%.

Beyond fuel, which has a major influence on any ship, the management of Fresh Water (FW), grey black water (GBW) is particularly critical for luxury cruise ships, where comfort standards and service levels are significantly higher. On luxury cruise ship, the capacity of FW tanks is typically comparable to that of fuel tanks. FW can be supplied in most ports, albeit at different price, and/or produced onboard through evaporators, making use of waste heat from engine cooling systems, and/or reverse osmosis systems powered by electricity. Ship operations may be simulated either with or without onboard freshwater production. In all cases, FW production is assumed to occur only during navigation phases, while an automatic FW bunkering policy is applied whenever the tank level at departure falls below 60%. Under such conditions, FW tanks are refilled up to 90%.

Freshwater consumption is modelled using an average value representative of luxury Mediterranean cruise operations, equal to 0.24 t/(person day) for the total number of people onboard, including both passengers and crew. The consumed FW is stored onboard in GBW tanks, except during navigation phases when treated GBW may be discharged at sea. Even in this case, 5% of the treated volume is assumed to remain onboard to account for treatment residuals. When the GBW tank filling level exceeds 60% leaving a residual onboard volume corresponding to 10% of the total tank capacity.

For a properly planned itinerary, a luxury cruise ship is assumed to operate close to its maximum passenger capacity, carrying a full payload of guests and nearly the entire nominal crew complement during navigation, transit, and manoeuvring phases. When the ship is in port, passengers

Table 3.2: Passenger and crew occupancy ratio and related standard deviation

	At Sea	At Berth
mean pax occupancy	0.93	0.63
pax occupancy st. dev.	0.02	0.03
mean crew occupancy	0.98	0.82
crew occupancy st. dev.	0.01	0.01

and a portion of the crew are expected to disembark. Based on statistical data representative of luxury cruise operations, the probability distributions of passenger and crew occupancy ratios are modelled as Gaussian, with mean values and standard deviations given in Table 3.2. After Monte Carlo sampling (MC) sampling, the passenger numbers derived from the generated occupancy ratios are rounded to the nearest integer and limited to values between zero and the corresponding maximum capacity [3].

The ship's power system is modelled as illustrated in Figure 3.16, which also presents the adopted nomenclature for powers and efficiencies. The system embeds fixed-pitch propellers, typically two, driven by PEM, which can embedded in a POD or drive a traditional shaft line.

The power demand for auxiliaries (P_{aux}) is defined as a linear function of the remaining overall power demand obtained excluding auxiliaries as ($P_{noaux} = P_{prop} + P_{other} - P_{aux}$). Additionally, the loads associated with air conditioning chillers (P_{ch}) are modelled as bilinear functions of the external air temperature T_a. Other electric loads detailed in the simulation model include those related to FW production (P_{FW}), as it can be deactivated based on phase or simulation requirements.

Environmental data for constructing probability distributions utilised in MC sampling are gathered from various sources. In particular, statistical characterisations of sea conditions are taken from [59],which provides sea scatter diagrams covering almost all regions worldwide. These datasets describe the probability of occurrence of sea states identified by the significant wave height $H_{1/3}$ and zero-crossing period T_z resolved over eight wave directions δ,and for each of the four seasons. On the basis of these data, a procedure is implemented to generate a generic deterministic sea state through MC sampling. First, the eight scatter diagrams relevant to the geographical area and season of the itinerary under investigation are selected. Subsequently, the cumulative density function of the wave direction, $cdf(\delta)$ is obtained by fitting the eight probability values corresponding to the directions reported in [59]. The random wave direction is then sampled as:

$$\delta_r = cdf^{-1}(rnd) \tag{3.99}$$

where rnd is a random number in $[0, 1]$ interval.After δ is determined, the corresponding scatter diagram is selected for further analysis. The cumulative joint probability distribution $cdf(T_z, \delta_r)$ is then fitted using the 11 discrete values of T_z provided in the selected scatter diagram. By

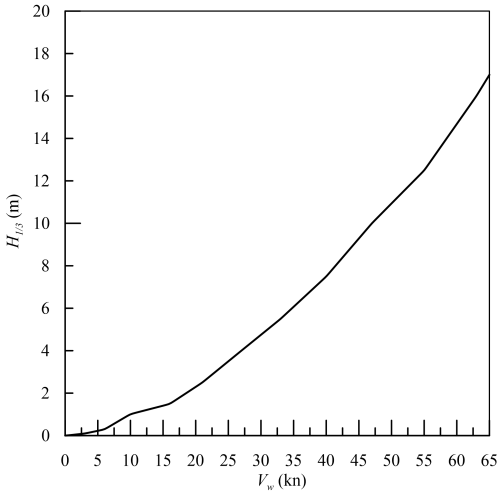

Figure 3.18: Wind-wave relation according to Beaufort scale

applying the same inverse cumulative approach adopted in Equation 3.99, the random zero crossing period T_{z_r} is generated. Finally, the empirical cumulative joint probability distribution $cdf(H_{1/3}, T_{z_r}, \delta_r)$ is defined using only the 15 probabilities related to $H_{1/3}$ reported in the scatter diagram column whose T_z interval contains T_{z_r}. The random $H_{1/3_r}$ is defined with the same approach defined in Equation 3.99. The wind is assumed to be correlated with the sea state, with the wind direction γ considered identical to the wave direction ($\gamma = \delta$). Hence, it is implicitly assumed that wind has generated the random sea state. Wind speed V_w is calculated as a function of $H_{1/3}$ based on the Beaufort scale as shown in Figure 3.18. Monthly average sea current speed V_c and direction β are assessed following Pilot Charts [60].
The probability density function for the average daily air temperature $pdf(T_a)$ is defined through kernel fitting using observations from the past ten years in each area defined in [59]. Kernel function is defined as:

$$pdf(x) = \frac{1}{nh} \sum_{i}^{n} K\left(\frac{x - x_i}{h}\right) \tag{3.100}$$

where x is the random variable, $x_1, ..., x_n$ is the data sample, K is the normal smoothing function [61] and h the bandwidth given by:

$$h = \sigma \left(\frac{4}{3n}\right)^{1/5} \tag{3.101}$$

where σ is the standard deviation of the sample [62]. With this process, a cumulative probability density function $cdf(T_a)$ is also established for each month under consideration. The same approach defined in Equation 3.99 is used for the generation of a random value from the $cdf(T_a)$. Air temperature and other environmental data are presumed to be uncorrelated. Air density is computed as a function of T_a, assuming a pressure of 101.325 kPa. Sea salinity (sa) and

sea surface temperature (SST) are considered as consistently averaged values. These values are determined on a monthly basis using statistical data from the preceding ten years, which is sourced from [63], and kept constant on all the randomly generated deterministic scenarios. Sea density ρ_w and kinematic viscosity ν_w are evaluated as functions of SST and sa following [64, 65]. The entire simulation process is summarised in the flow chart shown in Figure 3.19

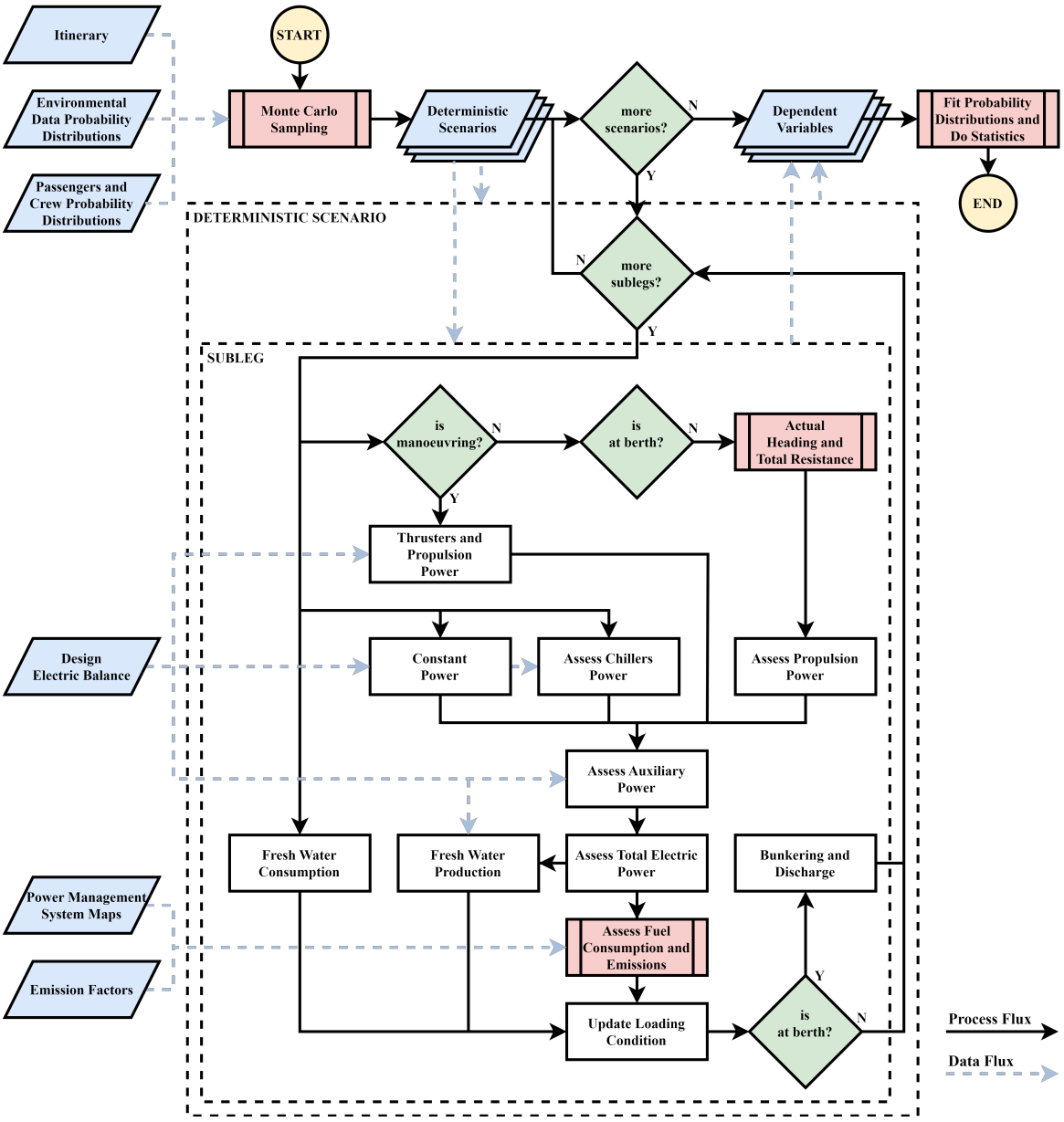

Figure 3.19: Flowchart of the proposed probabilistic simulation process [3]

The ship loading condition is updated at the beginning of each subleg and depends on MGO, FW, and GBW tank levels, as well as passenger and crew occupancy, treated as gaussian random variables, as already mentioned. Realistic bunkering and discharge policies are implemented, and the resulting draught directly affects hydrodynamic resistance.

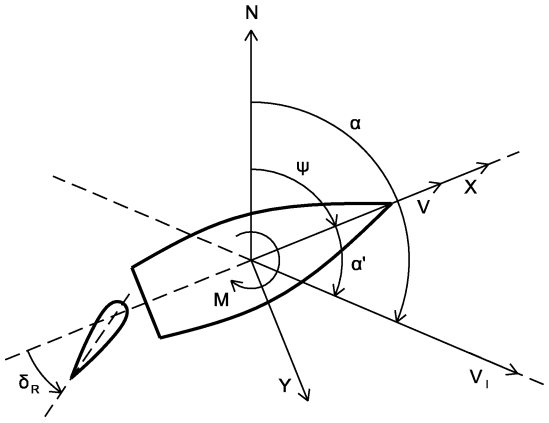

Figure 3.20: Ship fixed reference system and conventions for angles and speeds

For a subleg of the itinerary with a length d_l, the ship is considered to move at a constant speed over the ground V_l along the direction α of the leg (true course). Nevertheless, to counteract environmental forces and maintain the desired true course, the ship's heading angle ψ deviates from α of an angle $\alpha' = \alpha - \psi$, leading to a different effective required thrust and a non-null rudder angle δ_R compared to the calm water case. To capture such behaviour, this study uses a 3-DoF quasi-dynamic model, focusing on the degrees of freedom associated with longitudinal drift force, transversal drift force, and yawing moment. In Figure 3.20, conventions for angles and speeds are defined. All absolute angles are measured from the North direction and are considered positive in the clockwise direction.

All angles referred to the ship's heading (denoted by $'$) are measured from the direction of the ship's bow and are considered positive in the clockwise direction. Furthermore, the ship-fixed reference system $OXYZ$ used to measure forces and moments is defined in the Figure 3.20. This system is utilized to formulate the equilibrium equations of the ship, with its origin positioned at the midship section, having the X-axis facing stern to bow, the Y-axis facing port to starboard, and the Z-axis facing down (yawing moments are positive clockwise). It is noteworthy that, according to this convention, the advance speed $V = V_l \cdot \cos\alpha'$ is the component of ship speed V_l along the X-axis. However, the actual longitudinal and transverse speed components, u_{r_c} and v_{r_c}, relative to the ship must be calculated considering current speed and direction

Given a subleg, the equilibrium of all the forces acting on the ship can be expressed in the ship-fixed reference system. Given that the required speed over the ground and true course is known (as defined in the itinerary), the unknowns in the system include the heading of the ship ψ, the rudder angle δ_R, and the effective longitudinal force exerted by the propeller, denoted as R_T. This force is devoted to counterbalancing all the longitudinal components of other forces. The symbol R_T is chosen, as it is commonly used to define the effective power of the ship

($P_E = R_T \cdot V = T \cdot (1-t)$) where T is the propeller thrust and t the thrust deduction factor, representing the power required to sustain the ship's advance speed V.

3.3.1 System of Equations

For the 3-DoF model, the equilibrium equations are as follows:

$$\begin{cases} 0 = R_T + X_{hydro}(\psi) + X_{wind}(\psi) + X_{wave}(\psi) + X_{rud}(\psi, R_T, \delta_R) \\ 0 = Y_{hydro}(\psi) + Y_{wind}(\psi) + Y_{wave}(\psi) + Y_{rud}(\psi, R_T, \delta_R) \\ 0 = M_{hydro}(\psi) + M_{wind}(\psi) + M_{rud}(\psi, R_T, \delta_R) \end{cases} \tag{3.102}$$

where X, Y, and M denote the longitudinal forces, transversal forces, and yawing moments, respectively, in the ship-fixed reference system. The subscript $hydro$ denotes the hydrodynamic forces and moments originating from the interaction between the hull and fluid in calm water considering the current effect (in particular, X_{hydro} is the hull base resistance corrected to account for active stabilizers, fouling, loading condition and shallow water), $wind$ represents those related to the wind, $wave$ corresponds to those associated with the actual sea state (in particular, X_{wave} is commonly defined as added resistance in waves), and rud accounts for the forces generated by the rudder. The system is nonlinear in the variables $\mathbf{x} = (\psi, R_T, \delta_R)$. Consequently, it is solved here using a trust-region dogleg algorithm [66, 67], which is grounded in the interior-reflective Newton method while employing a subspace trust-region approach, as detailed in [68] and [69]. During each iteration, the algorithm approximates the solution to a large linear system by utilizing the preconditioned conjugate gradients method. The tolerance on the solution has been set to 0.001 N and 0.001 Nm for forces and moments, respectively while the following initial condition is adopted:

$$\mathbf{x}_0 = (\alpha, X_{hydro}(\alpha) + X_{wind}(\alpha) + X_{wave}(\alpha), 0) \tag{3.103}$$

The resistance curve in calm water, accounting for the effect of fixed appendages, denoted as $R_b(u_{r_c})$. However, it is usually associated with the design draught T_{des} and does not consider the actual loading condition, shallow water, retractable appendages, and hull fouling. Therefore, at the onset of each subleg, it is corrected to accommodate these factors, resulting in the corrected resistance $R_c(u_{r_c})$. This corrected resistance is then utilised in the computation of hydrodynamic forces.

Firstly, fouling leads to an increase in hull roughness and, consequently, resistance. The additional resistance due to fouling is assessed here using an empirical method to incorporate the increase in hull roughness [70]. The method considers two components of hull roughness M_{aa}: a linear increase of 2.8 μm/month while in port and a component related to biofouling accumu-

lation, considered only after the end of the anti-fouling paint lifespan. It is assumed that the initial hull roughness M_{aa_0} and the anti-fouling paint's lifespan are 100 µm and 1 year, respectively. After dry-docks, the hull roughness is presumed to return to the initial value [71], while after hull polishing at sea, only the biofouling effect on hull roughness is removed. Moreover, since anti-fouling paint is not applied during at-sea hull polishing operations, biofouling accumulation begins immediately after polishing. Once M_{aa} is determined, the additional resistance due to fouling is calculated as [72, 73]:

$$R_{rough}(u_{r_c}) = \frac{1}{2}\rho_w S(dC_F(M_{aa}) - dC_F(M_{aa_0}))u_{r_c}^2 \tag{3.104}$$

where dC_F is defined as:

$$dC_F(M_{aa}) = 105\left[\left(\frac{M_{aa}\cdot 10^{-6}}{L_{WL}}\right)^{\frac{1}{3}} - 0.64\right]\cdot 10^{-3} \tag{3.105}$$

Subsequently, the obtained resistance is adjusted to accommodate the loading condition. At the onset of each subleg, the ship's loading condition is updated by evaluating the filling factors of fuel, FW, and GBW tanks, as previously described. This adjustment induces changes in the ship's displacement and draught, thereby modifying the ship's resistance. In the context of cruise ships, characterized by a short interval between maximum and minimum seagoing draughts, the resistance correction is also relatively modest. Nonetheless, it is accounted for here according to the Admiralty formula:

$$R_{fc}(u_{r_c}) = [R_b(u_{r_c}) + R_{rough}(u_{r_c}) + R_{fins}(u_{r_c})]\left(\frac{T}{T_{des}}\right)^{\frac{2}{3}}\frac{\rho_w}{1025} \tag{3.106}$$

where T and T_{des} are the actual and design draughts respectively.
Finally, the obtained resistance $R_{fc}(u_{r_c})$ is once again adjusted to account for the shallow water effect, resulting in the final $R_c(u_{r_c})$. In the context of the studied problem, which aims to define the probability distribution of emissions for the entire itinerary, the impact of shallow water is significant only when long sublegs at high speed are navigated in shallow water. Therefore, the most concerning condition is incipient shallow water, modelled here according to the empirical Lackenby formulation, as recommended by ITTC [74, 75]. The method complements the classical Schlichting method with a similar approach. Given a reference speed, the effect of shallow water resistance is modelled by introducing a speed loss while keeping the resistance constant. In the Lackenby method, the non-dimensional speed loss factor $\Delta u_{r_c}/u_{r_c}$ due to incipient shallow water is given by:

$$\frac{\Delta u_{r_c}}{u_{r_c}} = 0.1242\left(\frac{A_M}{h^2} - 0.05\right) + 1 - \sqrt{\tanh\left(\frac{gh}{u_{r_c}^2}\right)} \tag{3.107}$$

where h is the water depth in m, A_M midship section area underwater in m^2 and u_{r_c} the open water ship speed in m/s.

The hydrodynamic forces are calculated by considering the impact of the ship's speed and sea current. The longitudinal component is determined through interpolation on the corrected resistance curve R_c. The current's longitudinal component of the relative speed u_{r_c} is considered as the actual speed:

$$X_{hydro}(\psi) = -R_c(u_{r_c}) = -R_c\left(V_{r_c}(\psi)\cos[\beta'_r(\psi)]\right) \tag{3.108}$$

where $V_{r_c}(\psi)$ and $\beta'_r(\psi)$ are the relative speed of the sea current and its angle from the heading, respectively. The transversal component of the hydrodynamic force and the yawing moment are evaluated according to [76] as:

$$\begin{aligned} Y_{hydro}(\psi) &= \tfrac{1}{2}\rho_w A_D [V_{r_c}(\psi)]^2 C_{Y_h}(\psi) \\ M_{hydro}(\psi) &= \tfrac{1}{2}\rho_w A_D L_{OA} [V_{r_c}(\psi)]^2 C_{M_h}(\psi) \end{aligned} \tag{3.109}$$

where A_D is the lateral projected area underwater, considering the actual draught, L_{OA} is the overall length of the ship, and the coefficients $C_{Y_h}(\psi)$ and $C_{M_h}(\psi)$ are given according with [76]

The wind forces are evaluated using Blendermann's method [77] considering the relative speed of the wind. The forces are then assessed as:

$$\begin{aligned} X_{wind}(\psi) &= \tfrac{1}{2}\rho_a A_F [V_{r_w}(\psi)]^2 C_{X_w}(\psi) \\ Y_{wind}(\psi) &= \tfrac{1}{2}\rho_a A_L [V_{r_w}(\psi)]^2 C_{Y_w}(\psi) \\ M_{wind}(\psi) &= \tfrac{1}{2}\rho_a A_L L_{OA} [V_{r_w}(\psi)]^2 C_{M_w}(\psi) \end{aligned} \tag{3.110}$$

where ρ_a is the air density, A_F and A_L are the frontal and lateral projected areas of the ship above the waterline, considering the actual draught, $V_{r_w}(\psi)$ is the relative speed of the wind (apparent wind), and $C_{X_w}(\psi)$, $C_{Y_w}(\psi)$, and $C_{M_w}(\psi)$ are the Blendermann's coefficients [77].

Wave forces are decomposed into two components: added resistance in waves X_{wave} and transversal drift force Y_{wave}. The added resistance in regular waves $R_{AW}/\zeta^2(\omega_e, \psi)$ has been assessed according to a statistical method [78] accounting for diffraction effects [79] and introducing semi-empirical parameters to approximate the added resistance under different wave headings. The drift force in regular waves $F_Y/\zeta^2(\omega_e, \psi)$ has been assessed with another statistical method [80] having similar features. Both forces in regular waves are computed as a function of encounter frequency ω_e, actual heading angle $\chi = \psi - \delta$, and thus, are derived as a

function of the angle ψ.
Given the $H_{1/3}$ and T_z identifying the sea state in a subleg, the sea spectrum is defined according to the Pierson-Moskowitz formulation [81] expressed as a function of wave frequency ω as:

$$S_\zeta(\omega) = \frac{Ag^2}{\omega^5} \exp\left[-B\left(\frac{g}{\omega}\right)^4\right] \tag{3.111}$$

where:

$$\begin{aligned} A &= 4\pi^3 \left(\tfrac{H_{1/3}}{gT_z^2}\right)^2 \\ B &= \tfrac{16\pi^3}{(gT_z)^4} \end{aligned} \tag{3.112}$$

which can be written as a function of ω_e as :

$$S_\zeta(\omega_e) = S_\zeta(\omega)\frac{g}{g - 2\omega V_l \cos(\psi - \delta)} \tag{3.113}$$

Wave forces are evaluated as [79, 82]:

$$\begin{aligned} X_{wave}(\psi) &= -2\int_0^\infty \tfrac{R_{AW}}{\zeta^2}(\omega_e, \psi) S_\zeta(\omega_e) d\omega_e \\ Y_{wave}(\psi) &= 2\int_0^\infty \tfrac{F_Y}{\zeta^2}(\omega_e, \psi) S_\zeta(\omega_e) d\omega_e \end{aligned} \tag{3.114}$$

The hydrodynamic forces exerted by the rudder are evaluated as follows:

$$\begin{aligned} &X_{rud}(\psi, R_T, \delta_R) = -L(\psi, R_T, \delta_R)\sin[\delta_R - \delta_e(\psi, R_T, \delta_R)] - D(\psi, R_T, \delta_R)\cos[\delta_R - \delta_e(\psi, R_T, \delta_R)] \\ &Y_{rud}(\psi, R_T, \delta_R) = -L(\psi, R_T, \delta_R)\cos[\delta_R - \delta_e(\psi, R_T, \delta_R)] + D(\psi, R_T, \delta_R)\sin[\delta_R - \delta_e(\psi, R_T, \delta_R)] \\ &M_{rud}(\psi, R_T, \delta_R) = -X_R Y_{rud}(\psi, R_T, \delta_R) \end{aligned} \tag{3.115}$$

where the attack angle δ_e, the lift force L and drag force D are defined as:

$$\begin{aligned} \delta_e(\psi, R_T, \delta_R) &= \delta_R + atan2[v_R(\psi, R_T), u_R(\psi, R_T)] \\ L(\psi, R_T, \delta_R) &= n_S \tfrac{1}{2}\rho_w A_R [V_R(\psi, R_T)]^2 C_L(\psi, \delta_R) \\ D(\psi, R_T, \delta_R) &= n_S \tfrac{1}{2}\rho_w A_R [V_R(\psi, R_T)]^2 C_D(\psi, \delta_R) \end{aligned} \tag{3.116}$$

where n_S is the number of propellers/rudders, A_R is the longitudinal projected area of the rudder or POD, X_R is the longitudinal coordinate of the A_R centre in the ship-fixed reference system, $V_R(\psi, R_T) = (u_R, v_R)$ is the speed of the incident flow on the rudder, whereas $C_D(\delta_R)$ and $C_L(\delta_R)$ are the drag and lift coefficients of the rudder, respectively. Since the rudder is used only to maintain the true course , and there is no interest in investigating ship manoeuvring, the lift coefficient has been evaluated using a linear derivative:

$$C_L(\psi, \delta_R) = \frac{\partial C_L}{\partial \delta_e}\delta_e(\psi, R_T, \delta_R) \tag{3.117}$$

where, according to [83], the derivative is estimated as:

$$\frac{\partial C_L}{\partial \delta_e} = 1.95\pi \frac{\lambda}{\lambda + 3} \tag{3.118}$$

with λ as the elongation ratio of the rudder. Concerning the drag coefficient, it shall consider only the increase in rudder resistance due to the rudder angle, as the null-angle resistance is already included in the calm water resistance. Thus, it is evaluated as a function of the generated lift [83]:

$$C_D(\psi, \delta_R) = \frac{[C_L(\psi, \delta_R)]^2}{0.86\pi\lambda} \tag{3.119}$$

The evaluation of flow speed on the rudder is carried out considering both the hull effect and the flow acceleration induced by the propeller. The advance speed V_A and propeller thrust T are evaluated as:

$$\begin{aligned} V_A(\psi) &= u_{r_c}(\psi)[1 - w(\psi)] \\ T(\psi, R_T) &= \frac{R_T}{n_S[1-t(\psi)]} \end{aligned} \tag{3.120}$$

where $V_{r_c}(\psi) = (u_{r_c}, v_{r_c})$ is the relative speed of the current, $w(\psi)$ and $t(\psi)$ are the wake fraction and the thrust deduction factor, both expressed as a function of ship speed and here evaluated by interpolation assuming the ship speed $u_{r_c}(\psi)$. Then, the components of the rudder incident flow speed are estimated as:

$$\begin{aligned} u_R(\psi, R_T) &= V_A(\psi)\frac{1+\sqrt{1+C_T(\psi,R_T)}}{2} \\ v_R(\psi) &= v_{r_c}(\psi) \end{aligned} \tag{3.121}$$

where $C_T(\psi, R_T)$ is the thrust loading coefficient of the propeller.

3.3.2 Ships with POD propulsion

To integrate the podded propulsion system into the mathematical model, the governing equations are modified by defining the steering angle δ_R as the azimuth rotation angle of the POD units. Consequently, the thrust is no longer purely longitudinal but is resolved into its longitudinal and transverse components. The advace speed will be:

$$V_{A_{Pod}}(\psi) = V_A(\psi) * cos(\delta_R) - v_{r_c} * (1 - w) * sin(\delta_R); \tag{3.122}$$

The induced speed along the POD axis V_i and the relative velocity components are defined as:

$$V_i = \frac{V_{A_{Pod}}(\psi) \cdot \left(1 + \sqrt{1 + C_{Th}}\right)}{2} - V_A \tag{3.123}$$

$$
\begin{aligned}
u_R(\psi, R_T) &= V_A(\psi) + V_i \cos \delta_R \\
v_R(\psi) &= v_{r_c} * (1 - w) - V_i \sin \delta_R
\end{aligned}
\tag{3.124}
$$

The effective angle of attack δ_{eff} and the resulting relative velocity V_{rel} are calculated as:

$$
\delta_{eff} = \delta_R + atan2(v_R(\psi), u_R(\psi, R_T)
\tag{3.125}
$$

$$
V_{rel} = \sqrt{u_R(\psi, R_T)^2 + v_R(\psi)^2}
\tag{3.126}
$$

Furthermore, the forces acting on the "rudder" are limited to those generated by the pod structure, which operate within the propeller's accelerated slipstream. While the propellers are still modeled using the Wageningen B-series, the hydrodynamic propulsion coefficients are determined using Flikkema's approach [57] instead of Holtrop's.
The force of the pod F_{Pod} based on a Holtrop-style approach for appendages where C_F is the friction factor of the ship with POD , S_{Pod} is the POD wetted surface, $(1 + k)_{Pod}$ a form factor assumed 2.7[56]:

$$
F_{pod} = n_s \cdot \frac{1}{2} \rho V_{rel}^2 S_{Pod} \cdot (1 + k)_{Pod} \cdot C_F
\tag{3.127}
$$

and the corrected rudder force components $L(\psi, R_T, \delta_R)_{Pod} and D(\psi, R_T, \delta_R)_{Pod}$ are:

$$
\begin{aligned}
L(\psi, R_T, \delta_R)_{Pod} &= L(\psi, R_T, \delta_R) - F_{pod} \cos(\delta_R - \delta_{eff}) \\
D(\psi, R_T, \delta_R)_{Pod} &= D(\psi, R_T, \delta_R) + F_{pod} \sin(\delta_R - \delta_{eff})
\end{aligned}
\tag{3.128}
$$

3.3.3 Fuel consumption and emissions assessment

Once the system is solved and the actual R_T has been assessed, the electric power demand from propulsion is assessed according to Section Ship Resistance and Propulsion and Section 3.2.3. Then, the overall power is obtained summing the previously defined P_{other}, obtaining the electric power demand P_el, required from the onboard power plant. Subsequently, through an appropriate mapping operation to model the Power Menagment System (PMS), the electric power demand is converted into fuel consumption, leading to the estimation of the corresponding equivalent tons of carbon dioxide ($CO_{2_{eq}}$) emitted.
On a cruise ship, as with all diesel-electric ships, electric power is supplied by multiple diesel generators. The number and load of active generators are regulated by the PMS or manually adjusted by engineer officers [84]. Current PMSs typically employ straightforward rules based on the load l_g of the generators, defined as:

$$
l_{g_i} = \frac{P_{el_i}}{\eta_G P_i^{max}}
\tag{3.129}
$$

where P_{el_i} is the actual electric power produced by the generator, P_i^{max} is the engine's maximum continuous rating, and η_G is the generator efficiency. The basic rules of a standard Power Management System (PMS) can be summarized as follows:

- All active diesel generators operate with an equal load l_g.
- If l_g exceeds an upper threshold (typically 0.85) for a specified time interval, an additional generator is automatically activated.
- If l_g falls below a lower threshold (typically 0.20) for a specified time interval, a generator is automatically deactivated.

In practice, generators often come in two different sizes, forming a father-son configuration, which complicates the PMS rules. Moreover, some ships may have generators using different types of fuel.
In the simulation process, these rules are represented through a mapping procedure that determines the fuel consumption fc_j in t/h for each j-th type of fuel as a function of the power P_{el}. Especially in the case of a father-son power plant, there can be multiple viable configurations of active engines. A configuration is deemed viable if the sum of the electric power of all n_a active generators equals P_{el}, and the global load l_g falls within the lower and upper thresholds. The global load of the power plant is defined as:

$$l_g = l_{g_1} = ... = l_{g_{n_a}} = \frac{P_{el}}{P_G} \tag{3.130}$$

where P_G is the maximum electric power provided by diesel generators and defined as:

$$P_G = \eta_G \sum_{i}^{n_a} P_i^{max} \tag{3.131}$$

For the k-th configuration, the fuel consumption in t/h of the j-th type of fuel can be evaluated as:

$$fc_{jk} = \sum_{i}^{n_{jk}} d_j SFOC_{ij}(l_{g_i}) P_i^{max} l_{g_i} \cdot 10^{-6} \tag{3.132}$$

where n_{jk} denotes the number of active generators utilizing the j-th fuel, d_j represents a coefficient accounting for depuration/filtering allowance (assumed to be 1 for MGO), and $SFOC_{ij}(l_{g_i})$ represents the specific fuel consumption in g/kWh of the i-th engine at load l_{g_i}. Considering all the viable configurations of the power plant, the fuel consumption map is given by:

$$fc(P_{el}) = \min_k \sum_{j}^{n_f} fc_{jk} \tag{3.133}$$

where n_f is the number of fuel types used. This means that, among the viable configurations, the one minimising the overall fuel consumption is chosen.
Given the fuel consumption for each fuel type utilized in the standard or optimal configuration, the corresponding emissions of equivalent tons of CO_2 for the analysed subleg are determined as:

$$CO_2e_l = \sum_{j}^{n_f} EF_j fc_j \frac{d_l}{V_l} \tag{3.134}$$

where d_l is the distance covered by the ship in the subleg and V_l its speed, both related to true route. The total emissions ($CO_{2_{eq}}$) can be calculated by summing the contributions from all sublegs of the itinerary. The emission factors used are sourced from [85]. Tank-to-Wake (TtW) emissions have been considered solely in accordance with currently enforced guidelines for operational index assessment [86, 87]. The emissions can be utilised to calculate the statutory indicators for the ship's environmental performance over the entire itinerary. In this context, the Carbon Intensity indicator (CII) is employed, although its efficacy has recently been questioned, and alternative formulations for cruise ships have been suggested [88]. According to the currently applicable regulations [89], the attained CII for a cruise ship, concerning a specific itinerary, can be defined as:

$$CII = \frac{CO_{2_{eq}}}{GT \cdot d} \tag{3.135}$$

where GT represents the gross tonnage of the ship, and d denotes the total distance covered in the itinerary (the sum of all d_l). The attained value is to be compared to a required value, which declines over the years according to [90]. Finally, based on its attained value and the corresponding year, the ship is assigned a grade ranging from A (best emissions ranking) to E (worst emissions ranking) as per [91].
For itineraries within European waters, the Greenhouse intensity factor (GHG_{int}) has been evaluated in accordance with the *Fit for 55* legislative package introduced by the European Union, specifically under the FuelEU Maritime regulation [92]. This framework aims to progressively reduce the lifecycle GHG emissions of energy used on board ships by imposing limits on the average GHG intensity of the energy consumed during voyages under EU jurisdiction.
Under FuelEU Maritime, the GHG intensity is defined on a well-to-wake (WtW) basis [93], which accounts not only for emissions produced during fuel combustion on board, but also for upstream emissions related to fuel production, processing, and distribution. The indicator is expressed in terms of grams of $CO_{2_{eq}}$ per unit of energy supplied to the ship.
The GHG intensity factor is calculated as an energy-weighted average over all energy carriers used during the voyage [94]:

$$GHG_{int} = f_{wind} \cdot (GHG_{WtT} + GHG_{TtW}) \tag{3.136}$$

where f_{wind} is is the remuneration factor for wind-assisted propulsion assumed 1, the GHG_{WtT} is the greenhouse gas intensity of the *Well-to-Tank* pathway (gCO_{2eq}/MJ). It accounts for emissions associated with the extraction, production, and transport of the fuel or electricity generation, and is calculted as:

$$GHG_{WtT} = \frac{\sum_i^{n_{\text{fuel}}} M_i \cdot LCV_i \cdot CO_{2eq_{WtT},i} + \sum_k^c E_k \cdot CO_{2eq_{electricity},k}}{\sum_i^{n_{\text{fuel}}} M_i \cdot LCV_i \cdot RWD_i + \sum_k^c E_k} \tag{3.137}$$

and GHG_{TtW} is the greenhouse gas intensity of the TtW pathway (gCO_{2eq}/MJ). It quantifies emissions released during combustion or energy utilisation on board the ship, including the impact of unburnt gases and it is calculated as:

$$GHG_{TtW} = \frac{\sum_i^{n_{\text{fuel}}} \sum_j^m M_{i,j} \cdot \left[\left(1 - \frac{1}{100} C_{\text{slip},j}\right) \cdot CO_{2_{eq},i,j} + \left(\frac{1}{100} C_{\text{slip},j} \cdot CO_{2eq_{TtW,slip},i,j}\right) \right]}{\sum_i^{n_{\text{fuel}}} M_i \cdot LCV_i \cdot RWD_i + \sum_k^c E_k} \tag{3.138}$$

where [92] M_i is the total mass of fuel i consumed,LCV_i the Lower Calorific Value of fuel i, $CO_{2eq_{WtT},i}$ the WtT emission factor for fuel i, E_k is the electricity supplied from external sources (e.g., On-shore Power Supply - OPS), $CO_{2eq_{electricity},k}$ is the emission intensity associated with the specific electricity grid k utilised, RWD_i the reward Factor for fuel i, introduced to incentivise the use of sustainable fuels or low-emission technologies, $C_{\text{slip},j}$ is the fuel slip coefficient for engine/technology j, expressed as a percentage of the fuel mass that passes through the system unburnt, $CO_{2_{eq},i,j}$ is the TtW emission factor for fuel i utilised with technology j and $CO_{2_{eq_{slip},i,j}}$ is the emission factor specifically associated with the fraction of unburnt fuel released into the atmosphere.

3.3.4 2^{nd} stage attributes definition

The probabilistic simulation generates mean μ, median Q_2, and third quartile Q_3 values for various operational metrics. By adopting a stochastic approach, the software determines probability distribution curves for fuel consumption, atmospheric pollutant emissions, fresh water consumption, and water production via reverse osmosis units and evaporators, alongside other operational outputs such as average power demand per voyage leg. The indices provided in the previous section will also be treated as probabilistic averages across the simulated scenarios.
Consequently, determining which attributes to include in the second ranking phase is crucial. If the non-dominated designs from the initial selection are evaluated for itineraries, the percentage of operational life spent on each specific itinerary must be defined. Seasonality must also be accounted for, as hotel loads fluctuate based on ambient conditions; for instance, the power required by chillers is directly dependent on the external air temperature. By defining the number

of itineraries g and the annual utilisation time fraction t_g, for each, the overall attribute value a is calculated as:

$$a = \sum_{1}^{g} a_g \cdot t_g \tag{3.139}$$

Where the sum of t_g equals 1 and a_g is the attribute for specific itinerary. By defining this set of operational attributes, it is possible to evaluate the ship's performance in scenarios that deviate from the nominal design conditions.

Following the definition of the operational attributes, their respective weights, the fuzzification process, and the Pareto filtering a TOPSIS algorithm was applied once again. This procedure enabled a second ranking specifically for the non-dominated designs.

Chapter 4

Application and Results

In this chapter, the proposed methodology will be applied to a luxury cruise ship.
The parametric ship model will be presented, the methodology implementation will be discussed and finally, the selection of the feasible design will be shown after applying the probabilistic simulation on the chosen itineraries.
Given that approximately 3965 designs will be simulated, the data for the central parametrised ship will be presented.

4.1 Parametric ship presentataion

Parametric modelling was implemented using Grasshopper, a visual programming environment integrated within Rhinoceros. As illustrated in Figure 4.1, the logic of Grasshopper is based on the use of functional components interconnected via a directed graph structure, commonly referred to as a data tree, where the data flow dictates the geometric generation. Figure 4.1 shows a complex Grasshopper definition used for parametric modelling. The script is composed of multiple interconnected components, organised into functional clusters highlighted in purple. The dense network of wires represents the data flow between different parts of the algorithm, indicating a high level of interdependency. The yellow components on the right correspond to the final outputs of the model. Overall, the image illustrates an advanced and highly customised parametric workflow.

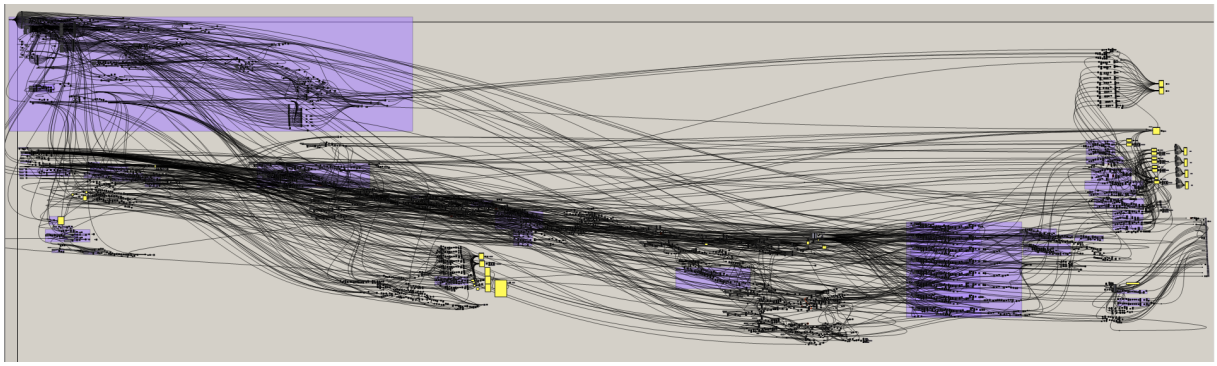

Figure 4.1: Grasshoper script

The modelling process started with the definition of the primary variables strictly applying the previously proposed methodology. The design variables and their respective ranges of variability were defined, the details of which are presented in Table 4.1.

The selected variables allow for precise modification of the hull geometry by adjusting pa-

Table 4.1: Design variables and variability ranges identified for the parametric model

Name	**Lower bound**	**Upper bound**	**Step**	**Unit**
PAX	796	1096	1	-
$NOPOD$	0	1	1	-
L_{OA}	218.000	260.000	-	m
$L_{SternProfile}$	0.950	1.000	0.010	-
$B/2$	14.300	17.300	-	m
$DK2$	2	6	-	-
$DK3$	1	5	-	-
$WheelDeck$	0	4	-	-
$HighDK$	1	5	-	-

rameters such as the length overall L_{OA}, the ship semi-breadth $B/2$, the shape of the stern profile $L_{SternProfile}$ as well as the inclusion or exclusion of a POD propulsion system. The $L_{stern_{profile}}$ coefficient modifies the length of the run, thereby determining the longitudinal extent of the stern's geometry. Concurrently, the superstructure is managed through the application of Boolean operators that regulate the presence of external areas for each deck. The notation adopted herein takes the BD as the primary datum.

Specifically, the boolean variable designated $DK2$ determines the inclusion of an external area on the embarkation deck, which houses the main public spaces such as the atrium and the theatre. As exemplified in Figure 4.2, the extent of this area depends on a variable dimensional parameter, which has been modelled to ensure that the boundary of the external space consistently coincides with a reinforced frame. This boolean can be set to 2 if there is no external area at the considered deck; otherwise, it is set to 6.

Figure 4.2: External area applied to the embarkation deck

A similar logic was applied to the first passenger cabin deck with $DK3$; as shown in Figure 4.3, the depth of the recess is controlled by a dimensional slider, configured to align the start of the superstructure with the first available reinforced frame. This boolean can be set to 1 if there is no external area at the considered deck; otherwise, it is set to 5.

Figure 4.3: External area applied to the first passenger cabin deck

Subsequent passenger decks do not feature recessed external areas; instead, they allow for the configuration of cabins or suites at both the bow and stern with the option of extended balconies, which can develop not only along the ship's side but also longitudinally towards the extremities. A third Boolean ($WheelDeck$) operator regulates the presence of external areas on the wheelhouse deck (Figure 4.4) , which constitutes the uppermost level intended for passenger cabins. This boolean can be set to 0 if there is no external area at the considered deck; otherwise, it is set to 4.

Figure 4.4: External area boolean on Wheelhouse deck

Finally, a further Boolean ($HighDK$) manages the open spaces on the highest deck (Figure 4.5) , where the ship has been modelled to include outboard walkways and aft areas for a potential

swimming pool. This boolean can be set to 1 if there is no external area at the considered deck; otherwise, it is set to 5.

Figure 4.5: External area boolean on highest deck

The deckhouses were also modelled on this deck as two distinct structures separated by the pool area, with the aft deckhouse configured to accommodate the funnel casing.
By varying the identified Boolean parameters, different superstructure configurations can be achieved. This includes, for instance, a ship featuring external areas on all designated decks, as shown in Figure 4.6, or a configuration entirely without external spaces, as illustrated in Figure 4.7.

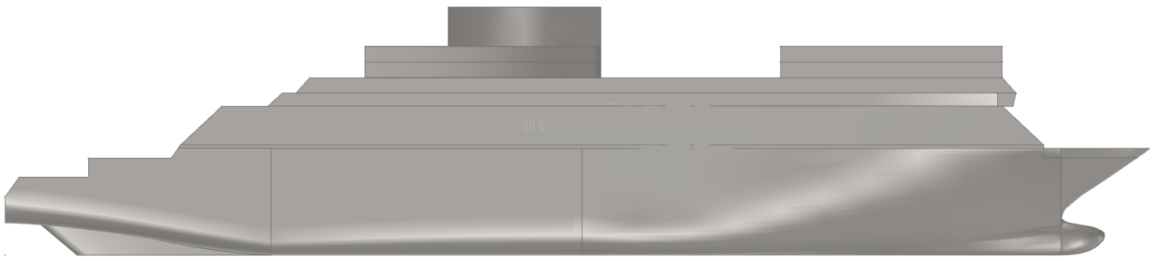

Figure 4.6: External areas on all designated decks

Figure 4.7: Configuration entirely without external spaces

This approach enables a comprehensive exploration of different architectural solutions by simply adjusting the logical inputs within the parametric model.
One of the primary variables in the model is the passenger capacity, a parameter whose variability is intrinsically linked to the total number of cabins and the required crew size. For a luxury cruise ship, the crew-to-passenger ratio is established at approximately 0.646, signifying more

than one crew member for every two passengers; concurrently, it is assumed that a standard balcony cabin accommodates an average of two people. Therefore, any fluctuation in the number of passengers necessitates a corresponding adjustment in both the cabin count and the crew complement. The interplay between the passenger capacity and the presence of external areas directly governs the number of decks dedicated to accommodation. Given that the number of cabins on the first passenger deck is limited by the available surface area, achieving the required capacity may necessitate an additional cabin deck compared to a configuration without external areas, where the internal floor space is inherently more extensive.

By employing the variables defined in Table 4.1, 3965 models were generated using the Monte Carlo sampling methodology. The design generation process was carried out using modeFrontier., which systematically adjusted the input variables for each design iteration to produce the respective three-dimensional models. Certain parameters, however, were maintained constant across all designs, as summarised in Table 4.2. A uniform cabin size was adopted for all projects

Table 4.2: Main ship parameters

Symbol	Description	Value
T_{des}	Design draught [m]	7.2
V_{des}	Design speed [kn]	19
V_{max}	Maximum speed [kn]	20
h_B	Bulb center height above keel [m]	3.47
C_X	Midship coefficient [-]	0.934
screw	Propulsion type	Twin Screw
$CSTERN$	Stern shape parameter [-] [56]	10
D	Propeller diameter [m]	4.6
Z	Number of blades [-]	6
L_{cab}	Cabin length [m]	12.3
B_{cab}	Cabin widht [m]	3.0
s	Frame spacing [mm]	750
n_{Evap}	Number of evaporators [-]	2
n_{Osmos}	Number of reverse osmosis units [-]	2

to ensure a consistent structural frame spacing throughout the models; this spacing is intrinsically linked to the cabin width, established at 3 m. Similarly, the range selected for the length overall was determined by considering the longitudinal spacing of the pillars, set at intervals of approximately 6 m. The definition of a fixed grid and the longitudinal position of the funnel facilitated the subdivision of each design into MFZ. Based on the passenger numbers, the minimum stair width required for evacuation was calculated in compliance with statutory regulations. Regarding the sizing of the stairways, the worst-case scenario was taken into account. With reference to the values presented in Table 4.3, the number of people per deck was calculated as the sum of the occupants originating from MFZ 2 and MFZ 3. This approach accounts for the emergency condition in which passengers from both zones converge into the same stair-

Table 4.3: N person per deck to embarkation Deck

DK	MFZ 1	MFZ 2	MFZ 3	MFZ 4
1^{st} Cab	62	52	52	60
2^{nd} Cab	58	52	52	62
3^{rd} Cab	55	52	52	58
4^{th} Cab	22	52	16	6

case, thereby necessitating maximum evacuation capacity. This task was executed via a Python script integrated within the Grasshopper model, which extracted the passenger count per MFZ and determined the minimum stair dimensions according to the number of decks. Once the staircase width and the overall cabin dimensions (including balconies) were established, the remaining corridor width was calculated. While regulations mandate a minimum corridor width of 900 mm, a threshold of 1100 mm was adopted for this study to provide a sufficient margin for the inclusion of fire extinguishers and handrails.

The designs that successfully passed the initial topological screening were analysed using a custom-made script developed in MATLAB. Those projects that failed to satisfy the constraint regarding minimum corridor width were discarded and flagged with the error code: "Topology, T0011, Corridors width < 1100 mm". The geometric and functional values defined in Section 3.1.3 were extracted from the parametric model, with Table 4.4 providing an illustrative example of the data generated for a simulated ship.

Table 4.4: Ship principal particulars of one of the simulated ship

Symbol	**Description**	**Value**
GT	Gross Tonnage (GT)	79688
L_{OA}	Length overall [m]	258
L_{WL}	Length on waterline [m]	248.20
L_{BP}	Length between perpendiculars [m]	248.20
B	Breadth moulded [m]	32.6
∇	Displacement volume [m^3]	37818.54
LCF	Longitudinal center of flotation [m]	109.43
LCB	Longitudinal center of buoyancy [m]	117.93
A_{BT}	Transverse bulb area [m^2]	18.87
C_B	Block coefficient [-]	0.647
A_{WP}	Waterplane area [m^2]	6816.98
C_{WP}	Waterplane area coefficient [-]	0.840
A_T	Transom immersed area at zero speed [m^2]	5.44

Continued on next page

Symbol	Description	Value
S	Wetted hull surface [m^2]	15847.14
i_E	Entrance angle coefficient [-] [56]	18.95
LE	Bow waterline entrance length [m]	82.93
LR	Stern waterline run length [m]	34.84
kyy	Longitudinal inertia radius [m]	62.05
A_{l_a}	Lateral windage area [m^2]	7345.59
sl	Lateral windage area centroid longitudinal position [m] [77]	-9.81
A_{f_a}	Transverse windage area [m^2]	1233.24
sf	Transverse windage area centroid height [m]	19.51
A_{l_w}	Lateral projected area underwater [m^2]	1690.85
A_X	Maximum section area [m^2]	219.44
P/D	Pitch diameter ratio [-]	1.105
A_E/A_0	Expanded area ratio [-]	0.739
isPod	Pod propulsion flag: 1 podded ship, 0 shaft line [-]	1
S_{pod}	Pod wetted surface [m^2]	49.93
PAX	Pax on board	996
$CREW$	Crew member	644

For the functional organisation of the decks located above the bulkhead deck, the internal spaces were categorised into macro-areas as follows:

- Passenger Cabins.
- Internal Public Spaces.
- External Public Spaces.
- Crew and Technical Areas.
- Wheelhouse and Deckhouse.
- Casing and Trunk.

The aforementioned macro-areas were further subdivided according to their respective MFZ, with the longitudinal, transverse, and vertical centres of gravity calculated for each areas. Tables in Appendix A provides an illustrative example of this spatial breakdown for one of the simulated ships (*Cruise_110*).
In contrast, a volumetric modelling approach was employed for the decks situated below the

BD. Each compartment was assigned a unique identification code (Type coloumn in Table B.1) based on its contents and functional type, providing the necessary data for the development of a comprehensive weight estimate:

- Ballast Room = 0,
- Thruster Room = 1,
- Tank Room = 2,
- Engine Room = 3,
- PEM Room = 4,
- Auxiliaries Room = 5,
- Technical Room = 6

A summary table categorising these rooms is provided in Appendix B for the *Cruise_110*. Furthermore, the longitudinal, transverse, and vertical centres for every individual compartment were recorded, ensuring precise mapping of the volume and weight distribution throughout the lower hull.

For each ship satisfying the minimum corridor width constraint, it was possible to determine the specific deck lengths, breadths, and heights. An example of a ship from the database is presented in Table 4.5. To ensure structural continuity and streamline the integration between the hull and the superstructure, the longitudinal positioning of the external areas was constrained to the primary framing layout. Specifically, based on the boolean parameters defining the presence of open decks, the superstructure boundaries were aligned with the nearest web frames according to the defined frame spacing. This approach ensures that the superstructure's end bulkheads are positioned directly above reinforced structural members capable of supporting the design loads.

In every instance, the vertical positions of the bulkhead deck, the preceding deck, and the two subsequent public decks remain constant. Regarding the vertical position of the double bottom, the SOLAS regulations were applied by placing it at $B/20$. Conversely, the vertical positions of the passenger cabin decks may vary according to the design requirements, particularly when an additional deck is necessitated by the presence of external areas which restrict the available space for cabin placement.

4.2 Ship resistance, propulsion and generation

A service speed of 19 knots and a maximum speed of 20 knots were assumed for all models. Based on the output variables obtained from the parametric modelling, the Holtrop-Mennen

Table 4.5: Deck lengths, breadths, and heights for one of simulated ship

L_{decks} (m)	B_{decks} (m)	Z_{Decks} (m)
185.646	20.140	0.000
232.587	30.854	1.630
240.341	31.994	7.000
239.192	32.600	9.800
242.532	32.600	12.600
245.877	32.600	16.800
213.000	32.600	21.000
193.000	32.600	23.800
187.000	32.600	26.600
181.000	32.600	29.400
175.000	32.600	32.200
165.000	32.600	35.000
156.000	32.600	38.360
102.000	23.016	41.720
102.000	23.016	45.080

method was applied to estimate total resistance, an example of which is illustrated for a simulated ship in Figure 4.8.

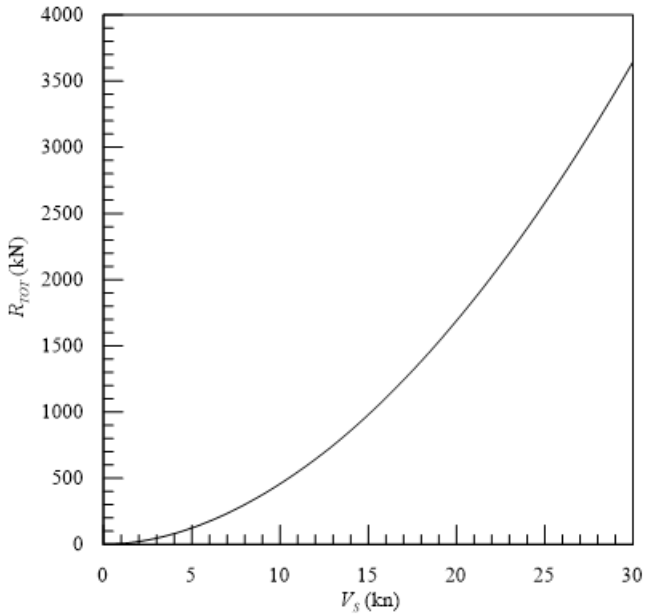

Figure 4.8: Ship resistance

The propeller selection process was conducted by calculating the propulsive coefficients according to the Holtrop-Mennen method for conventional hulls and the Flikkema method for podded ships. Utilising the Wageningen B-series polynomials, various propellers were generated across a range of pitch-to-diameter ratios, ultimately selecting the one demonstrating the highest open-

water efficiency. An open-water propeller diagram for a simulated ship is presented in Figure 4.9.

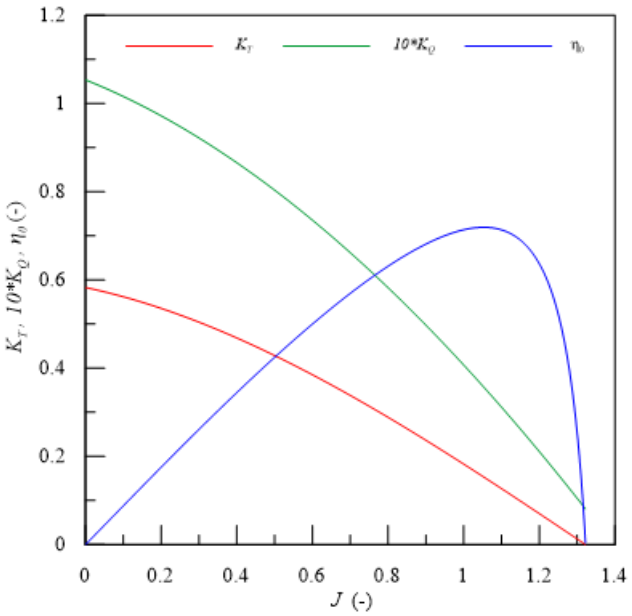

Figure 4.9: Screw diagram

Subsequently, the selection of either the POD unit or the PEM was performed. PEM or POD databases, summarised in Appendix D (Table D.1) , were utilised for this purpose. Table 4.6 outlines the efficiency assumptions adopted to determine the brake power required for the selection of the propulsion machineries. Finally, dimensional and propulsive feasibility checks

Table 4.6: Efficiency assumptions

η_{Mek}	η_{Conv}	η_{Tran}	η_{POD}	η_G	η_{sw}
0.97	0.95	0.95	0.96	0.97	0.999

were executed. A ship was rejected if the volume allocated for the PEM/POD was insufficient, if the pod or propeller exceeded the stern aperture dimensions, if there was potential mechanical interference between the two propellers or with the skeg, if the compartment width/length was narrower than the machinery footprint, or if the actual attainable speed remained below the specified maximum speed despite the machinery selection.

Subsequently, an estimation of the maximum electrical load was conducted for both seagoing and harbour conditions to establish a preliminary electrical balance. Table 4.7 provides an example of elaborated electric balance. Based on the underlying assumptions, the power consumption for the chillers and the onboard fresh water production machinery was isolated and calculated as shown in Table 4.8. Once the preliminary electrical balance was determined, the selection of the DG was performed. A father-son configuration consisting of four diesel

Table 4.7: Electric Balance

ID	NServS	NServW	NmaxS	NmaxW	ManS	ManW	HarbS	HarbW
Hull	219.066	219.066	219.066	219.066	2351.724	2351.724	12.525	12.525
Safety	407.632	407.632	407.632	407.632	441.820	441.820	173.425	173.425
Prop.	14956.533	14956.533	17346.097	17346.097	0.000	0.000	0.000	0.000
Engine	2390.321	2384.461	2390.321	2384.461	2351.724	2311.109	871.296	882.335
HVAC	6604.518	5717.781	6604.518	5717.781	6083.482	5279.956	3028.739	3070.736
Galley	781.361	815.069	781.361	815.069	708.149	613.984	154.180	161.363
Acc.	25.647	23.343	25.647	23.343	58.537	61.545	68.715	72.382
Lights	2134.421	2482.267	2134.421	2482.267	5374.317	6279.192	495.861	576.671
Total	27519.499	27006.152	29909.064	29395.717	17369.754	17339.331	4804.740	4949.437

Table 4.8: Chiller and Fresh water machineries electric balance

Type	NServS	NServW	NmaxS	NmaxW	ManS	ManW	HarbS	HarbW
Chiller	4461.814	3139.348	4461.814	3139.348	4052.573	2852.443	1715.902	1081.482
FW Mac	329.147	329.533	329.147	329.533	0.000	0.000	0.000	0.000

generators was adopted. From a database of engines, summarised in Appendix D (Table D.2), the configuration that best satisfied the power demand was selected. In this instance as well, dimensional checks were carried out to ensure the engines' footprint was compatible with the two dedicated engine rooms, and designs that failed to meet these geometric constraints were rejected, Table 4.9.

Table 4.9: Propulsion and generation rejection error

Type	Code	Description
Geometry	G0011	POD over the baseline
Geometry	G0012	POD over the ship breadth
Geometry	G0013	POD rotation interference
Geometry	G0014	Not enough space in the POD room
Geometry	G0015	PEM over the double bottom
Geometry	G0016	PEM over the ship breadth
Geometry	G0017	Propeller diameter interference
Geometry	G0018	Not enough space in the PEM room
Propulsion	P001	Maximum speed not reached
Propulsion	P002	No power plant configuration available

4.3 Ship tanks, weigth and stability

The estimation of volumes dedicated to fuel oil, fresh water, ballast water, black water, and grey water was subsequently performed. For the case study under consideration, the ships are powered exclusively by MGO, thereby eliminating the requirement for onboard exhaust gas scrubbers. The formulae presented in Section 3.2.5 were applied, and a representative exam-

ple for a simulated ship is provided in Table 4.10. Within this framework, a ship was subject

Table 4.10: Weigth results

W_{st} (t)	W_{ct} (t)	W_{ms} (t)	W_{EngAux} (t)	W_{HVAC} (t)	W_{El} (t)	W_{Gal} (t)	W_{Cab} (t)	W_{Pub} (t)	$W_{prop_{res}}$ (t)	DWT (t)
18634	1461	1537	1846	670	1124	92	3870	1579	2452	4492

to rejection if the available tank capacities were found to be insufficient relative to the estimated requirements. Regarding the ballast tanks, only the previously defined "Ballast type" rooms were considered. Conversely, fuel oil and fresh water tanks were allocated to "Tank" and "Void" rooms, specifically excluding double bottom spaces as these regions are unsuitable for the storage of such liquids. GBW tanks, however, were permitted within the double bottom volumes. The volumetric analysis was conducted by progressively subtracting the required capacities based on a predefined priority sequence, starting with MGO, followed by FW and GBW. Heeling tanks were not included in the analysis as the current parametric modelling remains strictly symmetrical, although future developments may incorporate such modifications. Table 4.11 outlines the specific error categories that lead to the rejection of a ship design.

For those ships satisfying the tank volume constraints, a preliminary weight estimate was con-

Table 4.11: Tank, weight and stability rejection

Type	Code	Description
FUEL	A001	Not enough space in volume in Tank Rooms
FW	A002	Not enough space in volume in Tank Rooms
GBW	A003	Not enough space in volume in double bottom
WB	A004	Not enough space in volume in Ballast Rooms
Weight	B001	The ship is bowed
Weight	B002	Ballast tons under minimun
Weight	B003	Ballast tons above maximun
Weight	B004	Weigth > bouyancy
Stability	S001	KGlimit criteria not compliant

ducted using the regression formulae detailed in Section 3.2.4. The total weight was distributed across the macro-areas generated by the parametric modelling. By utilising available databases, it was possible to define the percentage-based specific weight distribution for each macro-area. Table 4.12 details the coefficients applied to each weight component relative to the considered macro-areas. The residual weight was distributed across the volumes of the rooms located below the bulkhead deck. The results obtained for the various macro-volumes of *Cruise_110* ship, categorised by MFZ, are detailed in the tables within Appendix C . Subsequently, the longitudinal and vertical positions of the centre of gravity were calculated. Prior to determining the centre of gravity using Varignon's theorem based on the known centres of each area divided

Table 4.12: Weigth area and volume coefficients

ID	W_{ct}	W_{ms}	W_{EngAux}	W_{HVAC}	W_{El}	W_{Gal}	W_{Cab}	W_{Pub}	$W_{prop_{res}}$
Internal Public Spaces	0.000	0.000	0.000	0.000	0.000	0.752	0.200	0.235	0.000
Passenger Cabins	0.000	0.000	0.000	0.000	0.000	0.000	0.350	0.000	0.000
Crew areas	0.000	0.000	0.000	0.000	0.000	0.000	0.450	0.000	0.000
External Public Spaces	0.736	0.324	0.000	0.000	0.000	0.000	0.000	0.565	0.000
Trunk and technical spaces	0.189	0.000	0.650	0.750	0.750	0.048	0.000	0.000	0.412
Residual	0.075	0.676	0.350	0.250	0.250	0.200	0.000	0.200	0.588

by MFZ, the weights of the diesel generators and propulsion motors, specifically calculated for each design and accounting for their onboard placement, were added to the propulsion weight component ($W_{prop_{res}}$).

Following the calculation of the lightship weight and the deadweight using the formula presented in Section 3.2.5, ships with a total weight exceeding their displacement were rejected. MGO, GBW, FW are considered in deadweight regression. The remaining ships underwent stability check to ensure an even keel condition. Based on the longitudinal positions of the centre of gravity and the centre of buoyancy, the volume of ballast water required to trim the ship was calculated. The ballast water quantity was constrained by the maximum capacity of the ballast tanks and the difference between total weight and displacement, ensuring that the equilibrium between weight and buoyancy remained valid.

The ships were then analysed based on their trim angle; those found to be trimmed by the bow were rejected, whereas ships on an even keel or trimmed by the stern were accepted. Table 4.11 lists the error categories for project rejection. Once the necessary ballast for trimming was determined, the vertical and longitudinal positions of the centre of gravity were updated. The vertical position of the centre of gravity was then compared against the limiting KG permitted by the three criteria cited in Section 3.2.6. Should at least one of these criteria remain unsatisfied, the ship was rejected with the corresponding error category.

4.4 Attributes and 1st Step Ranking

The attributes for the 1st selection stage were defined focusing on parameters that deck technical performance and economic viability. The first attribute considered is the ratio of ballast water weight to total displacement (W_{WB}/Δ), incorporating both the weight components required for reaching even keel condition and the design design draught. A high value in this ratio suggests a suboptimal weight distribution, as it forces the ship to carry non-remunerative weight, thereby diminishing overall transport efficiency. Hence, a low value of this attributes favours designs having a good alignment between LCG and LCB, as well as a good agreement between weight and buoyancy forces. Although the ballast water ratio W_{WB}/Δ represents a small fraction of displacement and has limited operational relevance for luxury cruise ships, it remains a useful concept-design indicator, as it reflects the degree of mass–buoyancy consis-

tency and longitudinal balance achieved without corrective non-remunerative weight . From a commercial perspective, the Gross Tonnage per Passenger ratio (GT/PAX) was identified as an attribute to be minimised. A lower value in this metric indicates higher passenger density relative to ship size, which optimises construction costs and port/canal fees per passenger. This attribute also favours the maximization of carried passengers. Similarly, while a low GT/PAX may conflict with the experiential definition of luxury, its inclusion in the first selection stage serves as an economic efficiency proxy, ensuring that candidate designs do not rely on excessive enclosed volume per passenger. The implicit assumption is that all designs already satisfy a minimum luxury threshold, and that GT/PAX is controlled rather than optimised for minimum value.

Finally, energy efficiency was addressed through the average SFOC and the fuel consumption per nautical mile (fc/nm). Once the electrical balance for each individual project was established, and taking into account the selected configuration alongside the ISO SFOC values specified in the engine datasheets, it was possible to determine the hourly fuel consumption for the various operational modes. Specifically, the SFOC was calculated for both the seagoing condition ($SFOC_{nav}$) at service speed and the harbour stay condition ($SFOC_{port}$). The average SFOC ($\overline{SFOC}$) was calculated by integrating the operational profiles for both seagoing and harbour conditions, the latter estimated at 120 days per year, allowing for an assessment of the diesel generators' actual efficiency across the entire operational cycle. With t_p defined as the ratio of annual days spent in port to the total number of days in a year, the attribute was calculated as follows:

$$\overline{SFOC} = SFOC_{port} \cdot t_p + SFOC_{nav} \cdot (1 - t_p) \tag{4.1}$$

The fc/nm attribute, which must be minimised, represents the fuel consumed for every nautical mile travelled at design speed; this is a critical parameter not only for reducing operational expenditure (OPEX) but also for enhancing the ship's environmental profile in compliance with current emission regulations, in particular CII.

To conduct a qualitative ranking of the design variants, a subjective weight was assigned to each attribute based on its strategic and technical significance relative to the other parameters, using AHP method. High priority was given to W_{WB}/Δ due to fundamental role in assure an high feasibility of the alternative. The fuzzification of this attribute was specifically calibrated to target an ideal value of zero, establishing a range between the maximum and minimum permissible ballast. Notably, the inclusion of small negative ballast values and higher positive ballast values as a lower bound and upper bound, respectively, allows the model to avoid rejecting projects with low weight surplus or moderate buoyancy surplus, ensuring that highly efficient configurations, which might otherwise be clipped by the membership function, are retained for further refinement in the next stages of design process. Nevertheless, alternatives with almost

null ballast are preferred.

Regarding volumetric and economic indicators, the attribute GT/PAX was categorised as being between medium and high importance. This attribute is targeted for minimisation to encourage designs with higher volumetric efficiency per passenger, thereby reducing capital expenditure and port-related fees.

Finally, propulsive and energy efficiency were incorporated by assigning medium importance to both the $\overline{SFOC}$ and fc/nm. Both attributes were subjected to minimisation to ensure reduced operational expenditure and enhanced environmental compliance.

Table 4.13 provides a comprehensive summary of the selected attributes, including their respective weights, fuzzification types [1], and variability ranges.

A total of 3965 cases were simulated, resulting in 93 feasible designs. Following the application of the Pareto frontier, 32 non-dominated projects were identified. The pie chart presented in Figure 4.10 illustrates that approximately 49% of the projects were rejected due to topological constraints, specifically where the corridor width was below the mandatory 1100 mm limit. The second most frequent cause for exclusion, accounting for roughly 40% of the cases, pertained to ballast-related issues. Approximately 11% of the designs were excluded due to propulsion errors, with the remainder rejected based on geometric and stability constraints.

Table 4.13: Design attributes at 1^{st} Step Ranking

Attributes	Weight	Type	$\overline{y}$	y_{j*}	y_j^*	units
W_{WB}/Δ	0.5	1	0	-0.005	0.05	-
GT/PAX	0.25	3	68.846	68.846	102.292	-
$\overline{SFOC}$	0.125	3	168.284	168.284	181.411	g/(kWh)
fc/nm	0.125	3	0.376	0.376	0.538	t/nm

[1] 1 - Attribute converging towards a target value $\overline{x}$; 2 - Attribute to be maximised; 3 - Attribute to be minimised; 4 - Attribute diverging from a specific value $\overline{x}$

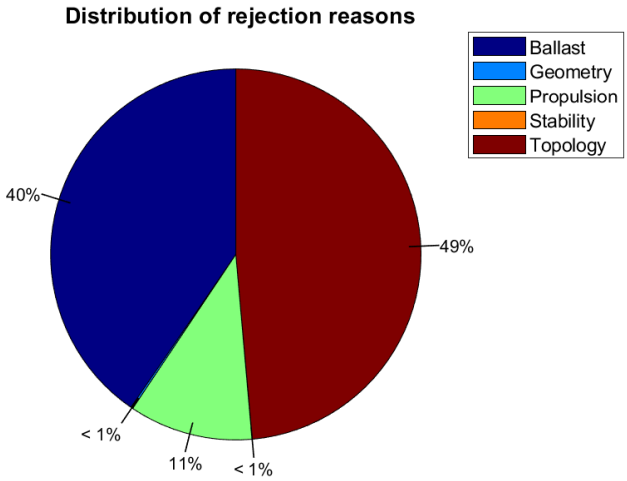

Figure 4.10: Distribution of rejection reasons

By analysing the specific causes within each error category 100% of the rejections for the "Geometry", "Stability", "Propulsion" and "Topology" categories were attributed respectively to "G0011: POD over the baseline", "S001: KGlimit criteria not compliant", " P001: Maximum speed not reached" and "Topology, T0011, Corridors width < 1100 mm" . In detail, regarding "Ballast" errors, the pie chart in Figure 4.11 shows that approximately 87% of these failures are classified as "B004: Weight > bouyancy", 10% as "B001: The ship is bow by trim", and the remaining 3% as "B003: Ballast tons above maximun". The latter condition occurs when the ballast water weight required to satisfy the weight-buoyancy equilibrium and trim requirements exceeds the total available capacity of the dedicated ballast tanks.

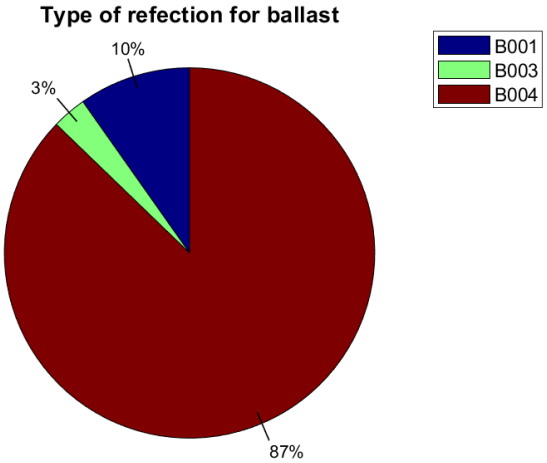

Figure 4.11: Type of refection for ballast

Following the identification of the feasible designs, the selection of the optimal onboard power

plant configuration was conducted. The pie chart in Figure 4.12 illustrates the probabilistic distribution of the selected configurations within the valid sample space. The legend categorises each entry by the manufacturers, and the specific engines model.
The pie chart illustrates the relative frequency of the main engine configurations selected during the sampling of the vessel population. There is a clear prevalence of solutions based on MAN engines, which together account for over 59% of the sample, with the (14V32/44CR + 14V32/44CR) combination being the most frequent at 25%. Regarding the manufacturer Wärtsilä, the most represented configuration is the (12V31 + 14V31) at 29%.
It is interesting to note that "father and son" configurations are the most frequent, offering greater flexibility in meeting electrical and propulsion demands across different operational conditions.

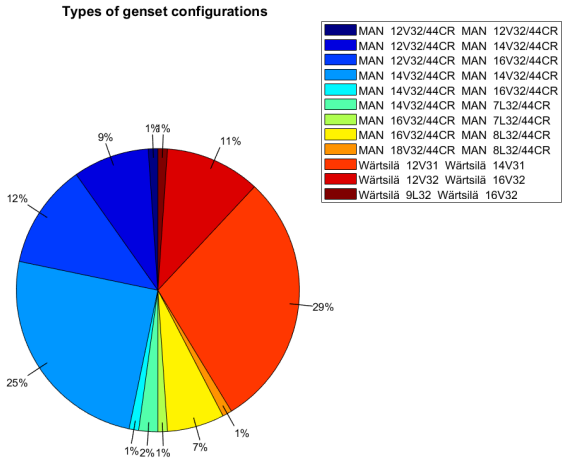

Figure 4.12: Types of genset configurations

The non-dominated designs belonging to the Pareto frontier were subsequently analysed using the TOPSIS method to establish a performance ranking. Table 4.14 presents the decision variables, performance attributes, and the respective weighting coefficients applied within the TOPSIS algorithm. The ship ranked in the first position has been identified as the feasible ship for this initial step.

4.4.1 Variable - variable analisys

An analysis of the design space is now conducted on a variable-by-variable basis. In the plots presented in Figures 4.13 to 4.18, red markers denote unfeasible projects, while blue markers represent feasible but dominated ships. Green markers indicate the non-dominated projects identified through Pareto frontier screening, and the yellow marker highlights the best ship selected following the 1st stage process. Figure 4.13 displays the stern vault coefficient $L_{SternProfile}$ as a function of the ship's B. As observed, the feasible design space is predominantly distributed towards larger beams; narrower ships were systematically rejected due to non-compliance with the mandatory minimum corridor width constraint of 1100 mm.

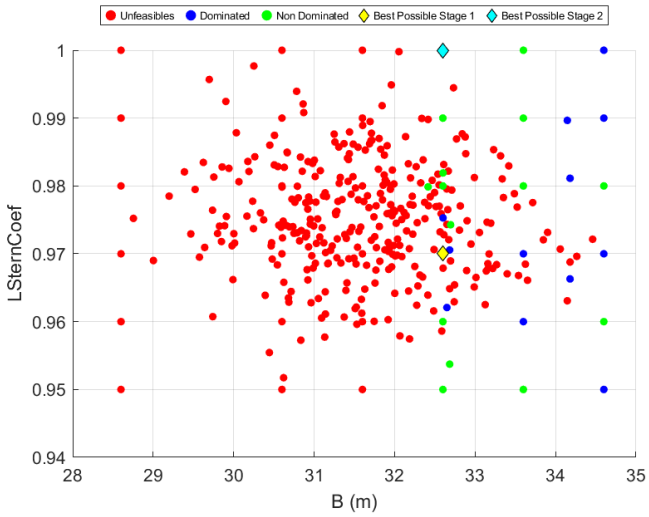

Figure 4.13: B vs $L_{SternProfile}$

The analysis now examines the correlation between the B and its passenger capacity , as presented in Figure 4.14. The distribution of data points clearly highlights the impact of the topological constraint regarding the minimum corridor width. A high density of unfeasible projects is observed for B values below approximately 32.5 m; this confirms that, regardless of passenger capacity, a cross-section that is too narrow fails to accommodate the mandatory internal circulation requirements.

The positioning of the best possible ship (1st stage) is of particular interest: it is situated at the upper extremity, around 1100 passengers and near the lower bound of the feasibility range for the beam. This distribution indicates that the ranking model favoured a configuration capable of maximising number of passengers while maintaining the minimum beam necessary for feasibility. This choice is optimal from a hydrodynamic perspective, as a restricted beam contributes to reducing hull resistance and, consequently, overall fuel consumption.

Table 4.14: First Step ranking

Pos	ID	L_{OA} (m)	B (m)	NO POD (-)	PAX (-)	$L_{Stern_{Profile}}$ (-)	$DK2$ (-)	$DK3$ (-)	$WheelDeck$ (-)	$HighDK$ (-)	W_{WB}/Δ (-)	GT/PAX (-)	$\overline{SFOC}$ g/kWh	fc/nm t/nm	d_k^+ (-)	d_k^- (-)	C_k (-)
1	'Cruise_1210'	258.000	32.600	1	1096	0.970	6	5	0	1	0.002	72.751	174.998	0.513	0.127	0.535	0.809
2	'Cruise_2928'	260.000	33.600	1	996	0.950	2	5	0	5	0.003	83.402	170.803	0.441	0.125	0.497	0.799
3	'Cruise_3561'	242.000	32.600	0	996	0.960	6	5	0	5	0.007	76.092	174.879	0.510	0.145	0.477	0.767
4	'Cruise_3763'	243.734	32.696	1	900	0.974	2	5	0	1	0.006	81.189	174.253	0.492	0.148	0.475	0.762
5	'Cruise_2276'	242.000	32.600	1	1096	1.000	2	5	4	5	0.014	68.886	169.592	0.458	0.142	0.455	0.762
6	'Cruise_1981'	248.000	32.600	1	996	1.000	2	5	0	1	0.007	76.557	174.800	0.512	0.149	0.473	0.761
7	'Cruise_1928'	248.000	32.600	1	896	0.950	2	5	0	1	0.008	83.625	169.963	0.460	0.146	0.457	0.758
8	'Cruise_736'	258.000	32.600	1	896	0.990	6	5	0	1	0.003	84.325	175.084	0.509	0.169	0.487	0.742
9	'Cruise_560'	248.000	32.600	1	996	0.950	6	5	0	1	0.007	77.118	180.042	0.505	0.172	0.472	0.733
10	'Cruise_110'	258.000	32.600	1	996	0.990	6	5	0	1	0.005	80.008	179.881	0.508	0.177	0.476	0.729
11	'Cruise_904'	258.000	34.600	1	896	0.980	6	5	0	1	0.001	89.653	175.088	0.492	0.191	0.503	0.725
12	'Cruise_1817'	258.000	34.600	1	896	0.960	6	5	0	1	0.003	89.710	174.899	0.487	0.190	0.486	0.719
13	'Cruise_3285'	242.000	32.600	1	796	0.950	2	5	0	1	0.006	93.363	170.138	0.450	0.200	0.456	0.695
14	'Cruise_556'	248.000	32.600	1	996	0.980	6	5	0	1	0.011	77.051	180.045	0.507	0.193	0.432	0.691
15	'Cruise_2575'	254.000	33.600	1	796	1.000	6	5	4	5	0.001	102.291	170.722	0.454	0.258	0.497	0.658
16	'Cruise_1421'	248.000	32.600	1	996	0.950	6	5	0	1	0.019	77.118	170.523	0.456	0.200	0.379	0.655
17	'Cruise_2812'	242.000	32.600	1	1096	0.960	6	1	0	1	0.022	68.846	169.777	0.450	0.220	0.391	0.640
18	'Cruise_476'	248.000	32.600	1	996	0.970	6	5	0	1	0.021	77.074	170.284	0.447	0.217	0.363	0.627
19	'Cruise_931'	258.000	32.600	1	796	0.990	6	5	0	1	0.014	94.918	170.391	0.449	0.243	0.379	0.609
20	'Cruise_1821'	248.000	32.600	1	996	0.970	6	5	0	1	0.024	77.074	177.089	0.443	0.258	0.328	0.560
21	'Cruise_3144'	242.000	32.600	0	896	0.950	6	5	0	5	0.024	80.511	169.298	0.457	0.257	0.325	0.558
22	'Cruise_3409'	242.000	33.600	0	996	0.990	6	5	0	1	0.027	79.819	169.188	0.448	0.281	0.306	0.521
23	'Cruise_149'	258.000	32.600	1	796	1.000	6	5	0	1	0.022	94.888	170.306	0.443	0.292	0.306	0.512
24	'Cruise_1827'	248.000	32.600	1	996	0.950	6	5	0	1	0.027	77.118	177.088	0.443	0.290	0.300	0.509
25	'Cruise_3772'	224.766	32.602	0	1023	0.982	6	5	0	5	0.037	74.024	169.424	0.453	0.368	0.272	0.425
26	'Cruise_1916'	248.000	32.600	0	996	1.000	6	1	0	1	0.038	74.946	169.097	0.452	0.375	0.265	0.414
27	'Cruise_3744'	236.354	32.684	0	937	0.954	2	5	0	5	0.043	76.188	168.826	0.466	0.427	0.237	0.357
28	'Cruise_1163'	248.000	32.600	0	996	0.990	6	1	0	1	0.046	74.968	168.979	0.470	0.456	0.236	0.342
29	'Cruise_2101'	218.000	33.600	0	996	0.980	6	5	4	1	0.051	72.403	173.283	0.376	0.495	0.255	0.340
30	'Cruise_200'	228.000	32.600	0	896	0.980	2	5	0	1	0.045	77.663	168.284	0.453	0.454	0.225	0.332
31	'Cruise_3694'	242.457	32.416	0	919	0.980	2	5	4	1	0.050	78.587	168.928	0.452	0.500	0.212	0.297
32	'Cruise_3219'	242.000	32.600	0	796	0.990	6	5	0	5	0.048	93.530	176.182	0.425	0.509	0.104	0.169

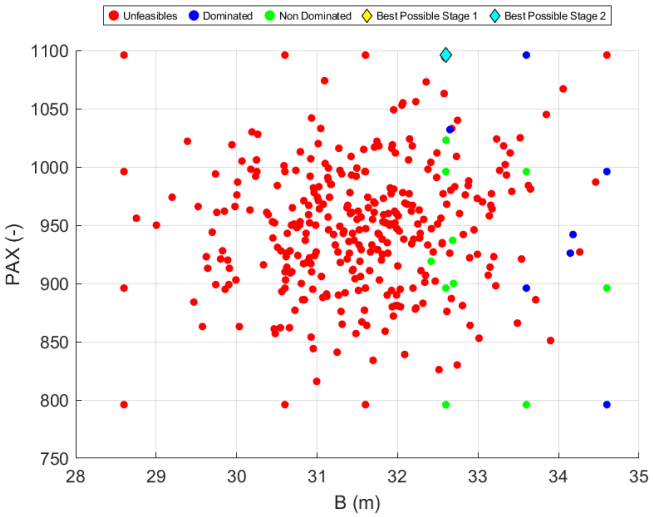

Figure 4.14: B vs PAX

The examination of the design space continues with the analysis of the relationship between the L_{OA} versus B, as illustrated in Figure 4.15.

A distinct horizontal separation is observed at approximately 32.5 m of B; below this threshold, almost all projects are classified as unfeasible due to the topological constraint requiring a minimum corridor width of 1100 mm. In contrast, the length overall exhibits a more heterogeneous distribution, spanning a range between 218 m and 260 m.

The best possible ship (1st stage) is strategically positioned at the far right of the plot, near the maximum L_{OA} simulated value while maintaining a beam at the lower bound of the feasibility range. This positioning indicates that the model prioritised increasing length over beam to maximise both efficiency and transport capacity.

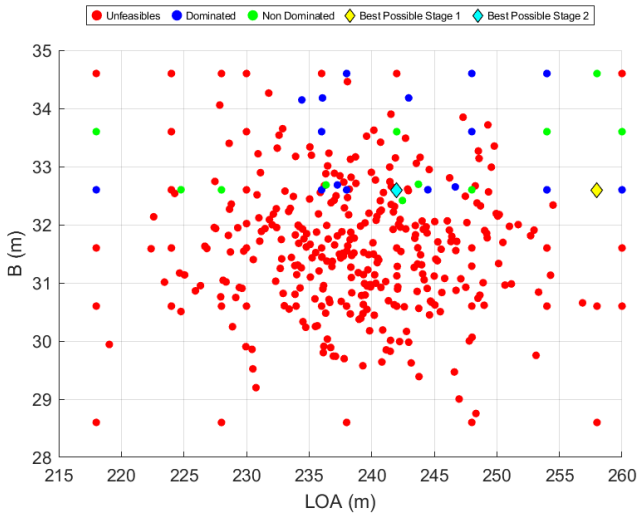

Figure 4.15: L_{OA} vs B

The examination of the design space now focuses on the relationship between the L_{OA} and the $L_{SternProfile}$, as illustrated in Figure 4.16. The distribution of results highlights how the combination of these two geometric parameters significantly influences both the feasibility and the optimality of the ship design.

Observation of the plot reveals a concentration of unfeasible projects in the central region of the simulated space, particularly for lengths between 230 m and 245 m. Conversely, the dominated and non-dominated units tend to cluster towards the higher values of length overall.

The best possible ship (1st stage) is positioned at an L_{OA} of approximately 258 m, confirming the model's tendency to favour longer hulls to maximise volumetric capacity and passenger count. Regarding the $L_{Stern_{Profile}}$ parameter, the chosen unit features a value of 0.97. This positioning indicates that, for a given high length, an intermediate stern coefficient provides the best compromise between aft weight distribution and the hull's hydrodynamic performance. This configuration avoids the stability issues or excessive resistance that would typically characterise extreme coefficient values when combined with such a significant length overall.

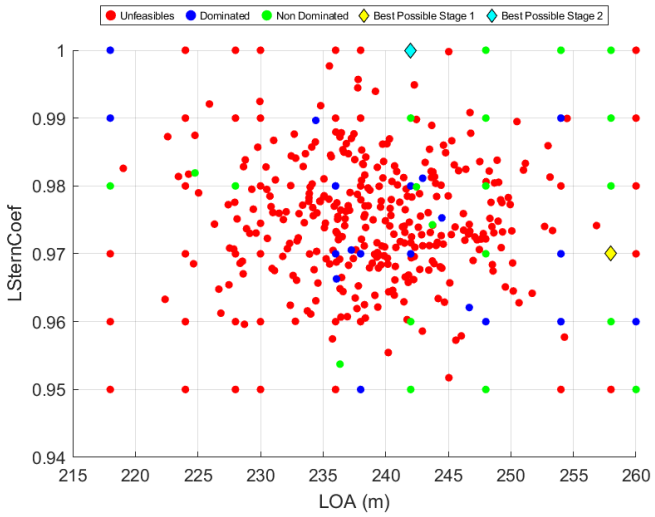

Figure 4.16: L_{OA} vs $L_{Stern_{Profile}}$

The examination of the design space goes on with the analysis of the relationship between L_{OA} and its PAX, as illustrated in Figure 4.17. The distribution of results highlights how these two variables serve as the primary drivers for the profitability and volumetric efficiency of the design.

The best possible ship (1st stage) through the ranking process is located at the point of maximum passenger capacity and maximum length overall. This positioning is significant; it indicates that, among all feasible units, the model identified the largest configuration as the most high-performing.

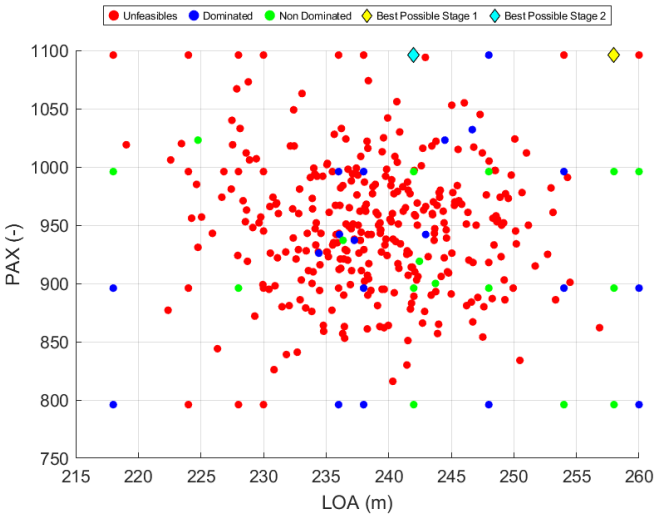

Figure 4.17: L_{OA} vs PAX

The analysis continues by examining the relationship between PAX and the $L_{Stern_{Profile}}$, as illustrated in Figure 4.18. This plot enables an assessment of how the choice of aft geometry interacts with the ship's payload capacity to determine the overall feasibility and efficiency of the design.

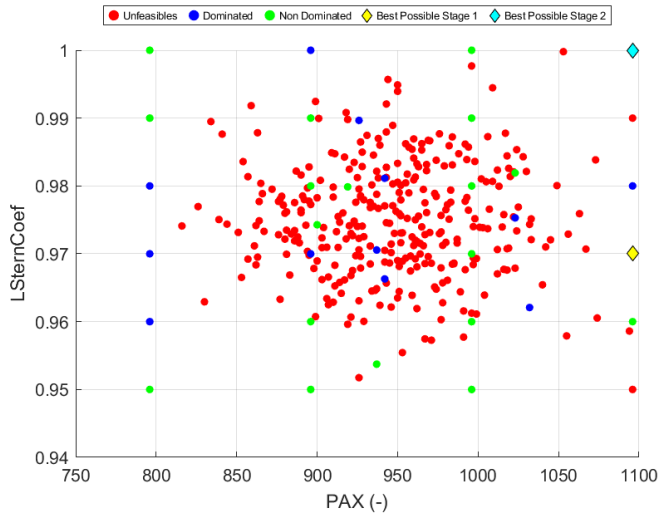

Figure 4.18: PAX vs $L_{Stern_{Profile}}$

4.4.2 Variable - attribute analisys

The analysis now shifts to the variable-attribute examination, aimed at evaluating the functional performance of the design space. In Figures 4.20 to 4.34, only feasible units are displayed to provide a clearer visualization of the efficiency distribution. The plots allow for a distinct

separation between dominated ships (blue markers) and those situated on the Pareto frontier (green markers), which represent the upper bound of achievable performance for the considered criteria. The yellow marker highlights the best possible ship (1st stage) identified during the first-step ranking process, representing the feasible compromise solution within the feasible set. The analysis continues with an examination of the relationship between the W_{WB}/Δ versus B , as illustrated in Figure 4.19. This plot focuses exclusively on feasible units, highlighting the trade-off between stability requirements and deadweight efficiency.

Observation of the distribution reveals that the majority of feasible solutions are clustered around a beam of approximately 32.6 m. Within this region, theW_{WB}/Δ varies significantly, ranging from near-zero values to over 0.05. The Pareto frontier defines the lower bound of this distribution, identifying designs that satisfy hydrostatic equilibrium with the minimum required amount of onboard ballast.

The best possible ship (1st stage) is positioned at the lower extremity of the Pareto frontier for the 32.6 m beam, exhibiting a near W_{WB}/Δ zero value. This positioning is highly significant for design efficiency. Minimising ballast requirements allows for a reduction in total displacement for a given useful volume, directly translating into lower hull resistance and a reduction in both fuel consumption and emissions.

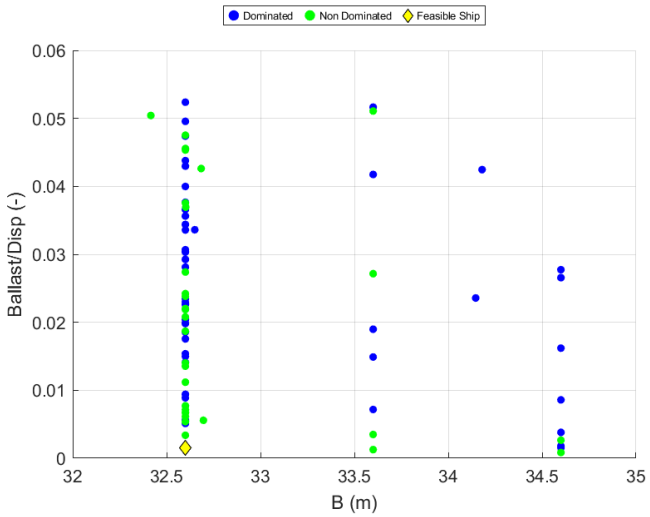

Figure 4.19: B vs W_{WB}/Δ

The analysis of performance attributes continues with the fc/nm as a function of the B, as illustrated in Figure 4.20. This plot enables an assessment of the energy efficiency of the feasible units only, highlighting how geometric choices directly influence the operational and environmental impact of the design.

From the data distribution, it is observed that most configurations cluster at a beam value of approximately 32.6 m, where fuel consumption varies between 0.42 and 0.54 t/nm. The Pareto

frontier identifies the designs that minimise fuel consumption for each specific beam value. Notably, a non-dominated unit with a wider beam achieves the absolute minimum consumption value, suggesting that a slightly wider hull may, in certain scenarios, offer better propulsive efficiency.

The best possible ship (1st stage), while not the absolute best in terms of minimum consumption, records a value of approximately 0.51 t/nm. This choice indicates that the ranking process balanced fuel efficiency against other attributes. Consequently, the model favoured a compromise solution that ensures high operational profitability alongside sustainable energy consumption.

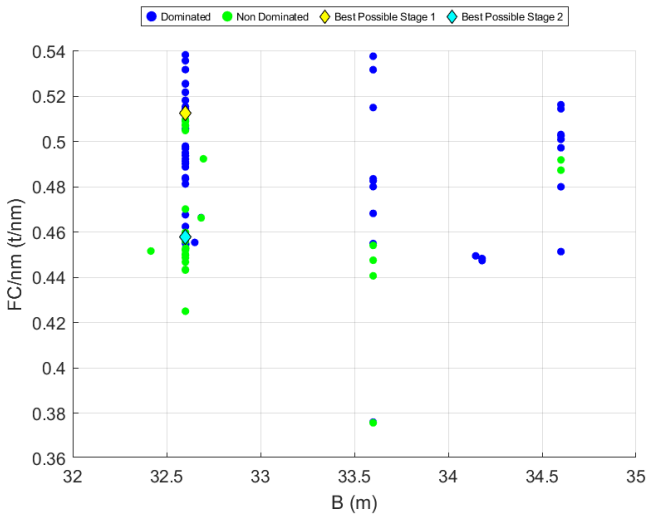

Figure 4.20: B vsfc/nm

The analysis continues by examining the GT/PAX as a function of B, as illustrated in Figure 4.21.

The plot shows that the majority of feasible units cluster at a beam of approximately 32.6 m, with GT/PAX values ranking widely between 68 and 98. The Pareto frontier defines the lower bound of this data set, identifying designs that maximise internal space utilisation by offering the lowest gross tonnage volume required per passenger. Additionally, a non-dominated unit at a wider beam is observed, featuring a high comfort ratio.

The best possible ship (1st stage) is positioned at the lower end of the distribution for the 32.6 m beam, with a GT/PAX value of approximately 73.

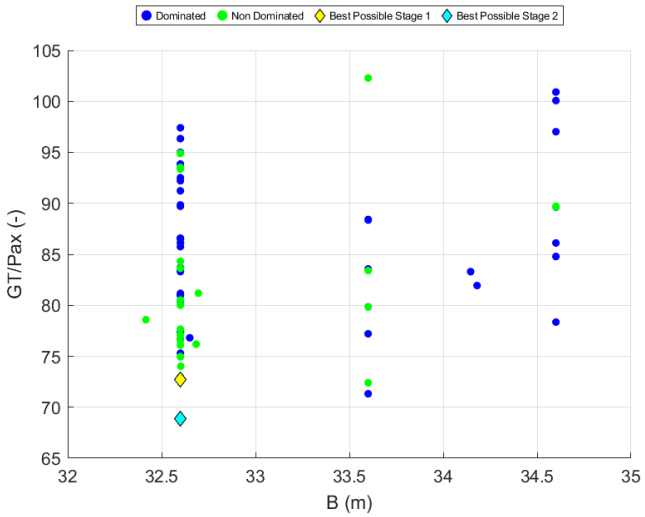

Figure 4.21: B vs GT/PAX

The analysis proceeds with the examination of the relationship between the $\overline{SFOC}$ attribute and the B variable, as illustrated in Figure 4.22.

Observation of the plot reveals that best possible ship (1st stage)s cluster around specific discrete beam values, with the highest concentration at 32.6 m. Within this region, $\overline{SFOC}$ values vary significantly, ranging from approximately 168 g/kWh to 180 g/kWh. The Pareto frontier identifies configurations that minimise specific consumption for each beam value, representing the selection of the most technically efficient engine sets.

The best possible ship (1st stage) exhibits an $\overline{SFOC}$ value of approximately 175 g/kWh at a beam of 32.6 m. Although configurations with lower specific consumption exist within the same beam range, the selection of the unit reflects a global optimisation strategy.

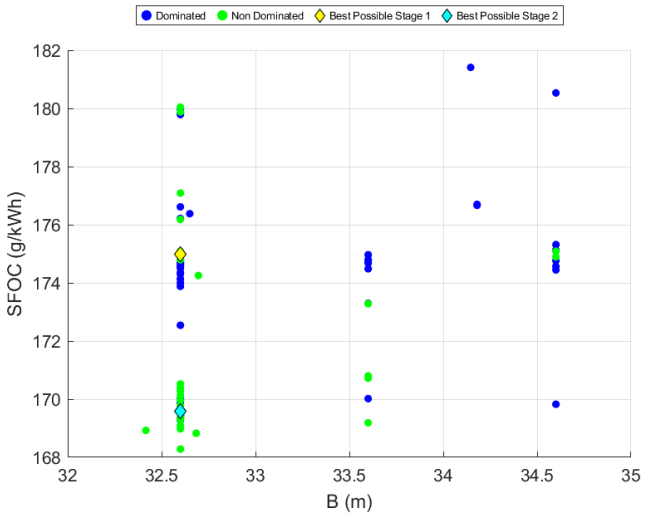

Figure 4.22: B vs $\overline{SFOC}$

Figure 4.23 illustrates the relationship between W_{WB}/Δ attribute and L_{OA} variable . The plot shows a significant dispersion of feasible solutions, with ships on the Pareto frontier tending to occupy the minimum ballast levels for each simulated length interval.
The best possible ship (1st stage) is located at the far right of the graph, combining the maximum length overall with a W_{WB}/Δ value close to zero.

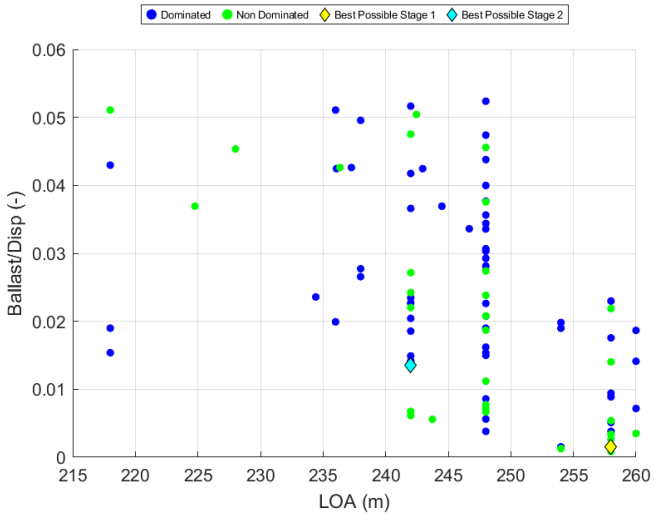

Figure 4.23: L_{OA} vs W_{WB}/Δ

Figure 4.24 shows the fc/nm as a function of the L_{OA}.
A clear proportional trend emerges from the distribution of results: as the overall length of the ship increases, there is a corresponding rise in fuel consumption per mile. This phenomenon is physically attributable to the higher displacement and greater wetted surface area characteristic of longer hulls. The Pareto frontier identifies the configurations that minimise energy expenditure for each length interval, representing the hull forms with the best hydrodynamic efficiency or the most high-performing propulsion systems.
The best possible ship (1st stage) is positioned at a length of approximately 258 m, with a fuel consumption of about 0.51 t/nm. This unit exhibits higher absolute consumption compared to shorter ships, maybe beacuse the attribute is less important than other.

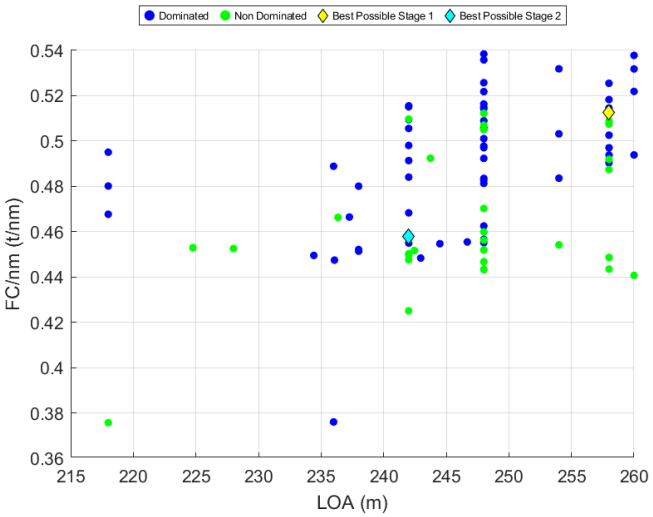

Figure 4.24: L_{OA} vs fc/nm

Figure 4.25 shows the GT/PAX as a function of the L_{OA}.
. This parameter is crucial for defining the ship's service standard, as a higher GT/Pax value is generally associated with increased availability of public spaces and a superior level of comfort for guests.
The best possible ship (1st stage) is located at a length of approximately 258 m, exhibiting a GT/PAX value of about 73. This positioning is particularly noteworthy: the unit lies below the main cluster of data points and even below the Pareto frontier observed for other lengths. This indicates that the best possible ship (1st stage) has been optimised for maximum commercial efficiency, offering a generous volume in absolute terms but distributed across a high passenger count.

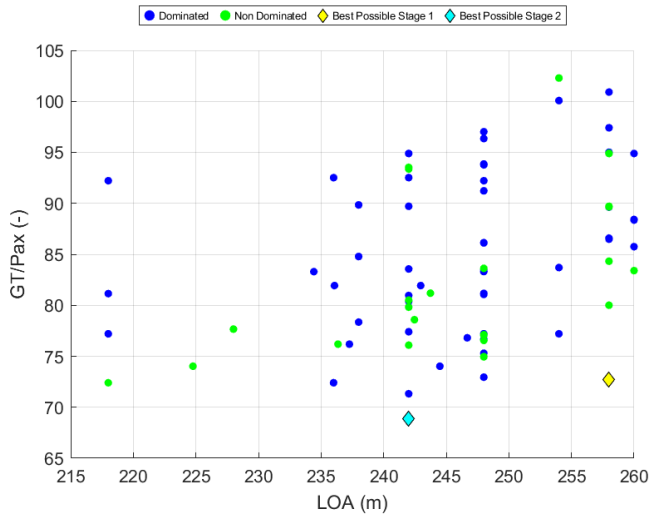

Figure 4.25: L_{OA} vs GT/PAX

Figure 4.26 shows the $\overline{SFOC}$ as a function of the L_{OA}.
The best possible ship (1st stage) is positioned at anL_{OA} of approximately 258 m with an SFOC value of 175 g/kWh. Although this unit does not sit on the Pareto frontier for minimum specific consumption, its selection indicates a system-wide optimisation. The value of 175 g/kWh suggests the adoption of an engine configuration that provides an ideal compromise between energy efficiency, operational reliability, and the capacity to meet the high electrical load requirements necessary for a ship of this size and passenger capacity.

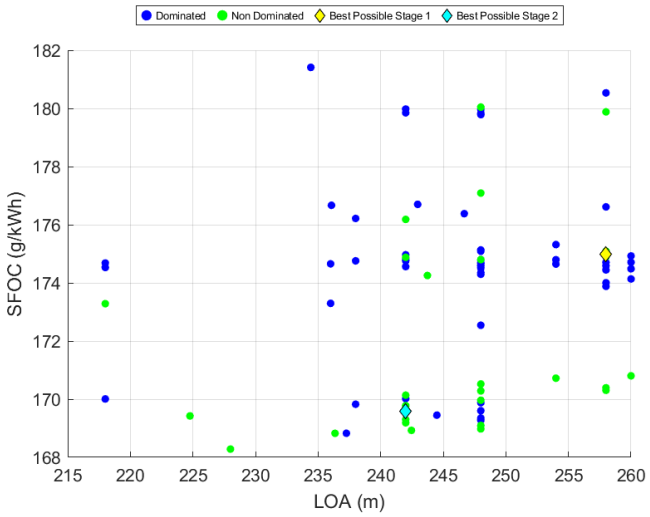

Figure 4.26: L_{OA} vs $\overline{SFOC}$

Figure 4.27 shows the W_{WB}/Δ as a function of the $L_{Stern_{Profile}}$.
The best possible ship (1st stage) is positioned at an $L_{Stern_{Profile}}$ of 0.97, recording an extremely low, nearly zero W_{WB}/Δ value. This result highlights the decision of the selected design: the stern configuration has been calibrated to ensure the necessary stability without burdening the ship with deadweight. Operating with minimum ballast allows the best possible ship (1st stage) to maintain a reduced displacement, directly optimising propulsive efficiency and reducing the environmental impact associated with the transport of ballast water.

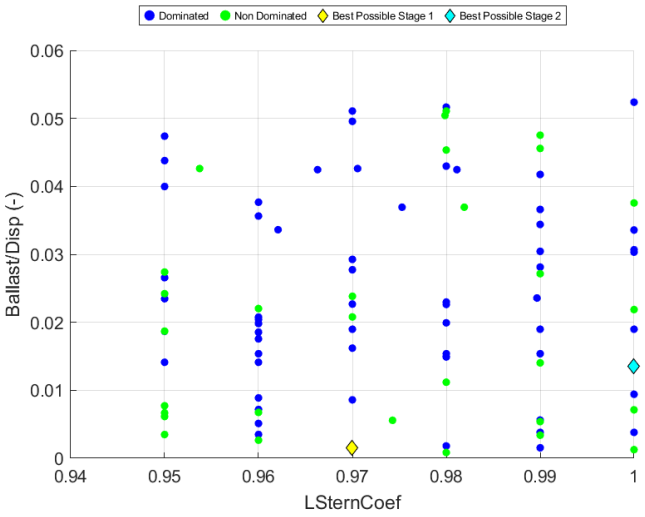

Figure 4.27: $L_{SternProfile}$ vs W_{WB}/Δ

Figure 4.28 shows the fc/nm as a function of the $L_{Stern_{Profile}}$.
The best possible ship (1st stage) is positioned at an $L_{Stern_{Profile}}$ of 0.97, with a fc/nm of approximately 0.51 t/nm. Although units with lower consumption exist for the same coefficient, the best possible ship (1st stage) represents an optimal equilibrium point: the 0.97 value ensures the necessary volume for aft technical compartments and a smooth water flow to the propellers.

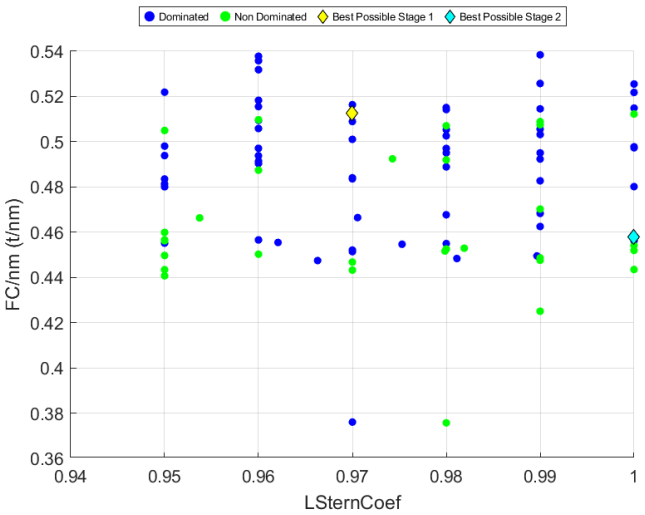

Figure 4.28: $L_{Stern_{Profile}}$ vs fc/nm

Figure 4.29 shows the GT/PAX as a function of the $L_{Stern_{Profile}}$.
The best possible ship (1st stage) is positioned at an $L_{Stern_{Profile}}$ of 0.97, recording a GT/PAX value of approximately 73. This positioning is particularly significant: the unit sits in the lower portion of the data cluster, indicating a design choice oriented towards volumetric efficiency

and the maximisation of carrying capacity. Despite the medium-sized stern (0.97), the ship maintains a highly competitive tonnage-to-passenger ratio.

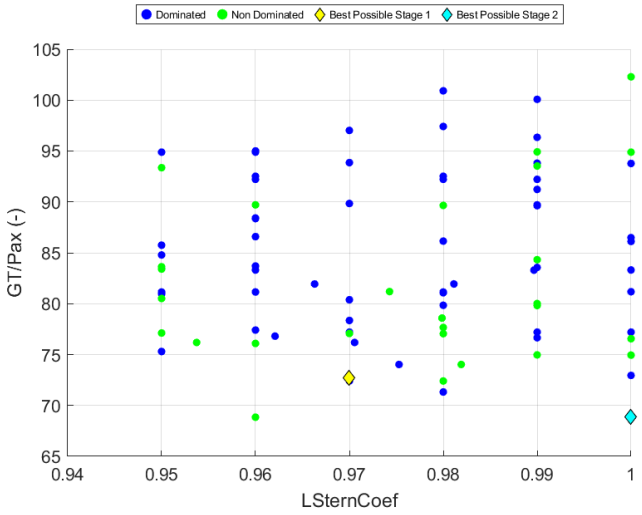

Figure 4.29: $L_{Stern_{Profile}}$ vs GT/PAX

Figure 4.30 shows the $\overline{SFOC}$ as a function of the $L_{Stern_{Profile}}$.
The best possible ship (1st stage) is positioned at an $L_{Stern_{Profile}}$ of 0.97 with an $\overline{SFOC}$ value of 175 g/kWh. This choice indicates that for the selected unit, priority was given to an engine configuration that ensures high reliability and electrical load capacity, even if it is not the absolute lowest specific consumption solution. This positioning is consistent with a global optimisation strategy, where component efficiency is balanced against the requirements for powering a high-density passenger ship.

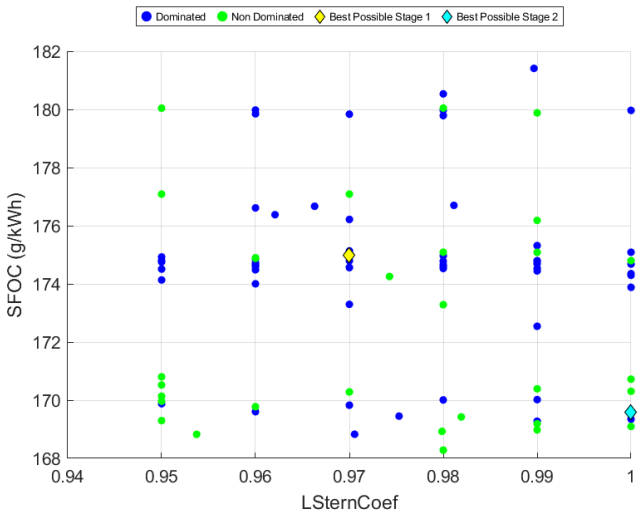

Figure 4.30: $L_{Stern_{Profile}}$ vs $\overline{SFOC}$

Figure 4.31 shows the W_{WB}/Δ as a function of the PAX.
The best possible ship (1st stage) is positioned within the maximum capacity cluster, with approximately 1096 passengers, and stands out for a W_{WB}/Δ value near zero. This result is particularly noteworthy: despite the ship belonging to the category with the highest passenger count, and potentially the highest centre of gravity, the selected design manages to operate almost without liquid ballast. Such efficiency ensures a reduced operational displacement, which directly translates into lower hull resistance and optimised fuel consumption compared to other, less balanced solutions.

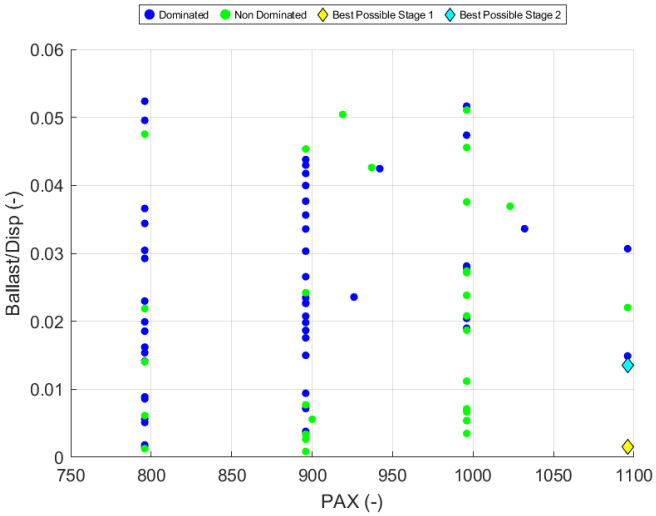

Figure 4.31: PAX vs W_{WB}/Δ

Figure 4.32 shows the fc/nm as a function of the PAX.
It is observed that as the number of passengers increases, fuel consumption per mile generally tends to rise due to larger hull dimensions and higher energy demands for hotel services.
The best possible ship (1st stage) is located within the highest capacity cluster, with approximately 1096 passengers, recording an fc/nm value of approximately 0.51 t/nm. Although this unit exhibits higher absolute consumption compared to ships in smaller clusters, it represents a local optimum for its category.

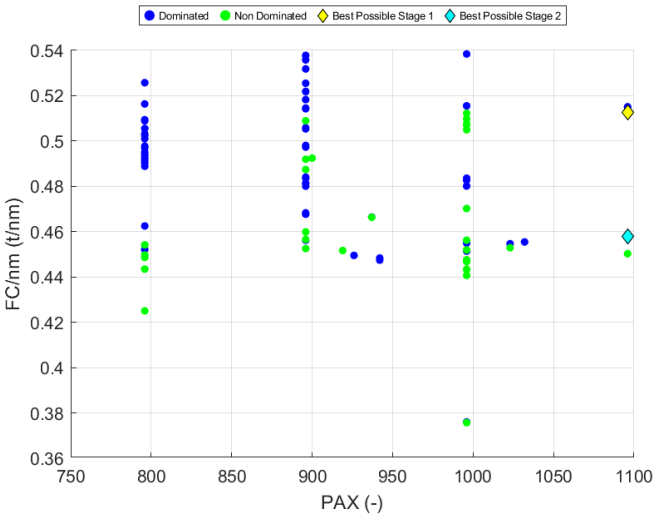

Figure 4.32: PAX vs fc/nm

Figure 4.33 shows the GT/PAX as a function of the PAX.

The data distribution reveals a clear downward trend in the GT/PAX attribute as the total number of passengers increases. This correlation suggests that, in larger ships, the volume allocated to each guest tends to decrease, thereby optimising gross tonnage to maximise carrying capacity.

The best possible ship (1st stage) is positioned within the maximum capacity cluster, with 1096 passengers, and exhibits a GT/PAX of approximately 73. Although the GT/PAX is among the lowest in the dataset, the ship maintains an absolute gross tonnage sufficient to provide all necessary services, demonstrating excellent management of internal volumes relative to its large transport capacity.

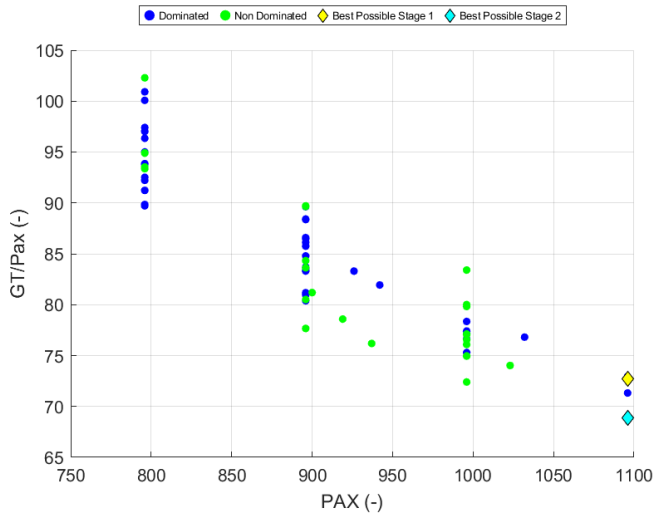

Figure 4.33: PAX vs GT/PAX

Figure 4.34 shows the $\overline{SFOC}$ as a function of the PAX.
The best possible ship (1st stage) is located within the highest capacity cluster with approximately 1096 passengers and an $\overline{SFOC}$ value of 175 g/kWh. Although options with lower specific consumption exist, the selection of 175 g/kWh for the chosen unit indicates an optimisation aimed at ensuring superior power reserves and operational reliability, which are necessary to manage the high electrical demand (hotel load) required by a ship with over one thousand passengers. This configuration represents the optimal compromise between energy efficiency and functional performance for a ship of this commercial size.

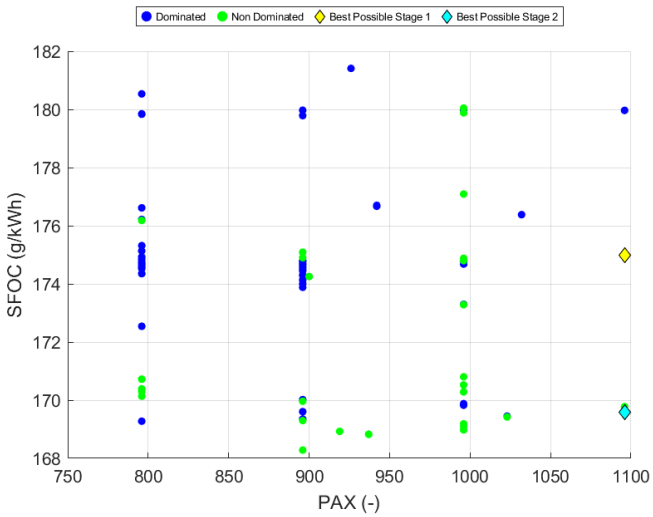

Figure 4.34: PAX vs $\overline{SFOC}$

4.4.3 Attribute - Attribute analisys

An "attribute-by-attribute" analysis of the results obtained during the first optimisation step is now conducted. Figure 4.35 to 4.40 illustrate the distributions. Figure 4.35 shows the fc/nm as a function of the W_{WB}/Δ.
The plot reveals a heterogeneous data dispersion, reflecting the complex trade-off between hydrostatic stability and hull resistance. The Pareto frontieridentifies configurations that minimise consumption for each required ballast level; a slight trend towards lower minimum consumption is observed as the ballast ratio increases towards medium values (0.02÷0.03), suggesting that trim by stern may, in some cases, lead to lower resistance, despite the greater amount of water ballast loaded onboard. The best possible ship (1st stage) is positioned at a point of significant operational interest: it features a W_{WB}/Δ value near zero associated with a consumption of approximately 0.51 t/nm

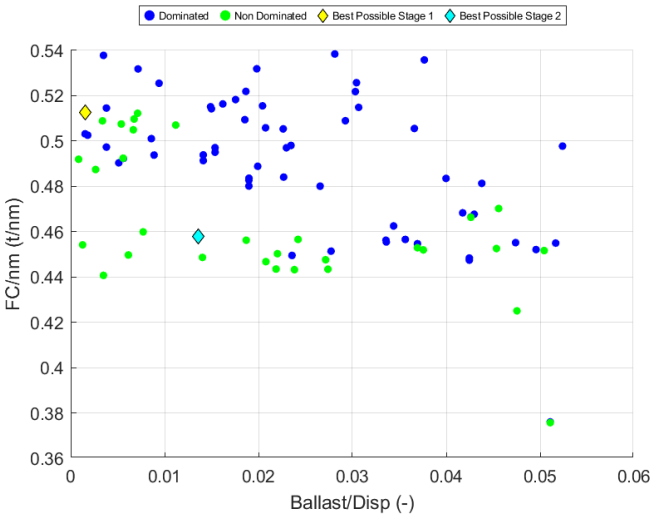

Figure 4.35: W_{WB}/Δ vs fc/nm

Figure 4.36 shows the GT/PAX as a function of the W_{WB}/Δ.

The plot reveals a rather dispersed data distribution, reflecting the diverse design philosophies adopted to reconcile internal volumes with hydrostatic trim. The Pareto frontier identifies designs that manage to provide a specific space standard per passenger while minimising ballast usage; it is noted that for high GT/PAX values (above 95), the ballast requirement tends to stabilise, whereas for lower ratios, the variability is at its peak.

The best possible ship (1st stage) is positioned in an extremely favourable area of the diagram: it exhibits a GT/PAX value of approximately 73 associated with a ballast ratio near zero. This result is particularly significant: the unit not only optimises gross tonnage utilisation to accommodate a high number of passengers (high commercial efficiency) but does so while maintaining an excellent hydrostatic balance that requires no corrective deadweight. Such a configuration confirms the validity of the selected hull, which is capable of supporting a "dense" layout without penalising operational displacement with ballast water.

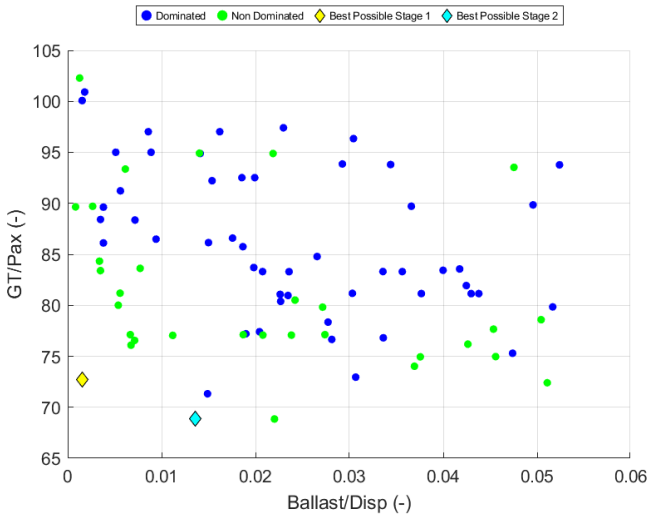

Figure 4.36: W_{WB}/Δ vs GT/PAX

Figure 4.37 shows the $\overline{SFOC}$ as a function of the W_{WB}/Δ.

The plot reveals a data distribution organised into well-defined horizontal bands, corresponding to different $\overline{SFOC}$ technological levels (approximately 169, 175, and 180 g/kWh). The Pareto frontier (green dots) identifies the most efficient engines for each ballast level; it is observed that ballast requirements vary widely (from 0 to 0.05) within each consumption band, confirming that the need for ballast water depends on hull geometry rather than specific engine performance.

The best possible ship (1st stage) is positioned within the intermediate efficiency band, with an $\overline{SFOC}$ value of 175 g/kWh, and stands out for a ballast ratio near zero. This positioning indicates excellent system-wide optimisation: while other variants with the same engine require up to 5% ballast relative to displacement to maintain trim, the selected ship achieves intrinsic stability. This choice ensures that the energy produced by the engines is not wasted on transporting ballast weight, thereby maximising the ship's actual operational efficiency despite not adopting the engine with the absolute lowest specific consumption.

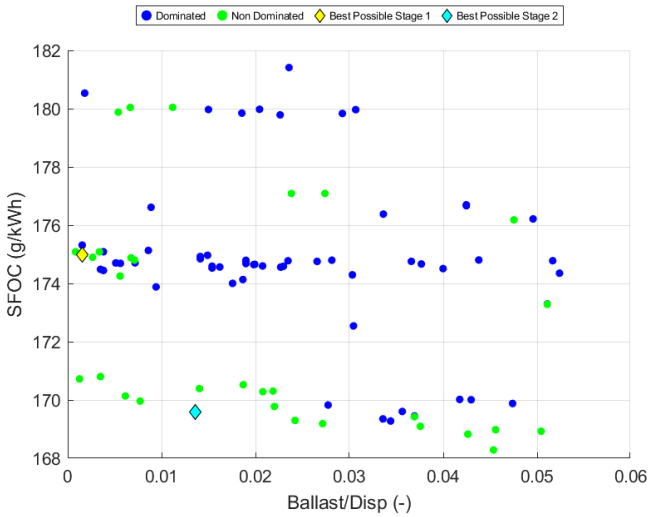

Figure 4.37: W_{WB}/Δ vs $\overline{SFOC}$

Figure 4.38 shows the fc/nm as a function of the GT/PAX.
The best possible ship (1st stage) is positioned on the left side of the diagram, with a GT/PAX value of approximately 73 and a consumption of 0.51 t/nm. Although the absolute consumption is in the higher range of the distribution, this is justified by the fact that the ship operates with the maximum possible number of passengers, ensuring high economic efficiency per passenger carried.

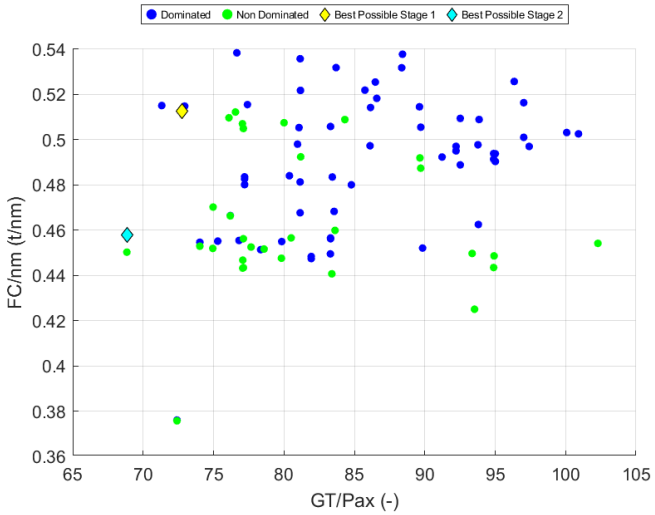

Figure 4.38: GT/PAX vs fc/nm

Figure 4.39 shows the $\overline{SFOC}$ as a function of the GT/PAX.
The data distribution reveals that $\overline{SFOC}$ values are organised into distinct horizontal bands, corresponding to different technological engine options (primarily around 169, 175, and 180 g/kWh). The Pareto frontier (green dots) identifies configurations that maximise efficiency for

each comfort level; it is observed that engine efficiency remains substantially constant across the entire GT/PAX spectrum, confirming that the choice of the propulsion plant is independent of passenger density on board.
The best possible ship (1st stage) is positioned within the intermediate consumption band with an SFOC of 175 g/kWh and a GT/PAX value of approximately 73

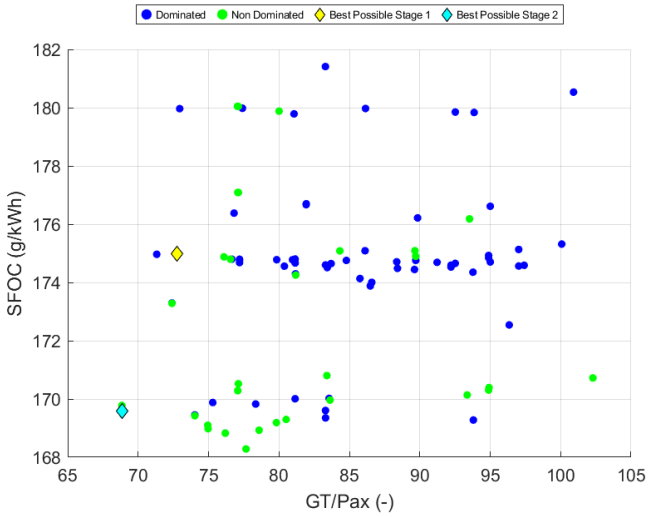

Figure 4.39: GT/PAX vs $\overline{SFOC}$

Figure 4.40 shows the fc/nm as a function of the $\overline{SFOC}$.
The best possible ship (1st stage) is located in the central cluster with an SFOC of 175 g/kWh and records a consumption of approximately 0.51 t/nm. Although it does not adopt the engine configuration with the lowest specific consumption (169 g/kWh band), the selected ship is positioned at the upper end of its respective cluster in terms of fc/nm. This confirms that the best possible ship (1st stage) is selected considering other attributes.

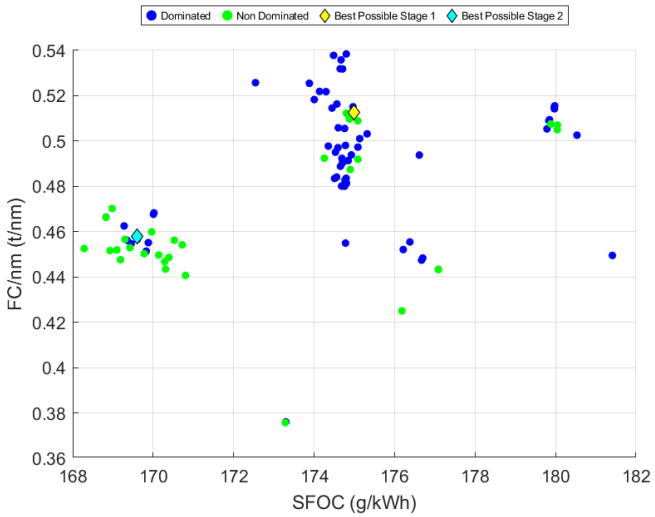

Figure 4.40: $\overline{SFOC}$ vs fc/nm

4.5 Probabilistic simulation and 2nd Ranking

The probabilistic analysis of fuel consumption and pollutant emissions commenced with the selection of a specific operational itinerary. To evaluate whether the ranking generated by the mathematical model remains robust under real-world conditions, three additional operational attributes were integrated into the framework. These include CII, the GHG_{int}, and the net balance between freshwater consumption and onboard production. The CII, established by the IMO as a mandatory operational measure, rates ships based on their CO_2 emissions relative to capacity and distance travelled, effectively compelling operators to maintain high efficiency standards. Complementing this, the GHG_{int}, introduced under the European Union's FuelEU Maritime framework, provides a comprehensive well-to-wake assessment of the fuel's emission profile.

Beyond the environmental considerations, the GHG_{int} introduces direct financial accountability; exceeding the 2025 regulatory threshold of 91.16 $gCO_{2_{eq}}$/MJ necessitates a financial penalty for the shipowner, typically indexed to the market price of Very Low Sulphur Fuel Oil (VLSFO) equivalent. Furthermore, the discrepancy between freshwater demand and onboard generation was analysed to assess the trade-off between harbour bunkering and self-sufficiency. While purchasing water in port incurs specific fees and harbour duties, excessive onboard production, often achieved through energy-intensive desalination plants, can lead to increased electrical plant loads, subsequently elevating fuel consumption and emissions. Consequently, the optimisation targets were set to minimise both the CII and GHG_{int}, whereas the freshwater balance was fuzzified to target an ideal value of zero. Table 4.15 details these additional operational attributes, including their respective fuzzification methods and variability ranges.

In accordance with the European Union's "Fit for 55" legislative framework, a representative

Table 4.15: Design attributes at 2^{st} Step Ranking

Attributes	Weight	Type	$\overline{y}$	y_{j_*}	y_j^*	units
W_{WB}/Δ	0.179	1	0	-0.005	0.05	-
GT/PAX	0.179	3	68.846	68.846	102.292	-
$\overline{SFOC}$	0.119	3	168.284	168.284	181.411	g/(kWh)
fc/nm	0.06	3	0.376	0.376	0.538	t/nm
CII	0.143	3	10	10	25	-
GHG_{int}	0.179	3	0	0	91.16	$gCO_{2_{eq}}/MJ$
$(FWc - FW_{Prod})$	0.143	1	0	-500	500	t

Mediterranean cruise itinerary was selected for this case study, as this region represents one of the most densely traversed maritime areas globally. The itinerary, presented in Figure 4.41, comprises a weekly voyage departing from and returning to the port of Genoa, with scheduled calls at Civitavecchia, Palermo, Ibiza, Valencia, and Marseille.

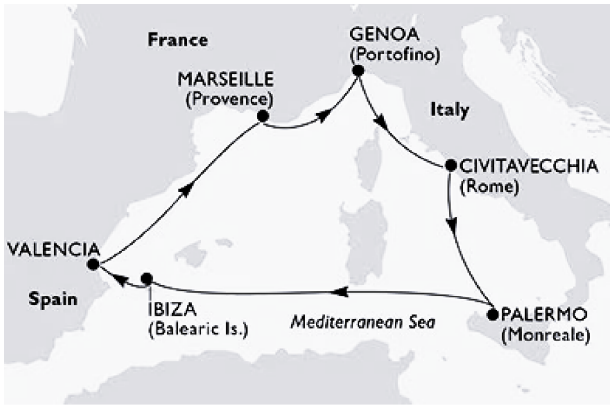

Figure 4.41: Tested itinerary [3]

To evaluate operational performance, 35 stochastic scenarios were generated by integrating wave statistics from [59] with the methodology detailed in Section 3.3. The baseline departure date was established as 28 April 2025, reflecting the onset of the summer season for the determination of onboard electrical loads. Environmental variability was captured through a Monte Carlo simulation that sampled sea-state conditions across a five-day window (from 26 to 30 April) over a seven-year historical period preceding the target date. This methodology provided a robust probabilistic characterisation of the environmental conditions the ship is expected to encounter during its operational life.

The route discretization is detailed in Appendix E, with the voyage subdivided into several sub-legs. Port stays are discretized into two-hour intervals, with the exception of the initial and final periods of each call, which are reserved for the shore power connection. Following the manoeuvring and transit phases, the ship maintains a constant speed within each sub-leg; this

operational speed deviates from the 19-knot design speed to provide a more realistic simulation of actual service conditions. For each ship, a drydocking event on 31/12/2024 was assumed to simulate approximately four months of hull fouling.
Based on the specific engine configuration of each ship, PMS strategy maps were generated. In accordance with [3], a linear load-sharing strategy for the power plant was adopted. For instance, by implementing a "father-son" configuration, the load distribution profile illustrated in Figure 4.42 is obtained.

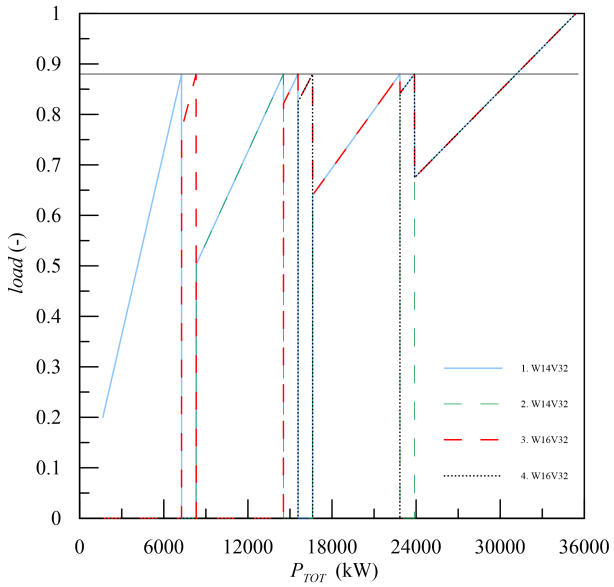

Figure 4.42: Generation station map: engines load as function of power

As observed, the load on the initial operating engine increases linearly with power demand until it reaches approximately 88% of its capacity, at which point a second unit is engaged. The total load is then equally distributed between the two engines, which both subsequently increase their output linearly. This sequential process continues with the activation of the third and fourth engines, eventually leading to a simultaneous linear increase across all four units toward maximum power.
The integration of probabilistic simulations in the second optimisation step marks a crucial transition: from a purely static evaluation of the design to a dynamic and stochastic vision of the ship's operational life. Within this framework, although the external environmental conditions remain constant across the entire database, the interaction between the ship's morphology and atmospheric agents leads to significant variations in performance. The differences in fuel consumption and emissions observed in the results largely stem from the management of aerodynamic drag, where variations in the longitudinal wind-exposed area and its centre of application alter the intensity of wind-induced forces and moments. Similarly, current-related forces are governed by the geometry of the underwater hull, particularly the overall length and beam,

which define the wetted surface area and resistance.
A discriminating factor in manoeuvrability and overall efficiency is the choice of propulsion system: the distinction between the use of PODs or a traditional shaft line directly influences rudder forces and the ship's ability to maintain its course with minimal energy expenditure. The results of these simulations, detailed in the appendix, provide a comprehensive statistical mapping via fuel consumption probability curves for the 32 non-dominated ships. Utilising parameters such as the mean (μ), median (Q_2), and the third quartile (Q_3) allows for the quantification of not only the expected performance but also the operational risk profile, identifying the probability of consumption exceeding nominal values in 25% of the most critical scenarios. To define the attributes, mean of CII, GHG_{int} and $(FW_c - FW_{Prod})$ simulation results is used. Once the fuzzification phase was completed and the decision weights defined, the application of the TOPSIS method enabled an update of the original ranking by incorporating these new operational attributes. No design are filtered by Pareto filtering but the data presented in Table 4.16 show how the relative positioning of the solutions has shifted: ships that appeared technically superior in the first step may have lost ground due to higher sensitivity to environmental variables or a more elevated risk profile.

Table 4.16: Second step ranking

Pos	ID	L_{OA} (m)	B (m)	NO POD (-)	PAX (-)	$L_{Stern_{Profile}}$ (-)	W_{WB}/Δ (-)	GT/PAX (-)	$\overline{SFOC}$ (g/kWh)	fc/nm t/nm	CII (-)	GHG ($gCO_{2_{eq}}$/MJ)	$(FW_c - FW_{prod})$ (t)	d_k^+ (-)	d_k^- (-)	C_k (-)
1	'Cruise_2276'	242.000	32.600	1	1096	1.000	0.014	68.886	169.592	0.458	15.404	78.147	-195.952	0.122	0.245	0.667
2	'Cruise_2928'	260.000	33.600	1	996	0.950	0.003	83.402	170.803	0.441	14.108	78.162	-305.222	0.114	0.223	0.662
3	'Cruise_1928'	248.000	32.600	1	896	0.950	0.008	83.625	169.963	0.460	15.865	78.190	-410.082	0.115	0.217	0.654
4	'Cruise_2812'	242.000	32.600	1	1096	0.960	0.022	68.846	169.777	0.450	15.303	78.133	-193.460	0.134	0.231	0.634
5	'Cruise_1421'	248.000	32.600	1	996	0.950	0.019	77.118	170.523	0.456	15.202	78.155	-303.243	0.121	0.204	0.628
6	'Cruise_476'	248.000	32.600	1	996	0.970	0.021	77.074	170.284	0.447	15.031	78.132	-296.314	0.121	0.203	0.626
7	'Cruise_3763'	243.734	32.696	1	900	0.974	0.006	81.189	174.253	0.492	16.667	78.236	-414.344	0.137	0.212	0.607
8	'Cruise_1210'	258.000	32.600	1	1096	0.970	0.002	72.751	174.998	0.513	15.294	78.239	-219.456	0.158	0.239	0.601
9	'Cruise_3144'	242.000	32.600	0	896	0.950	0.024	80.511	169.298	0.457	16.183	78.155	-406.991	0.129	0.194	0.600
10	'Cruise_3561'	242.000	32.600	0	996	0.960	0.007	76.092	174.879	0.510	15.816	78.206	-320.512	0.148	0.217	0.593
11	'Cruise_3285'	242.000	32.600	1	796	0.950	0.006	93.363	170.138	0.450	15.800	78.166	-505.584	0.148	0.214	0.590
12	'Cruise_1981'	248.000	32.600	1	996	1.000	0.007	76.557	174.800	0.512	16.283	78.272	-326.885	0.150	0.215	0.588
13	'Cruise_3409'	242.000	33.600	0	996	0.990	0.027	79.819	169.188	0.448	14.516	78.132	-299.789	0.140	0.187	0.572
14	'Cruise_736'	258.000	32.600	1	896	0.990	0.003	84.325	175.084	0.509	16.136	78.238	-423.093	0.158	0.208	0.568
15	'Cruise_904'	258.000	34.600	1	896	0.980	0.001	89.653	175.088	0.492	15.064	78.224	-422.088	0.165	0.205	0.555
16	'Cruise_1817'	258.000	34.600	1	896	0.960	0.003	89.710	174.899	0.487	14.977	78.214	-419.145	0.162	0.200	0.553
17	'Cruise_560'	248.000	32.600	1	996	0.950	0.007	77.118	180.042	0.505	15.447	78.186	-310.291	0.172	0.208	0.547
18	'Cruise_1821'	248.000	32.600	1	996	0.970	0.024	77.074	177.089	0.443	14.762	78.096	-288.132	0.149	0.179	0.546
19	'Cruise_1916'	248.000	32.600	0	996	1.000	0.038	74.946	169.097	0.452	15.518	78.139	-301.565	0.161	0.192	0.544
20	'Cruise_3772'	224.766	32.602	0	1023	0.982	0.037	74.024	169.424	0.453	15.050	78.107	-268.076	0.163	0.194	0.543
21	'Cruise_931'	258.000	32.600	1	796	0.990	0.014	94.918	170.391	0.449	15.294	78.135	-499.514	0.162	0.191	0.542
22	'Cruise_110'	258.000	32.600	1	996	0.990	0.005	80.008	179.881	0.508	14.915	78.190	-310.091	0.177	0.202	0.533
23	'Cruise_2575'	254.000	33.600	1	796	1.000	0.001	102.291	170.722	0.454	14.340	78.155	-506.328	0.193	0.219	0.532
24	'Cruise_556'	248.000	32.600	1	996	0.980	0.011	77.051	180.045	0.507	15.489	78.190	-311.085	0.176	0.196	0.528
25	'Cruise_1827'	248.000	32.600	1	996	0.950	0.027	77.118	177.088	0.443	14.746	78.095	-287.584	0.157	0.173	0.524
26	'Cruise_2101'	218.000	33.600	0	996	0.980	0.051	72.403	173.283	0.376	14.170	77.876	-252.353	0.196	0.210	0.518
27	'Cruise_3744'	236.354	32.684	0	937	0.954	0.043	76.188	168.826	0.466	16.480	78.170	-367.393	0.178	0.186	0.511
28	'Cruise_149'	258.000	32.600	1	796	1.000	0.022	94.888	170.306	0.443	15.221	78.125	-496.600	0.170	0.175	0.508
29	'Cruise_200'	228.000	32.600	0	896	0.980	0.045	77.663	168.284	0.453	16.168	78.081	-390.452	0.182	0.187	0.507
30	'Cruise_1163'	248.000	32.600	0	996	0.990	0.046	74.968	168.979	0.470	15.826	78.179	-311.272	0.191	0.185	0.492
31	'Cruise_3694'	242.457	32.416	0	919	0.980	0.050	78.587	168.928	0.452	16.015	78.136	-377.798	0.198	0.178	0.474
32	'Cruise_3219'	242.000	32.600	0	796	0.990	0.048	93.530	176.182	0.425	14.876	78.049	-486.713	0.228	0.128	0.360

Chapter 5

Discussion

The analysis of the obtained results is now presented. Table 5.1 reports the ranking after applying the probabilistic simulation to the 32 non-dominated ships belonging to the Pareto frontier. As can be observed, the probabilistic simulation has modified the ordering of the feasible designs according to the considered attributes and their associated weights.
The operational attributes favour ships characterised by a small difference between water consumed and water produced and by low GT values. As can be seen, the values in the "water consumed – water produced" attribute column (Table 4.16) are always negative: evaporators and reverse-osmosis units tend to produce more water than is consumed. Under operating conditions, this results in a reduction in the amount of ballast water that needs to be taken on board. In operational phases it is therefore possible to ballast less, allow the ship to adjust its floating position using only the FW, and then fill the ballast tanks to reach a condition of zero or slightly stern-trimmed trim
With respect to ship length, a variability range between 224 m and 260 m is observed, with the highest concentration of designs between 240 m and 245 m, which lies within the typical limits of luxury cruise ships. One might have expected the selection to converge towards shorter ships; however, from an operational standpoint this is not always confirmed. In terms of seakeeping, smaller ships tend to be more affected by wave action, and the results show that their average SFOC is higher than that of longer ships. This may be related to the sea states encountered during operation, which can force the engines to operate outside their optimal ranges, thus favouring the adoption of higher installed power in order to redistribute the load around approximately 85%, where the optimal efficiency condition is typically achieved.
It is also noted that the ship *Cruise_2928* remains in the same position even after the operational analysis. An examination of its dimensions shows that it is the largest ship in the dataset, with a length of 260 m and a GT of 83,068. The ship therefore does not fall within the luxury cruise ship class, despite its favourable operational characteristics. Nevertheless, it may represent a useful reference case for future studies aimed at investigating the downsizing of cruise ships

Table 5.1: Ship ranking main results

ID	Step 2 Pos	Step 1 Pos	GT (GT)	L_{OA} (m)	B (m)	C_B (-)	LCG (m)	KG (m)	W_{st} (t)	∇ (m^3)	A_{l_a} (m^2)	A_{f_a} (m^2)	A_{l_w} (m^2)	A_{f_w} (m^2)	$A_{Pax_{tot}}$ (m^2)	$A_{Pub_{tot}}$ (m^2)	$A_{Ext_{tot}}$ (m^2)	$TrunkTec_{tot}$ (m^2)	$A_{Crew_{tot}}$ (m^2)	P_{tot} (kW)
C_2276	1	5	75499	242.0	32.6	0.649	110.2	19.3	17068	35551	7023	1219	1576	219	21202	23752	4354	11352	7532	30680
C_2928	2	2	83068	260.0	33.6	0.649	116.9	19.5	19540	39094	7496	1162	1691	226	20905	34278	10880	9044	8515	30680
C_1928	3	7	74928	248.0	32.6	0.648	113.1	18.9	17570	36343	6970	1130	1619	219	22699	30810	10193	9622	7772	30680
C_2812	4	17	75455	242.0	32.6	0.647	110.3	19.4	17068	35416	7023	1219	1576	219	21202	24836	4354	11583	8073	30680
C_1421	5	16	76810	248.0	32.6	0.651	112.8	19.8	17652	36550	7096	1233	1619	219	22206	27676	6808	11944	8068	30680
C_476	6	18	76766	248.0	32.6	0.649	112.9	19.6	17652	36412	7096	1233	1619	219	21246	27128	4768	11563	8731	30680
C_3763	7	4	73070	243.7	32.7	0.648	110.8	18.7	17244	35861	6770	1137	1588	220	23216	29166	4612	11224	8475	32480
C_1210	8	1	79735	258.0	32.6	0.650	115.8	19.4	18634	37962	7346	1233	1691	219	22277	23232	5021	8856	8882	32480
C_3144	9	21	72138	242.0	32.6	0.651	110.1	18.8	16990	35621	6702	1134	1576	219	23143	30134	4538	12411	8258	30680
C_3561	10	3	75788	242.0	32.6	0.651	110.2	19.7	17068	35621	7056	1217	1576	219	24388	25850	4296	10034	8086	32480
C_3285	11	13	74317	242.0	32.6	0.646	110.4	19.1	16990	35349	6980	1123	1576	219	22983	32969	10134	9429	8036	30680
C_1981	12	6	76251	248.0	32.6	0.648	113.0	19.1	17570	36343	7113	1120	1619	219	23978	31522	4446	8986	8485	32480
C_3409	13	22	79500	242.0	33.6	0.653	109.4	19.5	17981	36818	7170	1263	1576	226	21880	31763	4547	8843	8591	30680
C_736	14	8	75555	258.0	32.6	0.647	115.6	18.8	18548	37819	6985	1134	1691	219	22509	24702	4918	9973	8586	32480
C_904	15	11	80329	258.0	34.6	0.647	115.3	19.0	20554	40149	6985	1203	1691	233	21692	27562	5220	11396	9723	32480
C_1817	16	12	80380	258.0	34.6	0.650	114.7	18.8	20554	40303	6985	1203	1691	233	21102	26148	5220	11279	9576	32480
C_560	17	9	76810	248.0	32.6	0.651	112.6	19.7	17652	36550	7096	1233	1619	219	22722	26974	4768	12058	8732	31360
C_1821	18	20	76766	248.0	32.6	0.649	113.0	19.5	17652	36412	7096	1233	1619	219	20398	27145	4768	12058	8768	28800
C_1916	19	26	74646	248.0	32.6	0.650	112.7	18.9	17570	36486	6930	1132	1619	219	22109	30037	4676	10226	8215	30680
C_3772	20	25	75727	224.8	32.6	0.654	110.6	19.2	17312	36154	7001	1233	1594	219	21689	23199	4656	10817	8481	30680
C_931	21	19	75555	258.0	32.6	0.647	116.2	18.7	18548	37819	6985	1134	1691	219	20405	26189	4918	10649	8918	30680
C_110	22	10	79688	258.0	32.6	0.647	116.0	19.4	18634	37819	7346	1233	1691	219	21502	25630	5021	8862	9140	31360
C_2575	23	15	81424	254.0	33.6	0.649	115.1	19.4	19127	38456	7352	1163	1662	226	20807	25319	10707	8900	8465	30680
C_556	24	14	76743	248.0	32.6	0.648	113.0	19.6	17652	36343	7096	1233	1619	219	22796	27172	4768	11574	8731	31360
C_1827	25	24	76810	248.0	32.6	0.651	112.6	19.5	17652	36550	7096	1233	1619	219	20361	27145	4768	12058	8658	28800
C_2101	26	29	72113	218.0	33.6	0.649	98.4	19.6	15575	32919	6544	1252	1403	226	20884	41644	9547	12203	7708	24360
C_3744	27	27	71388	236.4	32.7	0.653	106.9	18.4	16521	34991	6611	1127	1535	220	23474	29455	4363	11236	8139	30680
C_149	28	23	75531	258.0	32.6	0.646	117.2	18.6	18548	37746	6985	1134	1691	219	19963	26252	4918	9846	8807	30680
C_200	29	30	69586	228.0	32.6	0.651	103.2	18.5	15654	33512	6489	1123	1475	219	21112	22231	4060	8789	6668	30680
C_1163	30	28	74668	248.0	32.6	0.651	112.5	18.9	17570	36553	6930	1132	1619	219	23031	30037	4676	9741	8511	30680
C_3694	31	31	72221	242.5	32.4	0.651	109.9	18.7	16868	35496	6752	1127	1579	218	22456	30025	4536	11121	7131	30680
C_3219	32	32	74450	242.0	32.6	0.653	109.5	19.0	16990	35751	6980	1123	1576	219	21778	32969	10134	10610	8099	27320

and the development of an intermediate class between luxury and mega cruise ships. It can further be observed that heavier ships and those with higher C_B values tend to drop in the ranking, most likely due to the potential increase in frictional resistance which, under operational conditions, leads to higher fuel consumption and associated pollutant emissions. The analysis therefore favours lighter ships with an optimal distribution of onboard volumes.
From an operational perspective, ships with a smaller wind-exposed area are preferred, as a reduced lateral surface significantly decreases wind-induced drift. In dimensional terms, ships with a lower wetted surface area are considered more advantageous, since, in addition to reducing hull fouling accumulation, they also limit the action of drift forces due to currents and waves.
From an economic optimization perspective, the market tends to reward units with a low GT/PAX , aiming to concentrate maximum potential revenue within the smallest possible gross volume to reduce port fees and construction costs. However, the analysis of project *Cruise_2101* highlights the limits of this approach. This unit features the most extensive public area in the dataset against a relatively low GT, but its ranking at 26^{th} place in the operational Step 2 emphasizes its overall inefficiency. This phenomenon can be explained by examining the vertical center of gravity, which is among the highest: the excessive development of superstructures to accommodate public spaces on a smaller hull compromises stability and drastically increases the A_{l_a}, making the ship extremely vulnerable to leeway and increasing fuel consumption in real-world sea conditions.
The results also indicate a preference for designs with a conventional shaft line rather thanPOD propulsion. With the former configuration, from a weight-balance perspective, the longitudinal positioning of the PEM room (which depends on the length of the stern profile) allows it to be located closer to the centre of flotation, which is advantageous for trim studies.
The focal point of the analysis was the minimisation of the GT/PAX ratio, in order to achieve a better distribution of volumes on board. It can be observed that the total area allocated to cabins tends to be maximised, favouring ships with higher revenue-earning capacity. Furthermore, the analysis also seeks to maximise both the public area and the external deck area. Providing larger public areas per passenger improves the onboard experience during navigation, allowing the installation of restaurants, atrium and leisure spaces. External areas are likewise maximised: increasing them leads to a reduction in GT per passenger and allows the shipowner to exploit these spaces economically by installing swimming pools, sun decks and similar facilities, in line with the demands of a market in which the average passenger tends to be older. There is also a tendency to increase the space allocated to technical areas within the central spine, in order to accommodate a greater number of auxiliary rooms such as air-conditioning stations, laundries, and so forth. Crew areas, finally, depend on the number of passengers carried. The analysis of structural weights and installed power further confirms this trend. While preliminary design tends to favor longer, high-capacity ships for their theoretical efficiency in calm waters,

operational simulation rewards units with a more balanced ratio between the lateral underwater area and the windage area. The ships occupying the top positions in the final ranking show greater resilience to environmental loads, where the impact of currents and waves on the submerged hull is managed with a lower power demand compared to oversized vessels. The results demonstrate that the GT/PAX ratio must be subordinate to the integrity of the vessel system: the economic advantage of a compact ship densely packed with public areas is nullified if it is not accompanied by correct center-of-gravity management and a superstructure configuration that minimizes negative wind interaction.

As shown in Figure 5.1, which plots the number of passengers against the length overall , the operational analysis favors a more compact ship while maintaining a constant passenger capacity. This results in a significant reduction in the GT/PAX attribute, effectively optimizing the distribution of onboard volumes for passenger use. Consequently, a more efficient and compact design is achieved without compromising the required service standards. Furthermore, from a hydrodynamic perspective, the smaller ship exhibits lower resistance, leading to reduced fuel consumption and lower total installed power

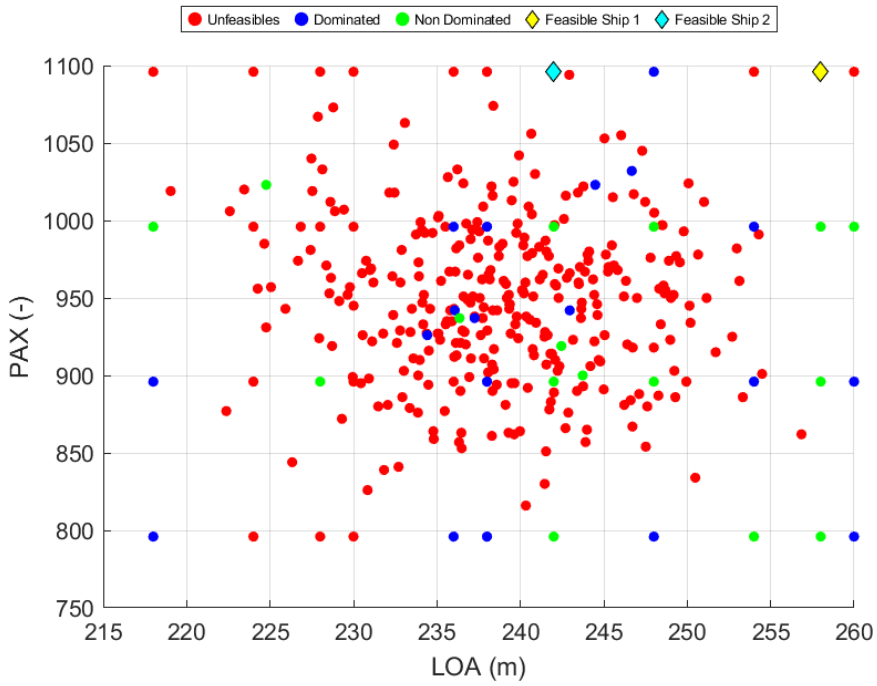

Figure 5.1: L_{OA} vs PAX

The analysis of the top-ranked configurations in the two ranking phases is now presented.. Both ship maintain the same passenger capacity and beam. Project *Cruise_2276*, which climbs from fifth to first place in Step 2, embodies the optimal equilibrium point between geometric footprint and operational functionality. While maintaining a length overall of only 242 meters, this

ship features a more conservative weight distribution and a significantly lower windage area compared to longer units such as *Cruise_1210*. It is noteworthy that *Cruise_2276* reserves a considerable surface area for technical trunks, suggesting that the operational survival of a design depends on the ability to integrate onboard systems without saturating every available volume with passenger areas. The operational performance discrepancy is primarily linked to the superstructure configuration, which is critical in defining the windage area. The *Cruise_1210* ship, which initially ranked first in the preliminary design stage, features extensive external areas on the first public deck ($DK2$) and the embarkation deck ($DK3$). In contrast, *Cruise_2276* features external areas located at the embarkation deck ($DK3$), the wheelhouse deck, and the uppermost deck.

Due to its shorter length overall, *Cruise_2276* drastically reduces its windage area, thereby minimizing the leeway effect caused by wind. Regarding the GT/PAX ratio, with an equal number of passengers, *Cruise_2276* proves more economically advantageous, as a lower volume per passenger allows the shipowner to optimize onboard space and increase revenue potential.

Analysis of the installed power shows that *Cruise_2276* requires 30680 kW compared to the 32480 kW of *Cruise_1210*, a direct consequence of the different dimensions. It is noted, however, that while *Cruise_1210* consumes more fuel per nautical mile and has a higher $SFOC$, it maintains a lower average CII because the index is indexed to the GT. Nevertheless, in terms of GHG_{int} factor, *Cruise_1210* emits a higher amount of $CO_{2_{eq}}$ per MJ.

A further distinction arises in water management: for the same number of passengers, *Cruise_1210* produces more fresh water than *Cruise_2276*. Crucially, the increase in the lateral underwater area is significant: the impact of currents and waves on the hull exerts a greater force than the wind on the superstructure, leading to higher overall fuel consumption.

Figure 5.2 shows a comparison of the longitudinal profiles of the two top-ranking ships. The ship in the upper part of the figure is *Cruise_2276*, while *Cruise_1210* is shown below.

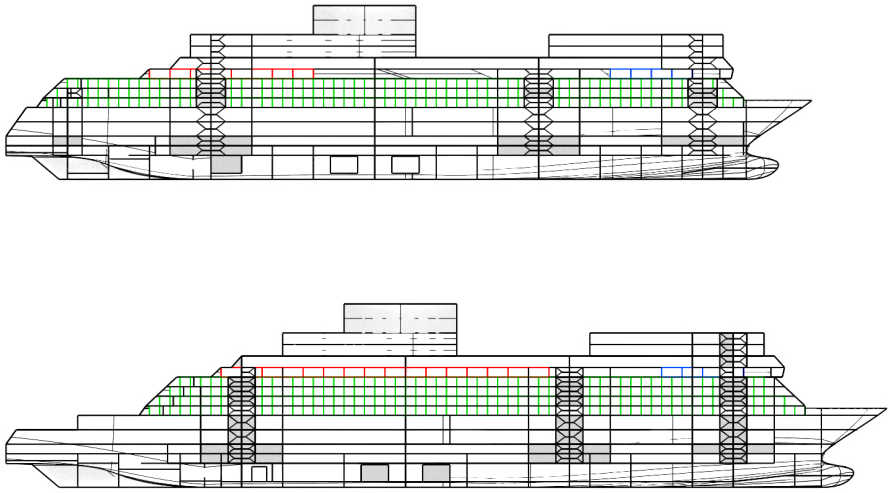

Figure 5.2: Longitudinal ship profiles. Above *Cruise_2276* below *Cruise_1210*

In Figure 5.2, passenger cabins on the passenger deck are shown in green, the suites on the deck hosting the navigation bridge are shown in red, and the officers' cabins, located immediately adjacent to the bridge, are shown in blue.

It can be observed that the parametric modelling has generated different configurations. The number of passengers in the two configurations is nevertheless the same: both ships accommodate 714 passenger cabins with balconies. Owing to the different arrangement of the external areas, the ship *Cruise_1210* features one additional deck devoted to cabins. As previously discussed, the parametric ship model was developed to determine the minimum number of decks to be allocated to passenger cabins and to saturate the wheelhouse deck with the remaining cabins, assessing the possibility of introducing suites whenever the available deck area allowed it. As can be seen, in both cases the wheelhouse deck includes suites (in red), albeit in different numbers. For *Cruise_2276*, the presence of larger external areas has allowed a greater portion of the wheelhouse deck to be devoted to luxury cabins, whereas ship 1 accommodates fewer suites but offers larger public areas. The identification of decision-making criteria is, therefore, fundamental in determining the feasible ship configuration by balancing technical requirements with expected operational performance. By establishing both objective and subjective weights, it is possible to generate a curated list of designs that satisfy mission requirements, integrating design variables and real-world operational scenarios into a single analytical framework. The innovative contribution of incorporating three-dimensional modeling provides a rapid and visual representation of the vessel during the early design stages, facilitating the understanding of spatial and volumetric distribution. Figure 5.3 displays detailed cross-sections of the two projects that emerged as the top candidates following the first design analysis phase and the second operational validation phase, respectively, highlighting the structural and functional differences that prompted the shift in the ranking hierarchy.

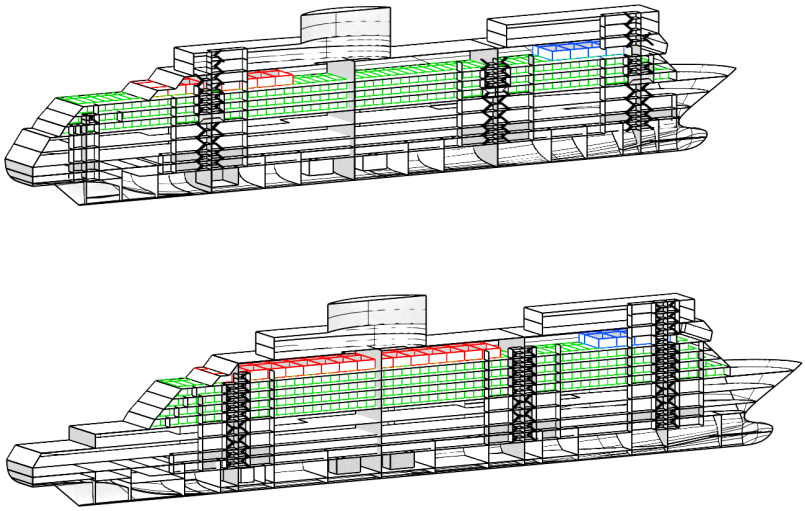

Figure 5.3: Ship section. Above *Cruise_2276* below *Cruise_1210*

Chapter 6

Conclusions

In conclusion, the proposed methodology provides an alternative and at the same time complementary contribution to traditional design approaches. It represents an alternative to the classical spiral design typically adopted in the maritime sector and an integration of multi-attribute decision-making methods, in which, in addition to the mathematical model, parametric modelling and operational software for the calculation of fuel consumption and pollutant emissions are employed. In this way, the design process is not limited to static assessments but incorporates, from the very early stages, a quantitative evaluation of operational and environmental performance.

The use of parametric modelling makes it possible to determine, from the preliminary design phases, the shapes, areas and volumes of a luxury cruise ship. Parametric modelling, depending on how it is implemented, makes it possible to accommodate in a structured way the main shipowner's requirements, particularly with respect to the definition of decks, passenger areas, public spaces and the external surfaces of the ship. By defining geometric, functional and volumetric parameters, it becomes possible to directly control the spatial arrangement, the relationships between different areas, and the compliance with capacity, comfort and functionality requirements, which are central aspects in the design of a luxury cruise ship.

Although parametric modelling requires greater care in the initial definition of parameters, since such frameworks are not necessarily standardised across different design offices and are therefore strongly dependent on designers experience and know-how, it offers a key strategic advantage: the ability to generate a coherent three-dimensional model already at the early conceptual stages. This makes it possible to move rapidly from qualitative and functional requirements to a quantitative geometric representation of the ship, allowing volumes, areas, weights and centres of gravity to be assessed from the outset.

Furthermore, a well-structured parametric model enables the systematic exploration of a wide design space, as variations in the parameters are automatically translated into alternative ship configurations. This supports trade-off analyses between architectural requirements, hydrody-

namic performance, structural constraints and operational needs, thereby reducing the risk of late-stage design changes. In this sense, parametric modelling is not merely a geometric representation tool but becomes a driver of the decision-making process, directly linking design choices to the technical and operational performance of the ship.
It has been observed that the ranking obtained at the first step is partly revised after the application of a probabilistic operational software. The operational analysis can therefore overturn the initial priorities and, consequently, the project selection, shifting the focus towards a ship that performs not only well under design conditions but also under real operating conditions.
From a technical point of view, the ship that proves to be overall the best is the *Cruise_2276* for navigation in Mediterranean Sea. Although, in order to meet the design condition, it requires a larger amount of ballast to be carried than the *Cruise_1210*, it shows better operational qualities during service, considering that a ship rarely operates exactly at its design condition.

6.1 Research innovation and contribution

In addition to providing a complementary alternative to traditional ship design methodologies, this research introduces several original and innovative contributions to the field of luxury cruise ship preliminary design.
A first element of innovation lies in the systematic adoption of multiple three-dimensional models throughout the different stages of the design process. Unlike conventional approaches, which often rely on simplified geometrical representations in the early phases, the proposed methodology enables the generation and continuous refinement of coherent 3D models from the conceptual stage onwards. This multi-level modelling framework allows designers to progressively increase geometric and functional resolution while preserving consistency between successive design phases. As a result, architectural, volumetric and performance-related assessments can be conducted within a unified and traceable modelling environment.
A further significant contribution is represented by the development of an original mathematical model specifically tailored to luxury cruise ships. To the best of the author's knowledge, comparable comprehensive parametric–mathematical frameworks dedicated to this ship category are currently lacking in the open literature. The proposed model integrates geometric, functional, operational and environmental parameters into a single structured formulation, allowing the complex interactions between layout, weight distribution, energy consumption and emissions to be quantitatively analysed from the earliest design stages. This represents an important advancement with respect to existing approaches, which often focus on limited subsets of design variables or on specific subsystems.
Moreover, the methodology enables systematic comparison among multiple design alternatives

and reference projects. By embedding different configurations within a common parametric and analytical framework, the proposed approach facilitates objective benchmarking across heterogeneous design solutions. This capability supports evidence-based decision-making and reduces the reliance on purely qualitative assessments or designer intuition. The availability of comparable datasets also enhances the transparency and reproducibility of the design process, fostering a more rigorous evaluation of competing concepts.

Overall, the integration of multi-stage three-dimensional modelling, an original mathematical formulation for luxury cruise ships, and a structured framework for inter-project comparison constitutes a novel contribution to preliminary ship design practice. The proposed methodology not only improves the efficiency of the early design process but also strengthens its analytical robustness, providing designers and shipowners with more reliable tools for informed strategic decision-making.

6.2 Future Developments

Although the present study demonstrates the effectiveness of the proposed methodology, several promising directions for future research and development can be identified.

A primary area of further investigation concerns the extension of parametric modelling towards a more detailed and physically representative description of onboard systems and spatial arrangements. In particular, future work may focus on the explicit parametrisation of the positioning of main machinery, auxiliary systems and major functional areas typical of luxury cruise ships. This would enable a more realistic assessment of weight distribution, accessibility, safety and maintenance requirements already at the preliminary design stage. In this context, the development of asymmetric hull parametrisations could be pursued in order to incorporate transverse stability analyses, including the modelling of heeling tanks and their operational strategies for achieving transverse equilibrium under different loading conditions.

Another relevant development concerns the integration of generative artificial intelligence techniques into the early phases of plant and systems modelling. AI-based tools could be employed to automatically generate preliminary layouts of propulsion, energy and auxiliary systems starting from the predefined positions of main machinery. Such approaches may significantly accelerate the conceptual design phase and support designers in exploring unconventional or highly optimised configurations.

Further extensions of the parametric framework may include the detailed modelling of tanks located below the watertight bulkhead deck, as well as the parametrisation of compartment positioning to ensure compliance with applicable safety and damage stability regulations. This would allow regulatory constraints to be directly embedded within the optimisation and decision-making process, reducing the risk of late-stage redesigns.

In addition, future research may address the parametrisation of superstructures in order to limit the number of rejected design solutions caused by excessive trim or unfavourable longitudinal weight distributions. By incorporating superstructure geometry and mass properties into the parametric model, it would be possible to more effectively control longitudinal balance and trim behaviour from the earliest design stages.

The flexibility of the proposed framework also opens the possibility of varying the position and geometry of the funnel, thereby generating alternative ship configurations characterised by different architectural, aerodynamic and functional features. Similarly, the parametrisation of cabin dimensions and layouts could be extended to allow the adoption of multiple accommodation standards, supporting different levels of luxury and market positioning. This approach would enable systematic analyses of the trade-offs between passenger comfort, revenue potential and technical constraints.

Future developments may also include the detailed modelling of crew accommodation spaces and of the areas located below the watertight bulkhead deck, which are currently represented in a simplified manner. A more comprehensive representation of these spaces would improve the accuracy of weight, stability and habitability assessments.

Finally, the introduction of parametric representations of structural elements, such as pillars, stiffeners and major supporting structures, represents a further important research direction. Integrating structural layouts into the early-stage parametric model would facilitate preliminary evaluations of structural feasibility, load paths and space occupation, promoting a closer interaction between naval architecture, structural engineering and architectural design from the outset. This study also provides a basis for several future developments. In particular, an economic model could be implemented in order to introduce a design attribute based on operating costs in addition to capital. Moreover, since operational simulations are strongly influenced by sea state and by the external forces acting on the ship, future work should also analyse ship behaviour on other itineraries typical of luxury cruise ships, possibly by integrating a seakeeping and manoeuvring models capable of defining dedicated operational attributes or constraints for the ship under different environmental conditions.

In addition, in future developments the use of parametric modelling could be extended to the generation of a preliminary general arrangement plan and a preliminary lines plan, fostering a fast transition to preliminary design stage.

Appendix A

Ship Area per MFZ

Below, an example of MFZ subdivision of the main areas selected in the parametric model of the decks located above the watertight bulkhead deck is presented for *Cruise_110*.

- Passenger Cabins.
- Internal Public Spaces.
- External Public Spaces.
- Crew Areas.
- Casings, Trunks and techical areas.

For each MFZ, the numerical values of the areas and the coordinates of their corresponding centroids are reported.

Table A.1: Passenger Cabins area per MFZ above bulkhead deck

MFZ 1				MFZ 2				MFZ 3				MFZ 4				MFZ 5				
Area (m^2)	X (m)	Y (m)	Z (m)	Area (m^2)	X (m)	Y (m)	Z (m)	Area (m^2)	X (m)	Y (m)	Z (m)	Area (m^2)	X (m)	Y (m)	Z (m)	Area (m^2)	X (m)	Y (m)	Z (m)	TOT (m^2)
0.00	0.00	0.00	0.00	0.00	0.00	0.00	0.00	0.00	0.00	0.00	0.00	0.00	0.00	0.00	0.00	0.00	0.00	0.00	0.00	0.00
0.00	0.00	0.00	0.00	0.00	0.00	0.00	0.00	0.00	0.00	0.00	0.00	0.00	0.00	0.00	0.00	0.00	0.00	0.00	0.00	0.00
0.00	0.00	0.00	0.00	0.00	0.00	0.00	0.00	0.00	0.00	0.00	0.00	0.00	0.00	0.00	0.00	0.00	0.00	0.00	0.00	0.00
664.20	55.50	0.00	21.00	1180.80	93.00	0.00	21.00	1180.66	141.00	0.00	21.00	1170.52	188.84	0.00	21.00	466.08	223.33	0.00	21.00	4662.26
848.70	54.72	0.00	23.80	1771.20	90.00	0.00	23.80	1180.80	141.00	0.00	23.80	1549.80	196.50	0.00	23.80	0.00	0.00	0.00	0.00	5350.50
590.40	57.00	0.00	26.60	1180.80	93.00	0.00	26.60	1180.80	141.00	0.00	26.60	1536.54	196.31	0.00	26.60	0.00	0.00	0.00	0.00	4488.54
516.60	58.50	0.00	29.40	1180.80	93.00	0.00	29.40	1180.80	141.00	0.00	29.40	1465.50	194.85	0.00	29.40	0.00	0.00	0.00	0.00	4343.70
295.20	66.00	0.00	32.20	1771.20	87.00	0.00	32.20	0.00	0.00	0.00	0.00	590.40	204.00	0.00	32.20	0.00	0.00	0.00	0.00	2656.80
0.00	0.00	0.00	0.00	0.00	0.00	0.00	0.00	0.00	0.00	0.00	0.00	0.00	0.00	0.00	0.00	0.00	0.00	0.00	0.00	0.00
0.00	0.00	0.00	0.00	0.00	0.00	0.00	0.00	0.00	0.00	0.00	0.00	0.00	0.00	0.00	0.00	0.00	0.00	0.00	0.00	0.00
0.00	0.00	0.00	0.00	0.00	0.00	0.00	0.00	0.00	0.00	0.00	0.00	0.00	0.00	0.00	0.00	0.00	0.00	0.00	0.00	0.00
0.00	0.00	0.00	0.00	0.00	0.00	0.00	0.00	0.00	0.00	0.00	0.00	0.00	0.00	0.00	0.00	0.00	0.00	0.00	0.00	0.00

Table A.2: Internal Public Spaces area per MFZ above bulkhead deck

MFZ 1				MFZ 2				MFZ 3				MFZ 4				MFZ 5				
Area (m^2)	X (m)	Y (m)	Z (m)	Area (m^2)	X (m)	Y (m)	Z (m)	Area (m^2)	X (m)	Y (m)	Z (m)	Area (m^2)	X (m)	Y (m)	Z (m)	Area (m^2)	X (m)	Y (m)	Z (m)	TOT (m^2)
0.00	0.00	0.00	0.00	0.00	0.00	0.00	0.00	0.00	0.00	0.00	0.00	0.00	0.00	0.00	0.00	0.00	0.00	0.00	0.00	0.00
2181.10	33.62	0.00	12.60	1361.80	92.11	0.00	12.60	1395.30	141.54	0.00	12.60	1340.30	187.99	0.00	12.60	474.07	226.69	0.00	12.60	6752.57
1305.10	41.64	0.00	16.80	1048.20	95.35	0.00	16.80	1213.60	139.10	0.00	16.80	1090.50	191.73	0.00	16.80	749.64	229.90	0.00	16.80	5407.04
184.08	46.12	0.00	21.00	113.29	93.00	0.00	21.00	113.29	141.00	0.00	21.00	113.29	189.00	0.00	21.00	100.32	226.54	0.00	21.00	624.27
192.68	47.19	0.00	23.80	113.29	93.00	0.00	23.80	113.29	141.00	0.00	23.80	113.29	189.00	0.00	23.80	247.92	229.19	0.00	23.80	780.47
111.80	51.34	0.00	26.60	113.29	93.00	0.00	26.60	113.29	141.00	0.00	26.60	113.29	189.00	0.00	26.60	146.96	226.99	0.00	26.60	598.63
104.72	53.24	0.00	29.40	113.29	93.00	0.00	29.40	113.29	141.00	0.00	29.40	113.29	189.00	0.00	29.40	123.36	224.78	0.00	29.40	567.95
145.80	62.98	0.00	32.20	408.48	106.01	0.00	32.20	1294.08	141.00	0.00	32.20	777.48	180.03	0.00	32.20	24.00	214.50	0.00	32.20	2649.84
195.60	66.00	0.00	35.00	1564.80	93.00	0.00	35.00	1564.80	141.00	0.00	35.00	1963.50	195.93	0.00	35.00	0.00	0.00	0.00	0.00	5288.70
0.00	0.00	0.00	0.00	1729.10	90.41	0.00	38.36	148.11	123.86	0.00	38.36	898.98	190.87	0.00	38.36	184.53	217.81	0.00	38.36	2960.72
0.00	0.00	0.00	0.00	0.00	0.00	0.00	0.00	0.00	0.00	0.00	0.00	0.00	0.00	0.00	0.00	0.00	0.00	0.00	0.00	0.00
0.00	0.00	0.00	0.00	0.00	0.00	0.00	0.00	0.00	0.00	0.00	0.00	0.00	0.00	0.00	0.00	0.00	0.00	0.00	0.00	0.00

Table A.3: External area per MFZ above bulkhead deck

MFZ 1				MFZ 2				MFZ 3				MFZ 4				MFZ 5				
Area (m^2)	X (m)	Y (m)	Z (m)	Area (m^2)	X (m)	Y (m)	Z (m)	Area (m^2)	X (m)	Y (m)	Z (m)	Area (m^2)	X (m)	Y (m)	Z (m)	Area (m^2)	X (m)	Y (m)	Z (m)	TOT (m^2)
0.00	0.00	0.00	0.00	0.00	0.00	0.00	0.00	0.00	0.00	0.00	0.00	0.00	0.00	0.00	0.00	0.00	0.00	0.00	0.00	0.00
0.00	0.00	0.00	0.00	0.00	0.00	0.00	0.00	0.00	0.00	0.00	0.00	0.00	0.00	0.00	0.00	0.00	0.00	0.00	0.00	0.00
586.80	12.00	0.00	16.80	0.00	0.00	0.00	0.00	0.00	0.00	0.00	0.00	0.00	0.00	0.00	0.00	0.00	0.00	0.00	0.00	586.80
586.80	30.00	0.00	21.00	0.00	0.00	0.00	0.00	0.00	0.00	0.00	0.00	0.00	0.00	0.00	0.00	490.09	243.11	0.00	21.00	1076.89
0.00	0.00	0.00	0.00	0.00	0.00	0.00	0.00	0.00	0.00	0.00	0.00	0.00	0.00	0.00	0.00	0.00	0.00	0.00	0.00	0.00
0.00	0.00	0.00	0.00	0.00	0.00	0.00	0.00	0.00	0.00	0.00	0.00	0.00	0.00	0.00	0.00	0.00	0.00	0.00	0.00	0.00
0.00	0.00	0.00	0.00	0.00	0.00	0.00	0.00	0.00	0.00	0.00	0.00	0.00	0.00	0.00	0.00	0.00	0.00	0.00	0.00	0.00
326.00	55.00	0.00	32.20	0.00	0.00	0.00	0.00	0.00	0.00	0.00	0.00	0.00	0.00	0.00	0.00	0.00	0.00	0.00	0.00	326.00
97.80	64.50	0.00	35.00	0.00	0.00	0.00	0.00	0.00	0.00	0.00	0.00	0.00	0.00	0.00	0.00	0.00	0.00	0.00	0.00	97.80
0.00	0.00	0.00	0.00	785.51	87.66	0.00	38.36	1365.90	143.58	0.00	38.36	782.20	192.75	0.00	38.36	0.00	0.00	0.00	0.00	2933.61
0.00	0.00	0.00	0.00	0.00	0.00	0.00	0.00	0.00	0.00	0.00	0.00	0.00	0.00	0.00	0.00	0.00	0.00	0.00	0.00	0.00
0.00	0.00	0.00	0.00	0.00	0.00	0.00	0.00	0.00	0.00	0.00	0.00	0.00	0.00	0.00	0.00	0.00	0.00	0.00	0.00	0.00

Table A.4: Casing and Trunk area per MFZ above bulkhead deck

MFZ 1				MFZ 2				MFZ 3				MFZ 4				MFZ 5				
Area (m^2)	X (m)	Y (m)	Z (m)	Area (m^2)	X (m)	Y (m)	Z (m)	Area (m^2)	X (m)	Y (m)	Z (m)	Area (m^2)	X (m)	Y (m)	Z (m)	Area (m^2)	X (m)	Y (m)	Z (m)	TOT (m^2)
67.68	63.00	0.00	9.80	980.21	108.07	0.00	9.80	67.68	159.00	0.00	9.80	135.36	189.00	0.00	9.80	67.68	219.00	0.00	9.80	1318.60
67.68	63.00	0.00	12.60	1003.50	110.35	0.00	12.60	67.68	159.00	0.00	12.60	135.36	189.00	0.00	12.60	67.68	219.00	0.00	12.60	1341.89
67.68	63.00	0.00	16.80	304.55	106.50	0.00	16.80	632.07	132.82	0.00	16.80	135.36	189.00	0.00	16.80	67.68	219.00	0.00	16.80	1207.33
129.72	57.50	0.00	21.00	270.71	93.00	0.00	21.00	270.71	141.00	0.00	21.00	270.71	189.00	0.00	21.00	67.68	219.00	0.00	21.00	1009.53
129.72	57.50	0.00	23.80	270.71	93.00	0.00	23.80	270.71	141.00	0.00	23.80	270.71	189.00	0.00	23.80	67.68	219.00	0.00	23.80	1009.53
112.80	59.00	0.00	26.60	270.71	93.00	0.00	26.60	270.71	141.00	0.00	26.60	270.71	189.00	0.00	26.60	67.68	219.00	0.00	26.60	992.61
95.88	60.50	0.00	29.40	270.71	93.00	0.00	29.40	270.71	141.00	0.00	29.40	270.71	189.00	0.00	29.40	67.68	219.00	0.00	29.40	975.69
0.00	0.00	0.00	0.00	270.71	93.00	0.00	32.20	270.71	141.00	0.00	32.20	270.71	189.00	0.00	32.20	0.00	0.00	0.00	0.00	812.13
0.00	0.00	0.00	0.00	0.00	0.00	0.00	0.00	0.00	0.00	0.00	0.00	0.00	0.00	0.00	0.00	0.00	0.00	0.00	0.00	0.00
0.00	0.00	0.00	0.00	0.00	0.00	0.00	0.00	0.00	0.00	0.00	0.00	0.00	0.00	0.00	0.00	0.00	0.00	0.00	0.00	0.00
0.00	0.00	0.00	0.00	85.97	101.78	0.00	41.72	0.00	0.00	0.00	0.00	108.35	195.46	0.00	41.72	0.00	0.00	0.00	0.00	194.32
0.00	0.00	0.00	0.00	0.00	0.00	0.00	0.00	0.00	0.00	0.00	0.00	0.00	0.00	0.00	0.00	0.00	0.00	0.00	0.00	0.00

Table A.5: Crew and Technical area per MFZ above bulkhead deck

MFZ 1				MFZ 2				MFZ 3				MFZ 4				MFZ 5				
Area (m^2)	X (m)	Y (m)	Z (m)	Area (m^2)	X (m)	Y (m)	Z (m)	Area (m^2)	X (m)	Y (m)	Z (m)	Area (m^2)	X (m)	Y (m)	Z (m)	Area (m^2)	X (m)	Y (m)	Z (m)	TOT (m^2)
2165.60	33.80	0.00	9.80	1361.80	92.11	0.00	9.80	2667.80	163.39	0.00	9.80	0.00	0.00	0.00	0.00	324.59	225.04	0.00	9.80	6519.79
0.00	0.00	0.00	0.00	0.00	0.00	0.00	0.00	0.00	0.00	0.00	0.00	0.00	0.00	0.00	0.00	0.00	0.00	0.00	0.00	0.00
0.00	0.00	0.00	0.00	0.00	0.00	0.00	0.00	0.00	0.00	0.00	0.00	0.00	0.00	0.00	0.00	0.00	0.00	0.00	0.00	0.00
0.00	0.00	0.00	0.00	0.00	0.00	0.00	0.00	0.00	0.00	0.00	0.00	0.00	0.00	0.00	0.00	0.00	0.00	0.00	0.00	0.00
0.00	0.00	0.00	0.00	0.00	0.00	0.00	0.00	0.00	0.00	0.00	0.00	0.00	0.00	0.00	0.00	0.00	0.00	0.00	0.00	0.00
0.00	0.00	0.00	0.00	0.00	0.00	0.00	0.00	0.00	0.00	0.00	0.00	0.00	0.00	0.00	0.00	0.00	0.00	0.00	0.00	0.00
0.00	0.00	0.00	0.00	0.00	0.00	0.00	0.00	1328.40	137.67	0.00	29.40	701.10	201.08	0.00	29.40	0.00	0.00	0.00	0.00	2029.50
0.00	0.00	0.00	0.00	0.00	0.00	0.00	0.00	0.00	0.00	0.00	0.00	590.40	204.00	0.00	32.20	0.00	0.00	0.00	0.00	590.40
0.00	0.00	0.00	0.00	0.00	0.00	0.00	0.00	0.00	0.00	0.00	0.00	0.00	0.00	0.00	0.00	0.00	0.00	0.00	0.00	0.00
0.00	0.00	0.00	0.00	0.00	0.00	0.00	0.00	0.00	0.00	0.00	0.00	0.00	0.00	0.00	0.00	0.00	0.00	0.00	0.00	0.00
0.00	0.00	0.00	0.00	0.00	0.00	0.00	0.00	0.00	0.00	0.00	0.00	0.00	0.00	0.00	0.00	0.00	0.00	0.00	0.00	0.00
0.00	0.00	0.00	0.00	0.00	0.00	0.00	0.00	0.00	0.00	0.00	0.00	0.00	0.00	0.00	0.00	0.00	0.00	0.00	0.00	0.00

Appendix B

Ship Compartiment room

Below, an example of MFZ subdivision of the main ship Compartiment room volumes selected in the parametric model of the decks located under the watertight bulkhead deck is presented for *Cruise_110*. For each MFZ, the numerical values of the volume, the coordinates of their corresponding centroids and the type of room are reported.

Table B.1: Ship compartment room volume and centre position

ID	V (m^3)	X	Y	Z	Type	ID	V (m^3)	X	Y	Z	Type
1	0.00	0.00	0.00	0.00	0	10	792.01	143.95	0.00	0.85	0
	843.95	13.03	0.00	6.50	0		3028.50	143.99	0.00	4.33	2
	1330.90	10.63	0.00	8.79	2		1593.70	144.00	0.00	8.40	5
	V (m^3)	X	Y	Z	Type		V (m^3)	X	Y	Z	Type
2	0.00	0.00	0.00	0.00	0	11	471.64	158.83	0.00	0.89	0
	874.19	27.72	0.00	5.20	1		1987.10	158.97	0.00	4.35	2
	1076.90	27.03	0.00	8.41	1		1061.20	159.00	0.00	8.40	5
	V (m^3)	X	Y	Z	Type		V (m^3)	X	Y	Z	Type
3	1990.10	43.31	0.00	3.59	0	12	201.06	167.93	0.00	0.91	0
	827.68	42.05	0.00	6.29	5		961.78	167.98	0.00	4.39	2
	1641.40	42.01	0.00	8.40	6		528.98	168.00	0.00	8.40	6
	V (m^3)	X	Y	Z	Type		V (m^3)	X	Y	Z	Type
4	546.56	57.37	0.00	1.04	0	13	320.16	176.65	0.00	0.94	0
	1998.60	57.01	0.00	4.44	2		1788.10	176.87	0.00	4.44	2
	1095.40	57.00	0.00	8.40	5		1044.00	176.97	0.00	8.41	6
	V (m^3)	X	Y	Z	Type		V (m^3)	X	Y	Z	Type
5	300.22	66.00	0.00	0.98	0	14	289.33	190.94	0.00	0.97	0
	1000.80	66.00	0.00	4.43	2		2133.00	191.46	0.00	4.55	2
	547.68	66.00	0.00	8.40	5		1423.20	191.71	0.00	8.42	6
	V (m^3)	X	Y	Z	Type		V (m^3)	X	Y	Z	Type
6	593.24	74.99	0.00	0.98	0	15	102.66	206.54	0.00	0.95	0
	1995.20	75.00	0.00	4.44	2		969.18	206.61	0.00	4.69	2
	1095.40	75.00	0.00	8.40	4		760.13	206.76	0.00	8.44	6
	V (m^3)	X	Y	Z	Type		V (m^3)	X	Y	Z	Type
7	766.63	89.98	0.00	0.87	0	16	98.17	221.34	0.00	0.93	0
	3022.70	90.00	0.00	4.33	2		785.05	220.62	0.00	4.78	2
	1592.60	90.00	0.00	8.40	5		753.59	220.98	0.00	8.47	1
	V (m^3)	X	Y	Z	Type		V (m^3)	X	Y	Z	Type
8	759.72	107.99	0.00	0.87	0	17	65.47	237.84	0.00	1.09	0
	3015.50	108.00	0.00	4.34	2		283.88	238.47	0.00	4.31	2
	1592.60	108.00	0.00	8.40	3		161.17	234.55	0.00	8.58	0
	V (m^3)	X	Y	Z	Type						
9	761.86	126.04	0.00	0.87	0						
	3014.90	126.00	0.00	4.34	2						
	1592.80	126.00	0.00	8.40	3						

Appendix C

Ship Weight per MFZ

Below, an example of MFZ subdivision of the main weight selected in the parametric model of the decks located above the watertight bulkhead deck is presented for *Cruise_110*.

- Passenger Cabins.
- Internal Public Spaces.
- External Public Spaces.
- Crew Areas.
- Casings, Trunks and techical areas.

For each MFZ, the numerical values of the areas and the coordinates of their corresponding centroids are reported.

Table C.1: Passenger Cabins weigth per MFZ above bulkhead deck

MFZ 1				MFZ 2				MFZ 3				MFZ 4				MFZ 5			
Weigth (t)	X (m)	Y (m)	Z (m)	Weigth (t)	X (m)	Y (m)	Z (m)	Weigth (t)	X (m)	Y (m)	Z (m)	Weigth (t)	X (m)	Y (m)	Z (m)	Weigth (t)	X (m)	Y (m)	Z (m)
0.00	0.00	0.00	0.00	0.00	0.00	0.00	0.00	0.00	0.00	0.00	0.00	0.00	0.00	0.00	0.00	0.00	0.00	0.00	0.00
0.00	0.00	0.00	0.00	0.00	0.00	0.00	0.00	0.00	0.00	0.00	0.00	0.00	0.00	0.00	0.00	0.00	0.00	0.00	0.00
0.00	0.00	0.00	0.00	0.00	0.00	0.00	0.00	0.00	0.00	0.00	0.00	0.00	0.00	0.00	0.00	0.00	0.00	0.00	0.00
59.77	55.50	0.00	21.00	106.25	93.00	0.00	21.00	106.24	141.00	0.00	21.00	105.33	188.84	0.00	21.00	41.94	223.33	0.00	21.00
76.37	54.72	0.00	23.80	159.38	90.00	0.00	23.80	106.25	141.00	0.00	23.80	139.46	196.50	0.00	23.80	0.00	0.00	0.00	0.00
53.13	57.00	0.00	26.60	106.25	93.00	0.00	26.60	106.25	141.00	0.00	26.60	138.26	196.31	0.00	26.60	0.00	0.00	0.00	0.00
46.49	58.50	0.00	29.40	106.25	93.00	0.00	29.40	106.25	141.00	0.00	29.40	131.87	194.85	0.00	29.40	0.00	0.00	0.00	0.00
26.56	66.00	0.00	32.20	159.38	87.00	0.00	32.20	0.00	0.00	0.00	0.00	53.13	204.00	0.00	32.20	0.00	0.00	0.00	0.00
0.00	0.00	0.00	0.00	0.00	0.00	0.00	0.00	0.00	0.00	0.00	0.00	0.00	0.00	0.00	0.00	0.00	0.00	0.00	0.00
0.00	0.00	0.00	0.00	0.00	0.00	0.00	0.00	0.00	0.00	0.00	0.00	0.00	0.00	0.00	0.00	0.00	0.00	0.00	0.00
0.00	0.00	0.00	0.00	0.00	0.00	0.00	0.00	0.00	0.00	0.00	0.00	0.00	0.00	0.00	0.00	0.00	0.00	0.00	0.00
0.00	0.00	0.00	0.00	0.00	0.00	0.00	0.00	0.00	0.00	0.00	0.00	0.00	0.00	0.00	0.00	0.00	0.00	0.00	0.00

Table C.2: Internal Public Spaces weight per MFZ above bulkhead deck

MFZ 1				MFZ 2				MFZ 3				MFZ 4				MFZ 5			
Weigth (t)	X (m)	Y (m)	Z (m)	Weigth (t)	X (m)	Y (m)	Z (m)	Weigth (t)	X (m)	Y (m)	Z (m)	Weigth (t)	X (m)	Y (m)	Z (m)	Weigth (t)	X (m)	Y (m)	Z (m)
0.00	0.00	0.00	0.00	0.00	0.00	0.00	0.00	0.00	0.00	0.00	0.00	0.00	0.00	0.00	0.00	0.00	0.00	0.00	0.00
230.52	33.62	0.00	12.60	143.93	92.11	0.00	12.60	147.47	141.54	0.00	12.60	141.66	187.99	0.00	12.60	50.10	226.69	0.00	12.60
137.94	41.64	0.00	16.80	110.78	95.35	0.00	16.80	128.27	139.10	0.00	16.80	115.25	191.73	0.00	16.80	79.23	229.90	0.00	16.80
19.46	46.12	0.00	21.00	11.97	93.00	0.00	21.00	11.97	141.00	0.00	21.00	11.97	189.00	0.00	21.00	10.60	226.54	0.00	21.00
20.36	47.19	0.00	23.80	11.97	93.00	0.00	23.80	11.97	141.00	0.00	23.80	11.97	189.00	0.00	23.80	26.20	229.19	0.00	23.80
11.82	51.34	0.00	26.60	11.97	93.00	0.00	26.60	11.97	141.00	0.00	26.60	11.97	189.00	0.00	26.60	15.53	226.99	0.00	26.60
11.07	53.24	0.00	29.40	11.97	93.00	0.00	29.40	11.97	141.00	0.00	29.40	11.97	189.00	0.00	29.40	13.04	224.78	0.00	29.40
15.41	62.98	0.00	32.20	43.17	106.01	0.00	32.20	136.77	141.00	0.00	32.20	82.17	180.03	0.00	32.20	2.54	214.50	0.00	32.20
20.67	66.00	0.00	35.00	165.38	93.00	0.00	35.00	165.38	141.00	0.00	35.00	207.52	195.93	0.00	35.00	0.00	0.00	0.00	0.00
0.00	0.00	0.00	0.00	182.75	90.41	0.00	38.36	15.65	123.86	0.00	38.36	95.01	190.87	0.00	38.36	19.50	217.81	0.00	38.36
0.00	0.00	0.00	0.00	0.00	0.00	0.00	0.00	0.00	0.00	0.00	0.00	0.00	0.00	0.00	0.00	0.00	0.00	0.00	0.00
0.00	0.00	0.00	0.00	0.00	0.00	0.00	0.00	0.00	0.00	0.00	0.00	0.00	0.00	0.00	0.00	0.00	0.00	0.00	0.00

Table C.3: External Public Spaces weight per MFZ above bulkhead deck

MFZ 1				MFZ 2				MFZ 3				MFZ 4				MFZ 5			
Weigth (t)	X (m)	Y (m)	Z (m)	Weigth (t)	X (m)	Y (m)	Z (m)	Weigth (t)	X (m)	Y (m)	Z (m)	Weigth (t)	X (m)	Y (m)	Z (m)	Weigth (t)	X (m)	Y (m)	Z (m)
0.00	0.00	0.00	0.00	0.00	0.00	0.00	0.00	0.00	0.00	0.00	0.00	0.00	0.00	0.00	0.00	0.00	0.00	0.00	0.00
0.00	0.00	0.00	0.00	0.00	0.00	0.00	0.00	0.00	0.00	0.00	0.00	0.00	0.00	0.00	0.00	0.00	0.00	0.00	0.00
420.59	12.00	0.00	16.80	0.00	0.00	0.00	0.00	0.00	0.00	0.00	0.00	0.00	0.00	0.00	0.00	0.00	0.00	0.00	0.00
420.59	30.00	0.00	21.00	0.00	0.00	0.00	0.00	0.00	0.00	0.00	0.00	0.00	0.00	0.00	0.00	351.28	243.11	0.00	21.00
0.00	0.00	0.00	0.00	0.00	0.00	0.00	0.00	0.00	0.00	0.00	0.00	0.00	0.00	0.00	0.00	0.00	0.00	0.00	0.00
0.00	0.00	0.00	0.00	0.00	0.00	0.00	0.00	0.00	0.00	0.00	0.00	0.00	0.00	0.00	0.00	0.00	0.00	0.00	0.00
0.00	0.00	0.00	0.00	0.00	0.00	0.00	0.00	0.00	0.00	0.00	0.00	0.00	0.00	0.00	0.00	0.00	0.00	0.00	0.00
233.66	55.00	0.00	32.20	0.00	0.00	0.00	0.00	0.00	0.00	0.00	0.00	0.00	0.00	0.00	0.00	0.00	0.00	0.00	0.00
70.10	64.50	0.00	35.00	0.00	0.00	0.00	0.00	0.00	0.00	0.00	0.00	0.00	0.00	0.00	0.00	0.00	0.00	0.00	0.00
0.00	0.00	0.00	0.00	563.02	87.66	0.00	38.36	979.02	143.58	0.00	38.36	560.65	192.75	0.00	38.36	0.00	0.00	0.00	0.00
0.00	0.00	0.00	0.00	0.00	0.00	0.00	0.00	0.00	0.00	0.00	0.00	0.00	0.00	0.00	0.00	0.00	0.00	0.00	0.00
0.00	0.00	0.00	0.00	0.00	0.00	0.00	0.00	0.00	0.00	0.00	0.00	0.00	0.00	0.00	0.00	0.00	0.00	0.00	0.00

Table C.4: Casing and Trunk weight per MFZ above bulkhead deck

MFZ 1				MFZ 2				MFZ 3				MFZ 4				MFZ 5			
Weigth (t)	X (m)	Y (m)	Z (m)	Weigth (t)	X (m)	Y (m)	Z (m)	Weigth (t)	X (m)	Y (m)	Z (m)	Weigth (t)	X (m)	Y (m)	Z (m)	Weigth (t)	X (m)	Y (m)	Z (m)
48.79	63.00	0.00	9.80	706.63	108.07	0.00	9.80	48.79	159.00	0.00	9.80	97.58	189.00	0.00	9.80	48.79	219.00	0.00	9.80
48.79	63.00	0.00	12.60	723.42	110.35	0.00	12.60	48.79	159.00	0.00	12.60	97.58	189.00	0.00	12.60	48.79	219.00	0.00	12.60
48.79	63.00	0.00	16.80	219.55	106.50	0.00	16.80	455.66	132.82	0.00	16.80	97.58	189.00	0.00	16.80	48.79	219.00	0.00	16.80
93.52	57.50	0.00	21.00	195.15	93.00	0.00	21.00	195.15	141.00	0.00	21.00	195.15	189.00	0.00	21.00	48.79	219.00	0.00	21.00
93.52	57.50	0.00	23.80	195.15	93.00	0.00	23.80	195.15	141.00	0.00	23.80	195.15	189.00	0.00	23.80	48.79	219.00	0.00	23.80
81.32	59.00	0.00	26.60	195.15	93.00	0.00	26.60	195.15	141.00	0.00	26.60	195.15	189.00	0.00	26.60	48.79	219.00	0.00	26.60
69.12	60.50	0.00	29.40	195.15	93.00	0.00	29.40	195.15	141.00	0.00	29.40	195.15	189.00	0.00	29.40	48.79	219.00	0.00	29.40
0.00	0.00	0.00	0.00	195.15	93.00	0.00	32.20	195.15	141.00	0.00	32.20	195.15	189.00	0.00	32.20	0.00	0.00	0.00	0.00
0.00	0.00	0.00	0.00	0.00	0.00	0.00	0.00	0.00	0.00	0.00	0.00	0.00	0.00	0.00	0.00	0.00	0.00	0.00	0.00
0.00	0.00	0.00	0.00	0.00	0.00	0.00	0.00	0.00	0.00	0.00	0.00	0.00	0.00	0.00	0.00	0.00	0.00	0.00	0.00
0.00	0.00	0.00	0.00	61.98	101.78	0.00	41.72	0.00	0.00	0.00	0.00	78.11	195.46	0.00	41.72	0.00	0.00	0.00	0.00
0.00	0.00	0.00	0.00	0.00	0.00	0.00	0.00	0.00	0.00	0.00	0.00	0.00	0.00	0.00	0.00	0.00	0.00	0.00	0.00

Table C.5: Crew and Technical weight per MFZ above bulkhead deck

MFZ 1				MFZ 2				MFZ 3				MFZ 4				MFZ 5			
Weigth (t)	X (m)	Y (m)	Z (m)	Weigth (t)	X (m)	Y (m)	Z (m)	Weigth (t)	X (m)	Y (m)	Z (m)	Weigth (t)	X (m)	Y (m)	Z (m)	Weigth (t)	X (m)	Y (m)	Z (m)
0.00	33.80	0.00	9.80	0.00	92.11	0.00	9.80	0.00	163.39	0.00	9.80	0.00	0.00	0.00	0.00	0.00	225.04	0.00	9.80
0.00	0.00	0.00	0.00	0.00	0.00	0.00	0.00	0.00	0.00	0.00	0.00	0.00	0.00	0.00	0.00	0.00	0.00	0.00	0.00
0.00	0.00	0.00	0.00	0.00	0.00	0.00	0.00	0.00	0.00	0.00	0.00	0.00	0.00	0.00	0.00	0.00	0.00	0.00	0.00
0.00	0.00	0.00	0.00	0.00	0.00	0.00	0.00	0.00	0.00	0.00	0.00	0.00	0.00	0.00	0.00	0.00	0.00	0.00	0.00
0.00	0.00	0.00	0.00	0.00	0.00	0.00	0.00	0.00	0.00	0.00	0.00	0.00	0.00	0.00	0.00	0.00	0.00	0.00	0.00
0.00	0.00	0.00	0.00	0.00	0.00	0.00	0.00	0.00	0.00	0.00	0.00	0.00	0.00	0.00	0.00	0.00	0.00	0.00	0.00
0.00	0.00	0.00	0.00	0.00	0.00	0.00	0.00	0.00	137.67	0.00	29.40	0.00	201.08	0.00	29.40	0.00	0.00	0.00	0.00
0.00	0.00	0.00	0.00	0.00	0.00	0.00	0.00	0.00	0.00	0.00	0.00	0.00	204.00	0.00	32.20	0.00	0.00	0.00	0.00
0.00	0.00	0.00	0.00	0.00	0.00	0.00	0.00	0.00	0.00	0.00	0.00	0.00	0.00	0.00	0.00	0.00	0.00	0.00	0.00
0.00	0.00	0.00	0.00	0.00	0.00	0.00	0.00	0.00	0.00	0.00	0.00	0.00	0.00	0.00	0.00	0.00	0.00	0.00	0.00
0.00	0.00	0.00	0.00	0.00	0.00	0.00	0.00	0.00	0.00	0.00	0.00	0.00	0.00	0.00	0.00	0.00	0.00	0.00	0.00
0.00	0.00	0.00	0.00	0.00	0.00	0.00	0.00	0.00	0.00	0.00	0.00	0.00	0.00	0.00	0.00	0.00	0.00	0.00	0.00

Appendix D

Machineries database

Below is the database of diesel generators, POD and PEM used for machinery selection, including their corresponding weights.

Table D.1: POD/PEM database

Type (-)	Model (-)	Power (kW)	Speed (rpm)	Length (m)	Width (m)	Heigth (m)	tilt angle (deg)	Weight (t)
POD	VO1600	10000	220	8.50	4.50	8.00	3.00	116.00
POD	VO1800	13500	190	9.40	4.80	8.30	4.00	148.00
POD	VO2100	20500	170	10.10	5.00	9.60	4.00	172.00
POD	VO2300	22500	155	10.60	5.50	10.70	4.00	220.00
POD	VO2500	25000	140	11.70	6.00	12.00	0.00	270.00
PEM	M3HXD	20000	120	6.72	5.12	5.88	0.00	155.00

Table D.2: Diesel Generator database

Supplier	Model	Power	Speed	Dry mass	Length	Height	Width
-	-	(kW)	(rpm)	(t)	(mm)	(mm)	(mm)
Wärtsilä	8V31SG	4240	720	94.3	9100	4150	3600
Wärtsilä	10V31SG	5300	720	107.2	9900	4150	3600
Wärtsilä	12V31SG	6360	720	122.3	11300	4200	3600
Wärtsilä	14V31SG	7420	720	138.4	11900	4300	3600
Wärtsilä	16V31SG	8480	720	150.4	12540	4300	3600
Wärtsilä	6L20DF	1110	1200	16.9	5325	2825	2070
Wärtsilä	8L20DF	1480	1200	20.8	6030	2875	2070
Wärtsilä	9L20DF	1665	1200	23.9	6535	2925	2070

Continued on next page

Supplier	Model	Power	Speed	Dry mass	Length	Height	Width
-	-	(kW)	(rpm)	(t)	(mm)	(mm)	(mm)
Wärtsilä	8V31DF	4240	720	94.3	9100	4150	3600
Wärtsilä	10V31DF	5300	720	107.2	9900	4150	3600
Wärtsilä	12V31DF	6360	720	122.3	11300	4200	3600
Wärtsilä	14V31DF	7420	720	138.4	11900	4300	3600
Wärtsilä	16V31DF	8480	720	150.4	12540	4300	3600
Wärtsilä	6L34DF	2880	720	57	8700	3795	2290
Wärtsilä	8L34DF	3840	720	76	10410	3975	2690
Wärtsilä	9L34DF	4320	720	87	10475	3975	2890
Wärtsilä	12V34DF	5760	720	96	10075	3820	3060
Wärtsilä	16V34DF	7680	720	121	11175	3920	3060
Wärtsilä	8V31	4720	720	94.3	9100	4150	3600
Wärtsilä	10V31	5900	720	107.2	9900	4150	3600
Wärtsilä	12V31	7080	720	122.3	11300	4200	3600
Wärtsilä	14V31	8260	720	138.4	11900	4300	3600
Wärtsilä	16V31	9440	720	150.4	12540	4300	3600
Wärtsilä	6L32	3360	720	57	8345	3745	2490
Wärtsilä	8L32	4480	720	76	10410	4010	2690
Wärtsilä	9L32	5040	720	86	10505	4010	2890
Wärtsilä	12V32	6720	720	100	10700	4130	3060
Wärtsilä	16V32	8960	720	127	11465	4445	3360
Wärtsilä	6L32	3360	720	57	8345	3745	2490
Wärtsilä	8L32	4480	720	76	10410	4010	2690
Wärtsilä	9L32	5040	720	86	10505	4010	2890
Wärtsilä	12V32	6720	720	100	10700	4130	3060
Wärtsilä	16V32	8960	720	127	11465	4445	3360

Continued on next page

Supplier	Model	Power	Speed	Dry mass	Length	Height	Width
-	-	(kW)	(rpm)	(t)	(mm)	(mm)	(mm)
MAN	5L23/30DF	625	720	17.3	3469	2749	1210
MAN	6L23/30DF	750	720	19	3839	2749	1210
MAN	7L23/30DF	875	720	21.4	4209	2749	1210
MAN	8L23/30DF	1000	720	23.3	4579	2749	1210
MAN	5L28/32DF	1050	720	32.6	4321	2835	1490
MAN	6L28/32DF	1260	720	36.3	4801	3009	1490
MAN	7L28/32DF	1470	720	39.4	5281	3009	1490
MAN	8L28/32DF	1680	720	40.7	5761	3009	1490
MAN	9L28/32DF	1890	720	47.1	6241	3009	1490
MAN	6L35/44DF	3360	720	76	6270	4631	2360
MAN	7L35/44DF	3920	720	84	6900	4867	2360
MAN	8L35/44DF	4480	720	91	7480	4867	2360
MAN	9L35/44DF	5040	720	96	8110	4867	2360
MAN	12V32/44CR	7200	720	117	5382	5014	4260
MAN	14V32/44CR	8120	720	131	6012	5014	4260
MAN	16V32/44CR	9600	720	144	6642	5014	4260
MAN	18V32/44CR	10800	720	159	7272	5014	4260
MAN	20V32/44CR	12000	720	172	7902	5014	4260
MAN	6L32/44CR	3600	720	71	10738	4768	2490
MAN	7L32/44CR	4060	720	78	11268	4768	2490
MAN	8L32/44CR	4800	720	84	11798	4955	2573
MAN	9L32/44CR	5400	720	91	12328	4955	2573
MAN	10L32/44CR	6000	720	97	12858	4955	2573
MAN	12V32/40	6000	720	101	11045	4850	3365
MAN	14V32/40	7000	720	113	11710	4850	3365

Continued on next page

Supplier	Model	Power	Speed	Dry mass	Length	Height	Width
-	-	(kW)	(rpm)	(t)	(mm)	(mm)	(mm)
MAN	16V32/40	8000	720	126	12555	5245	3730
MAN	18V32/40	9000	720	138	13185	5245	3730
MAN	6L32/40	3000	720	70.5	9755	4622	2360
MAN	7L32/40	3500	720	74.3	10285	4622	2360
MAN	8L32/40	4000	720	81.8	11035	4840	2360
MAN	9L32/40	4500	720	85.8	11565	4840	2360
MAN	5L27/38	-	720	40	6832	3712	1480
MAN	6L27/38	2100	720	44.5	7557	3712	1480
MAN	7L27/38	2450	720	50.4	8002	3899	1480
MAN	8L27/38	2800	720	58.2	8667	3899	1480
MAN	9L27/38	3150	720	64.7	9112	3899	1480
MAN	5L27/38 Mk2	1500	720	40	6832	3712	1480
MAN	6L27/38 Mk2	1980	720	44.5	7557	3712	1480
MAN	7L27/38 Mk2	2310	720	50.4	8002	3899	1480
MAN	8L27/38 Mk2	2640	720	58.2	8667	3899	1480
MAN	9L27/38 Mk2	2970	720	64.7	9112	3899	1480
MAN	5L23/30H Mk3	850	720	16.8	5581	2621	1210
MAN	6L23/30H Mk3	1020	720	18.4	6001	2621	1210
MAN	7L23/30H Mk3	1190	720	20.7	6421	2621	1210
MAN	8L23/30H Mk3	1360	720	22.5	6841	2621	1210
MAN	9L23/30H Mk3	1530	720	24.5	7261	2621	1210
MAN	5L23/30H Mk2	710	720	16.8	5581	2621	1210
MAN	6L23/30H Mk2	852	720	18.4	6001	2621	1210
MAN	7L23/30H Mk2	994	720	20.7	6421	2621	1210
MAN	8L23/30H Mk2	1136	720	22.5	6841	2621	1210

Continued on next page

Supplier	Model	Power	Speed	Dry mass	Length	Height	Width
-	-	(kW)	(rpm)	(t)	(mm)	(mm)	(mm)
MAN	5L23/30DF	625	720	17.3	5671	2746	1210
MAN	6L23/30DF	750	720	19	6091	2749	1210
MAN	7L23/30DF	875	720	24.1	6511	2749	1210
MAN	8L23/30DF	1000	720	23.3	6931	2749	1210
MAN	5L21/31DF	1000	900	22.2	6049	3074	1220
MAN	6L21/31DF	1320	900	25.7	6456	3161	1220
MAN	7L21/31DF	1540	900	29.2	6791	3161	1220
MAN	8L21/31DF	1760	900	32.7	7146	3161	1220
MAN	9L21/31DF	1980	900	36.2	7636	3267	1220

Appendix E

Simulated itinerary

Below the intinerary subdivev by subleg regarding a tipical West Mediterrean itinerary. For each row is specified the type of the itineray (stay in port, manoeuvreing, transit or navigation phase of the itynerary), the latitude ϕ, longitude θ, the length, the time Δt and the speed V_l of the sublegs.

Table E.1: Detailed Schedule and discretisation of original itinerary

ID	type	ϕ	θ	ψ	length	Δt	V_l	ID	type	ϕ	θ	ψ	length	Δt	V_l
	-	(deg)	(deg)	(deg)	(nm)	(h)	(kn)		-	(deg)	(deg)	(deg)	(nm)	(h)	(kn)
1	Port	44.41	8.92	0	0.00	2.00	0.00	133	Man	41.36	2.17	209	0.40	0.20	2.00
2	Port	44.41	8.92	0	0.00	2.00	0.00	134	Man	41.36	2.17	207	0.03	0.02	2.01
3	Port	44.41	8.92	0	0.00	2.00	0.00	135	Transit	41.35	2.17	207	0.41	0.04	10.94
4	Port	44.41	8.92	0	0.00	2.00	0.00	136	Transit	41.34	2.17	191	0.50	0.05	10.91
5	Port	44.41	8.92	0	0.00	2.00	0.00	137	Transit	41.32	2.17	188	0.96	0.09	10.89
6	Port	44.41	8.92	0	0.00	1.00	0.00	138	Transit	41.32	2.17	162	0.47	0.04	10.90
7	Man	44.41	8.92	192	0.27	0.13	2.00	139	Transit	41.30	2.17	169	1.05	0.10	10.91
8	Man	44.40	8.92	143	0.23	0.12	2.00	140	Transit	41.29	2.18	167	0.61	0.06	10.93
9	Transit	44.40	8.92	143	0.07	0.01	7.59	141	Nav	41.28	2.18	167	0.57	0.03	17.42
10	Transit	44.40	8.92	173	0.32	0.04	7.47	142	Nav	41.23	2.21	154	3.15	0.18	17.44
11	Transit	44.39	8.93	124	0.53	0.07	7.50	143	Nav	41.27	2.28	57	3.59	0.21	17.45
12	Transit	44.39	8.94	117	0.35	0.05	7.51	144	Nav	41.31	2.36	57	4.48	0.26	17.45
13	Transit	44.39	8.94	135	0.36	0.05	7.48	145	Nav	41.35	2.44	57	4.48	0.26	17.45
14	Transit	44.38	8.95	170	0.56	0.07	7.52	146	Nav	41.39	2.53	57	4.48	0.26	17.45
15	Transit	44.37	8.95	164	0.31	0.04	7.49	147	Nav	41.43	2.61	57	4.48	0.26	17.45
16	Nav	44.31	8.97	164	3.84	0.31	12.30	148	Nav	41.47	2.69	57	4.48	0.26	17.45
17	Nav	44.26	8.89	233	4.51	0.37	12.30	149	Nav	41.51	2.78	57	4.47	0.26	17.45
18	Nav	44.22	8.81	233	4.51	0.37	12.30	150	Nav	41.55	2.86	57	4.47	0.26	17.45
19	Nav	44.17	8.72	233	4.51	0.37	12.30	151	Nav	41.59	2.94	57	4.47	0.26	17.45
20	Nav	44.13	8.64	233	4.51	0.37	12.30	152	Nav	41.63	3.02	57	3.90	0.22	17.45
21	Nav	44.08	8.56	233	4.51	0.37	12.30	153	Nav	41.68	3.10	50	4.90	0.28	17.45
22	Nav	44.04	8.47	233	4.52	0.37	12.30	154	Nav	41.73	3.18	50	4.90	0.28	17.45
23	Nav	43.99	8.39	233	4.52	0.37	12.30	155	Nav	41.79	3.27	50	4.89	0.28	17.45
24	Nav	43.95	8.31	233	4.52	0.37	12.30	156	Nav	41.84	3.35	50	4.89	0.28	17.45
25	Nav	43.90	8.22	233	4.52	0.37	12.30	157	Nav	41.89	3.43	50	4.89	0.28	17.45
26	Nav	43.85	8.14	233	4.52	0.37	12.30	158	Nav	41.94	3.52	50	4.89	0.28	17.45
27	Nav	43.81	8.06	233	4.53	0.37	12.30	159	Nav	41.96	3.55	50	1.88	0.11	17.45
28	Nav	43.76	7.97	233	4.53	0.37	12.30	160	Nav	42.03	3.63	45	5.27	0.30	17.45
29	Nav	43.72	7.89	233	4.53	0.37	12.30	161	Nav	42.09	3.71	45	5.27	0.30	17.45

Continued on next page

ID	type	ϕ	θ	ψ	length	Δt	V_l	ID	type	ϕ	θ	ψ	length	Δt	V_l
	-	(deg)	(deg)	(deg)	(nm)	(h)	(kn)		-	(deg)	(deg)	(deg)	(nm)	(h)	(kn)
30	Nav	43.67	7.81	233	4.53	0.37	12.30	162	Nav	42.15	3.80	45	5.27	0.30	17.45
31	Nav	43.63	7.72	233	4.54	0.37	12.30	163	Nav	42.21	3.88	45	5.26	0.30	17.45
32	Nav	43.58	7.64	233	4.54	0.37	12.30	164	Nav	42.26	3.94	45	3.92	0.22	17.45
33	Nav	43.54	7.56	233	4.54	0.37	12.30	165	Nav	42.32	4.03	45	5.27	0.30	17.45
34	Nav	43.49	7.47	233	4.54	0.37	12.30	166	Nav	42.39	4.11	45	5.27	0.30	17.45
35	Nav	43.45	7.39	233	4.54	0.37	12.30	167	Nav	42.45	4.19	45	5.27	0.30	17.45
36	Nav	43.40	7.31	233	4.55	0.37	12.30	168	Nav	42.51	4.28	45	5.26	0.30	17.45
37	Nav	43.35	7.22	233	4.55	0.37	12.30	169	Nav	42.57	4.36	44	5.26	0.30	17.45
38	Nav	43.31	7.14	233	4.55	0.37	12.30	170	Nav	42.64	4.44	44	5.26	0.30	17.45
39	Nav	43.26	7.06	233	4.55	0.37	12.30	171	Nav	42.70	4.53	44	5.25	0.30	17.45
40	Nav	43.22	6.97	233	4.56	0.37	12.30	172	Nav	42.76	4.61	44	5.25	0.30	17.45
41	Nav	43.17	6.89	233	4.56	0.37	12.30	173	Nav	42.82	4.69	44	5.25	0.30	17.45
42	Nav	43.13	6.81	233	4.56	0.37	12.30	174	Nav	42.89	4.78	44	5.25	0.30	17.45
43	Nav	43.08	6.72	233	4.56	0.37	12.30	175	Nav	42.95	4.86	44	5.24	0.30	17.45
44	Nav	43.04	6.64	233	4.56	0.37	12.30	176	Nav	43.01	4.94	44	5.24	0.30	17.45
45	Nav	43.02	6.62	233	1.08	0.09	12.30	177	Nav	43.02	4.95	44	0.50	0.03	17.45
46	Nav	42.99	6.54	243	4.11	0.33	12.30	178	Nav	43.08	5.03	44	5.22	0.30	17.45
47	Nav	42.96	6.45	243	4.11	0.33	12.30	179	Nav	43.12	5.08	44	3.20	0.18	17.45
48	Nav	42.93	6.37	243	4.11	0.33	12.30	180	Nav	43.18	5.17	44	5.21	0.30	17.46
49	Nav	42.91	6.32	243	2.59	0.21	12.30	181	Nav	43.19	5.18	44	0.90	0.05	17.46
50	Nav	42.93	6.24	283	3.76	0.31	12.30	182	Nav	43.26	5.17	352	4.31	0.25	17.45
51	Nav	42.94	6.15	283	3.76	0.31	12.30	183	Nav	43.32	5.25	44	4.88	0.28	17.43
52	Nav	42.95	6.07	283	3.76	0.31	12.30	184	Nav	43.37	5.33	49	4.80	0.28	17.46
53	Nav	42.97	5.99	283	3.76	0.31	12.30	185	Nav	43.38	5.35	49	1.25	0.07	17.46
54	Nav	42.98	5.93	283	2.52	0.21	12.30	186	Transit	43.35	5.30	229	2.80	0.57	4.90
55	Nav	42.99	5.85	286	3.80	0.31	12.30	187	Transit	43.35	5.31	107	0.44	0.09	4.89
56	Nav	43.01	5.76	286	3.80	0.31	12.30	188	Transit	43.35	5.32	120	0.32	0.07	4.91
57	Nav	43.03	5.68	286	3.80	0.31	12.30	189	Transit	43.35	5.33	122	0.45	0.09	4.89
58	Nav	43.05	5.60	286	3.80	0.31	12.30	190	Man	43.35	5.32	302	0.19	0.11	1.67
59	Nav	43.06	5.51	286	3.80	0.31	12.30	191	Man	43.34	5.33	124	0.31	0.19	1.67
60	Nav	43.08	5.43	286	3.80	0.31	12.30	192	Port	43.34	5.33	0	0.00	2.00	0.00
61	Nav	43.10	5.35	286	3.79	0.31	12.30	193	Port	43.34	5.33	0	0.00	2.00	0.00
62	Nav	43.11	5.26	286	3.79	0.31	12.30	194	Port	43.34	5.33	0	0.00	2.00	0.00
63	Nav	43.13	5.18	286	3.79	0.31	12.30	195	Port	43.34	5.33	0	0.00	2.00	0.00
64	Nav	43.15	5.10	286	3.79	0.31	12.30	196	Port	43.34	5.33	0	0.00	1.00	0.00
65	Nav	43.16	5.06	286	1.50	0.12	12.30	197	Man	43.35	5.32	306	0.46	0.23	2.00
66	Nav	43.17	4.98	286	3.79	0.31	12.30	198	Man	43.35	5.32	295	0.04	0.02	2.00
67	Nav	43.19	4.90	286	3.79	0.31	12.30	199	Transit	43.35	5.31	295	0.82	0.03	23.90
68	Nav	43.21	4.81	286	3.79	0.31	12.30	200	Transit	43.34	5.28	228	1.45	0.06	24.08
69	Nav	43.22	4.73	286	3.79	0.31	12.30	201	Transit	43.31	5.26	207	1.74	0.07	23.98
70	Nav	43.24	4.65	286	3.79	0.31	12.30	202	Nav	43.27	5.23	207	2.87	0.18	15.64
71	Nav	43.26	4.56	286	3.79	0.31	12.30	203	Nav	43.19	5.30	150	5.77	0.37	15.65
72	Nav	43.28	4.48	286	3.79	0.31	12.30	204	Nav	43.17	5.31	150	0.83	0.05	15.65
73	Nav	43.29	4.40	286	3.79	0.31	12.30	205	Nav	43.12	5.39	133	5.00	0.32	15.64
74	Nav	43.31	4.31	286	3.78	0.31	12.30	206	Nav	43.07	5.47	133	4.48	0.29	15.64
75	Nav	43.33	4.23	286	3.78	0.31	12.30	207	Nav	43.03	5.55	119	4.18	0.27	15.64
76	Nav	43.35	4.15	286	3.78	0.31	12.30	208	Nav	43.00	5.63	119	4.18	0.27	15.64
77	Nav	43.36	4.09	286	2.74	0.22	12.30	209	Nav	42.96	5.72	119	4.19	0.27	15.64
78	Nav	43.32	4.00	239	4.22	0.34	12.30	210	Nav	42.93	5.80	119	4.19	0.27	15.64
79	Nav	43.29	3.92	240	4.22	0.34	12.30	211	Nav	42.90	5.88	119	4.19	0.27	15.64
80	Nav	43.27	3.88	240	2.10	0.17	12.30	212	Nav	42.89	5.89	119	0.32	0.02	15.64
81	Nav	43.23	3.80	238	4.32	0.35	12.30	213	Nav	42.89	5.97	90	3.66	0.23	15.64
82	Nav	43.19	3.71	238	4.32	0.35	12.30	214	Nav	42.89	6.06	90	3.66	0.23	15.64

Continued on next page

ID	type	ϕ	θ	ψ	length	Δt	V_l	ID	type	ϕ	θ	ψ	length	Δt	V_l
	-	(deg)	(deg)	(deg)	(nm)	(h)	(kn)		-	(deg)	(deg)	(deg)	(nm)	(h)	(kn)
83	Nav	43.15	3.63	238	4.32	0.35	12.30	215	Nav	42.89	6.14	90	3.66	0.23	15.64
84	Nav	43.11	3.55	238	4.32	0.35	12.30	216	Nav	42.89	6.22	90	3.66	0.23	15.64
85	Nav	43.08	3.46	238	4.32	0.35	12.30	217	Nav	42.89	6.31	90	3.66	0.23	15.64
86	Nav	43.04	3.38	238	4.32	0.35	12.30	218	Nav	42.89	6.39	90	3.66	0.23	15.64
87	Nav	43.01	3.33	238	2.58	0.21	12.30	219	Nav	42.89	6.41	90	0.95	0.06	15.64
88	Nav	42.93	3.32	186	5.03	0.41	12.30	220	Nav	42.91	6.49	71	3.88	0.25	15.65
89	Nav	42.85	3.30	186	5.03	0.41	12.30	221	Nav	42.94	6.58	71	3.88	0.25	15.65
90	Nav	42.78	3.29	186	4.04	0.33	12.30	222	Nav	42.95	6.64	71	2.98	0.19	15.65
91	Nav	42.70	3.31	172	5.05	0.41	12.30	223	Nav	43.00	6.72	53	4.59	0.29	15.64
92	Nav	42.61	3.33	172	5.05	0.41	12.30	224	Nav	43.04	6.81	53	4.59	0.29	15.64
93	Nav	42.53	3.34	172	5.05	0.41	12.30	225	Nav	43.09	6.89	53	4.58	0.29	15.64
94	Nav	42.45	3.36	172	5.05	0.41	12.30	226	Nav	43.14	6.97	53	4.58	0.29	15.64
95	Nav	42.36	3.37	172	5.05	0.41	12.30	227	Nav	43.14	6.99	53	0.70	0.04	15.64
96	Nav	42.32	3.38	172	2.78	0.23	12.30	228	Nav	43.19	7.07	53	4.57	0.29	15.64
97	Nav	42.24	3.36	191	5.10	0.41	12.30	229	Nav	43.23	7.15	53	4.56	0.29	15.64
98	Nav	42.15	3.34	191	5.10	0.41	12.30	230	Nav	43.28	7.24	53	4.56	0.29	15.64
99	Nav	42.07	3.32	191	5.10	0.41	12.30	231	Nav	43.33	7.32	53	4.56	0.29	15.64
100	Nav	41.99	3.29	191	5.10	0.41	12.30	232	Nav	43.37	7.40	53	4.56	0.29	15.64
101	Nav	41.90	3.27	191	5.10	0.41	12.30	233	Nav	43.42	7.49	53	4.56	0.29	15.64
102	Nav	41.86	3.26	191	2.49	0.20	12.30	234	Nav	43.46	7.57	53	4.55	0.29	15.64
103	Nav	41.81	3.18	232	4.76	0.39	12.30	235	Nav	43.51	7.65	53	4.55	0.29	15.64
104	Nav	41.76	3.09	232	4.76	0.39	12.30	236	Nav	43.55	7.73	53	4.32	0.28	15.64
105	Nav	41.71	3.01	232	4.76	0.39	12.30	237	Nav	43.60	7.82	51	4.65	0.30	15.64
106	Nav	41.66	2.93	232	4.76	0.39	12.30	238	Nav	43.65	7.90	51	4.65	0.30	15.64
107	Nav	41.62	2.85	232	4.77	0.39	12.30	239	Nav	43.70	7.98	51	4.65	0.30	15.64
108	Nav	41.57	2.76	232	4.77	0.39	12.30	240	Nav	43.75	8.07	51	4.64	0.30	15.64
109	Nav	41.52	2.68	232	4.77	0.39	12.30	241	Nav	43.79	8.15	51	4.64	0.30	15.64
110	Nav	41.47	2.60	232	4.77	0.39	12.30	242	Nav	43.84	8.23	51	4.64	0.30	15.64
111	Nav	41.42	2.51	232	4.77	0.39	12.30	243	Nav	43.89	8.32	51	4.64	0.30	15.64
112	Nav	41.37	2.43	232	4.78	0.39	12.30	244	Nav	43.94	8.40	51	4.63	0.30	15.64
113	Nav	41.32	2.35	232	4.78	0.39	12.30	245	Nav	43.99	8.48	51	4.63	0.30	15.64
114	Nav	41.27	2.26	232	4.78	0.39	12.30	246	Nav	44.04	8.57	51	4.63	0.30	15.64
115	Nav	41.26	2.24	232	1.16	0.09	12.30	247	Nav	44.09	8.65	51	4.63	0.30	15.64
116	Nav	41.28	2.18	298	2.93	0.24	12.30	248	Nav	44.13	8.73	51	4.63	0.30	15.64
117	Nav	41.30	2.18	346	0.83	0.07	12.31	249	Nav	44.18	8.82	51	4.62	0.30	15.64
118	Nav	41.33	2.16	340	2.21	0.18	12.31	250	Nav	44.23	8.90	51	4.62	0.30	15.64
119	Transit	41.32	2.17	160	0.83	0.17	4.80	251	Nav	44.25	8.93	51	1.82	0.12	15.64
120	Transit	41.33	2.17	342	0.63	0.13	4.80	252	Nav	44.31	9.00	40	4.54	0.29	15.63
121	Transit	41.35	2.17	10	1.32	0.28	4.80	253	Nav	44.36	8.97	337	3.17	0.20	15.66
122	Transit	41.37	2.18	26	1.22	0.25	4.80	254	Nav	44.38	8.96	334	1.49	0.10	15.62
123	Man	41.36	2.18	206	0.39	0.23	1.67	255	Transit	44.38	8.96	154	0.11	0.04	2.82
124	Man	41.36	2.18	55	0.11	0.07	1.67	256	Transit	44.39	8.95	337	0.46	0.16	2.83
125	Port	41.36	2.18	0	0.00	2.00	0.00	257	Transit	44.40	8.93	297	1.27	0.45	2.83
126	Port	41.36	2.18	0	0.00	2.00	0.00	258	Transit	44.40	8.92	314	0.28	0.10	2.83
127	Port	41.36	2.18	0	0.00	2.00	0.00	259	Transit	44.40	8.92	348	0.38	0.13	2.83
128	Port	41.36	2.18	0	0.00	2.00	0.00	260	Man	44.40	8.92	168	0.02	0.01	1.67
129	Port	41.36	2.18	0	0.00	2.00	0.00	261	Man	44.41	8.92	321	0.19	0.11	1.67
130	Port	41.36	2.18	0	0.00	1.00	0.00	262	Man	44.41	8.92	355	0.21	0.13	1.67
131	Port	41.36	2.18	0	0.00	1.00	0.00	263	Man	44.41	8.92	31	0.08	0.05	1.67
132	Man	41.36	2.18	241	0.07	0.04	2.00								

Appendix F

Step 2 variables-attributes comparison

Below the figures show the comparison between variable and variables, variables attributes and attributes-attributes for only the Non-dominated projects only for the Step 2 of the methodology.

F.1 Step 2 variables variables analisys

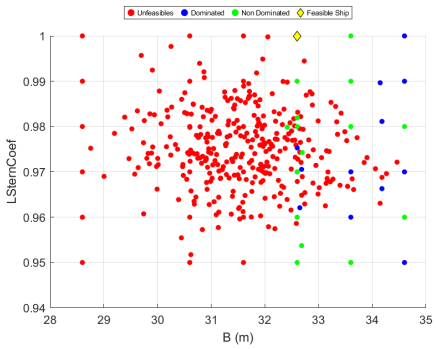

Figure F.1: B vs LSternCoef

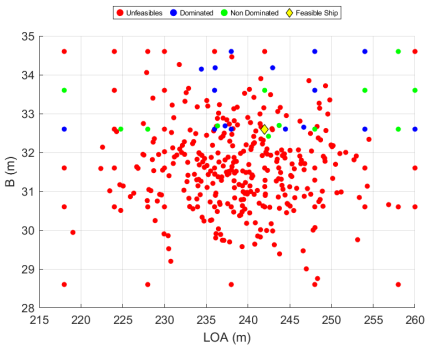

Figure F.3: L_{OA} vs B (m)

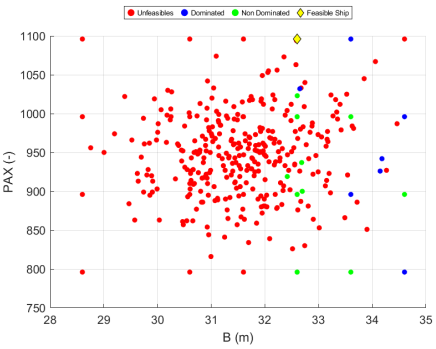

Figure F.2: B vs PAX

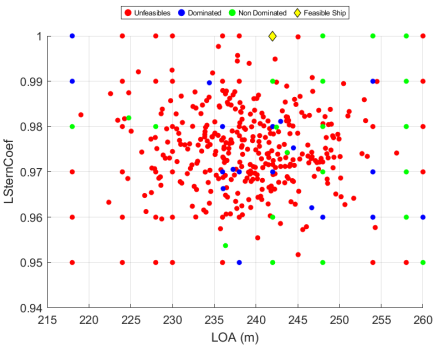

Figure F.4: L_{OA} vs LSternCoef

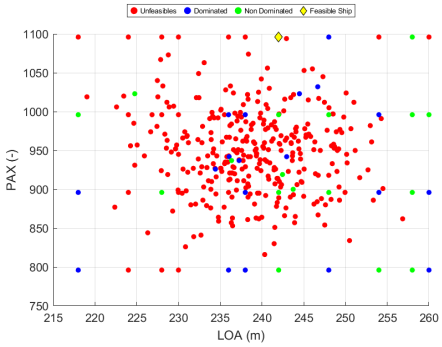

Figure F.5: L_{OA} vs PAX

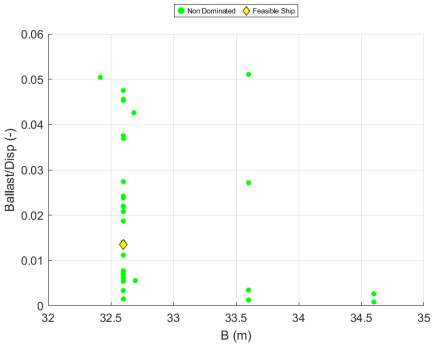

Figure F.8: B vs W_{WB}/Δ

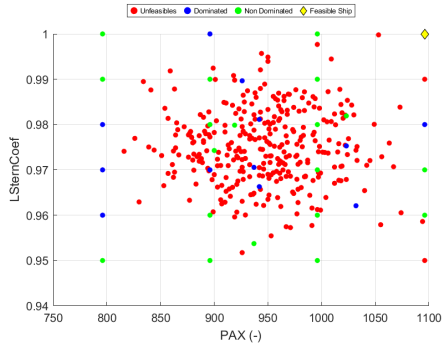

Figure F.6: PAX vs LSternCoef

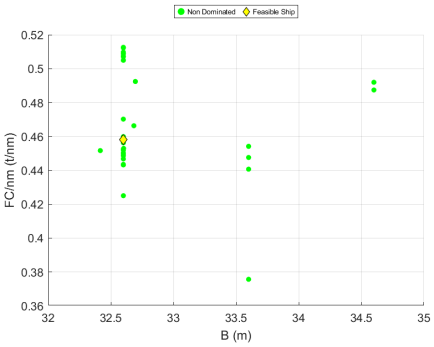

Figure F.9: B vs fc/nm

F.2 Step 2 variables attributes analisys

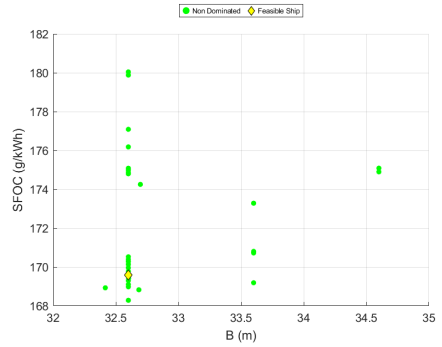

Figure F.7: B vs $\overline{SFOC}$

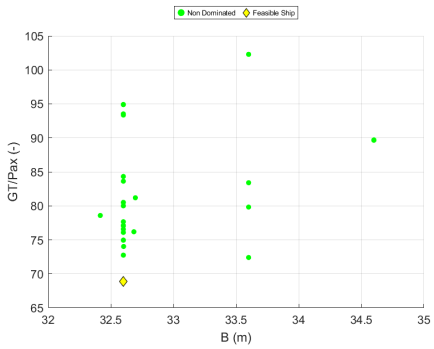

Figure F.10: B vs GT/PAX

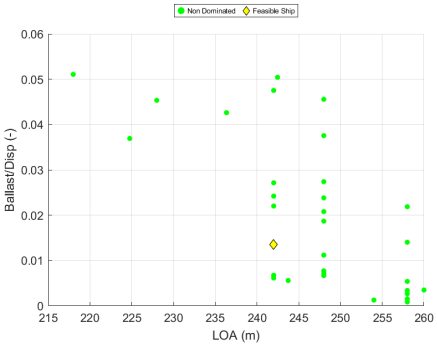

Figure F.11: L_{OA} vs W_{WB}/Δ

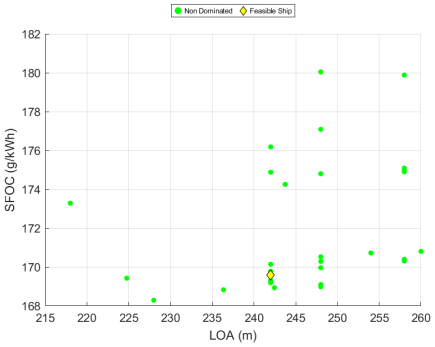

Figure F.14: L_{OA} vs $\overline{SFOC}$

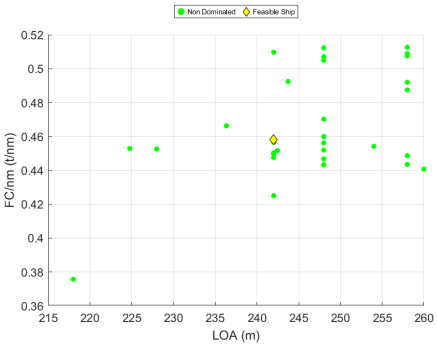

Figure F.12: L_{OA} vs fc/nm

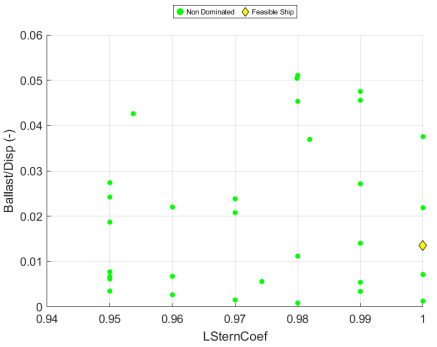

Figure F.15: $L_{Stern_{Profile}}$ vs W_{WB}/Δ

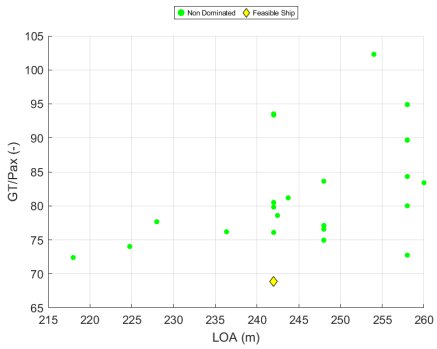

Figure F.13: L_{OA} vs GT/PAX

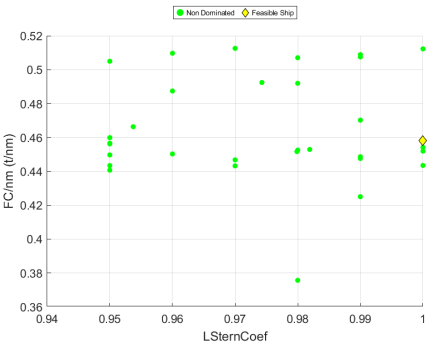

Figure F.16: $L_{Stern_{Profile}}$ vs fc/nm

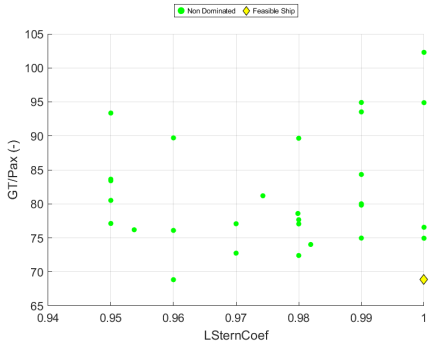

Figure F.17: $L_{Stern_{Profile}}$ vs GT/PAX

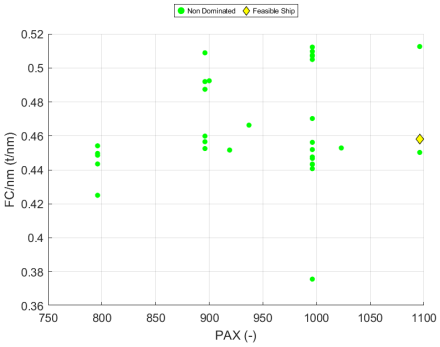

Figure F.20: PAX vs fc/nm

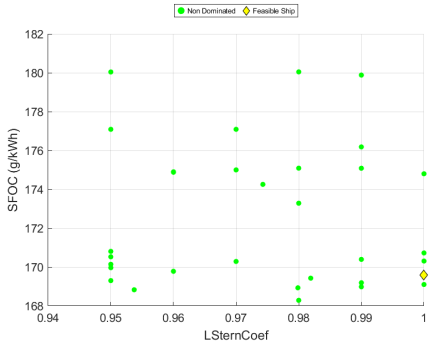

Figure F.18: $L_{Stern_{Profile}}$ vs $\overline{SFOC}$

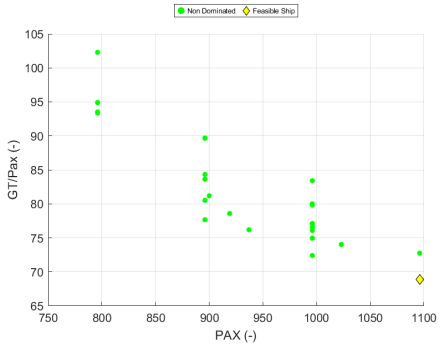

Figure F.21: PAX vs GT/PAX

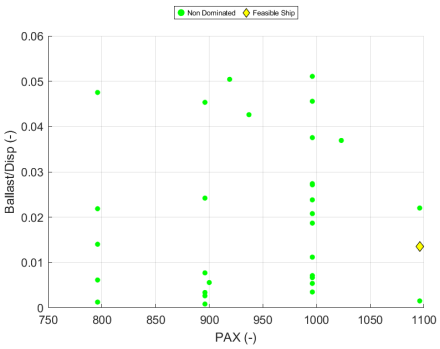

Figure F.19: PAX vs W_{WB}/Δ

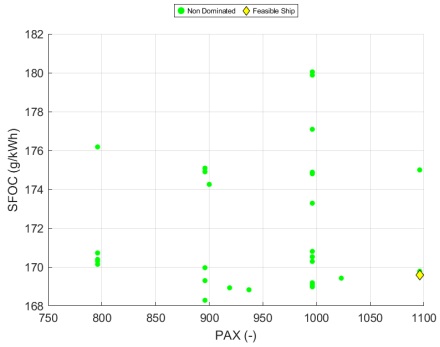

Figure F.22: PAX vs $\overline{SFOC}$

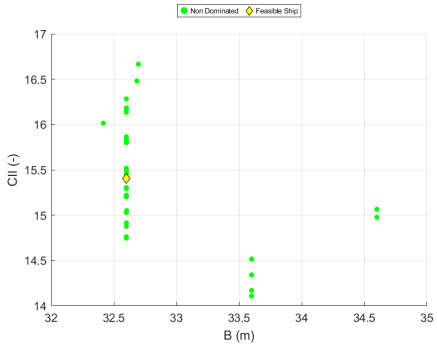

Figure F.23: B vs CII

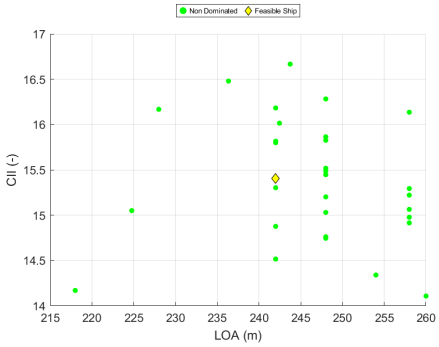

Figure F.26: L_{OA} vs CII

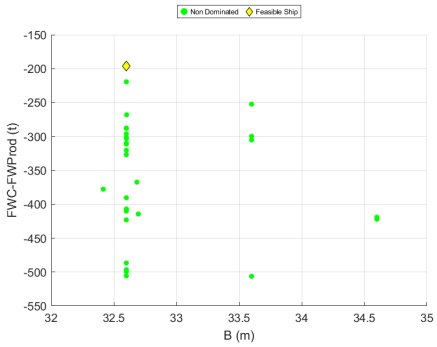

Figure F.24: B vs $(FWc - FW_{Prod})$

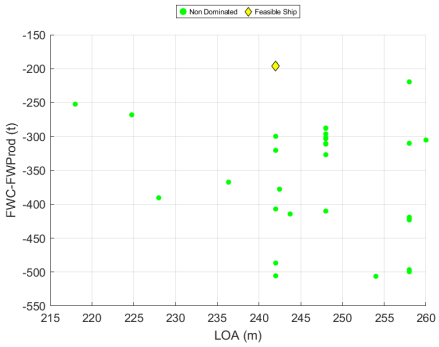

Figure F.27: L_{OA} vs $(FWc - FW_{Prod})$

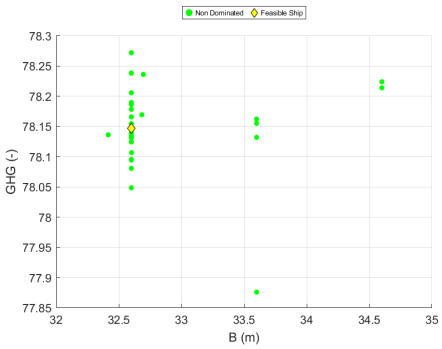

Figure F.25: B vs GHG

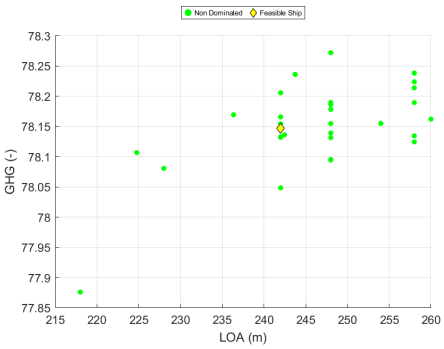

Figure F.28: L_{OA} vs GHG

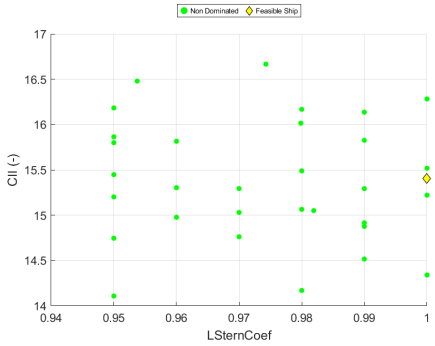

Figure F.29: $L_{Stern_{Profile}}$ vs CII

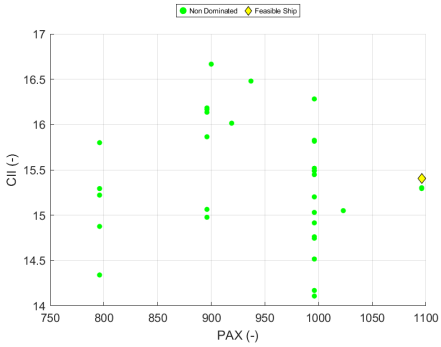

Figure F.32: PAX vs CII

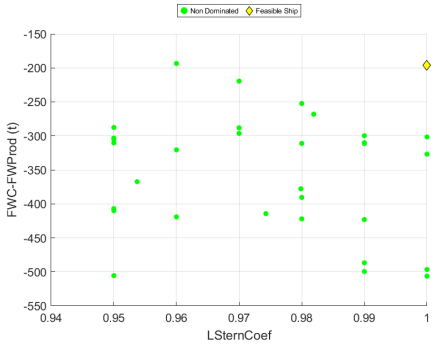

Figure F.30: $L_{Stern_{Profile}}$ vs $(FWc - FW_{Prod})$

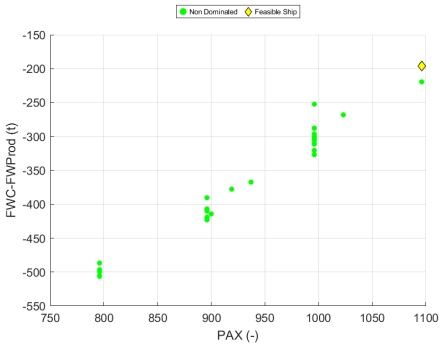

Figure F.33: PAX vs $(FWc - FW_{Prod})$

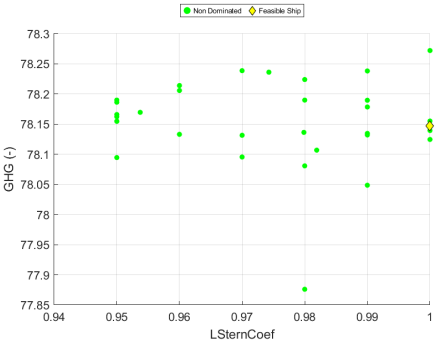

Figure F.31: $L_{Stern_{Profile}}$ vs GHG

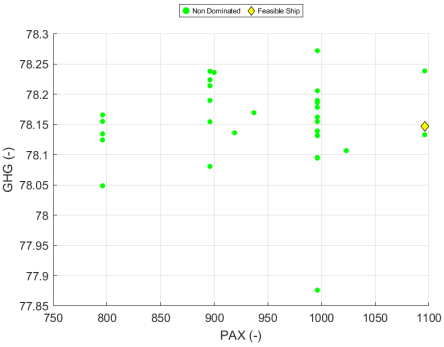

Figure F.34: PAX vs GHG

F.3 Step 2 attributes attributes analisys

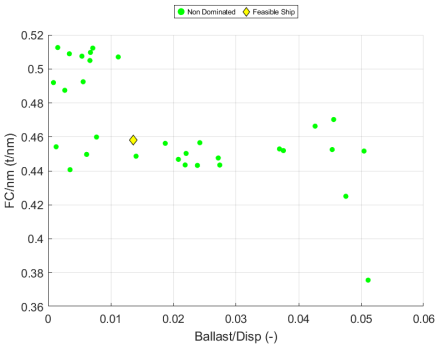

Figure F.35: W_{WB}/Δ vs fc/nm

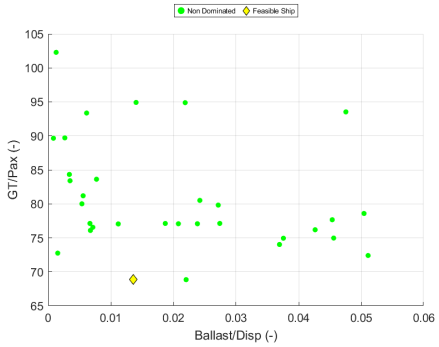

Figure F.36: W_{WB}/Δ vs GT/PAX

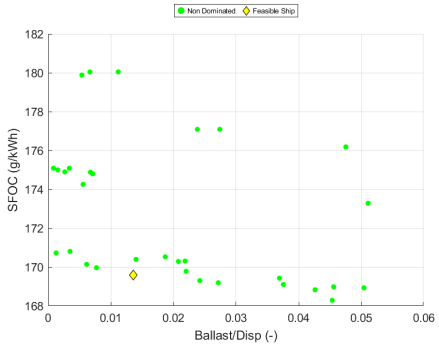

Figure F.37: W_{WB}/Δ vs $\overline{SFOC}$

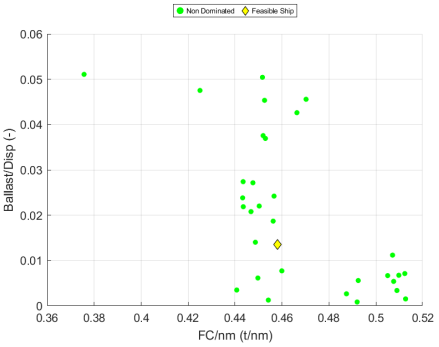

Figure F.38: fc/nm vs W_{WB}/Δ

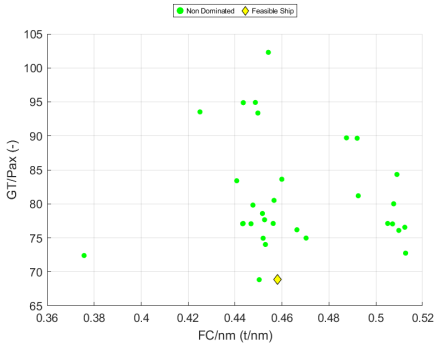

Figure F.39: fc/nm vs GT/PAX

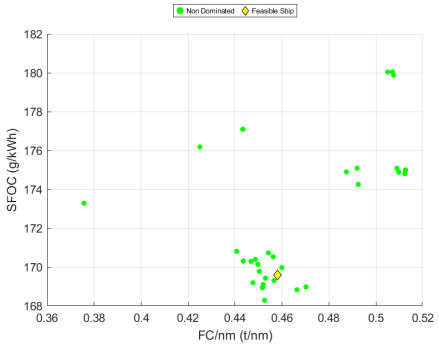

Figure F.40: fc/nm vs $\overline{SFOC}$

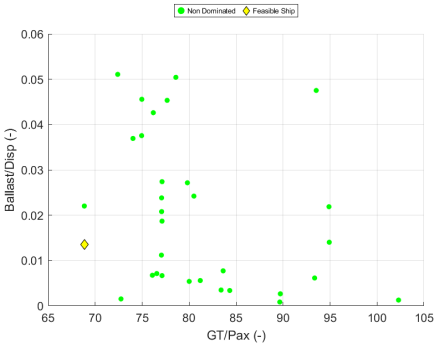

Figure F.41: GT/PAX vs W_{WB}/Δ

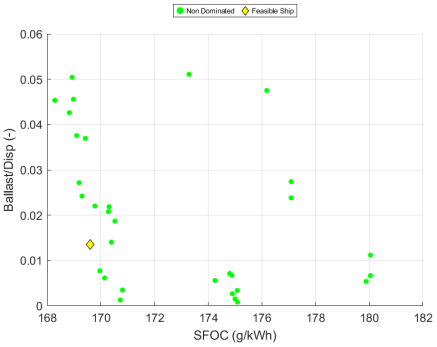

Figure F.44: $\overline{SFOC}$ vs W_{WB}/Δ

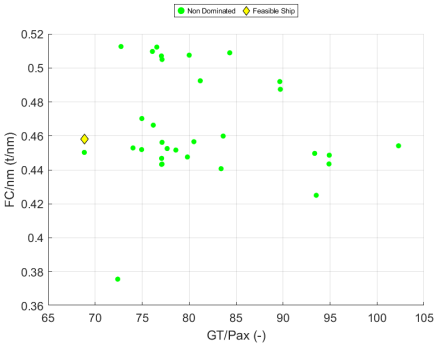

Figure F.42: GT/PAX vs fc/nm

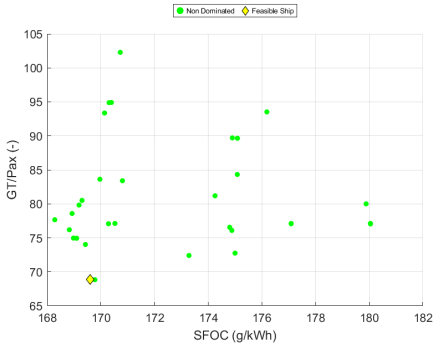

Figure F.45: $\overline{SFOC}$ vs GT/PAX

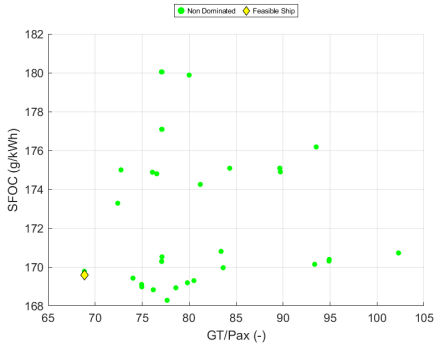

Figure F.43: GT/PAX vs $\overline{SFOC}$

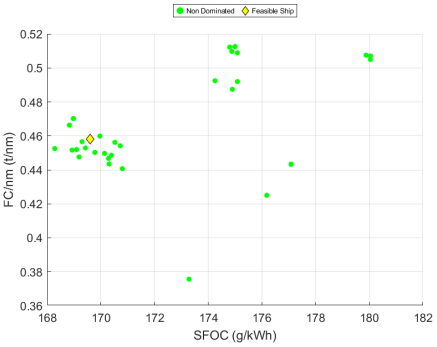

Figure F.46: $\overline{SFOC}$ vs fc/nm

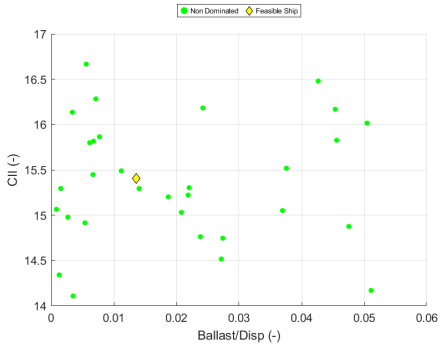

Figure F.47: W_{WB}/Δ vs CII

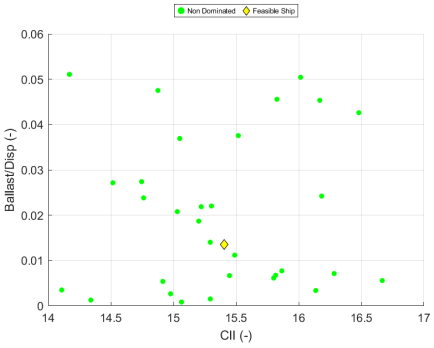

Figure F.50: CII vs W_{WB}/Δ

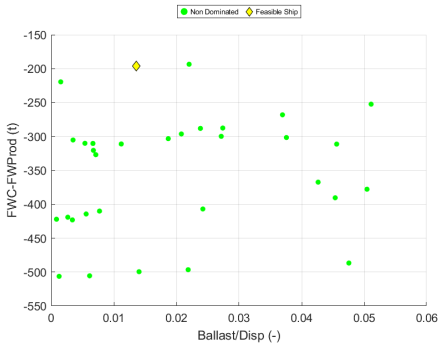

Figure F.48: W_{WB}/Δ vs $(FWc - FW_{Prod})$

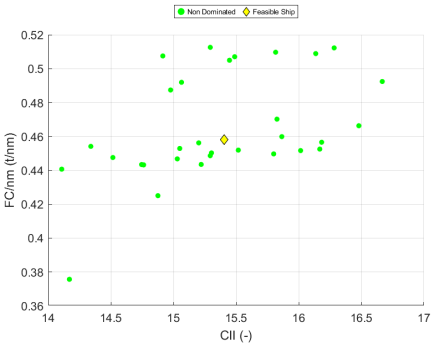

Figure F.51: CII vs fc/nm

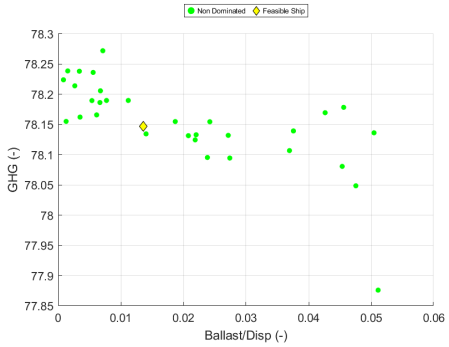

Figure F.49: W_{WB}/Δ vs GHG

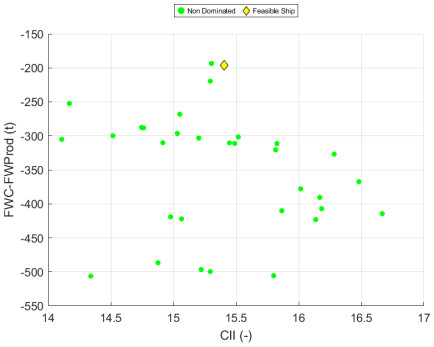

Figure F.52: CII vs $(FWc - FW_{Prod})$

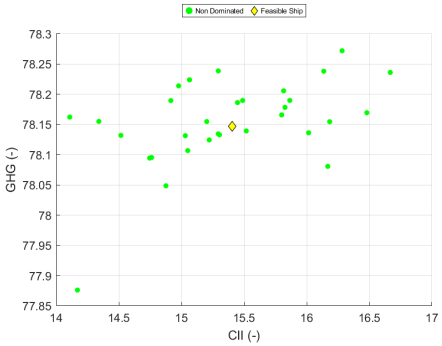

Figure F.53: CII vs GHG

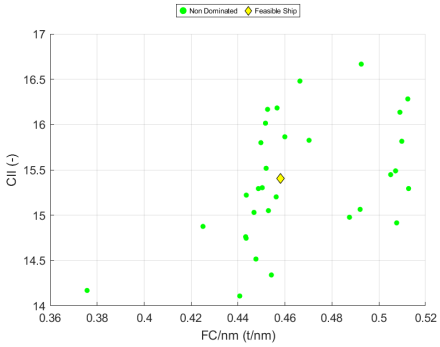

Figure F.56: fc/nm vs CII

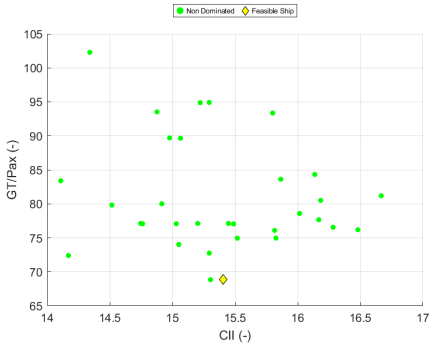

Figure F.54: CII vs GT/PAX

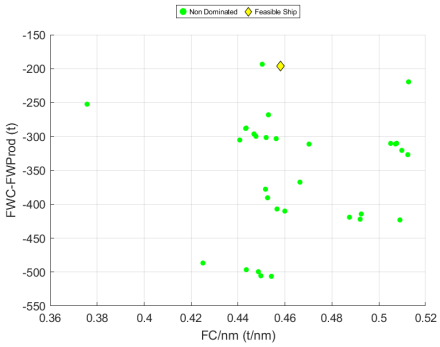

Figure F.57: fc/nm vs $(FWc - FW_{Prod})$

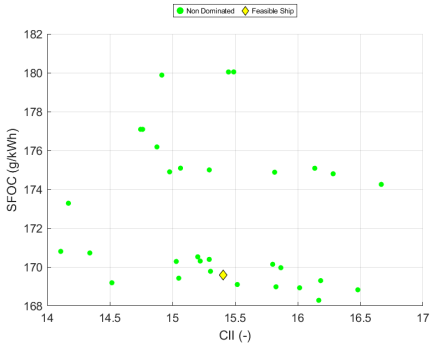

Figure F.55: CII vs $\overline{SFOC}$

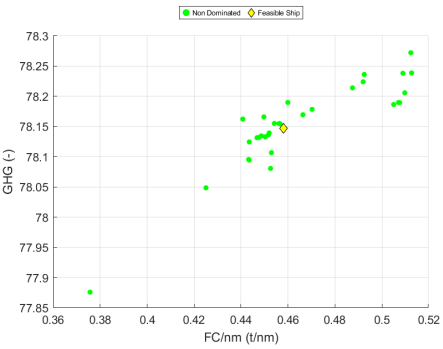

Figure F.58: fc/nm vs GHG

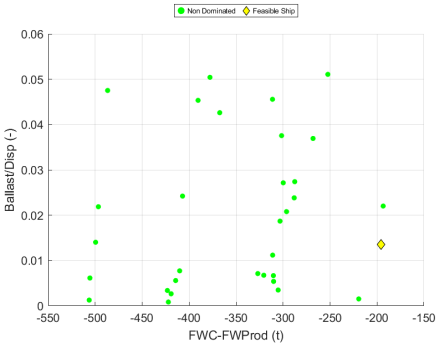

Figure F.59: $(FWc - FW_{Prod})$ vs W_{WB}/Δ

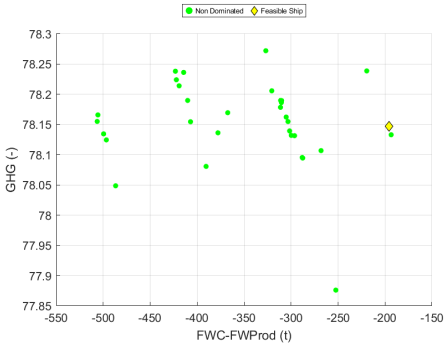

Figure F.62: $(FWc - FW_{Prod})$ vs GHG

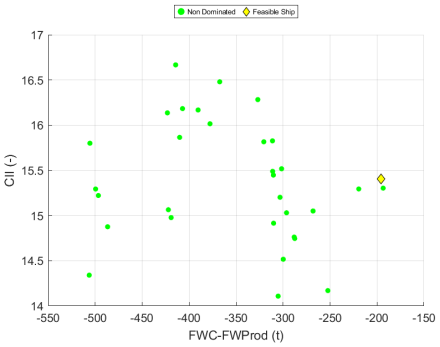

Figure F.60: $(FWc - FW_{Prod})$ vs CII

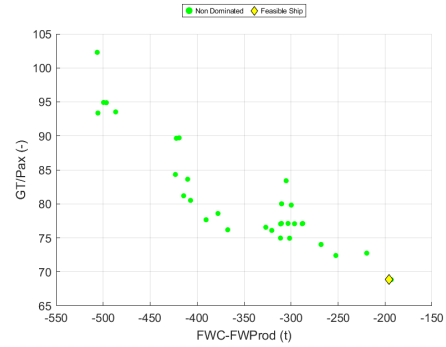

Figure F.63: $(FWc - FW_{Prod})$ vs GT/PAX

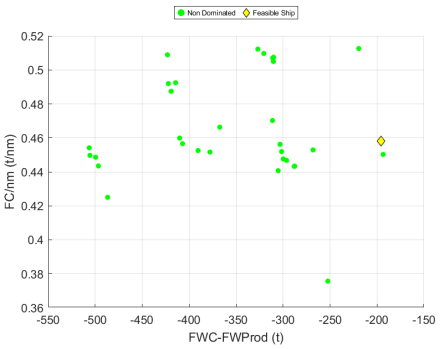

Figure F.61: $(FWc - FW_{Prod})$ vs fc/nm

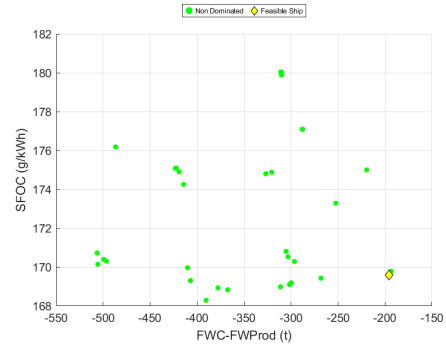

Figure F.64: $(FWc - FW_{Prod})$ vs $\overline{SFOC}$

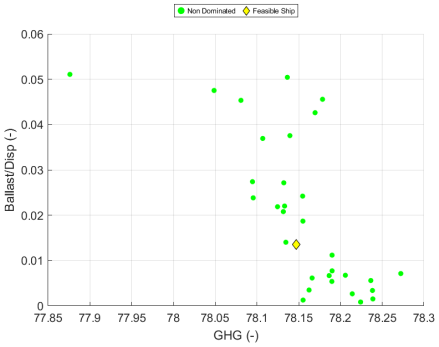

Figure F.65: GHG vs W_{WB}/Δ

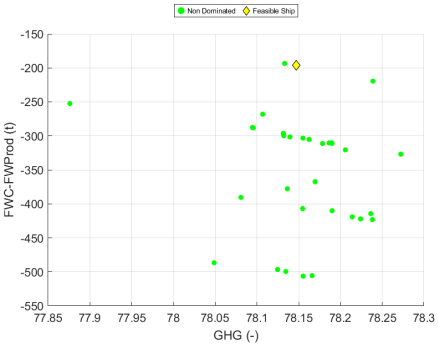

Figure F.68: GHG vs $(FWc - FW_{Prod})$

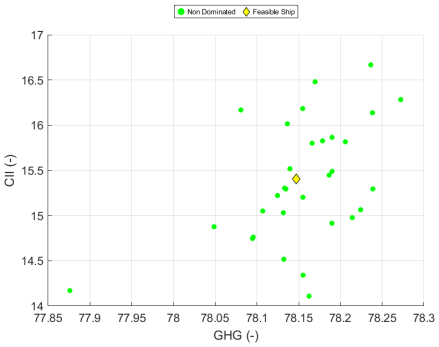

Figure F.66: GHG vs CII

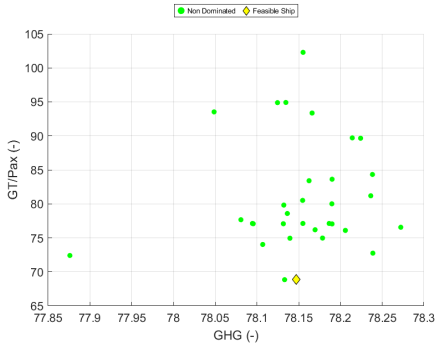

Figure F.69: GHG vs GT/PAX

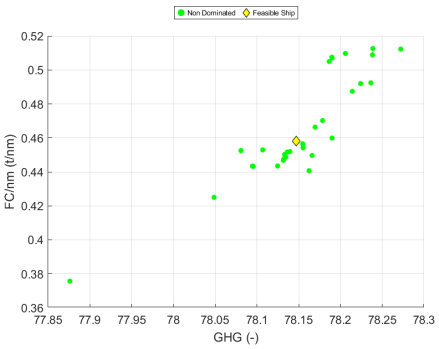

Figure F.67: GHG vs fc/nm

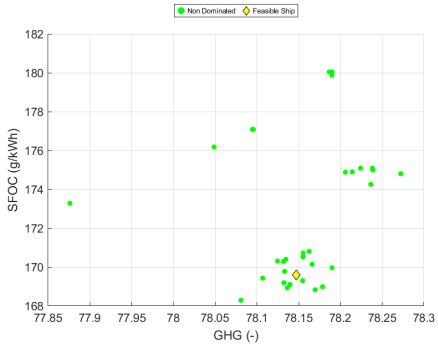

Figure F.70: GHG vs $\overline{SFOC}$

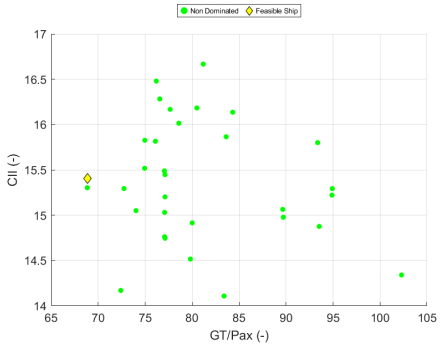

Figure F.71: GT/PAX vs CII

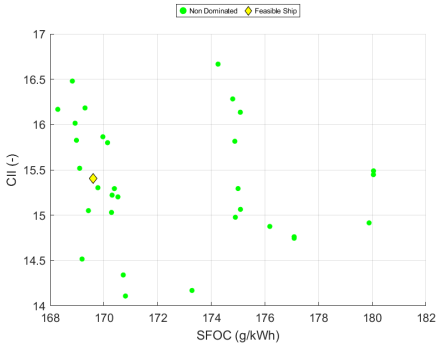

Figure F.74: $\overline{SFOC}$ vs CII

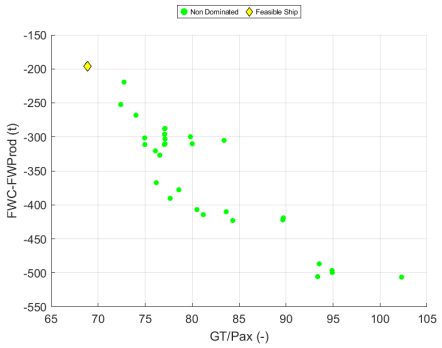

Figure F.72: GT/PAX vs $(FWc - FW_{Prod})$

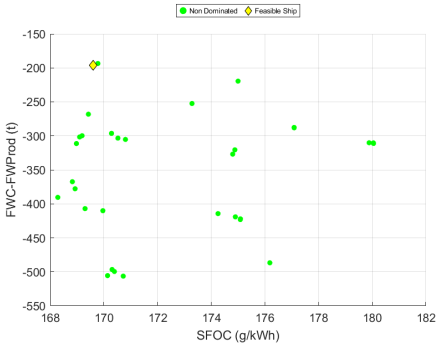

Figure F.75: $\overline{SFOC}$ vs $(FWc - FW_{Prod})$

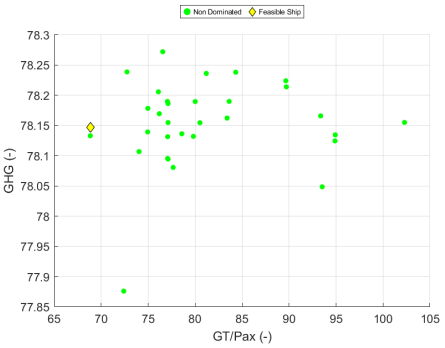

Figure F.73: GT/PAX vs GHG

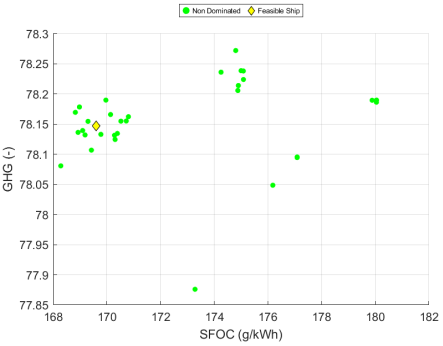

Figure F.76: $\overline{SFOC}$ vs GHG

Appendix G

Step1 vs Step2 variable-attribute analysis

Below the figures show the comparison between variable and variables, variables attributes and attributes-attributes for only the Non-dominated projects. The figures show the difference between the best possible desgin at 1^{st} stage and the best possible design at 2^{nd} stage of the methodology.

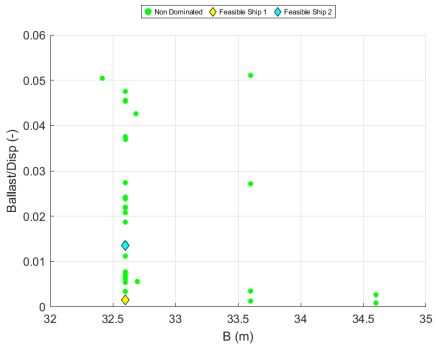

Figure G.1: B vs W_{WB}/Δ

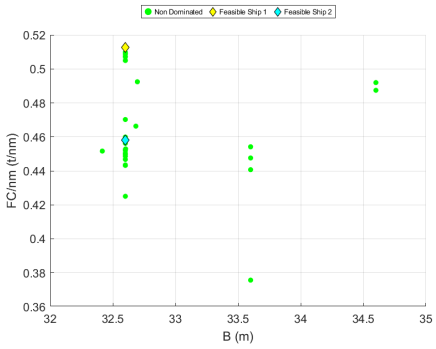

Figure G.3: B vs fc/nm

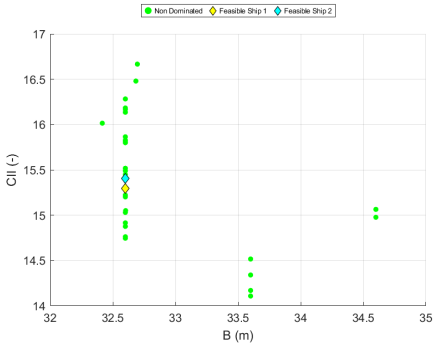

Figure G.2: B vs CII

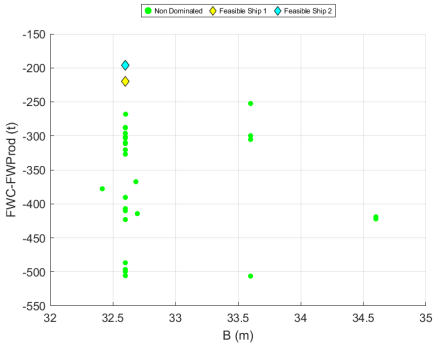

Figure G.4: B vs $(FWc - FW_{Prod})$

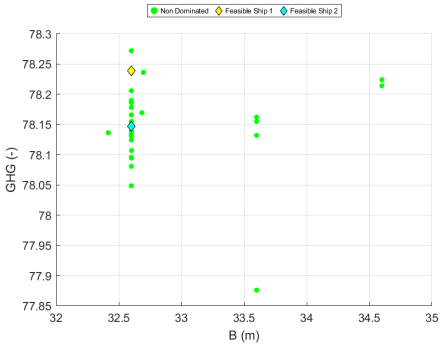

Figure G.5: B vs GHG

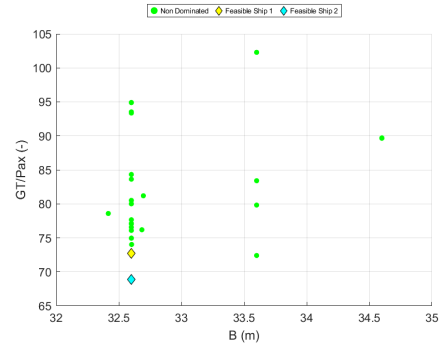

Figure G.6: B vs GT/PAX

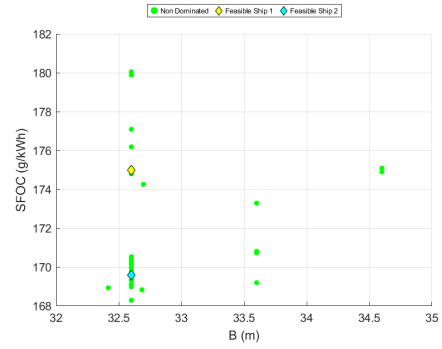

Figure G.7: B vs $\overline{SFOC}$

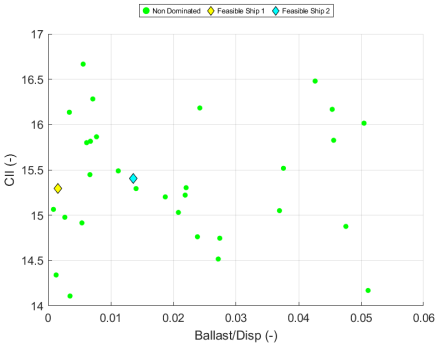

Figure G.8: W_{WB}/Δ vs CII

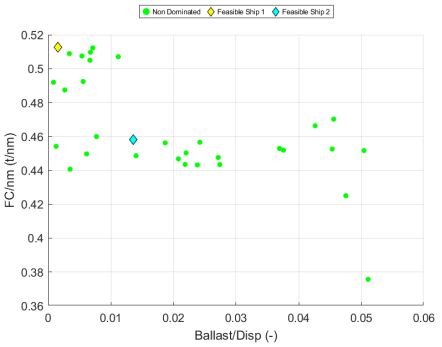

Figure G.9: W_{WB}/Δ vs fc/nm

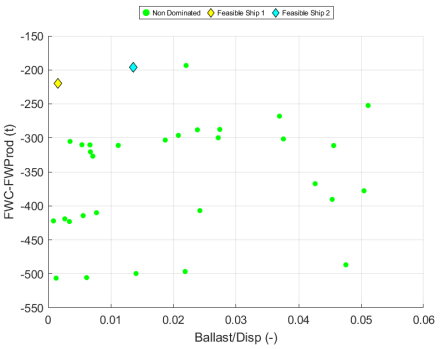

Figure G.10: W_{WB}/Δ vs $(FWc - FW_{Prod})$

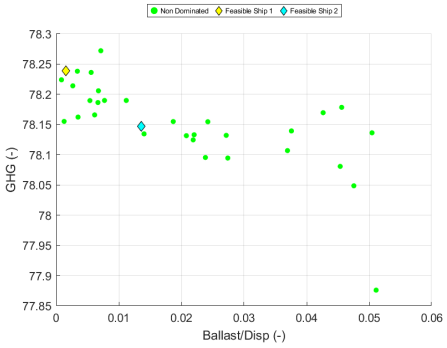

Figure G.11: W_{WB}/Δ vs GHG

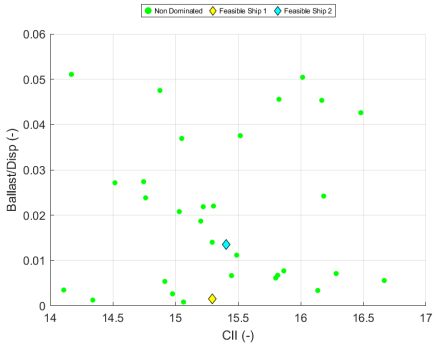

Figure G.14: CII vs W_{WB}/Δ

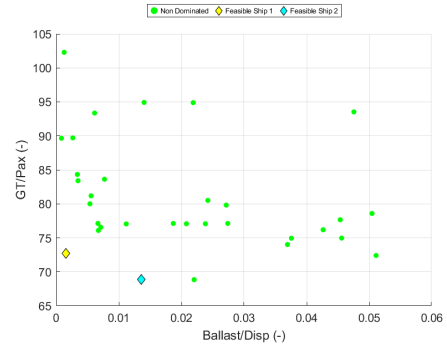

Figure G.12: W_{WB}/Δ vs GT/PAX

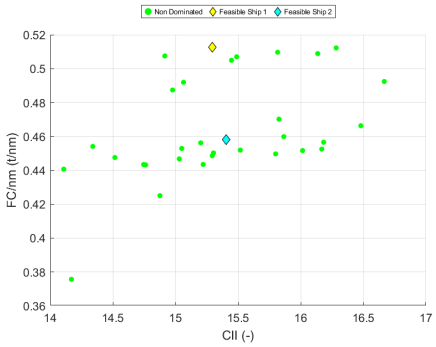

Figure G.15: CII vs fc/nm

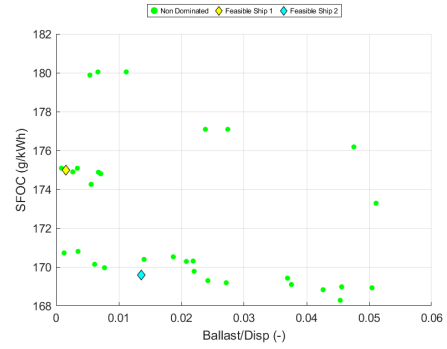

Figure G.13: W_{WB}/Δ vs $\overline{SFOC}$

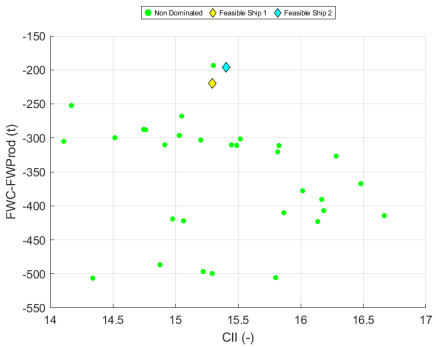

Figure G.16: CII vs $(FWc - FW_{Prod})$

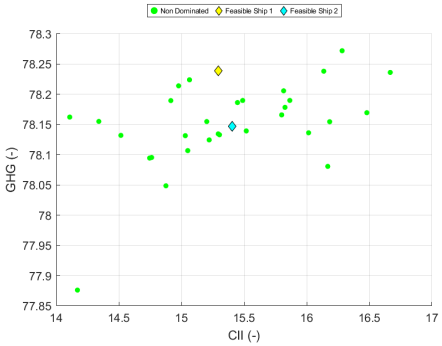

Figure G.17: CII vs GHG

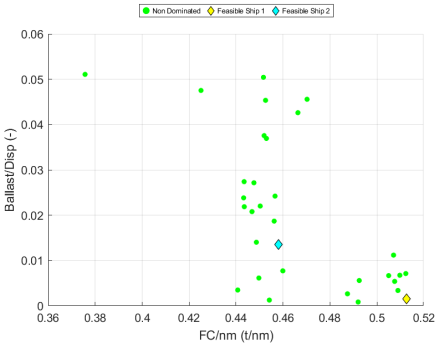

Figure G.20: fc/nm vs W_{WB}/Δ

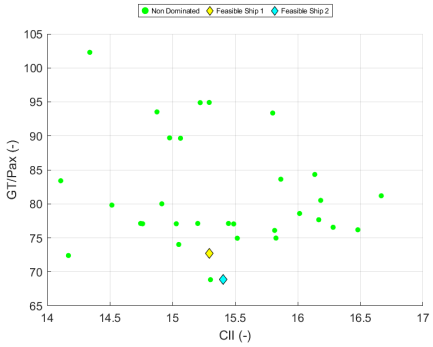

Figure G.18: CII vs GT/PAX

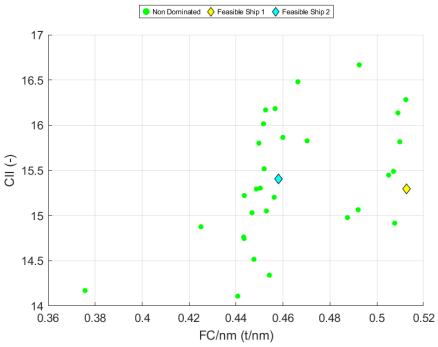

Figure G.21: fc/nm vs CII

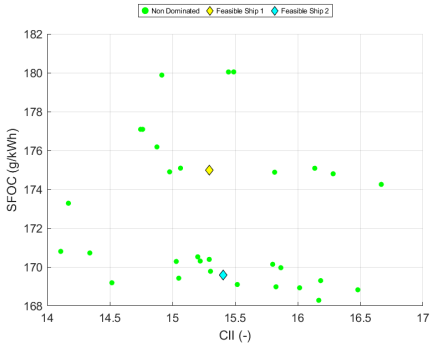

Figure G.19: CII vs $\overline{SFOC}$

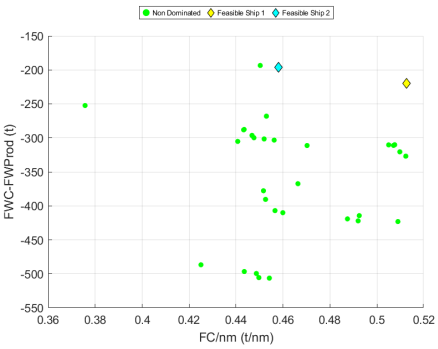

Figure G.22: fc/nm vs $(FWc - FW_{Prod})$

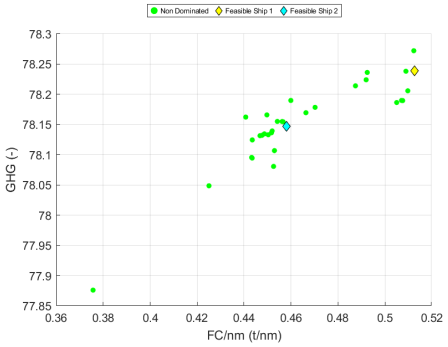

Figure G.23: fc/nm vs GHG

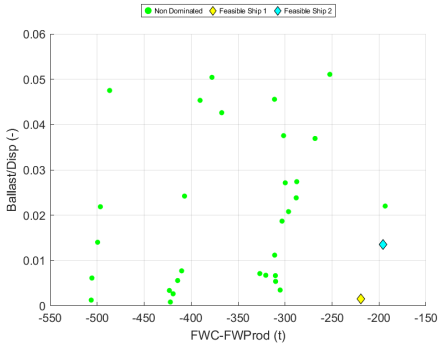

Figure G.26: $(FWc - FW_{Prod})$ vs W_{WB}/Δ

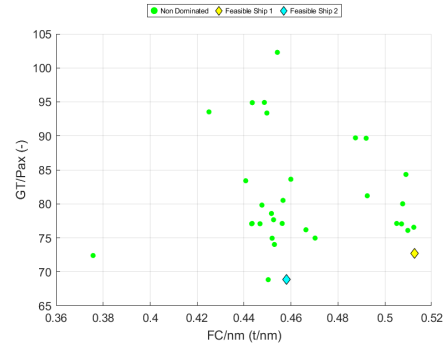

Figure G.24: fc/nm vs GT/PAX

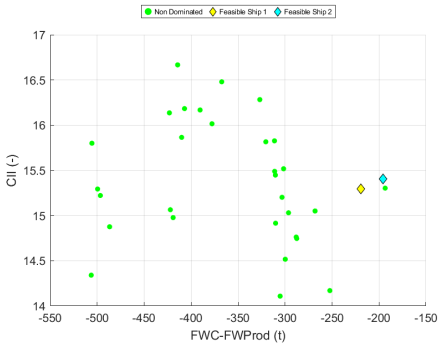

Figure G.27: $(FWc - FW_{Prod})$ vs CII

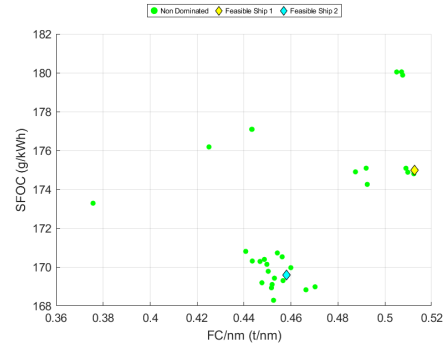

Figure G.25: fc/nm vs $\overline{SFOC}$

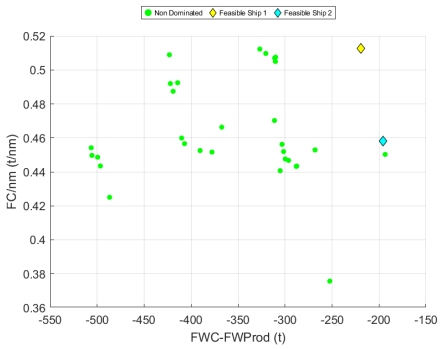

Figure G.28: $(FWc - FW_{Prod})$ vs fc/nm

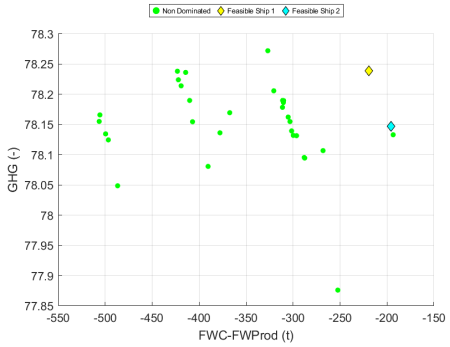

Figure G.29: $(FWc - FW_{Prod})$ vs GHG

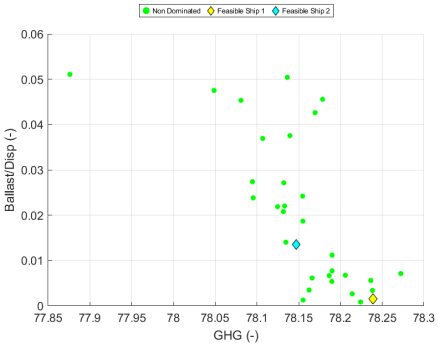

Figure G.32: GHG vs W_{WB}/Δ

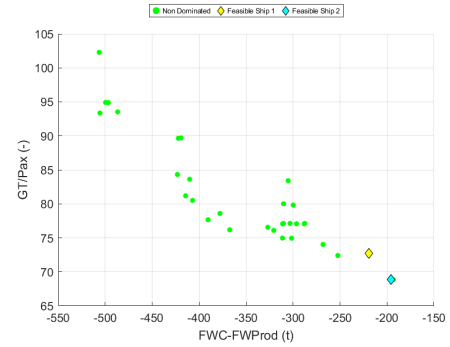

Figure G.30: $(FWc - FW_{Prod})$ vs GT/PAX

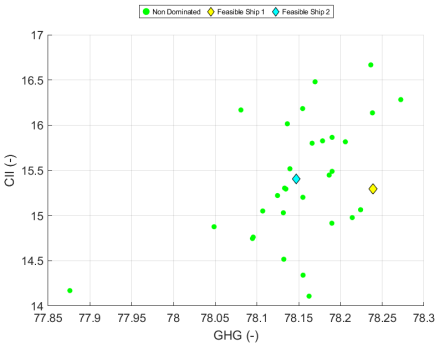

Figure G.33: GHG vs CII

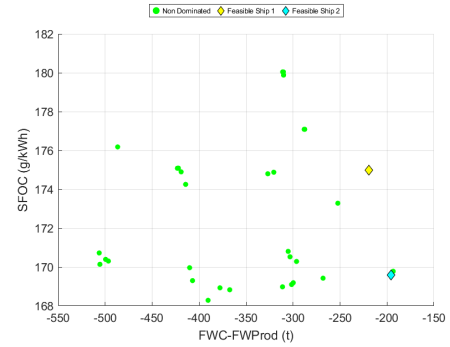

Figure G.31: $(FWc - FW_{Prod})$ vs $\overline{SFOC}$

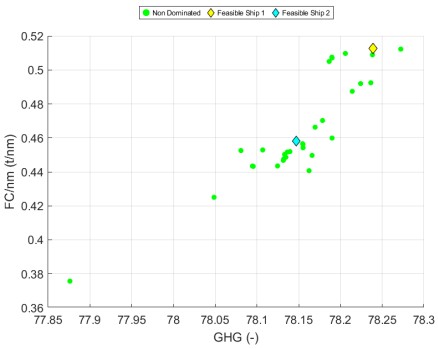

Figure G.34: GHG vs fc/nm

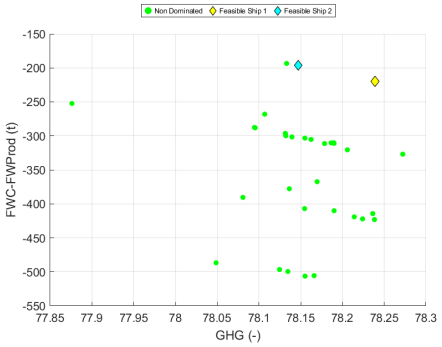

Figure G.35: GHG vs $(FWc - FW_{Prod})$

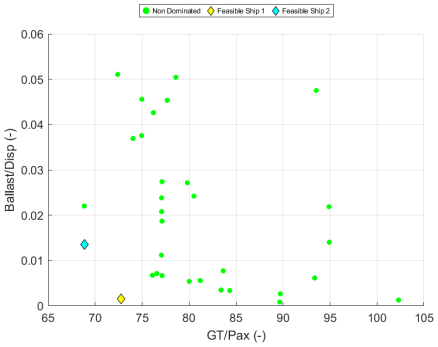

Figure G.38: GT/PAX vs W_{WB}/Δ

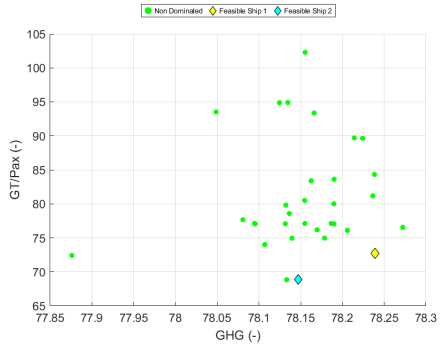

Figure G.36: GHG vs GT/PAX

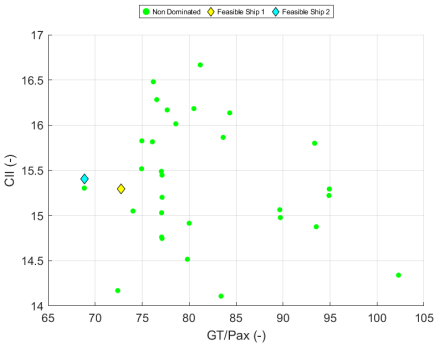

Figure G.39: GT/PAX vs CII

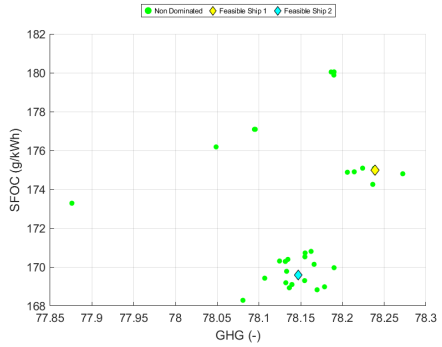

Figure G.37: GHG vs $\overline{SFOC}$

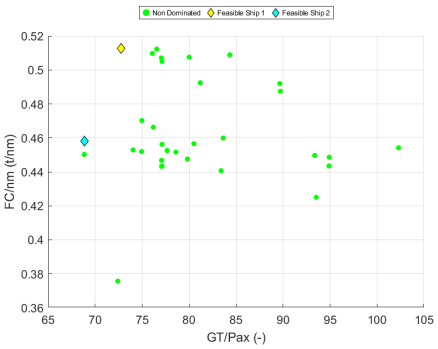

Figure G.40: GT/PAX vs fc/nm

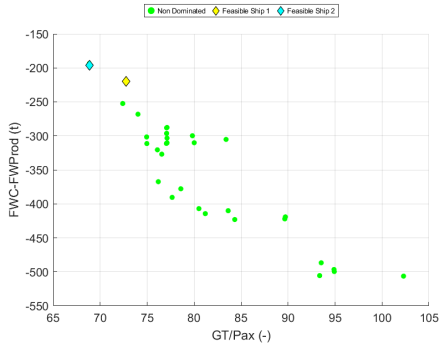

Figure G.41: GT/PAX vs $(FWc - FW_{Prod})$

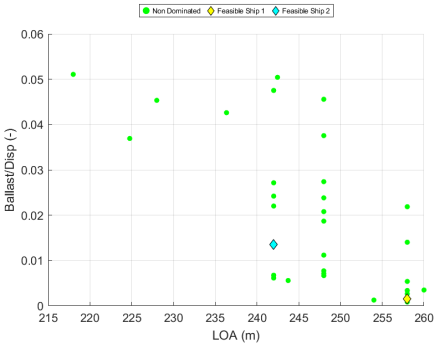

Figure G.44: L_{OA} vs W_{WB}/Δ

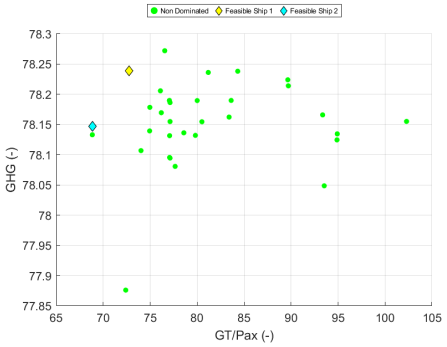

Figure G.42: GT/PAX vs GHG

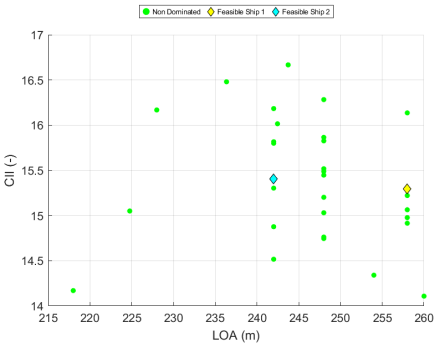

Figure G.45: L_{OA} vs CII

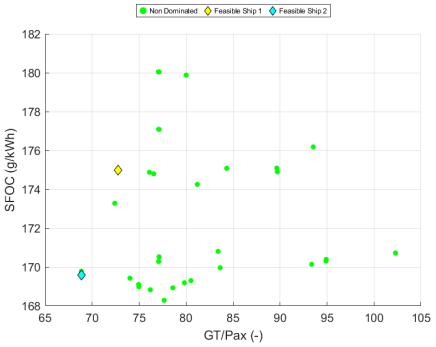

Figure G.43: GT/PAX vs $\overline{SFOC}$

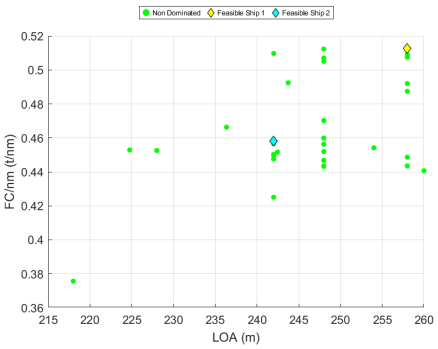

Figure G.46: L_{OA} vs fc/nm

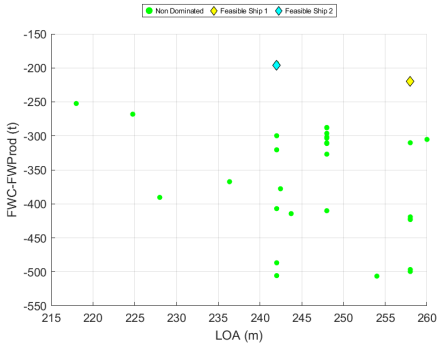

Figure G.47: L_{OA} vs $(FWc - FW_{Prod})$

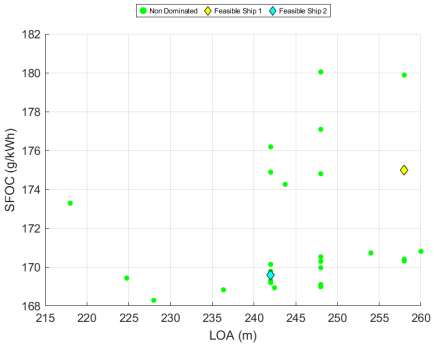

Figure G.50: L_{OA} vs $\overline{SFOC}$

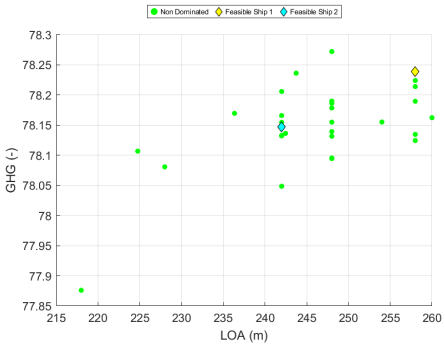

Figure G.48: L_{OA} vs GHG

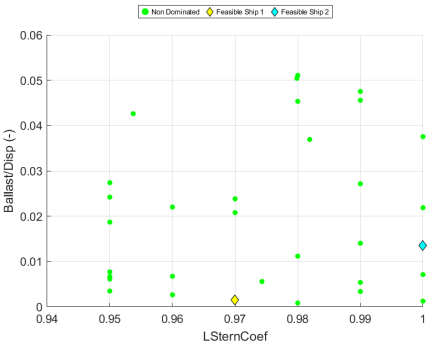

Figure G.51: $L_{Stern_{Profile}}$ vs W_{WB}/Δ

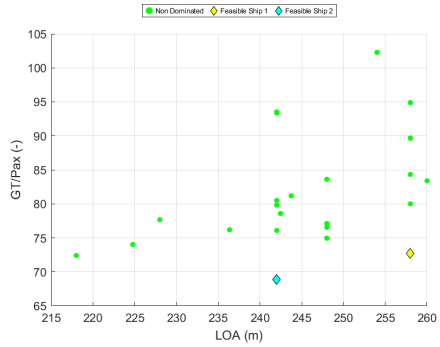

Figure G.49: L_{OA} vs GT/PAX

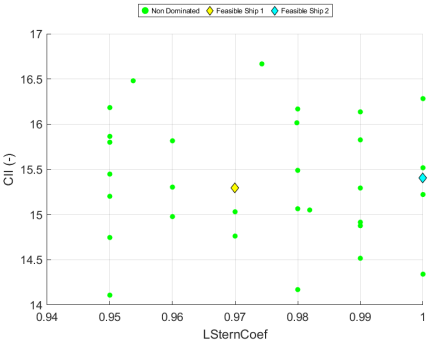

Figure G.52: $L_{Stern_{Profile}}$ vs CII

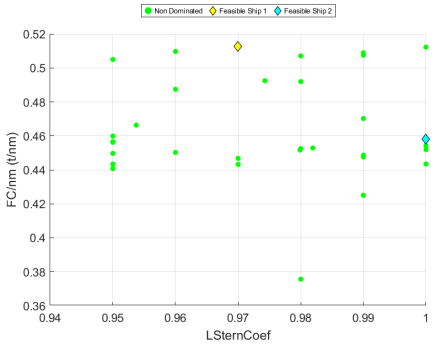

Figure G.53: $L_{Stern_{Profile}}$ vs fc/nm

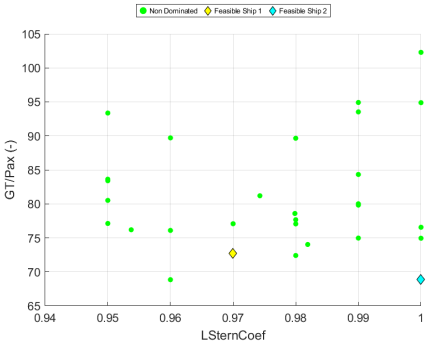

Figure G.56: $L_{Stern_{Profile}}$ vs GT/PAX

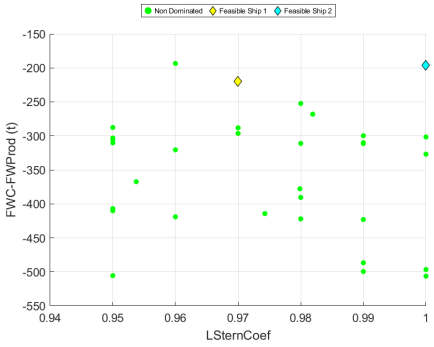

Figure G.54: $L_{Stern_{Profile}}$ vs $(FWc - FW_{Prod})$

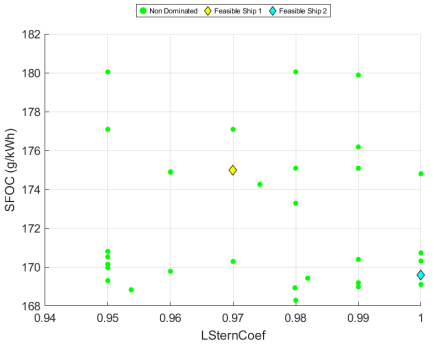

Figure G.57: $L_{Stern_{Profile}}$ vs $\overline{SFOC}$

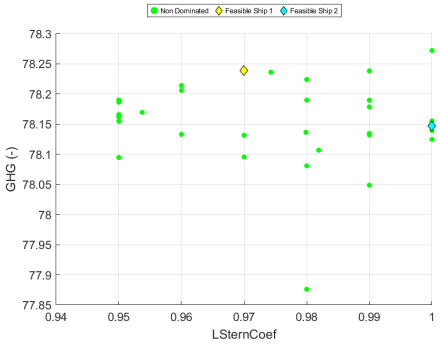

Figure G.55: $L_{Stern_{Profile}}$ vs GHG

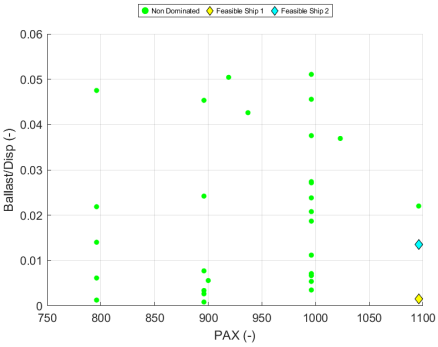

Figure G.58: PAX vs W_{WB}/Δ

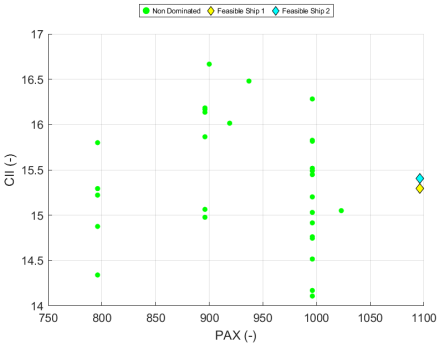

Figure G.59: PAX vs CII

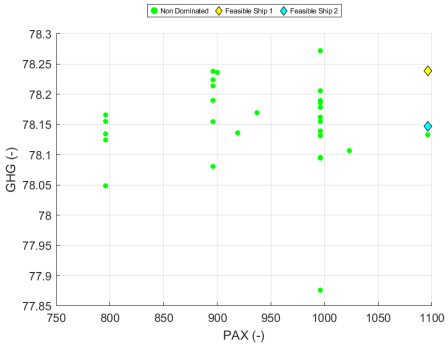

Figure G.62: PAX vs GHG

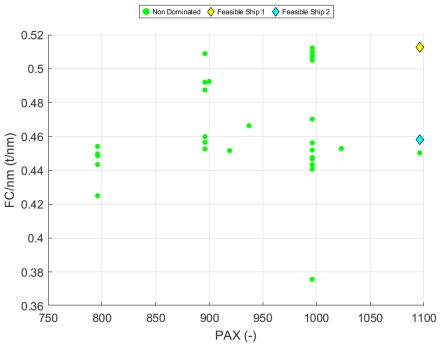

Figure G.60: PAX vs fc/nm

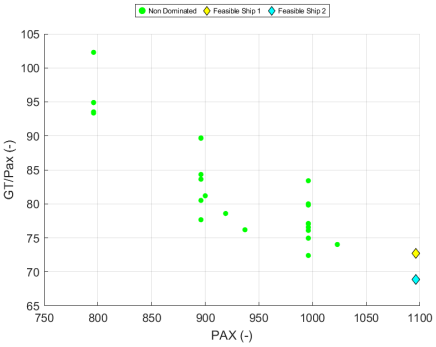

Figure G.63: PAX vs GT/PAX

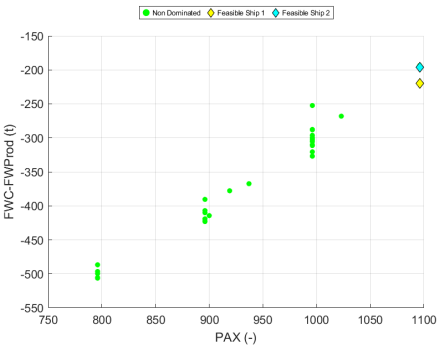

Figure G.61: PAX vs $(FWc - FW_{Prod})$

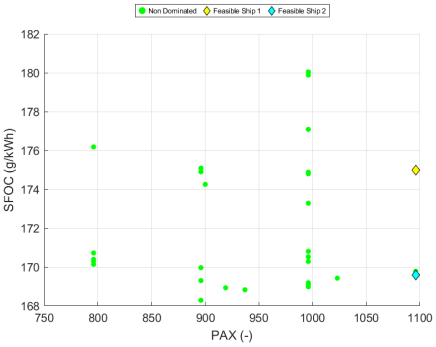

Figure G.64: PAX vs $\overline{SFOC}$

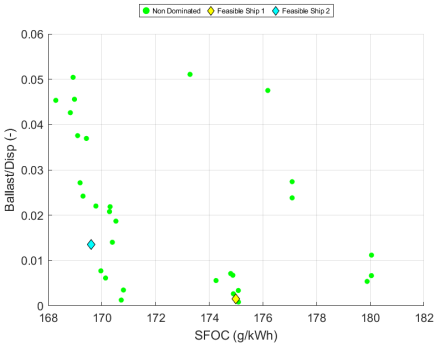

Figure G.65: $\overline{SFOC}$ vs W_{WB}/Δ

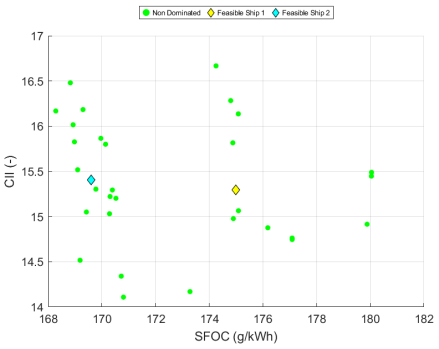

Figure G.66: $\overline{SFOC}$ vs CII

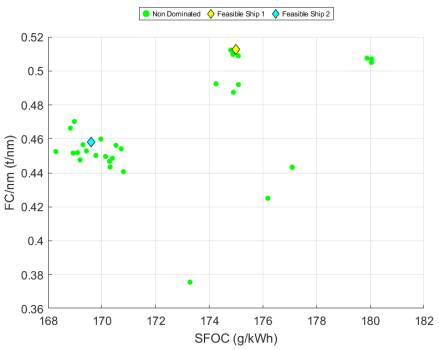

Figure G.67: $\overline{SFOC}$ vs fc/nm

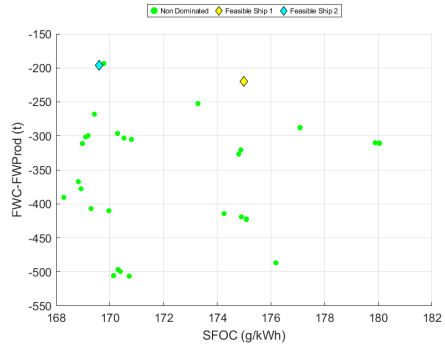

Figure G.68: $\overline{SFOC}$ vs $(FWc - FW_{Prod})$

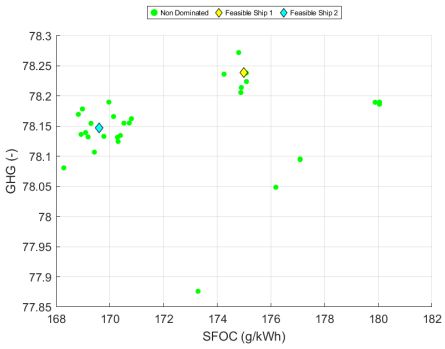

Figure G.69: $\overline{SFOC}$ vs GHG

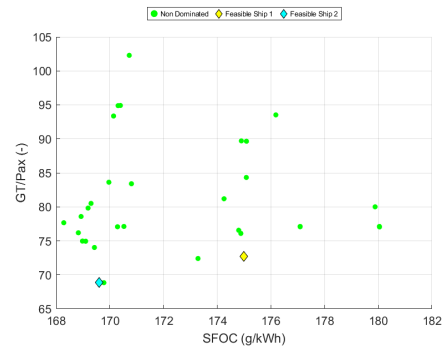

Figure G.70: $\overline{SFOC}$ vs GT/PAX

Appendix H

Simulation Results

From Figures H.1 to fig:fuel4 below the principal probablistic fuel consumption curves for Non dominated probabilistic simulations. In Table H.1 mean, median and 3^{rd} percentile results about fuel, fresh water consumption and fresh water producted and in Table H.2 mean, median and 3^{rd} percentile results about CII, GHG_{int} and $SFOC$.

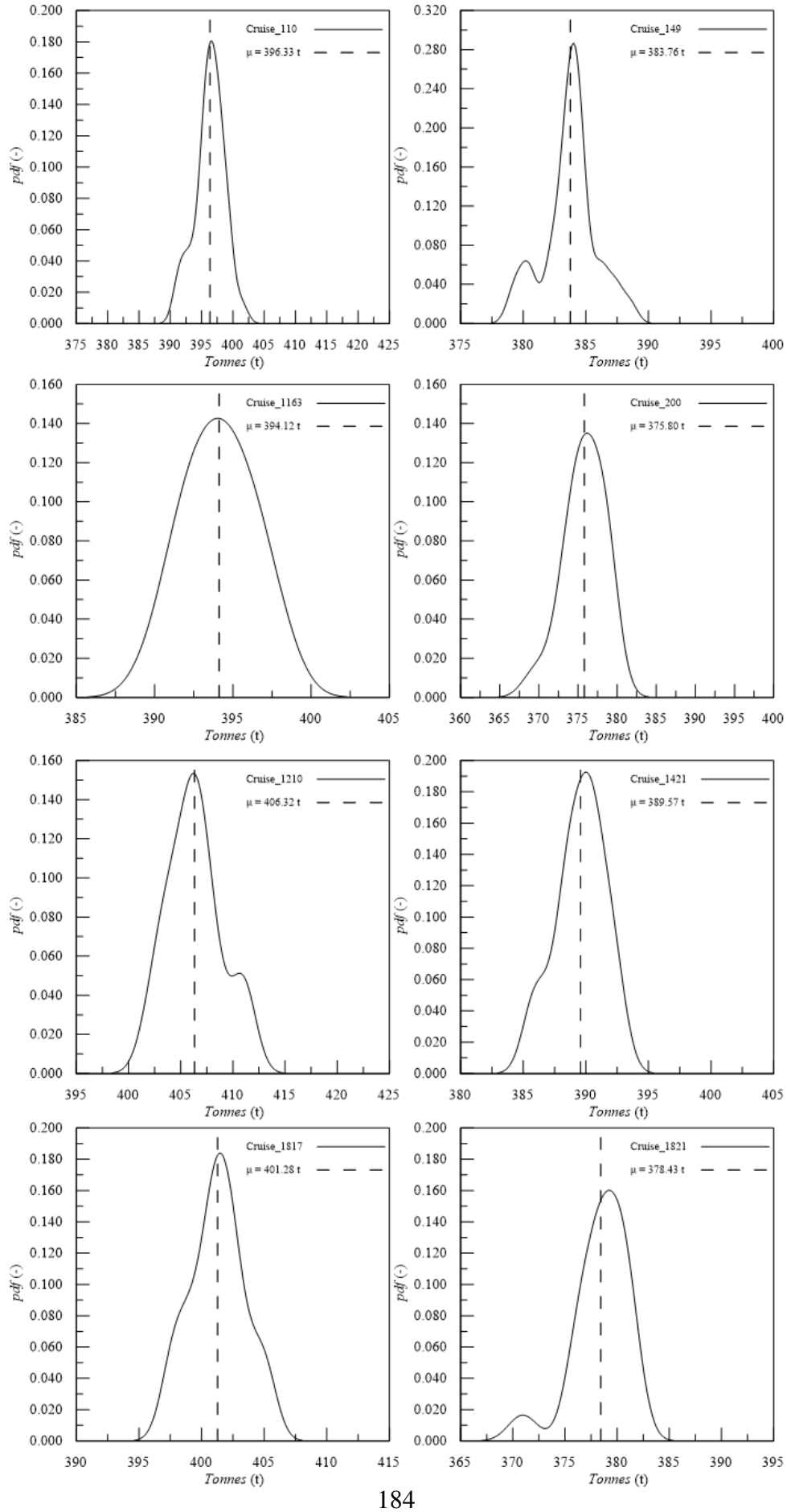

Figure H.1: Fuel consumption probabilty curve

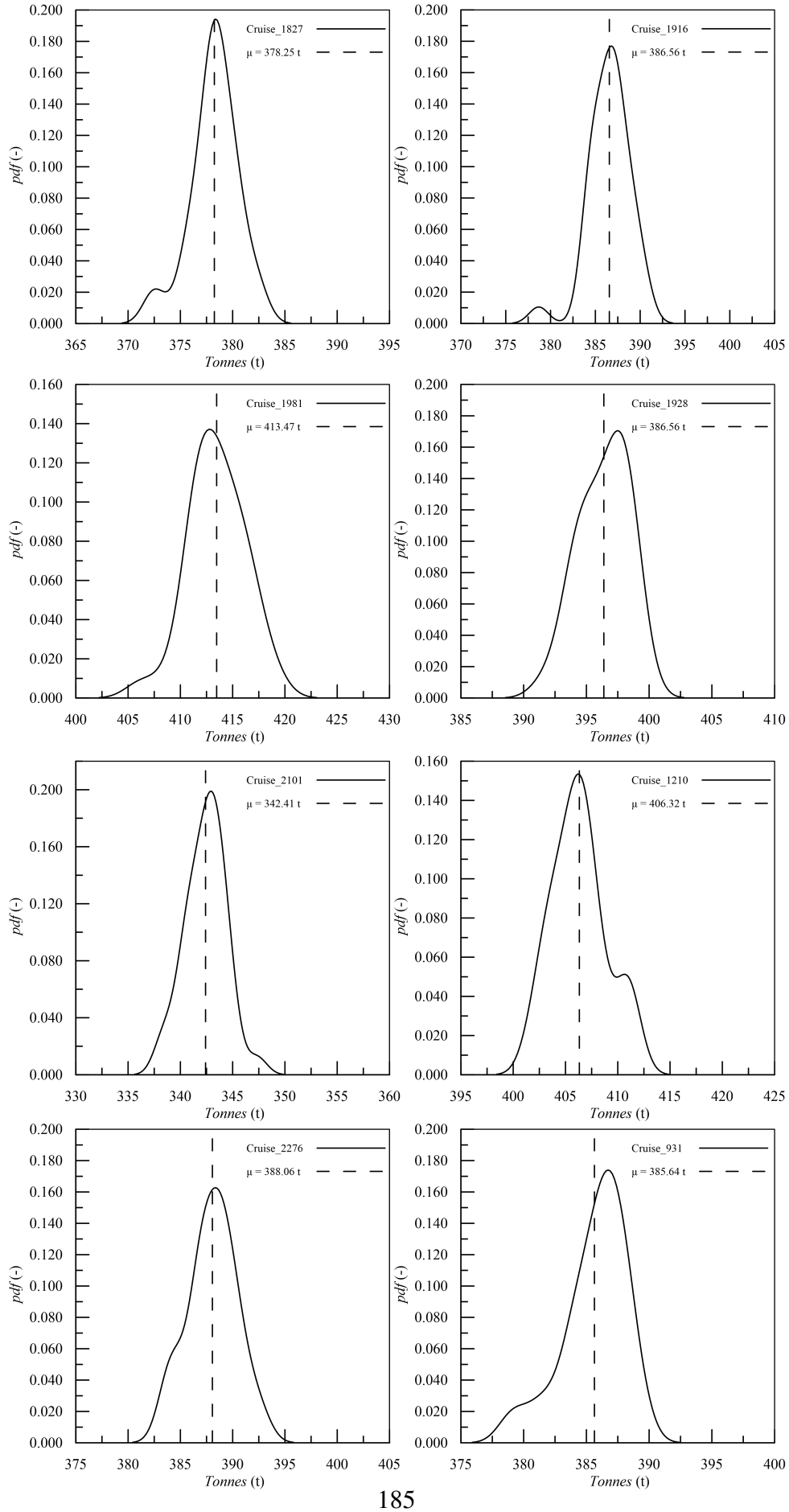

Figure H.2: Fuel consumption probabilty curve

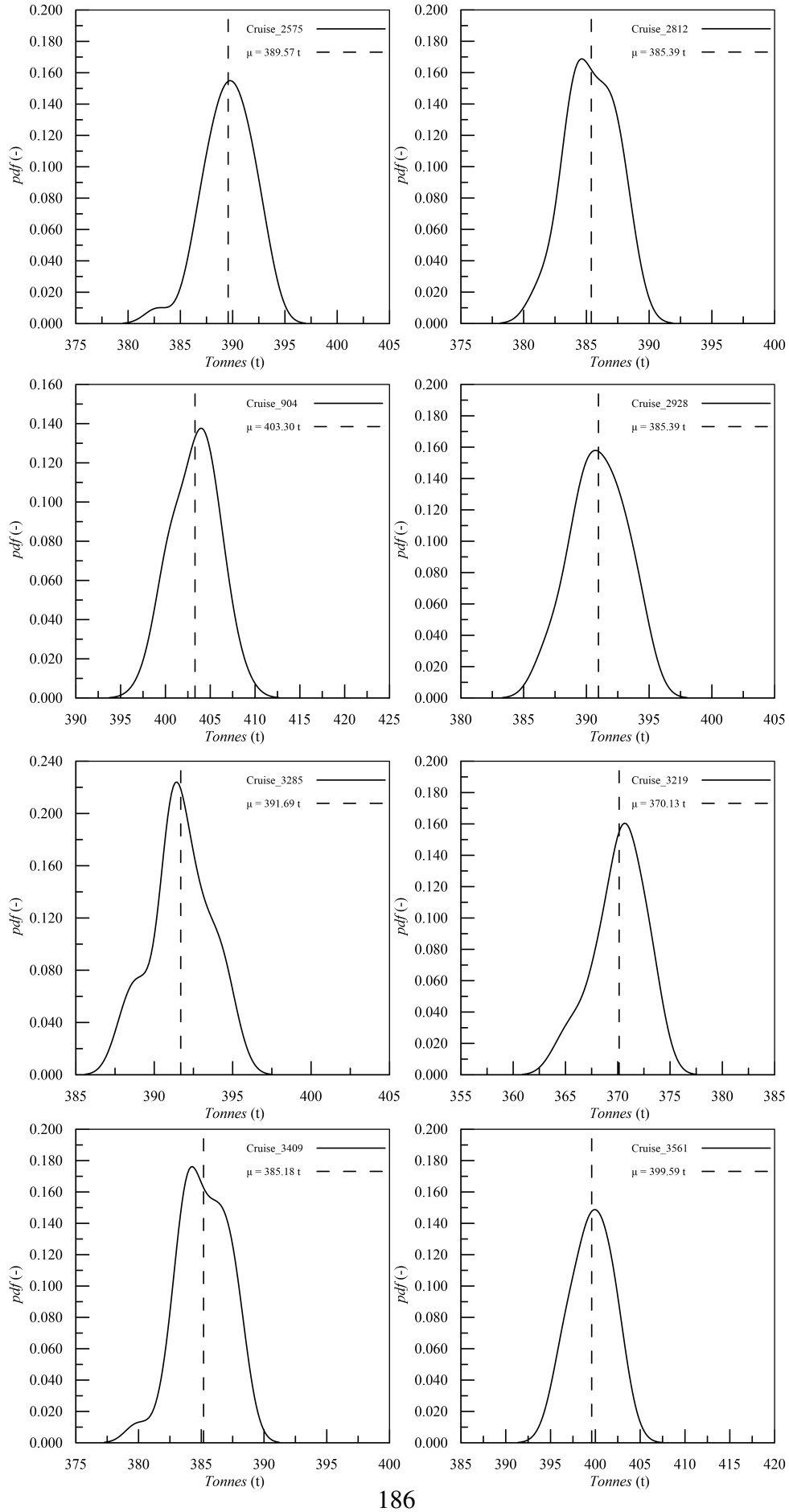

Figure H.3: Fuel consumption probabilty curve

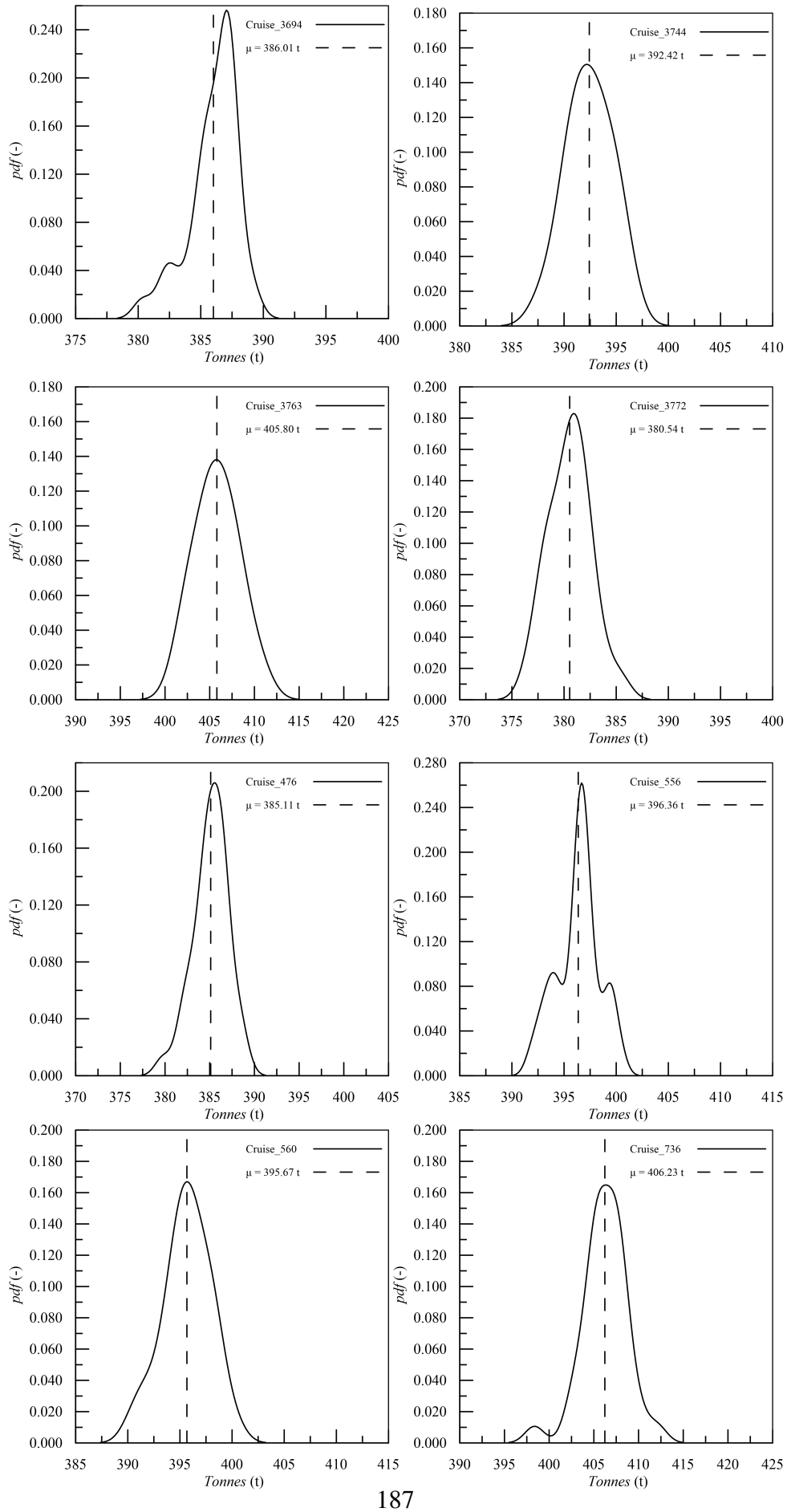

Figure H.4: Fuel consumption probabilty curve

Table H.1: mean, median and 3^{rd} percentile about fuel, fresh water consumption and fresh water producted

ID	fuel (t)			FW_c (t)			FW_{prod} (t)		
	μ	Q_1	Q_2	μ	Q_1	Q_2	μ	Q_1	Q_2
Cruise_2276	378	378	380	1008	1009	1033	1296	1296	1298
Cruise_2928	394	394	396	1008	1009	1033	1320	1320	1322
Cruise_1928	406	406	408	1110	1111	1137	1329	1329	1332
Cruise_2812	390	390	391	1008	1009	1033	1312	1312	1314
Cruise_1421	384	384	385	806	807	826	1303	1303	1305
Cruise_476	401	401	403	907	908	929	1326	1326	1328
Cruise_3763	378	379	380	1008	1009	1033	1296	1297	1299
Cruise_1210	396	397	398	1008	1009	1033	1318	1319	1321
Cruise_3144	387	387	388	1008	1009	1033	1310	1310	1312
Cruise_3561	396	397	398	907	908	929	1317	1317	1319
Cruise_3285	413	413	416	1008	1009	1033	1335	1335	1338
Cruise_1981	376	376	378	907	908	929	1297	1298	1299
Cruise_3409	342	343	344	1008	1009	1033	1261	1261	1263
Cruise_736	388	388	390	1110	1111	1137	1306	1306	1308
Cruise_904	390	390	391	806	807	826	1312	1313	1315
Cruise_1817	385	385	387	1110	1111	1137	1303	1304	1305
Cruise_560	391	391	393	1008	1009	1033	1314	1314	1316
Cruise_1821	389	390	391	907	908	929	1314	1314	1316
Cruise_1916	370	370	372	806	807	826	1293	1293	1295
Cruise_3772	392	392	393	806	807	826	1312	1312	1314
Cruise_931	385	385	387	1008	1009	1033	1308	1308	1310
Cruise_110	400	400	401	1008	1009	1033	1329	1330	1331
Cruise_2575	386	386	387	930	931	953	1308	1308	1310
Cruise_556	392	392	394	949	950	972	1316	1316	1318
Cruise_1827	406	406	408	911	912	934	1326	1326	1328
Cruise_2101	381	381	382	1035	1037	1061	1304	1304	1306
Cruise_3744	385	385	387	1008	1009	1033	1305	1305	1307
Cruise_149	396	397	398	1008	1009	1033	1319	1320	1322
Cruise_200	396	396	397	1008	1009	1033	1319	1319	1321
Cruise_1163	406	406	408	907	908	929	1330	1330	1332
Cruise_3694	403	403	405	907	908	929	1329	1329	1332
Cruise_3219	386	386	388	806	807	826	1306	1306	1309

Table H.2: mean, median and 3^{rd} percentile about CII, GHG_{int} and $SFOC$

ID	CII			GHG_{int} (gCO2eq/MJ)			$SFOC$ (g/kWh)		
	μ	Q_1	Q_2	μ	Q_1	Q_2	μ	Q_1	Q_2
Cruise_2276	14.746	14.753	14.802	78.095	78.096	78.200	198.7	198.6	198.8
Cruise_2928	15.826	15.826	15.897	78.179	78.179	78.285	198.4	198.4	198.5
Cruise_1928	15.294	15.285	15.361	78.239	78.239	78.340	198.5	198.5	198.6
Cruise_2812	15.202	15.208	15.264	78.155	78.156	78.263	199.0	198.9	199.0
Cruise_1421	15.221	15.227	15.271	78.125	78.124	78.232	199.4	199.4	199.5
Cruise_476	14.977	14.972	15.041	78.214	78.216	78.320	198.7	198.7	198.7
Cruise_3763	14.762	14.776	14.837	78.096	78.097	78.207	199.8	199.7	199.9
Cruise_1210	14.915	14.924	14.982	78.190	78.191	78.297	199.8	199.8	199.9
Cruise_3144	15.518	15.522	15.578	78.139	78.140	78.245	198.9	198.9	199.0
Cruise_3561	15.865	15.873	15.927	78.190	78.192	78.295	198.7	198.6	198.7
Cruise_3285	16.283	16.282	16.362	78.272	78.272	78.373	198.6	198.6	198.7
Cruise_1981	16.168	16.178	16.259	78.081	78.083	78.193	199.7	199.7	199.8
Cruise_3409	14.170	14.175	14.231	77.876	77.876	77.997	202.0	201.9	202.0
Cruise_736	15.404	15.414	15.478	78.147	78.148	78.255	199.1	199.1	199.2
Cruise_904	14.340	14.346	14.399	78.155	78.155	78.261	199.0	199.0	199.1
Cruise_1817	15.303	15.314	15.363	78.133	78.135	78.241	199.3	199.3	199.4
Cruise_560	14.108	14.111	14.166	78.162	78.163	78.267	199.0	198.9	199.1
Cruise_1821	16.183	16.185	16.247	78.155	78.155	78.261	198.7	198.7	198.8
Cruise_1916	14.876	14.891	14.947	78.049	78.052	78.162	200.2	200.2	200.3
Cruise_3772	15.800	15.801	15.856	78.166	78.166	78.273	198.9	198.9	199.0
Cruise_931	14.516	14.516	14.568	78.132	78.133	78.240	199.0	199.0	199.1
Cruise_110	15.816	15.822	15.891	78.206	78.206	78.312	198.3	198.2	198.3
Cruise_2575	16.015	16.028	16.074	78.136	78.137	78.246	199.0	199.0	199.1
Cruise_556	16.480	16.483	16.558	78.170	78.172	78.278	198.7	198.7	198.7
Cruise_1827	16.667	16.662	16.736	78.236	78.237	78.338	198.4	198.4	198.5
Cruise_2101	15.050	15.055	15.118	78.107	78.108	78.218	199.4	199.4	199.5
Cruise_3744	15.031	15.033	15.088	78.132	78.132	78.242	199.3	199.3	199.4
Cruise_149	15.489	15.493	15.548	78.190	78.193	78.291	198.6	198.6	198.7
Cruise_200	15.447	15.448	15.508	78.186	78.188	78.288	198.7	198.6	198.7
Cruise_1163	16.136	16.137	16.204	78.238	78.240	78.339	198.5	198.5	198.6
Cruise_3694	15.064	15.067	15.134	78.224	78.226	78.327	198.7	198.7	198.8
Cruise_3219	15.294	15.302	15.365	78.135	78.135	78.239	199.3	199.2	199.4

Bibliography

[1] V. Bucci, A. Marinò, I. Juricic, *Integrated ship design: Automated generation of production deliverables with new generation shipbuilding CAD systems*, Proc. Conf. Comput. Appl. Inf. Technol. Maritime. Ind (2013) pp. 1–14.

[2] IMO, Fire safety systems (fss) code, resolution MSC.98(73) (2015).

[3] L. Braidotti, S. Utzeri, S. Bertagna, V. Bucci, A fast simulation method for the probabilistic assessment of emissions in cruise ship's itinerary planning, Ocean Engineering 311 (2024) 118804.

[4] F. Altuntas, S. Altuntas, T. Dereli, Social network analysis of tourism data: A case study of quarantine decisions in covid-19 pandemic, International Journal of Information Management Data Insights 2 (2) (2022) 100108.

[5] B. S. Alonazi, T. H. Hassan, M. A. Abdelmoaty, A. E. Salem, M. I. Saleh, M. Y. Helal, Y. A. Mohamed, M. S. Abuelnasr, D. A. Gebreslassie, M. H. Aleedan, et al., Tourist behavior in the cruise industry post-covid-19: An examination of service quality, corporate image, and intentions to pay and revisit, Sustainability 15 (11) (2023) 8623.

[6] Cruise Lines International Association (CLIA), State of the Cruise Industry Report 2024 (April 2024).

[7] M. Kovačić, L. Silveira, Cruise tourism: Implications and impacts on the destinations of croatia and portugal, Pomorstvo 34 (1) (2020) 40–47.

[8] J. Dorigatti, T. Perić, G. J. Mrčelić, Cruise industry trends and cruise ships' navigational practices in the central and south part of the adriatic east coast affecting navigational safety and sustainable development, Applied Sciences 12 (14) (2022). doi:10.3390/app12146884.

[9] A. Coviello, R. Somma, Turismo crocieristico italiano: scenari e trend dopo la pandemia globale. Il test case di MSC, 2024, pp. 167–196.

[10] A. A. Pallis, G. K. Vaggelas, Cruise shipping and green ports: a strategic challenge, in: Green Ports, Elsevier, 2019, pp. 255–273.

[11] A. M. Kotrikla, E. Chortatsiani, Environmental sustainability in the cruise industry, Interdisciplinary Journal of Research and Development 9 (4. S2) (2022) 81–81.

[12] T. P. Zis, Prospects of cold ironing as an emissions reduction option, Transportation Research Part A: Policy and Practice 119 (2019) 82–95.

[13] Cruise Lines International Association (CLIA), State of the Cruise Industry Report 2024 (September 2023).

[14] P. Bjornsen, The growth of the market and global competition in the cruise industry, in: Cruise and Ferry Conference, Earls Court, London, 2003.

[15] R. H. Kamery, An overview of the cruise industry: An alternative to land-based vacations, Academy of Legal, Ethical, and Regulatory Issues 145 (2004).

[16] Cruise Industry News, 2023 luxury market report (2023).

[17] G. Trincas, Ship design: a Rational Approach, 2019.

[18] G. Trincas, V. Žanić, I. Grubišić, *Optimization Procedure for Preliminary Design of Fishing Vessels*, Proceedings 2nd Symposium on 'Technics & Technology in Fishing Vessels Vol 1 (1989) pp. 22–31.

[19] G. Hazelrigg, *A framework for Decision-Based Engeneering Design*, ASME Journal of Mechanical Design Vol 120 (1998) pp. 653–658.

[20] S. Shahak, Naval ship concept design: an evolutionary approach, Ph.D. thesis, Massachusetts Institute of Technology (1998).

[21] G. Trincas, F. Mauro, L. Braidotti, V. Bucci, *Handling the Path from Concept to Preliminary Ship Design*, In: Proceedings of the 13th International Marine Design Conference - IMDC 2018 (2018) pp. 3–19.

[22] G. Trincas, V. Žanić, I. Grubišić, *Comprehensive Concept Design of Fast Ro-Ro Ships by Multiattribute Decision-Making*, Proceedings, 4th International Marine Design Conference, IMDC 94 (1994) pp. 403–418.

[23] M. I. Zignego, D. Nicolini, E. Proia, Luxury cruise ship design: Evolution and new perspectives, in: Progress in Marine Science and Technology, Vol. 10, 2025, pp. 707–722. doi:10.3233/PMST250085.

[24] Y. Zhang, T. Sun, Z. Tao, J. Wu, X. Meng, Simulation and optimization of large passenger ship based on unity 3d, IAENG International Journal of Applied Mathematics 55 (7) (2025) 2269–2279.

[25] S. Helle, T. Nyyssönen, O. I. Heimo, L. Sakari, T. Lehtonen, Virtual reality applied to design reviews in shipbuilding, Multimodal Technologies and Interaction 9 (7) (2025). doi:10.3390/mti9070072.

[26] A. Buonomano, G. Del Papa, G. Giuzio, R. Maka, A. Palombo, G. Russo, Design and retrofit towards zero-emission ships: Decarbonization solutions for sustainable shipping, Renewable and Sustainable Energy Reviews 213 (2025) 115384. doi:10.1016/j.rser.2025.115384.

[27] W. Ma, G. Zhu, P. Gao, Study on evaluation of wave added resistance for safe return to port of large cruise ships, Ship Building of China 65 (3) (2024) 62–70.

[28] G. Vernengo, S. Brizzolara, D. Bruzzone, Hydrodynamic design of a fast semi-swath passenger ship for littoral applications: An automatic parametric optimization approach, in: Proceedings of ISOPE, 2014, pp. 787–795.

[29] A. Boiko, O. Bondarenko, Y. Davydenko, Hull parametric modeling of a small waterplane area twin hull ships, in: Experience of Designing and Application of CAD Systems in Microelectronics, 2019, p. 8779352.

[30] H. P. Crosby, Concept exploration of a surface effect patrol combatant using a multiobjective synthesis model, in: FAST 2021 Conference, 2021.

[31] D. Padolecchia, N. Taucer Marchesi, S. Bertagna, V. Bucci, 3d parametric modeling for ship concept design: A flexible approach to general arrangement plan, Progress in Marine Science and Technology 10 (2025) 1028–1037.

[32] G. D. Pillo, et al., A two-objective optimization of ship itineraries for a cruise company, 4OR 21 (4) (2023) 683–709.

[33] L. Zhen, et al., The effects of emission control area regulations on cruise shipping, Transportation Research Part D 62 (2018) 47–63.

[34] S. A. Wang, L. Zhen, D. Zhuge, Dynamic programming algorithms for selection of waste disposal ports in cruise shipping, Transportation Research Part B 108 (2018) 235–248.

[35] V. Bucci, G. Sulligoi, J. Chalfant, C. Chryssostomidis, Evolution in design methodology for complex electric ships, Journal of Ship Production and Design 37 (04) (2021) 215–227. doi:10.5957/JSPD.08190045.

[36] P. Y. Papalambros, Design science: why, what and how, Design Science 1 (2015) e1.

[37] I. Grubišić, V. Žanić, G. Trincas, *Sensitivity of Multiattribute Risk Analysis in Nuclear Emergency Management*, Risk Analysis Vol 20 (2000) pp. 455–467.

[38] P. Sen, J. Yang, *Multiple Criteria Decision Support in Engineering Design*, Springer-Verlag (1998).

[39] J. Venable, The role of theory and theorising in design science research, in: Proceedings of the 1st international conference on design science in information systems and technology (DESRIST 2006), Claremont, CA, 2006, pp. 1–18.

[40] V. Žanić, G. Trincas, I. Grubišić, *Multiattribute Decision-Making System Based on Random Generation of Nondominated Solutions: An Application to Fishing Vessel Design*, in 'Practical Design of Ships, Mobile Units, Elsevier Applied Science Vol 2 (1992) pp. 1443–160.

[41] G. W. Evans, Multiple criteria decision analysis for industrial engineering: Methodology and applications, CRC Press, 2016.

[42] G. Degan, L. Braidotti, A. Marinò, V. Bucci, Lctc ships concept design in the north europe-mediterranean transport scenario focusing on intact stability issues, Journal of Marine Science and Engineering 9 (3) (2021). doi:10.3390/jmse9030278.
URL https://www.mdpi.com/2077-1312/9/3/278

[43] V. Žanić, G. Trincas, I. Grubišić, *Mathematical Models for Ship Concept Design*, Proceedings Eighth Congress of the International Maritime Association of Mediterranean, IMAM'97 Vol 1 (1997) pp. 5.1–7–5.1–16.

[44] E. Lennon, J. Farr, R. Besser, Evaluation of multi-attribute decision making systems applied during the concept design of new microplasma devices, Expert Systems with Applications 40 (16) (2013) 6321–6329.

[45] G. Trincas, L. Braidotti, A. Vicenzutti, A. A. Tavagnutti, C. M. Cooke, J. Chalfant, V. Bucci, C. Chryssostomidis, G. Sulligoi, Integration of the power corridor concept in the early-phase design of electric naval ships using mathematical design models, in: International Marine Design Conference, 2024.

[46] B. C. Nehrling, Fuzzy set theory and general arrangement design, in: Computer Applications in the Automation of Shipyard Operation and Ship Design, 5thInternational Federation of Automatic Control, Laxenburg (Austria), 1985.

[47] P. Sen, J. Yang, *Design Decision Making Based upon Multiple Attribute Evaluations and Minimal Preference Iformation. Mathematical and Computer Modelling* (1994) pp. 107–124.

[48] R. W. Saaty, The analytic hierarchy process—what it is and how it is used, Mathematical modelling 9 (3-5) (1987) 161–176.

[49] E. E. Noble, P. P. Sanchez, A note on the information content of a consistent pairwise comparison judgment matrix of an ahp decision maker, Theory and Decision 34 (2) (1993) 99–108.

[50] J. Krejčí, J. Stoklasa, Aggregation in the analytic hierarchy process: Why weighted geometric mean should be used instead of weighted arithmetic mean, Expert Systems with Applications 114 (2018) 97–106. doi:https://doi.org/10.1016/j.eswa.2018.06.060.
URL https://www.sciencedirect.com/science/article/pii/S0957417418303981

[51] Z. Pavić, V. Novoselac, Notes on topsis method, International Journal of Research in Engineering and Science 1 (2) (2013) 5–12.

[52] R. Myers, D. Montgomery, C. AndersonCook, Response Surface Methodology, fourth edition, John Wiley and Sons Inc, 2016.

[53] K. M. Carley, N. Y. Kamneva, J. Reminga, *Response Surface Methodology*, CASOS Technical Report (2004).

[54] G. Box, J. Hunter, *Multi-Factor Experimental Designs for Exploring Response Surfaces*, The Annals of Mathematical Statistics 28(1) (1957) pp. 195–241.

[55] D. C. Montgomery, Design and Analysis of Experiments, Eighth Edition, John Wiley and Sons Inc, 2013.

[56] J. Holtrop, G. Mennen, et al., An approximate power prediction method, International Shipbuilding Progress 29 (335) (1982) 166–170.

[57] M. Flikkema, J. Holtrop, T. van Terwisga, A parametric power prediction model for tractor pods, in: T-POD Conference, Pole Mecanique Brestois, 2006, pp. 1–16.

[58] S. Utzeri, L. Braidotti, N. Norcia, A. Marino, Updated steel weight estimation for cruise ship concept design, in: Theory and Practice of Shipbuilding, IOS Press, 2024, pp. 35–45.

[59] N. Hogben, N. Dacunha, G. Oliver, Global Wave Statistics, British Maritime Technology Limited, 1986.

[60] NGIA, World port index - national geospatial-intelligence agency (2024). URL https://msi.nga.mil/Publications/APC

[61] N. J. Kotz, N. Balakrishnan, Continuous univariate distributions. vol. 1, hoboken (1993).

[62] A. W. Bowman, A. Azzalini, Applied smoothing techniques for data analysis: the kernel approach with S-Plus illustrations, Vol. 18, OUP Oxford, 1997.

[63] Intergovernmental Oceanographic Commission, Ioc, scor and iapso, 2010: the international thermodynamic equation of seawater, 2010: calculation and use of thermodynamic properties Manuals and Guides (56) (2010) 196 pp.

[64] T. J. McDougall, D. R. Jackett, D. G. Wright, R. Feistel, Accurate and computationally efficient algorithms for potential temperature and density of seawater, Journal of Atmospheric and Oceanic Technology 20 (5) (2003) 730–741. doi:https://doi.org/10.1175/1520-0426(2003)20<730:AACEAF>2.0.CO;2.

[65] F. Roquet, G. Madec, T. J. McDougall, P. M. Barker, Accurate polynomial expressions for the density and specific volume of seawater using the teos-10 standard, Ocean Modelling 90 (2015) 29–43. doi:https://doi.org/10.1016/j.ocemod.2015.04.002.

[66] M. J. Powell, A fortran subroutine for solving systems of nonlinear algebraic equations, Tech. rep., Atomic Energy Research Establishment, Harwell, England (United Kingdom) (1968).

[67] J. J. Moré, B. S. Garbow, K. E. Hillstrom, User guide for minpack-1, Tech. rep., CM-P00068642 (1980).

[68] T. F. Coleman, Y. Li, *An Interior, Trust Region Approach for Nonlinear Minimization Subject to Bounds.*, SIAM Journal on Optimization 6 (1996) pp. 418–445.

[69] T. F. Coleman, Y. Li, *On the Convergence of Reflective Newton Methods for Large-Scale Nonlinear Minimization Subject to Bounds.*, Mathematical Programming 67, number 2 (1994) pp. 189–224.

[70] M. Kresic, B. Haskell, Effects of propeller design–point definition on the performance of a propeller, Diesel Engine System with Regard to In–Service Roughness, Weather Conditions (1983) 195–224.

[71] A. F. Molland (Ed.), Chapter 5 - Powering, Butterworth-Heinemann, Oxford, 2008. doi:https://doi.org/10.1016/B978-0-7506-8987-8.00005-6.

[72] J. Malone, D. Little, Effects of hull foulants and cleaning/coating practices on ship performance and economics, Society of Naval Architects and Marine Engineers Vol.88 (1980).

[73] R. Townsin, D. Byrne, Speed, power and roughness: the economics of outer bottom maintenance, Society of Naval Architects and Marine Engineers Vol.122 (1980).

[74] ITTC, Recommended procedures and guidelines 7.5-04-01-01.2, analysis of speed/power trial data, Tech. rep. (2014).

[75] H. Lackenby, The effect of shallow water on ship speed, Shipbuilder and Marine Engineer 70 (1963) 446–450. doi:https://doi.org/10.1111/j.1559-3584.1964.tb04413.x.

[76] T. I. Fossen, Handbook of marine craft hydrodynamics and motion control, John Wiley & Sons, 2011. doi:10.1002/9781119994138.

[77] W. Blendermann, Book review: Practical ship and offshore structure aerodynamics (2014). doi:https://doi.org/10.1179/str.2014.61.2.004.

[78] S. Liu, A. Papanikolaou, Regression analysis of experimental data for added resistance in waves of arbitrary heading and development of a semi-empirical formula, Ocean Engineering 206 (2020) 107357.

[79] O. M. Faltinsen, Prediction of resistance and propulsion of a ship in a seaway, in: 13th Symposium on Naval Hydrodynamics, Tokyo, 1980, pp. 505–529.

[80] V. Jinkine, V. Ferdinande, *A method for predicting the added resistance of fast cargo ships in head waves*, Int.Shipbuild Prog.21(238) (1974) pp. 149–167.

[81] L. Moskowitz, W. Pierson, E. Mehr, *Wave spectra estimated from wave records obtained by the OWS Weather Explorer and OWS Weather Reporter* (1962-63).

[82] X. Lang, W. Mao, A semi-empirical model for ship speed loss prediction at head sea and its validation by full-scale measurements, Ocean Engineering 209 (2020) 107494. doi:https://doi.org/10.1016/j.oceaneng.2020.107494.
URL https://www.sciencedirect.com/science/article/pii/S0029801820305072

[83] A. F. Molland, S. R. Turnock, Marine rudders and control surfaces: principles data design and applications, Elsevier, 2011.

[84] N. Vasilikis, R. Geertsma, K. Visser, Operational data-driven energy performance assessment of ships: the case study of a naval vessel with hybrid propulsion, Journal of Marine Engineering & Technology 22 (2022) 1–17. doi:10.1080/20464177.2022.2058690.

[85] IMO, RESOLUTION MEPC.376(80) Adopted on 7 July 2023 - 2023 GUIDELINES ON LIFE CYCLE GHG INTENSITY OF MARINE FUELS (LCA GUIDELINES), Tech. rep., International Maritime Organization (2023).

[86] IMO, RESOLUTION MEPC.352(78) Adopted on 10 June 2022 - 2022 GUIDELINES ON OPERATIONAL CARBON INTENSITY INDICATORS AND THE CALCULATION METHODS (CII GUIDELINES, G1), Tech. rep., International Maritime Organization (2022).

[87] IMO, RESOLUTION MEPC.308(73) Adopted on 26 October 2018 - 2018 GUIDELINES ON THE METHOD OF CALCULATION OF THE ATTAINED ENERGY EFFICIENCY DESIGN INDEX (EEDI) FOR NEW SHIPS, Tech. rep., International Maritime Organization (2018).

[88] L. Braidotti, S. Bertagna, R. Rappoccio, S. Utzeri, V. Bucci, A. Marinò, On the inconsistency and revision of carbon intensity indicator for cruise ships, Transportation Research Part D: Transport and Environment 118 (2023) 103662. doi:10.1016/j.trd.2023.103662.

[89] IMO, Resolution MEPC.338(76) - 2021 GUIDELINES ON THE OPERATIONAL CARBON INTENSITY REDUCTION FACTOR RELATIVE TO REFERENCE LINES (CII REDUCTION FACTORS GUIDELINES, G3), Tech. rep., International Maritime Organization (2021).

[90] IMO, Resolution MEPC.337(76) - 2021 GUIDELINES ON THE REFERENCE LINES FOR THE USE WITH OPERATIONAL CARBON INTENSITY INDICATORS (CII REFERENCE LINES GUIDELINES, G2), IMO Document (2021).

[91] IMO, Resolution MEPC.339(76) - 2021 GUIDELINES ON THE OPERATIONAL CARBON INTENSITY RATING OF SHIPS (CII RATING GUIDELINES, G4), IMO Document (2021).

[92] International Maritime Organization, Resolution mepc.377(80): 2023 IMO strategy on reduction of GHG emissions from ships, Resolution, IMO, adopted on 7 July 2023 (2023).

[93] International Maritime Organization, Resolution mepc.395(82): 2024 guidelines for the development of a ship energy efficiency management plan (SEEMP), Resolution, IMO, adopted on 4 October 2024 (2024).

[94] International Maritime Organization, Resolution mepc.391(81): 2024 guidelines on life cycle GHG intensity of marine fuels (2024 LCA guidelines), Resolution, IMO, adopted on 22 March 2024 (2024).

UNIVERSITÀ
DEGLI STUDI
DI TRIESTE

Progetto "iNEST – Interconnected Nord-Est Innovation Ecosystem", ECS_00000043, è parte del programma di ricerca dell'ecosistema dell'innovazione a valere sulle risorse del Piano Nazionale per la Ripresa e Resilienza (PNRR), M4C2 – Investimento 1.5 Creazione e rafforzamento di "Ecosistemi dell'innovazione per la sostenibilità", Finanziato dall'Unione Europea, NextGenerationEU - CUP J43C22000320006